

Geological Survey of Finland

Bulletin 355

**Petrogenesis of the Proterozoic rapakivi
granites and related basic rocks of southeastern
Fennoscandia: Nd and Pb isotopic and general
geochemical constraints**

by **O. Tapani Rämö**



**Geologian tutkimuskeskus
Espoo 1991**

Geological Survey of Finland, Bulletin 355

PETROGENESIS OF THE PROTEROZOIC RAPAKIVI GRANITES
AND RELATED BASIC ROCKS OF SOUTHEASTERN
FENNOSCANDIA: Nd AND Pb ISOTOPIC AND GENERAL
GEOCHEMICAL CONSTRAINTS

by

O. TAPANI RÄMÖ

with 60 figures and 17 tables in the text and 4 appendices

ACADEMIC DISSERTATION

to be presented, with the permission of the Faculty of Science of the University of Helsinki,
for public criticism in Lecture Room 1 of the Department of Geology,
September 30, 1991, at 10 a.m.

GEOLOGIAN TUTKIMUSKESKUS
ESPOO 1991

Rämö, O. Tapani, 1991. Petrogenesis of the Proterozoic rapakivi granites and related basic rocks of southeastern Fennoscandia: Nd and Pb isotopic and general geochemical constraints. *Geological Survey of Finland, Bulletin 355*, 161 pages, 60 figures, 17 tables, and 4 appendices.

The Nd and Pb isotopic composition of 50 silicic and basic rock samples, combined with feldspar Pb and general geochemical data, are used to evaluate the origin and evolution of the Finnish and Soviet Karelian (1.65 to 1.54 Ga) rapakivi granites and penecontemporaneous diabase dykes and gabbroic and anorthositic rocks. Special emphasis is laid on the 1.64 Ga old Suomenniemi complex in south-eastern Finland.

The rapakivi granites occur as shallow-level multiple intrusions sharply transecting the surrounding bedrock. The Finnish granites were emplaced within the 1.9 Ga Svecofennian crust, while the Soviet Karelian granites were intruded in the contact zone between the Svecofennian crust and the Fennoscandian Archean craton. Geochemically, the rapakivi granites are metaluminous to slightly peraluminous subsolvus granites showing high K, K/Na, Fe/Mg, F, Ga, Ga/Al, Rb, Zr, Zn, and REE, as well as low Ca, Mg, P, and Sr, and hence are similar to the Phanerozoic subalkaline A-type granites. In the Suomenniemi complex, a minor peralkaline hyper-solvus intrusive phase (aegirine-augite alkali-feldspar syenite) also occurs.

Nd isotopic data on the Finnish granites show initial ϵ_{Nd} values ranging from -3.1 to -0.2 and T_{DM} model ages (topaz-bearing granites excluded) averaging 2.06 ± 0.03 (1 S.D.) Ga. Alkali feldspar Pb isotopic compositions have S&K μ_2 values that average 9.83 ± 0.08 (1 S.D.). These isotopic characteristics are very close to those measured for the Svecofennian crust and indicate that the Finnish rapakivi granites were derived from it. The Soviet Karelian granites exhibit more negative ϵ_{Nd} values (-8.1 to -5.7) and low Pb isotopic ratios (alkali feldspar μ_2 values 8.73 and 8.75). Mixing calculations suggest that these granites are about one-to-one mixtures of Proterozoic and Archean crustal material, and that the Archean lower crust presumably has a very unradiogenic Pb isotopic composition (apparent μ_2 value of about 8).

Major and trace element modeling of the granites of the Suomenniemi batholith suggests a felsic (ca. 73% SiO₂) parental magma which may have been generated by ca. 20% melting of an intermediate to acid (granodioritic) source. Calculations suggest that subsequent evolution of the parental magma was possibly controlled by fractionation of alkali feldspar, quartz, mafic silicates, and Fe-Ti-oxide (in the ratio 68/15/15/2), with trace amounts of apatite, zircon, and allanite. This resulted in a spectrum of rocks ranging from cumulates (hornblende granite, biotite-hornblende granite) to those precipitated from residual liquids (biotite granite, topaz-bearing granite). Isotopic data are indicative of some wall-rock assimilation.

The diabase dykes crystallized from evolved Fe-rich tholeiitic magmas. They are moderately enriched in the LREE and have ϵ_{Nd} values ranging from -1.2 to +1.6. The Pb isotopic compositions of the diabase dykes conform to the growth curve of average crustal Pb and define a secondary isochron with an age of 1854 ± 65 Ma, which is ca. 200 Ma in excess of their true crystallization age. The magma evolution of these dykes can be assessed by AFC modeling involving a plagioclase-dominated gabbro assemblage in which the amount of clinopyroxene exceeds that of olivine, and an upper crustal contaminant with $\epsilon_{Nd} = -3.6$ and Nd = 26 ppm. Incorporation

poration of Pb from the Svecofennian crust explains the age of the secondary isochron and variable U-Pb whole rock errorchrons as well. The gabbroic and anorthositic rocks are akin to lithologies encountered in the Proterozoic massive anorthosites. They also show an evolved character, variable ϵ_{Nd} values (-1.7 to +0.8), and Pb isotopic ratios that plot along the growth curve of average crustal Pb.

The rapakivi granites and related basic rocks are considered to derive from anorogenic magmas produced by partial melting in the upper mantle (diabase dykes, gabbroic and anorthositic rocks) and lower parts of the continental crust (rapakivi granites). This anorogenic magmatism may have been associated with the formation of an early Proterozoic supercontinent (Laurentia — Baltica) that promoted large-scale mantle upwellings, partial melting in the upper mantle, and subsequent anatexis of the continental crust.

Key words: igneous rocks, granites, rapakivi, gabbros, anorthosite, diabase, geochemistry, isotopes, neodymium, lead, genesis, Proterozoic, Finland

O. Tapani Rämö, Department of Geology, University of Helsinki, P.O. Box 115, SF-00171 Helsinki, Finland

ISBN 951-690-439-4

ISSN 0367-522-X

*To Kristiina,
Lotta, Sampo, and Milla*

CONTENTS

Introduction	9
Geologic setting	11
Mode of occurrence of the rapakivi granites and related basic rocks ..	11
The Suomenniemi complex	13
The Suomenniemi batholith	13
Coarse-grained biotite granite	16
Hornblende granite and biotite-hornblende granite	16
Hornblende-clinopyroxene-fayalite granite	18
Porphyritic biotite granite	18
Topaz-bearing granite	20
Alkali-feldspar syenite	20
Orbicular granite	23
Gabbro-anorthosite body	24
Quartz-feldspar porphyry dykes	24
Diabase dykes	25
Silicic-basic composite dykes	26
Alkali-feldspar diabases	28
The Lovasjärvi intrusion	31
Sampling	31
Rapakivi granites	33
Rapakivi granites of the Suomenniemi batholith	33
Rapakivi granites from the other intrusions	34
Alkali-feldspar syenites	31
Quartz-feldspar porphyry dykes	3
Diabase dykes and the Lovasjärvi intrusion	3
Gabbroic and anorthositic rocks	3
Analytical procedures	3
General geochemistry	3
Nd and Pb isotope geochemistry	3
General geochemical characteristics of the rapakivi granites and related basic rocks	3
Silicic rocks and alkali-feldspar syenites	3
Rapakivi granites and quartz-feldspar porphyry dykes	4
Alkali-feldspar syenites	4
Tectonomagmatic affinities and typology	4
Basic rocks	4
Diabase dykes and the Lovasjärvi intrusion	4
Gabbroic and anorthositic rocks	4
Nd and Pb isotope geochemistry	54
Notes on data presentation	54
Sm-Nd method	54
Pb-Pb method	54
Nd isotopic results	55
Finnish rapakivi granites, quartz-feldspar porphyry dykes, and alkali-feldspar syenites	55
Soviet Karelian rapakivi granites	55

Diabase dykes and the Lovasjärvi intrusion	62
Gabbroic and anorthositic rocks	62
Pb isotopic results	63
Finnish rapakivi granites, quartz-feldspar porphyry dykes, and alkali-feldspar syenites	63
Soviet Karelian rapakivi granites	67
Diabase dykes and the Lovasjärvi intrusion	67
Gabbroic and anorthositic rocks	71
Magma evolution in the Suomenniemi complex: silicic rocks and alkali-feldspar syenites	71
Processes producing chemical variation within felsic igneous suites	72
Methodology of modeling partial melting and fractional crystallization	76
Evolution of the granites of the Suomenniemi batholith	77
Partial melting vs. fractional crystallization	77
Fractional crystallization modeling	77
Isotopic implications	85
Quartz-feldspar porphyry dykes and alkali-feldspar syenites	87
Protolith of the Finnish rapakivi granites	88
Nd isotopic evidence	88
Pb isotopic evidence	90
Partial melting modeling: the main granite sequence of the Suomenniemi batholith	91
Depth of magma generation	93
Assessment of a possible protolith composition	94
Insights into the origin of the minor felsic intrusive phases in the Suomenniemi complex	99
Soviet Karelian rapakivi granites: a mixed source	101
Rapakivi granites as probes into lower continental crust: implications of the Nd and Pb isotopic data	103
Rapakivi-age basic rocks: mantle source characteristics and magma evolution	106
Evolution of the diabase dyke magmas	106
Primitive melts from a LIL-enriched mantle?	106
Qualitative constraints from petrography and major and trace element variations	108
Closed-system fractional crystallization modeling	111
Nd isotopic-compositional correlations	114
Combined assimilation-fractional crystallization modeling	116
Major element constraints on assimilation	121
Trace element variations	123
Model for the origin of uranogenic Pb in the diabases	126
Diabase whole rock U-Pb errorchrons	128
Origin of the gabbroic and anorthositic rocks	130
Nd isotopic constraints	130
Pb isotopic constraints	132
Discussion	132
Conclusions	138
Acknowledgements	139
References	140
Appendix 1: Chemical composition of the silicic rocks and alkali-feldspar syenites	150
Appendix 2: Chemical composition of the basic rocks	156
Appendix 3: Crystal/liquid partition coefficients used in modeling partial melting and fractional crystallization	161
Appendix 4: Geological map of the Suomenniemi complex	



INTRODUCTION

A hundred years ago, Sederholm (1891) introduced the Finnish term *rapakivi* to international geological literature in his pioneering paper on the *rapakivi* granites of southern Finland. The term, meaning disintegrated or crumbly rock illustrated the tendency of the *rapakivi* granites to weather more easily than other granitic rocks of Finland. Since the early days of Sederholm, southern Finland has been regarded as the type area of *rapakivi* granites. In the first half of the century, petrographical and geochemical works on Finnish *rapakivi* granites were published by Wahl (1925, 1947), Eskola (1928, 1930, 1949), Hackman (1934), and Sahama (1945, 1947). Later, studies have been carried out on petrology, petrography, and geochemistry (Savolahti, 1956, 1962; Vormaa, 1975, 1976; Haapala, 1977a; Törnroos, 1984), mineralogy (Haapala & Ojanperä, 1969; Simonen & Vormaa, 1969; Vormaa, 1971, 1972; Vormaa & Paasivirta, 1979), geochronology (Vaasjoki, 1977; Vaasjoki et al., 1988; Idman, 1989), intrusion mechanism (Bergman, 1986), and metallogeny (Haapala & Ojanperä, 1972a; Haapala, 1974, 1977b, 1988).

The Finnish *rapakivi* granites comprise four large batholiths (Wiborg, Åland or Ahvenanmaa, Laitila, and Vehmaa) and several smaller batholiths or stocks (Suomenniemi, Ahvenisto, Onas, Bodom, Obbnäs, Käkarsfjärd, Fjällskär, Eurajoki, Kokemäki, Reposaaari, and Siipyy) transecting the 1.9 Ga Svecofennian crust of southern Finland (Fig. 1). Quartz-feldspar porphyry dykes, compositionally akin to the granites, are often associated with the batholiths and stocks. The isotopic ages of the *rapakivi* granites and silicic dyke rocks range from 1.65 to 1.54 Ga (Vaasjoki et al., 1991; see also Vaasjoki, 1977).

The *rapakivi* granites are spatially and temporally associated with basic rocks, i.e. tholeiitic dykes (Subjotnian diabases) and minor gabbroic and anorthositic bodies. The tholeiitic dykes are in places cut by the *rapakivi* granites, but in other places the opposite relationship occurs, and in a few instances evidence for coexisting silicic and basic magmas is found (Laitala, 1984; Lindberg & Eklund, 1989; Rämö, 1989a). In contrast, the granites show an intrusive relationship to the gabbroic and anorthositic rocks; no difference, however, exists in the isotopic ages of these rocks (Vaasjoki, 1977; Suominen, 1987; Vaasjoki et al., 1991).

Presently used terminology differentiates between *rapakivi* granite and *rapakivi* texture (cf. Vormaa, 1976). *Rapakivi* texture (plagioclase-mantled alkali feldspar ovoids, two generations of alkali feldspar and quartz) is common in the Proterozoic *rapakivi* granites of Finland (although in some of the batholiths it may be rare or absent), but other granites with plagioclase-mantled alkali feldspar ovoids are commonly called *rapakivi* granites, regardless of age. Granites with *rapakivi* texture have been described from some Phanerozoic and Archean granites (e.g., Murakami & Imaoka, 1985; Sibiya, 1988), but they are most commonly found in middle to early Proterozoic anorogenic or postorogenic complexes in early Proterozoic orogenic belts (Bridgwater & Windley, 1973; Emslie, 1978; Anderson, 1983; Haapala, 1988). Proterozoic *rapakivi* granites are known to exist in most Precambrian shield areas. In addition to the Fennoscandian shield, they have been described for example from the Ukraine, U.S.S.R. (see Velikoslavinskiy et al., 1978), Greenland (Bridgwater et al., 1974), Canada (Emslie, 1978),

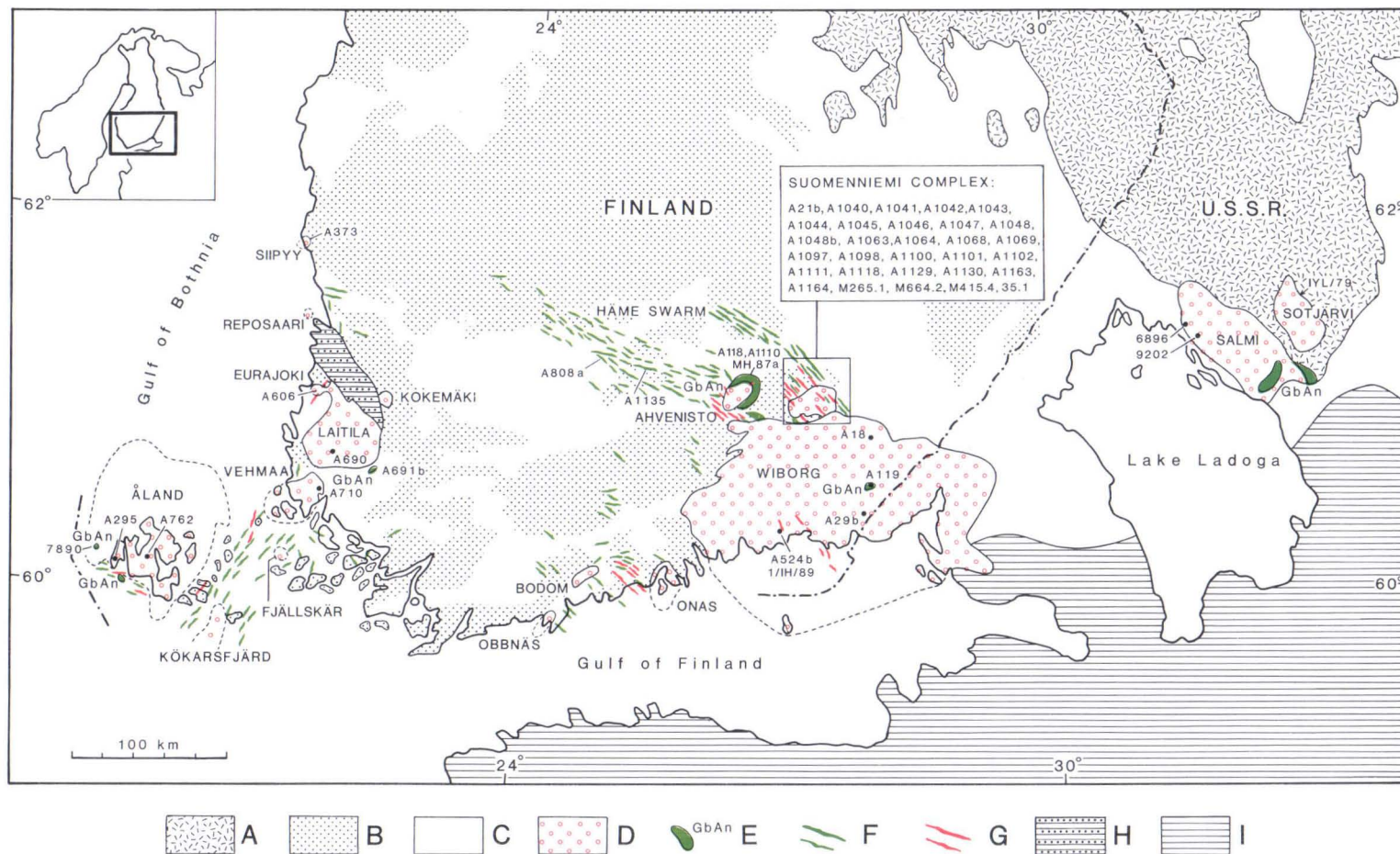


Fig. 1. Map showing the 1.65 to 1.54 Ga old rapakivi granite batholiths and stocks and associated gabbro-anorthosite bodies and basic and silicic dyke rocks of southern Finland and adjacent Soviet Karelia. Locations of the isotopic samples are denoted; for detailed sample sites in the Suomenniemi complex, see Appendices 1, 2, and 4. A: Archean craton; B: Proterozoic (Svecokarelian, 1.9 to 1.8 Ga) granitoid rocks; C: Proterozoic (mainly Svecokarelian) supracrustal rocks; D: rapakivi granite; E: gabbroic and anorthositic rocks; F: rapakivi-age (Subjotnian) diabase dykes; G: quartz-feldspar porphyry dykes; H: Jotnian (ca. 1.3 Ga) sandstone; I: Phanerozoic. Compiled after Bergman (1979), Ehlers and Ehlers (1978), Haapala (1977a), Idman (1989), Laitakari and Leino (1989), Leijärvi and Tyrväinen (1969), Meriläinen (1966), Papunen and Gorbunov (1985), Simonen (1973, 1979a, 1979b, and 1980), Simonen and Laitala (1972), Suominen (1979), Vaasjoki et al. (1988), Velikoslavinskiy et al. (1978), and Vormä (1980).

U.S.A. (Anderson, 1983), Brazil (Goni, 1961; Teixeira, 1990), Venezuela (Gaudette et al., 1978), China (Yu, 1989), and Australia (Wyborn et al., 1988).

Active geological research has focused on the rapakivi granites for a hundred years now, but the petrogenesis of these rocks is still controversial. Major problems regarding the petrogenesis of the rapakivi granites are (1) the source of the rapakivi granite magma, (2) the genetic relations between the rapakivi granites and the penecontemporaneous basic rocks, (3) the geotectonic framework in which these rocks were emplaced, (4) the overall relation of the rapakivi granites to the evolution of the continental crust, and (5) the origin of the rapakivi texture.

The aim of the present work is to discuss in detail the first two problems. To do this, a Nd and Pb isotopic and general geochemical study was carried out on the rapakivi granites and associated basic rocks of southern Finland. Because the Finnish rapakivi granite batholiths are typical rapakivi granite intrusions inasmuch as they all are found within the early Proterozoic crust, a few samples were also investigated from the two Soviet Karelian batholiths, Salmi and Sotjärvi (or Ulalega) (Fig. 1). The Soviet batholiths are located at the contact between the juvenile 1.9 Ga Svecofennian crust and the Fennoscandian Archean craton, and they were thought to provide information on the extent to which ancient continental crust was involved in the genesis of these granites.

The Suomenniemi complex on the northern

flank of the Wiborg rapakivi batholith (Fig. 1) was chosen for detailed study because relatively little information was available for the Suomenniemi rapakivi granite batholith and because the bedrock surrounding the batholith, with its abundant silicic and basic dyke rocks, was believed to be suitable for studying the problem of bimodal magmatism associated with rapakivi granites. The Suomenniemi complex was mapped in detail by the Department of Geology, University of Helsinki in 1986–88. The isotopic work presented in this study was performed in the Unit for Isotope Geology, Department of Petrology, Geological Survey of Finland in 1987–90.

First, the present work describes the mode of occurrence, petrography, and geochemistry of the Finnish rapakivi granites and penecontemporaneous basic rocks, with special reference to the Suomenniemi complex. Nd and Pb isotopic data on the silicic and basic rocks are dealt with next, with implications for intra-batholith magma evolution, source of the rapakivi granite magma, and isotopic composition of the lower continental crust. This is followed by a discussion on the mantle source characteristics and magma evolution of the rapakivi-age diabase dykes and gabbroic and anorthositic rocks. Finally, a petrogenetic model is suggested for the rapakivi granites and associated basic rocks. Preliminary results of this work have been reported by Haapala and Rämö (1987, 1988, 1990), Rämö (1989a, 1989b, 1990), Rämö et al. (1989, 1990), Vaasjoki and Rämö (1989), Rämö and Haapala (1991), and Vaasjoki et al. (1991).

GEOLOGIC SETTING

Mode of occurrence of the rapakivi granites and related basic rocks

The rapakivi granite batholiths and stocks of southeastern Fennoscandia cut sharply across the surrounding bedrock. They were emplaced at shallow crustal levels, often by multiple injections

of silicic magmas over long periods (e.g., emplacement of the Wiborg batholith took at least 25 Ma; Vaasjoki et al., 1991). Such features as sharp intrusive contacts, roof pendants, roof

breccias, and subvolcanic and volcanic members suggest that the present erosion level generally represents the upper parts of these epizonal intrusive complexes (Wahl, 1925, 1947; Vorma, 1975; Haapala, 1977a; Bergman, 1986). Some of the smaller intrusions show structures typical of centered complexes (Vorma, 1976; Haapala, 1977a, 1988). The effect of the rapakivi granite magmas on their immediate country rocks has been minor, largely due to the relatively high metamorphic grade of the bedrock. Vorma (1972), however, using the structural state of alkali feldspars in the rocks surrounding the Wiborg batholith, was able to recognize a thermal aureole around the batholith, presumably induced by the emplacement of the rapakivi magmas. Geophysical data indicate that the rapakivi batholiths are subhorizontal sheets not more than about 10 km thick, and that they may have deep roots (Laurén, 1970; Tuomi, 1988; Korja & Elo, 1990). The emplacement mechanisms were most probably cauldron subsidence and magmatic stoping (Sundsten, 1985; Bergman, 1986). Faults or deep fractures have, in several instances, obviously controlled the emplacement of the rapakivi granites.

The rapakivi granites of southeastern Fennoscandia can be divided into two age groups. The eastern Finnish intrusions (Wiborg, Suomensalmi, Ahvenisto, Onas, Bodom, and Obbnäs) show a range of U-Pb zircon ages from 1650 to 1620 Ma (Vaasjoki et al., 1991; M. Vaasjoki, pers. commun., 1991), while the western Finnish intrusions (Åland, Laitila, Vehmaa, Käkarsfjärd, Fjällskär, Kokemäki, Eurajoki, Reposaaari, and Siippy) and the Soviet Karelian batholiths (Salmi and Sotjärvi) have U-Pb zircon ages between 1590 and 1540 Ma (Suominen, 1987; Vaasjoki et al., 1988; Idman, 1989; Suominen, 1991; see also Vaasjoki, 1977).

The tholeiitic dyke rocks (Subjotnian diabbases) associated with the rapakivi granites of southeastern Finland comprise several west-northwest- or northwest-trending dyke swarms (Fig. 1) and show a range of isotopic ages from 1665 to 1635

Ma (Laitakari, 1987; Siivola, 1987; Suominen, 1987; Vaasjoki & Sakko, 1989; Vaasjoki et al., 1991). They usually have plagioclase phenocrysts and/or megacrysts set in a groundmass of plagioclase, olivine, clinopyroxene, and oxide. The largest of the dyke swarms is the roughly 250 km long and about 70 km wide Häme swarm (Fig. 1) extending from the northwestern flank of the Wiborg batholith through the belt of the Svecofennian plutonic and supracrustal rocks of southern Finland (Laitakari, 1969, 1987). The Häme swarm consists of at least two dyke sets that differ in age by some 20 Ma (Vaasjoki & Sakko, 1989). Other mafic dyke sets related to the eastern Finnish rapakivi intrusions are a swarm in the Suomensalmi complex that provides evidence for a third, slightly younger dyke event (Vaasjoki et al., 1991), a swarm north of the Ahvenisto complex (Laitakari & Leino, 1989), and scattered dykes along the southern coast of Finland in association with the Onas, Bodom, and Obbnäs plutons (Fig. 1). Wahl (1947) and Vorma (1975) present evidence for volcanic and subvolcanic mafic rocks most probably related to the diabase dykes of southeastern Finland. Tholeiitic dykes associated with the western Finnish intrusions comprise mainly northeast-trending swarms (Ehlers & Ehlers, 1977) but some roughly east-west-trending swarms also exist (Pihlaja, 1987; Lindberg & Eklund, 1989). These diabase dykes have isotopic ages close to those of the rapakivi granites of southwestern Finland (Suominen, 1987).

Most of the Finnish rapakivi granite batholiths are associated with minor gabbroic and anorthositic bodies that are found either as inclusions in rapakivi granite or as plutons at or close to the margins of the batholiths. By far the largest (ca. 70 km²) of the gabbroic and anorthositic bodies is the Ahvenisto gabbro-anorthosite complex (Fig. 1). It has been described in detail by Savolahti (1956) and Johanson (1984). The complex is associated with a biotite rapakivi granite batholith and also shows an abundance of intermediate monzodioritic rocks (Johanson, 1989).

Volumetrically the most important rock type in the complex is gabbronorite that is locally, especially in the southern part of the complex, altered to uralite gabbro. Other rock types include olivine gabbro, olivine gabbronorite, norite, leucogabbronorite, and anorthosite; minor occurrences of ilmenite-rich gabbronorites and very coarse-grained gabbropegmatites and leucogabbros are also encountered (Johanson, 1984). The age of the Ahvenisto gabbro-anorthosite complex is 1645 Ma (Vaasjoki et al., 1991).

Other gabbroic and anorthositic rocks related to the rapakivi granites of eastern Finland are anorthosite inclusions in the east-central part of the Wiborg batholith (e.g., at Ylämaa; Simonen, 1979a, 1979b), the Väärälampi body in the Suomenniemi batholith, and a minor anorthositic intrusion between the Ahvenisto complex and the Wiborg batholith (Lehijärvi & Tyrväinen, 1969; Tyrväinen, 1986). The anorthositic bodies of Väärälampi and Ylämaa are dated at 1636 and 1633 Ma, respectively (Vaasjoki et al., 1991;

Suominen, 1991).

Gabbroic and anorthositic rocks are also associated with the western Finnish and the Soviet Karelian batholiths. Close to the southeastern contact of the Laitila rapakivi granite batholith, at Kolinummi, there occurs an elongated anorthositic intrusion embedded in a Svecofennian garnet-cordierite gneiss (Nyfors, 1954; Vorma, 1976). It consists of various fine- to coarse-grained anorthositic rocks that occasionally show plagioclase crystals up to 15 cm in length. An U-Pb zircon age of about 1570 Ma was reported for the Kolinummi intrusion by Vaasjoki (1977). Minor gabbroic and anorthositic bodies are also found in the western and southwestern parts of the Åland batholith (Bergman, 1979; Suominen, 1987) and also in association with the Salmi batholith (Velikoslavinskiy et al., 1978). According to Suominen (1987), the anorthosites associated with the Åland batholith are about 1580 Ma old.

The Suomenniemi complex

The Suomenniemi complex consists of the Suomenniemi rapakivi granite batholith and spatially and temporally associated silicic and basic dyke rocks. A geological map of the complex is included as Appendix 4. Within the Suomenniemi batholith, a number of different rock types occur, ranging from low-silica hornblende-clinopyroxene-fayalite granite and hornblende granite to highly silicic topaz-bearing granite and peralkaline alkali-feldspar syenite. A small gabbro-anorthosite body also exists. The dyke rocks of the complex comprise quartz-feldspar porphyry and diabase that usually occur separately, but occasionally have intruded through the same fractures, producing composite dykes. Silicic-basic magma interaction in the complex is also demonstrated by diabases bearing alkali feldspar megacrysts (Rämö, 1989a). There also exists a

tholeiitic mafic intrusion at Lovasjärvi in the southwestern part of the complex, showing a close genetic association with the diabase dykes.

The Suomenniemi batholith

The Suomenniemi batholith is one of two satellite rapakivi granite bodies at the northwestern flank of the Wiborg batholith (Fig. 1, Appendix 4). It covers an area of approximately 365 km² and is well exposed, except in its west-central parts. The batholith has been described in unpublished theses (Pipping, 1956; Sundsten, 1985), but little has been published on the batholith: its lithology has briefly been commented on by Frosterus (1903), Vorma (1972, 1976), and Simonen and Tyrväinen (1981).

The Suomenniemi batholith cuts sharply across the surrounding early Proterozoic Svecofennian plutonic and supracrustal rocks that comprise microcline granite to the north and west, mica gneiss, quartz diorite, and granodiorite to the east, and mica gneiss, quartzite, and mafic schists to the south of the batholith (Simonen & Tyrväinen, 1965; Tyrväinen, 1990). The batholith presumably has a mutual contact with the Wiborg batholith in the southeast. The contact is not exposed, but Vormaa (1972) suggests that the Wiborg batholith probably is younger than the Suomenniemi batholith. This hypothesis is also consistent with the latest isotopic ages from the outer contact of the Wiborg batholith south of the Lovasjärvi intrusion where the rocks are

dated to be about 10 Ma younger than the granites in the Suomenniemi batholith (Vaasjoki et al., 1991).

The contacts of the Suomenniemi batholith against its country rocks dip usually gently away from the batholith in its western part where the granites show a distinct chill phase against the country rocks (Pipping, 1956; Simonen & Tyrväinen, 1981). Exposures of contact breccia are abundant along its northwestern and northeastern rims. In addition, country rock xenoliths, up to a few tens of meters across, have been found in the east-central and southwestern parts of the batholith (Appendix 4). The general outline of the contacts of the batholith seems to follow pre-existing northwest- and southwest-

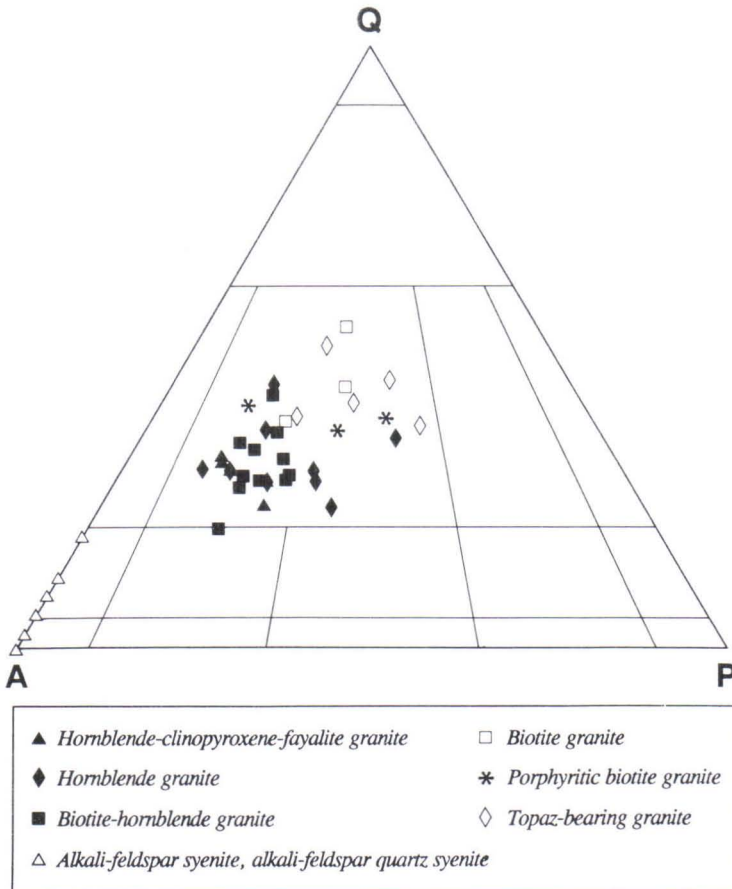


Fig. 2. Modal composition of the granites and alkali-feldspar syenites and alkali-feldspar quartz syenites of the Suomenniemi batholith shown in the APQ-diagram of Streckeisen (1973).

trending weakness zones in the bedrock (Sundsten, 1985). This has resulted in a zig-zag pattern, which in general is typical of centered complexes emplaced at shallow crustal levels (cf. Pitcher & Berger, 1972). Geophysical models suggests that the Suomenniemi batholith is about 3 km thick (Tuomi, 1988).

Previous studies (Pipping, 1956; Sundsten, 1985) have described two main granite types in the batholith: a coarse, even-grained to slightly porphyritic biotite granite that constitutes the bulk of the batholith in its western, central, and northern parts, and a coarse- and even-grained hornblende granite found in the southeastern part of the batholith. The present study indicates that the two rock types may gradually change from one to the other, as granites with varying amounts of biotite and hornblende are associated with the hornblende granite and biotite granite (Appendix 4). In outcrops the main granite types,

especially the biotite granite in the northern and western parts of the batholith, are usually rather homogeneous. Not infrequently, however, large heterogeneities exist, for instance, on a single outcrop, where a granite may vary from equigranular to distinctly porphyritic without necessarily showing sharp contacts.

In addition to the major granite types, several distinctive lithologies of small areal extent can be recognized in the batholith. These comprise fayalite-clinopyroxene-hornblende granite, porphyritic biotite granite, topaz-bearing granite, and alkali-feldspar syenite. Moreover, two occurrences of orbicular granite and a small gabbro-anorthosite body also occur. In the remainder of this section, short petrographic descriptions of the rock types are given. Representative modal compositions of the various felsic rock types in the batholith are plotted in the APQ-diagram (Streckeisen, 1973) in Fig. 2.

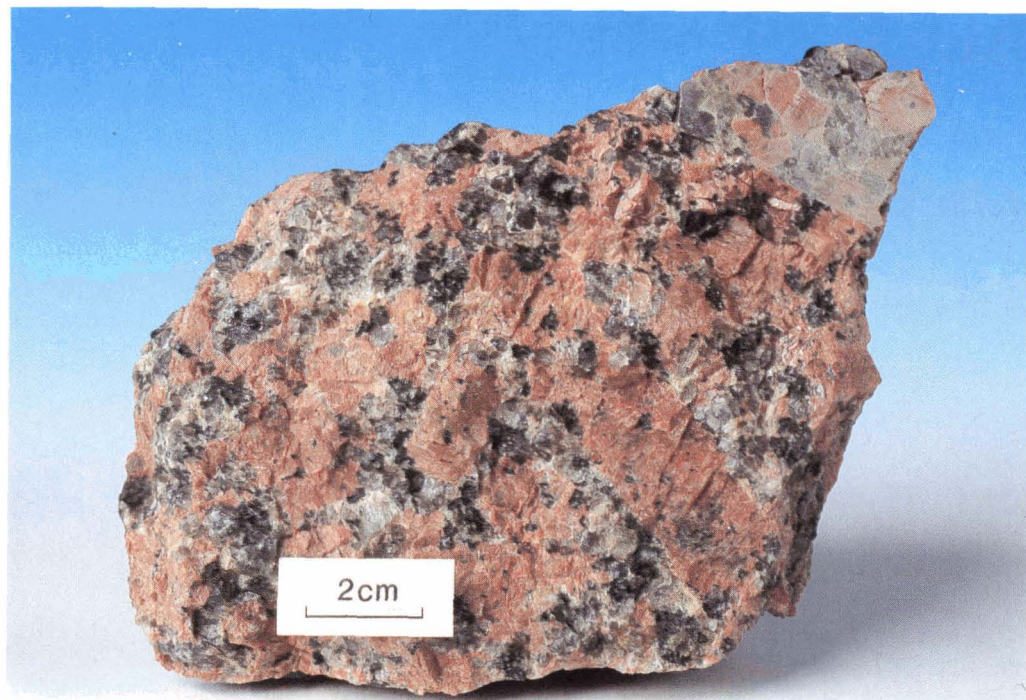


Fig. 3. Coarse-grained biotite granite (sample A1042) at Uiruvuori quarry, northern part of the Suomenniemi batholith. Photo by Jari Väättäinen.

Coarse-grained biotite granite

The coarse-grained biotite granite that constitutes the bulk of the batholith in its western, central, and northern parts is a red to pale red rock with an even-grained to slightly porphyritic texture showing predominant alkali feldspar crystals 2 to 4 cm across, conspicuous drop quartz, and biotite (Fig. 3). Scattered alkali feldspar ovoids with an average diameter of 5 cm also occur. At the contacts of the batholith the coarse-grained biotite granite grades to a distinctly porphyritic rock with scattered alkali feldspar and quartz phenocrysts in a medium-grained matrix with occasional hornblende.

Hornblende granite and biotite-hornblende granite

Hornblende granite and biotite-hornblende granite are found in the southern and southeast-

ern parts of the batholith (cf. Appendix 4). The relative proportions of the main mafic minerals (biotite, hornblende) and the grain size of the rocks vary considerably. The southeastern rim of the batholith is composed of a dark red, medium- to coarse-grained equigranular granite that has hornblende as the only main mafic mineral (Fig. 4). Toward north and west (i.e., where the bedrock is sufficiently exposed), the hornblende granite passes into a reddish grey equigranular granite with variable amounts of hornblende and biotite (Fig. 5). In the cores of the hornblende iddingsite pseudomorphs after fayalite and fayalite relics are often found. Plagioclase-phyric gabbro-anorthosite inclusions (Fig. 6) and plagioclase megacrysts are occasionally found in the hornblende granites and biotite-hornblende granites.

Sharp contacts between different granite types (e.g., between a coarse-grained biotite-hornblende granite and a more mafic hornblende-

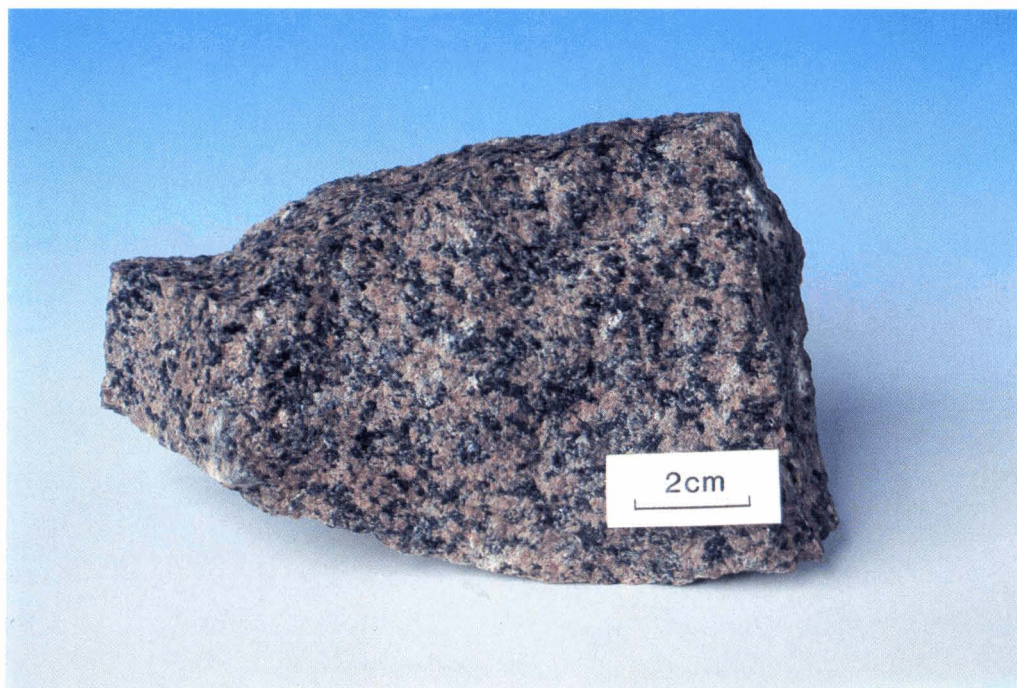


Fig. 4. Hornblende granite (sample A1043) at Pohjalampi, southeastern flank of the Suomenniemi batholith. Photo by Jari Väättäin.



Fig. 5. Biotite-hornblende granite (sample MKT-87-738.1) at Kuituranlahti, eastern part of the Suomenniemi batholith (Map 3132 09D, $x=6796.75$, $y=3528.45$). Photo by Jari Väätäinen.

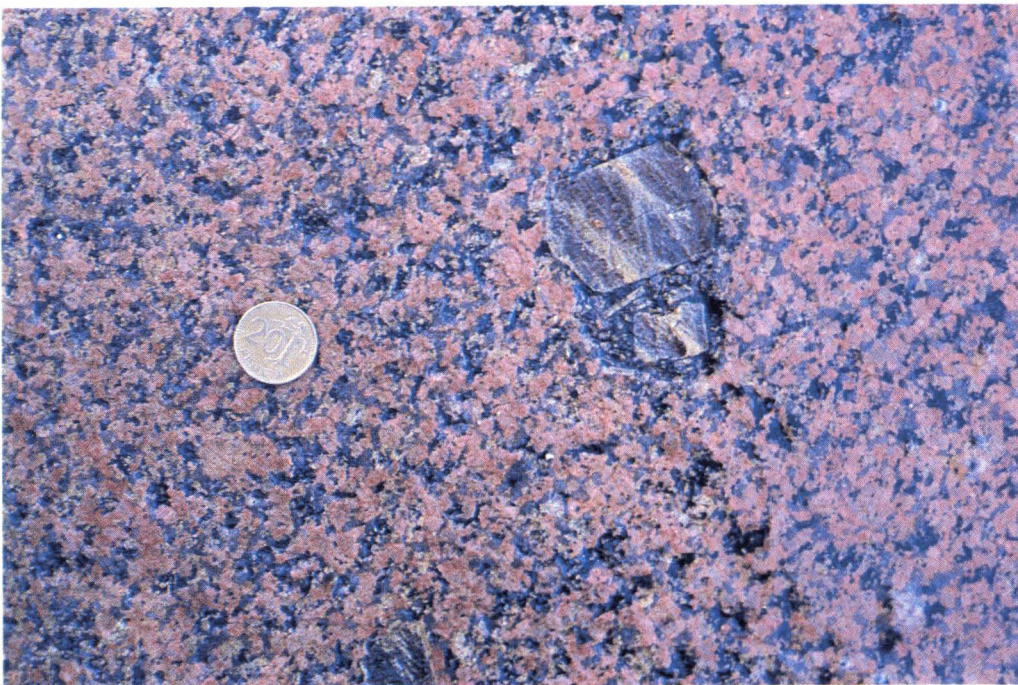


Fig. 6. Plagioclase-phyric gabbro-anorthosite inclusion embedded in biotite-hornblende granite on the island of Ärjätsaari, eastern part of the Suomenniemi batholith (Map 3132 09D, $x=6795.22$, $y=3526.77$). The diameter of the coin is 2.2 cm.

dominated granite) can be seen in a few outcrops in the eastern part of the batholith, but the relative ages of the rock types can not be indisputably defined. According to Vormaa (1976), the hornblende granite of the Suomenniemi batholith is younger than the coarse-grained biotite granite, but it is also possible that they are coeval and simply related to each other by fractionation processes, and hence sharp mutual contacts do not necessarily mean that they belong to distinctive intrusive phases, but may be the result of autointrusion under unstable crystallization conditions (e.g., rapid changes in pressure, cauldron subsidence perturbations) in the subvolcanic environment of emplacement of the batholith.

Hornblende-clinopyroxene-fayalite granite

Hornblende-clinopyroxene-fayalite granite is found as minor intrusive units within the south-

ern, east-central, and eastern parts of the batholith (Appendix 4). Typically, the rock is dark brownish gray, porphyritic with grayish alkali feldspar phenocrysts (diameter 1 to 2 cm) and a fine- to medium-grained groundmass of alkali feldspar, oligoclase, quartz, fayalite, clinopyroxene, and hornblende (Fig. 7). The hornblende-clinopyroxene-fayalite granite occurs as small patches within the hornblende granite and biotite-hornblende granite showing sharp and sometimes also brecciated contacts with them (Fig. 8). In accordance with the Fe-rich nature of the olivine in the rock, the clinopyroxene and hornblende are also Fe-rich (ferrohedenbergite and hastingsitic hornblende, respectively).

Porphyritic biotite granite

Porphyritic biotite granite occurs mainly in the northern and northwestern parts of the batholith.



Fig. 7. Hornblende-clinopyroxene-fayalite granite (sample A1130) at Sikolampi, eastern part of the Suomenniemi batholith. Photo by Jari Väättäin.

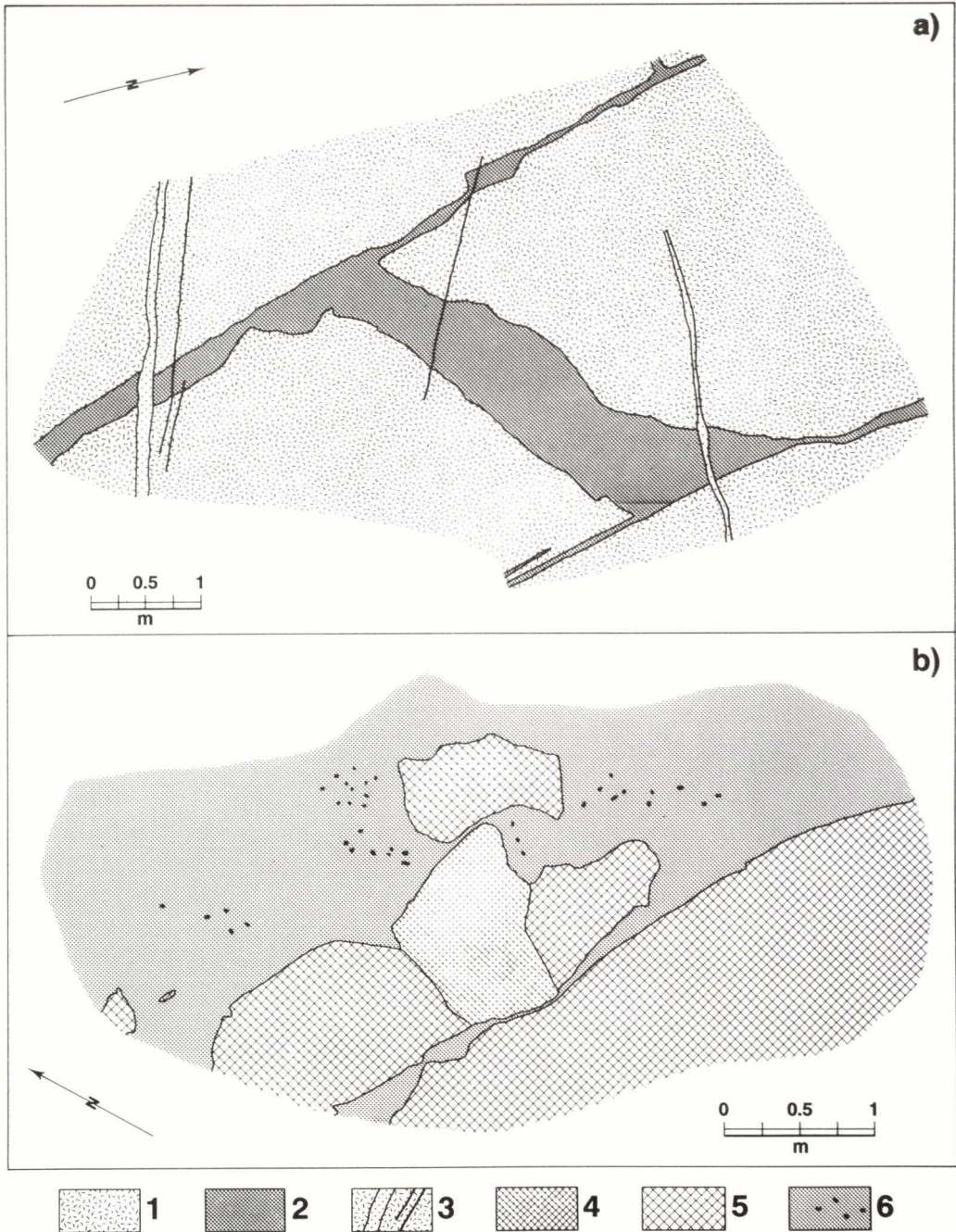


Fig. 8. Sketch maps showing the mode of occurrence of the hornblende-clinopyroxene-fayalite granite in the Suomenniemi batholith. (a) hornblende-clinopyroxene-fayalite granite brecciating biotite-hornblende granite at Sikolampi, eastern Suomenniemi batholith (Map 3132 09D, $x = 6799.36$, $y = 3528.34$). (b) hornblende-clinopyroxene-fayalite granite intruding hornblende granites at Sammakko-oriko, east-central Suomenniemi batholith (Map 3132 09B, $x = 6798.51$, $y = 3522.38$). 1: coarse-grained biotite-hornblende granite; 2: medium-grained hornblende-clinopyroxene-fayalite granite; 3: aplitic and pegmatitic veins; 4: medium- to coarse-grained hornblende granite; 5: coarse-grained hornblende granite; 6: medium- to coarse-grained slightly porphyritic hornblende-clinopyroxene-fayalite granite (dots denote clusters of alkali feldspar phenocrysts).

It shows distinctive euhedral alkali feldspar and quartz phenocrysts and an abundance of miarolitic microcavities; biotite is the only mafic silicate and sometimes occurs as poikilitic rosettes in the medium- to coarse-grained groundmass (Fig. 9). This rock type is areally quite restricted (the largest mappable unit occurs at Luotolahti in the northeastern corner of the batholith; Appendix 4), and occasionally shows sharp contacts against the coarse-grained biotite granite.

Topaz-bearing granite

Topaz-bearing granite is found as small patches within the coarse-grained biotite granite in the northern and western parts of the batholith (Appendix 4). The largest occurrence (1.5 by 3 km²) is found between Lake Lylysjärvi and Lake Kuivajärvi. The rock is normally a highly siliceous, pale red and porphyritic granite show-

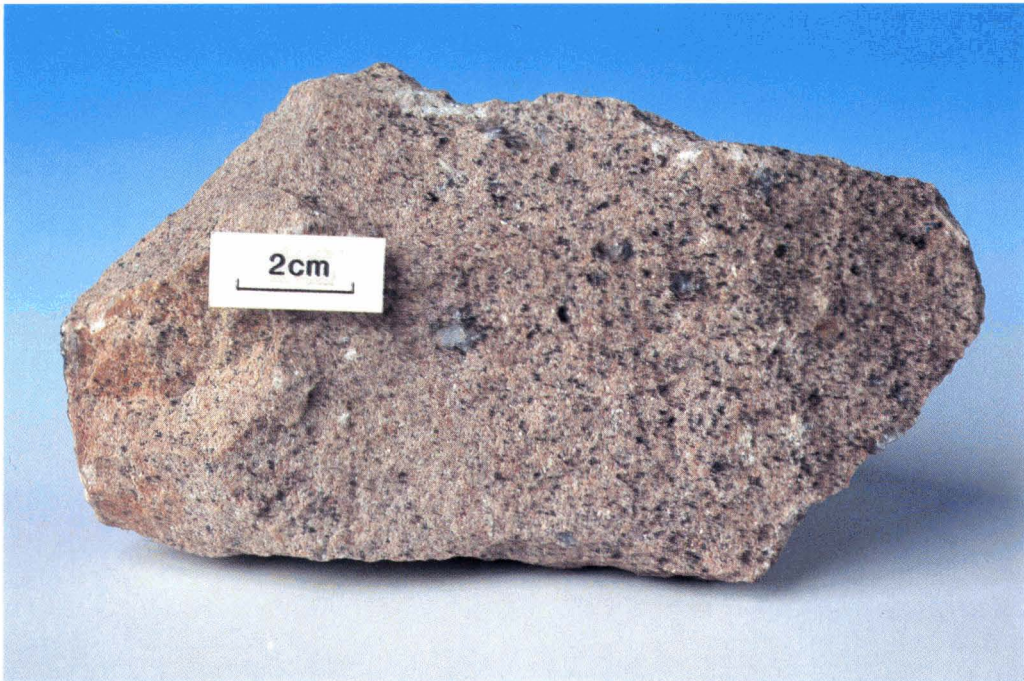
ing variable amounts of alkali feldspar and quartz phenocrysts, the latter often quite large (Fig. 10). The contact relationship of the topaz-bearing granites with the surrounding coarse-grained biotite granite is somewhat uncertain, but in at least at one location it intrudes it as dykes. The biotite in the topaz-bearing granite shows a relatively pale pleochroism and is often associated with some muscovite.

Alkali-feldspar syenite

Alkali-feldspar syenite and alkali-feldspar quartz syenite dykes that occur mainly in the east-central part of the batholith represent a new rock type in the Finnish rapakivi association. Most of the 15 dykes found so far trend northwest, are generally a few meters wide, show quite variable dips, and exhibit sharp contacts against the surrounding granites. They are typically deep vio-



Fig. 9. Porphyritic biotite granite (sample MKT-87-688.1) at Muikula, northwestern flank of the Suomenniemi batholith (Map 3141 04C, x = 6801.69, y = 3515.43). Photo by Jari Väättäinen.



a



b

Fig. 10. (a) aplitic topaz-bearing granite (sample A1097) at Pajulahti, north-central part of the Suomenniemi batholith. (b) porphyritic topaz-bearing granite (sample M664.2) at Vironvuoret, northwest-central part of the Suomenniemi batholith. Photos by Jari Väätäinen.



Fig. 11. Alkali-feldspar syenite (sample A1164) at Kirvessalmi, east-central part of the Suomenniemi batholith. Photo by Jari Väättäin.

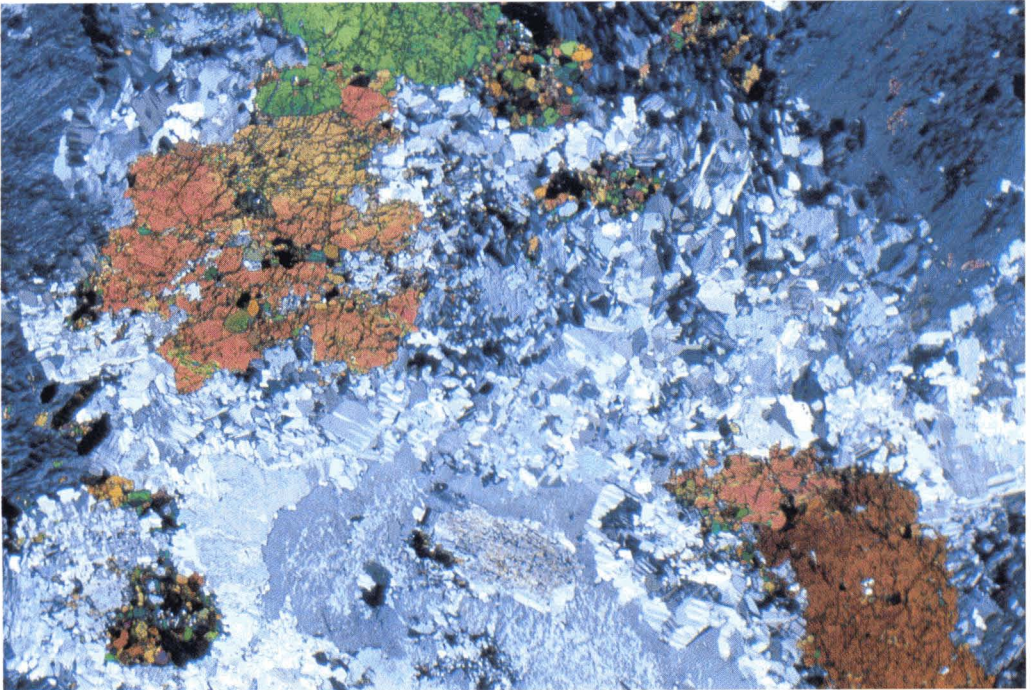


Fig. 12. Photomicrograph of alkali-feldspar syenite (sample A1111) showing mesoperthite grains with interstitial aegirine-augite (green to brownish red), albite, and alkali feldspar. Width of the figure corresponds to 1.1 cm. Crossed polars.

let red or violet red one-feldspar rocks showing euhedral mesoperthite phenocrysts and interstitial aggregates of aegirine-augite, alkali feldspar, and albite as the main constituents (Figs. 11 and 12). Some alkali amphibole, titanite, melanite garnet, oxide, and zircon are also encountered. Some of the dykes show intense post-crystallization alteration and have a greenish clin amphibole as the main mafic mineral. In modal composition, these rocks range from alkali-feldspar

syenites to alkali-feldspar quartz syenites (cf. Fig. 2) but in this work they are all referred to as alkali-feldspar syenites, unless otherwise stated.

Orbicular granite

Two occurrences of orbicular granite have been found in the Suomenniemi batholith, being the first orbicular rocks found within the Finn-



Fig. 13. Section through the center of an orbicule from an orbicular granite at Hämeenjärvi on the northwestern flank of the Suomenniemi batholith. An alkali feldspar grain constitutes the nucleus, whilst the mantle consists of alkali feldspar, quartz, biotite, and abundant fluorite. The orbicule measures 8 by 10 cm². Photo by Helsingin yliopiston kuvallaitos.

ish rapakivi granite batholiths. They occur as discrete pockets (0.5 to 2 m in diameter) in north-west-trending aplitic dykes cutting the coarse-grained biotite granite and biotite-hornblende granite in the northwestern and eastern parts of the batholith, respectively. The pockets are composed of undeformed, tightly-spaced, approximately spherical orbicules ranging from 5 to 20 cm in diameter. An alkali feldspar crystal constitutes the nucleus in the orbicules (Fig. 13), while their mantle consist of radially grown alkali feldspar, quartz, and green biotite or fayalite, with fluorite as a conspicuous minor component. The orbicular rock in the northwestern part of the batholith at Hämeenjärvi has been briefly described by Vaasjoki & Rämö (1989).

Gabbro-anorthosite body

A small gabbro-anorthosite body (100 by 300 m²) is found at Väärälampi on the northwestern flank of the Suomenniemi batholith (Appendix 4) where it lies between a Svecofennian garnet-bearing microcline granite and a medium-grained, slightly porphyritic biotite-hornblende granite belonging to the Suomenniemi batholith. The gabbro-anorthosite transects the microcline granite and has caused local melting near the contact. The contact with the biotite-hornblende granite is sharp and locally brecciated, the granite being indisputably younger. The exposed parts of the Väärälampi pluton consist of a heterogeneous, coarse-grained leucogabbro cut by a porphyritic gabbroanorthosite. The former is extensively altered and generally shows no primary ferromagnesian minerals. The gabbroanorthosite is better preserved showing a mafic medium-grained matrix, variable amounts of plagioclase phenocrysts (up to 20 cm long), and altered mafic inclusions (up to 10 cm across) that probably originally were pyroxene megacrysts. In addition to the leucogabbro and porphyritic gabbroanorthosite, later hydrothermal replacement veins of coarse-grained prehnite (M. Lehtinen, pers. commun.,

1988) are found within the body. Sizewise, the gabbro-anorthosite body at Väärälampi is insignificant compared with the Ahvenisto gabbro-anorthosite complex. It is, however, one example of the close relation of the Finnish rapakivi granites to massive anorthosites.

A detailed U-Pb zircon isotopic study has been conducted in order to date the Suomenniemi batholith (Vaasjoki et al., 1991). Dates have been obtained for two biotite granites, one hornblende granite, one hornblende-clinopyroxene-fayalite granite, one alkali-feldspar syenite, and the porphyritic gabbroanorthosite of the Väärälampi gabbro-anorthosite body. The results indicate that the Suomenniemi batholith was emplaced about 1640 Ma ago, and is thus somewhat younger than previously thought (cf. Vaasjoki, 1977).

Quartz-feldspar porphyry dykes

About 40 quartz-feldspar porphyry dykes are found in the Suomenniemi complex. The dykes trend northwest, dip vertically, are commonly 5 to 20 m wide, and cut both the Suomenniemi batholith and the Svecofennian country rocks (Appendix 4). The dykes often have dark and aphanitic margins, while the central parts are composed of alkali feldspar (rounded or angular), quartz, and plagioclase phenocrysts in a fine- to medium-grained granitic groundmass. Occasionally a mafic phenocryst phase is present, consisting of fine-grained aggregates of green amphibole, biotite, and chlorite. Some dykes show also some muscovite, and topaz is encountered as a minor groundmass phase in one dyke in the western part of the batholith. Scattered diabase globules, a few cm across, are found in a dyke southeast of Lake Ala-Kuomio in the northern part of the complex (Laitakari, 1987).

The age of the quartz-feldspar porphyry dykes of the Suomenniemi complex is well constrained, as four of them have been dated by U-Pb on zircon (Vaasjoki et al., 1991). The dykes register ages at about 1635 Ma, and hence the emplace-

ment of the quartz-feldspar porphyry dykes may represent a slightly later intrusive event than that of the granites of the Suomenniemi batholith.

Diabase dykes

A total of about 40 diabase dykes have been found in outcrops within the Suomenniemi complex. They have been previously described by Frosterus (1903), Simonen & Tyrväinen (1981), and Sundsten (1985). The dykes are vertical, cut sharply across the surrounding bedrock, and show a consistent trend toward the northwest. The width of the dykes ranges from a few cm to 50 m, but is normally 5 to 20 m. Geophysical data (cf. Tyrväinen, 1990) indicate that some of the dykes may be 15 or more km long. In the appended map (Appendix 4), however, only those parts of the dykes are indicated that can be followed in outcrops.

Most of the diabase dykes outcrop along a

5 km broad northwest-trending zone that extends from the rural center of Savitaipale across the northeastern part of the Suomenniemi batholith toward Pellosniemi (Appendix 4). In addition, some dykes are found to the northwest of the batholith. The majority of the dykes intrude the early Proterozoic rocks surrounding the Suomenniemi batholith; only three dykes have been found cutting granites within the batholith.

The dykes contain as primary magmatic minerals plagioclase (An_{60-67}), olivine (Fo_{40-50} , not always present), clinopyroxene ($Wo_{36-40}En_{33-38}Fs_{23-28}$), Fe-Ti-oxides, and sporadic apatite along with trace amounts of zircon. Green and colourless clinoamphiboles, biotite, and serpentine are typical of dykes that show post-crystallization alteration. Some of the dykes also have minor amounts of interstitial quartz and/or alkali feldspar.

Nearly all of the dykes have plagioclase phenocrysts, that usually amount to less than 10%. The phenocrysts are normally 1 to 2 cm

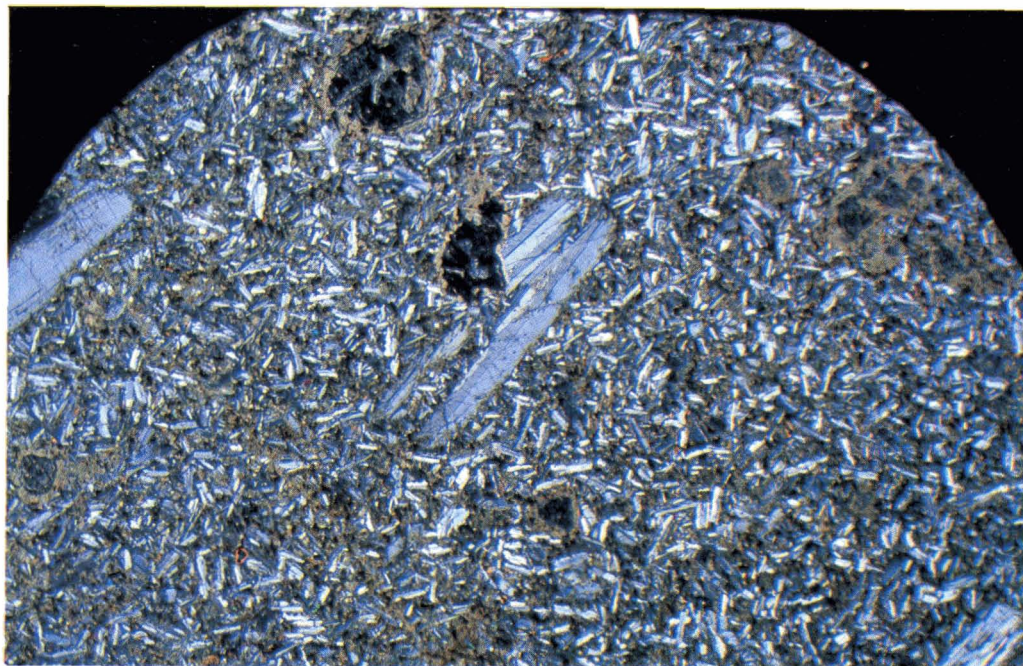


Fig. 14. Photomicrograph from a margin of a diabase dyke in the Suomenniemi swarm showing fresh plagioclase and completely altered olivine phenocrysts. Sample OTR-87-164.P2 (Map 3141 01D, $x = 6805.69$, $y = 3508.19$). Width of the figure corresponds to 2.4 cm. Crossed polars.

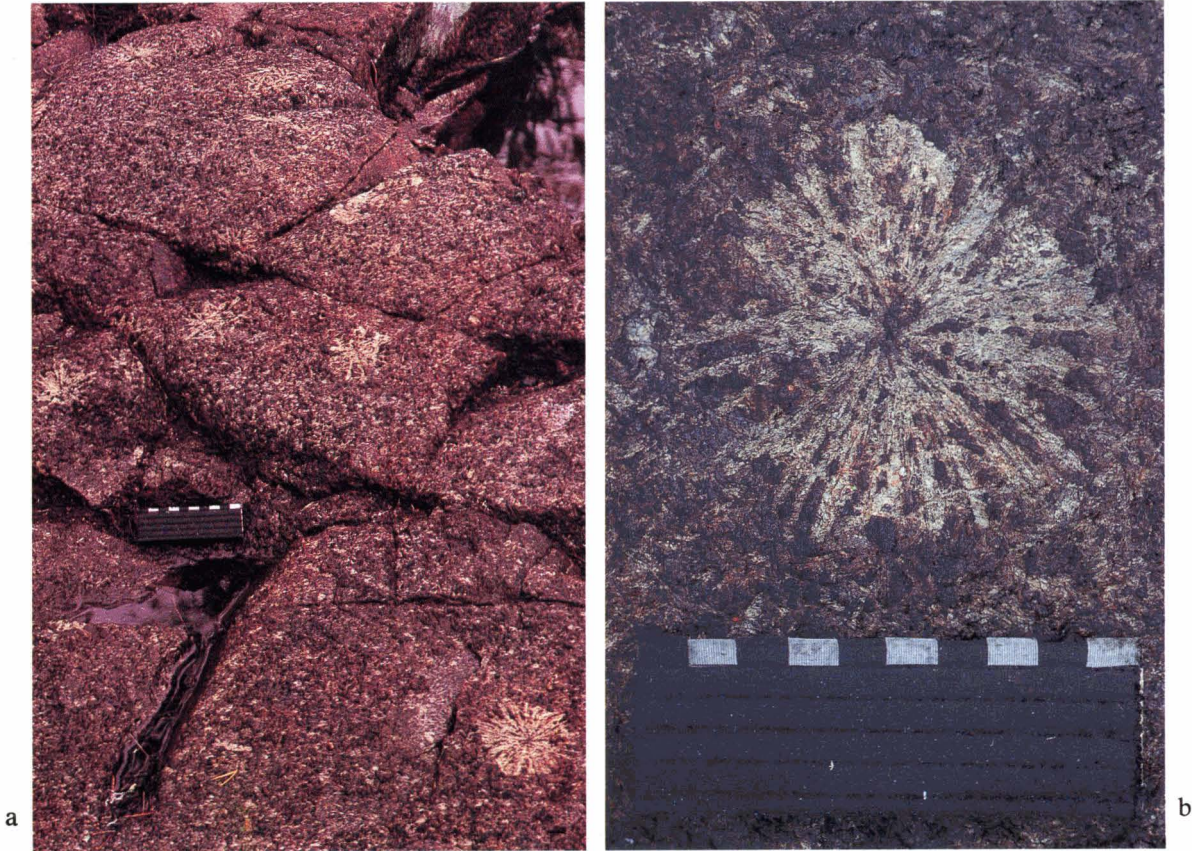


Fig. 15. Diabase dyke with plagioclase spherulites at Lehtoniemi, western part of the Suomenniemi complex (Map 3141 01C, $x=6802.78$, $y=3506.88$). (a) overview of the central part of the dyke, (b) close-up view of a spherulite. Length of the scale bar is 10 cm.

long, but also scattered plagioclase megacrysts (up to 15 cm in length) are often encountered in the dykes. Two dykes have been found that contain olivine phenocryst pseudomorphs (Fig. 14). The groundmass texture of the dykes is generally subophitic. A dyke at Lehtoniemi, west of Lake Ylä-Kuhanen, contains plagioclase spherulites (5 to 10 cm across) in a coarse-grained subophitic matrix of plagioclase, clinopyroxene, olivine, and Fe-Ti -oxide (Fig. 15).

The diabase dykes show little intra-dyke variation. Typically they have fine-grained to aphanitic margins, with a continuous increase in grain size toward the center. One dyke shows evidence for multiple intrusion of basic magma, but in general, indication of major intra-dyke variation,

such as the phenocryst-rich dyke centers in the Häme swarm proper (Laitakari, 1969) or ultra-basic cumulates described from the Subjotnian dykes in southwestern Finland (Pihlaja, 1987), have not been found in the dykes of the Suomenniemi swarm.

Silicic - basic composite dykes

The quartz-feldspar porphyry and diabase magmas usually occur as separate dykes in the northwest trending fracture system. In a few instances, however, they have intruded along the same fractures producing composite dykes. These composite dykes (and also the alkali-feldspar

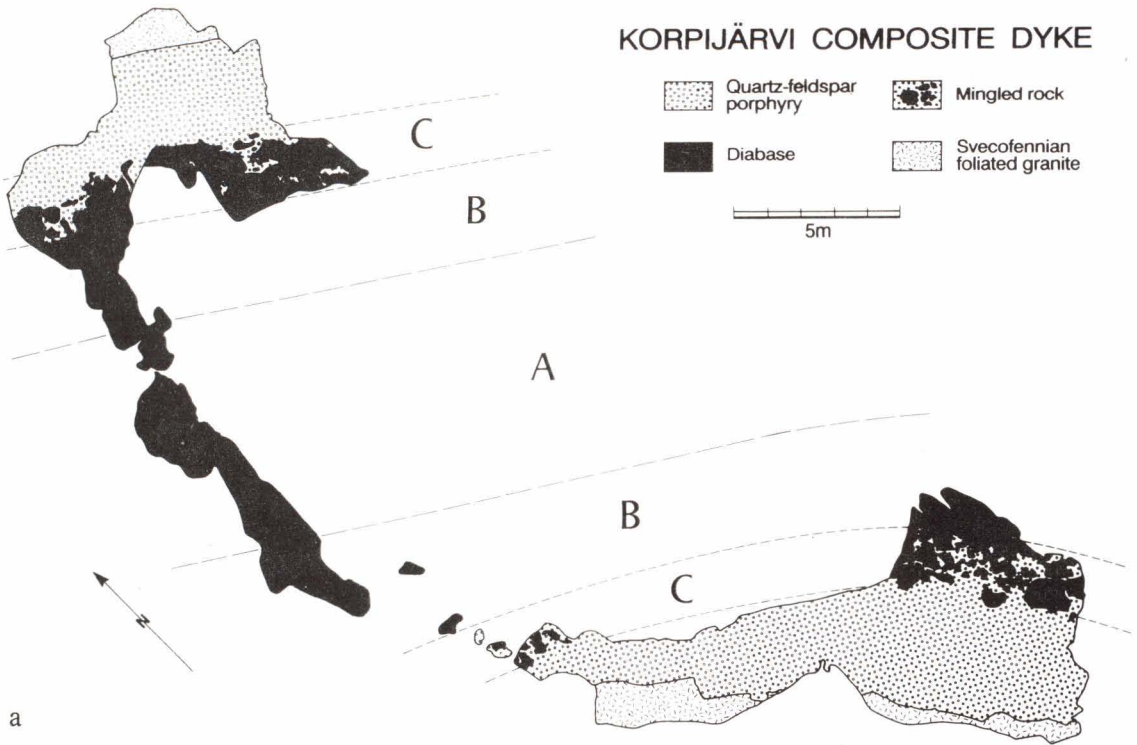


Fig. 16. (a) cross-section of the composite quartz-feldspar porphyry — diabase dyke north of Lake Korpijärvi, western part of the Suomenniemi complex (Map 3141 01C, $x = 6800.04$, $y = 3507.53$). Zones of xenocryst-free diabase (A), diabase with alkali feldspar and quartz xenocrysts (B), and intermingled diabase and quartz-feldspar porphyry (C) are indicated. (b) closer view of the lower mingled zone (C) showing diabase globules loaded with alkali feldspar and quartz xenocrysts as well as skeletal plagioclase phenocrysts, and quartz-feldspar porphyry in between the diabase globules. Length of the scale bar is 10 cm.

diabases described in the chapter that follows) are the subject of an ongoing petrographic, geochemical, and mineralogical study (Boyd & Rämö, in prep.), and only a brief description of the dykes is given here.

At the northwestern flank of the Suomenniemi batholith, north of Lake Korpjärvi, a 25 m wide composite dyke is found cutting a Svecofenian foliated granite. It has been briefly described by Pipping (1956), Simonen and Tyrväinen (1981), and Rämö (1989a). The dyke, which can be traced in outcrops for a distance of about 2.5 km, is composed of 3 m wide quartz-feldspar porphyry margins and a 15 m wide central olivine-free diabase (Fig. 16a). At the silicic-basic contacts, there are zones of mingled rock about 2 m wide in which diabase with alkali feldspar and quartz xenocrysts and skeletal plagioclase phenocrysts forms globules surrounded by quartz-feldspar porphyry matrix (Fig. 16b). The alkali feldspar and quartz xenocrysts exhibit textures caused by reaction with the surrounding basic magma: the alkali feldspar crystals have a micrographic margin and the quartz crystals are partly resorbed and mantled by amphibole. Going toward the center of the diabase portion, the alkali feldspar and quartz xenocrysts show, respectively, increasingly thick micrographic margins and amphibole mantles, and diminish in size until finally disappearing altogether so that much of the central part of the diabase is devoid of these silicic components.

At Kuusenhako, in the eastern part of the Suomenniemi complex, a different silicic-basic relationship is found. There a 20 m wide composite dyke with 1 m wide marginal olivine-free diabases and a central quartz-feldspar porphyry cuts rapakivi granites belonging to the Suomenniemi batholith (Fig. 17). The diabase margins exhibit chilled contacts against the rapakivi granite country rocks. The sharp and slightly sinuous contact between the diabase margins and the quartz-feldspar porphyry is also chilled. Quartz-feldspar porphyry apophyses intrude the diabase and mingle with basic material at the centre of

the margins forming a 10–20 cm wide zone of hybrid rock.

About 10 km southeast of the Kuusenhako dyke, on the island of Leinvihko near the rural center of Savitaipale, there is another composite dyke with diabase margins and a central quartz-feldspar porphyry. This was described in detail by Frosterus (1903); it differs from the dyke at Kuusenhako in having thicker diabase margins (3 to 4 m), and in lacking the zones of hybrid rock within the diabase margins.

Rämö (1989a) concluded that the sequences of intrusion of the silicic and basic magmas in the Korpjärvi and Kuusenhako dykes were different. In the Korpjärvi dyke, silicic magma intruded before basic magma, but the basic magma was emplaced before the silicic magma in the fracture was completely solidified. The hotter basic magma engulfed alkali feldspar and quartz phenocrysts from the crystallizing silicic magma and formed the zones of mingled rock. In the Kuusenhako dyke, the basic magma intruded first and was chilled against the surrounding rapakivi granites. The quartz-feldspar porphyry was emplaced when the central part of the diabase was still partially liquid, resulting in chilling of the residual basic magma against the cooler silicic magma. Finally, the silicic magma intruded the inner chilled zones of the diabase margins, mingling to some extent with the still molten central parts of the margins. By analogy, the latter mechanism also applies for the Leinvihko dyke, but in it the silicic magma possibly intruded the fracture somewhat later: no mafic magma appears to have been left within the basic margins as the quartz-feldspar porphyry apophyses intrude the margins without forming zones of mingled rock.

Alkali-feldspar diabases

In addition to the diabase — quartz-feldspar porphyry composite dykes, interaction of basic and silicic magmas in the Suomenniemi complex

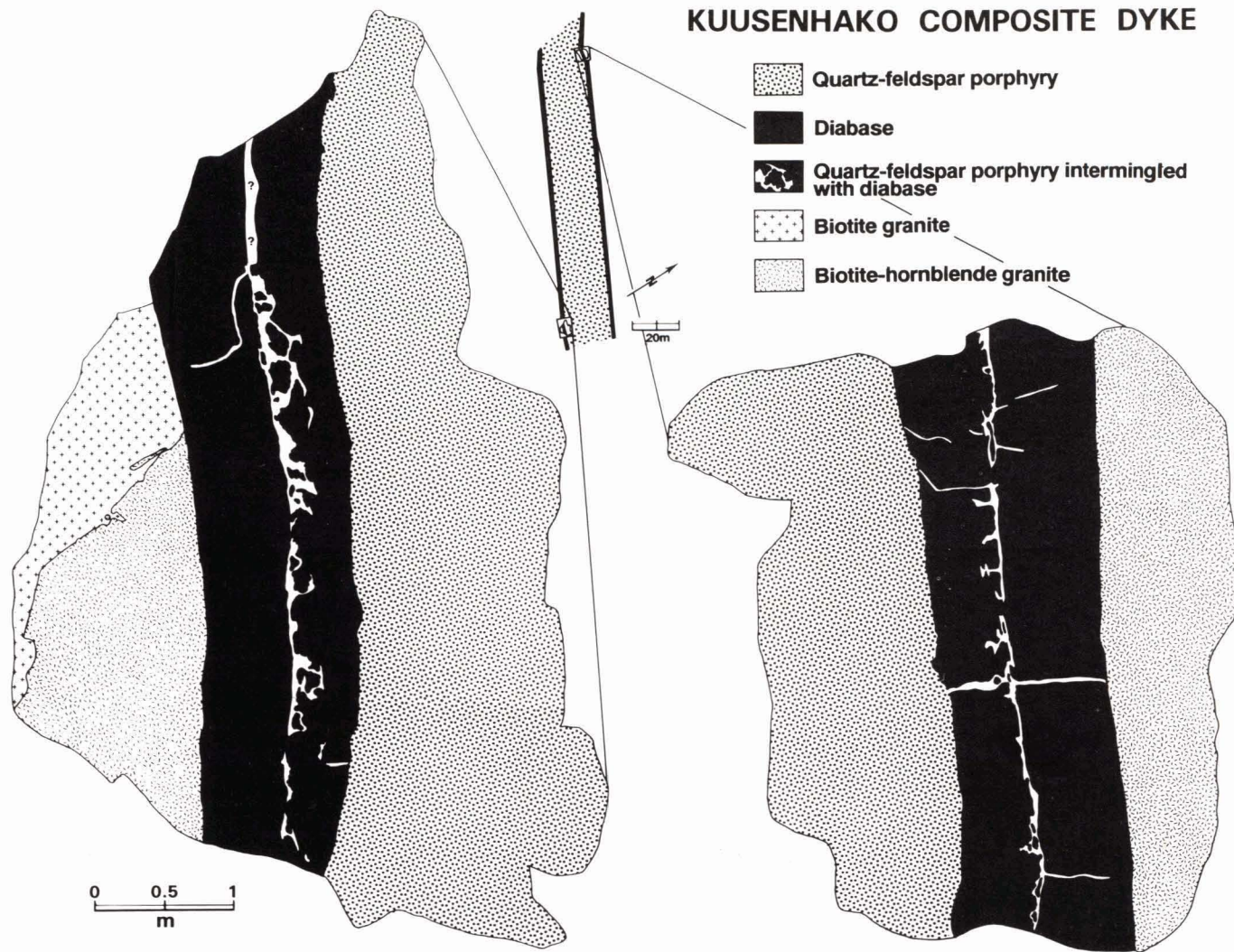


Fig. 17. Sketch map showing the geology of the composite diabase — quartz-feldspar porphyry dyke at Kuusenhako, eastern flank of the Suomeniemi batholith (Map 3132 09D, x = 6796.77, y = 3529.10).



Fig. 18. Photograph showing the northwestern exposed part of the Kirkkovouri diabase dyke with alkali feldspar megacrysts in the northern part of the Suomenniemi complex (Map 3141 05A, $x = 6812.45$, $y = 3513.20$). Some of the megacrysts are mantled with plagioclase. Length of the compass is 12 cm.

has also resulted in the intrusion of alkali-feldspar diabases. In the Kirkkovouri area, 10 km north of the Suomenniemi batholith, a 20 m wide diabase dyke with an exposed length of 400 m cuts Svecofennian migmatites. The northwestern end and the southeastern rims of the dyke consist of alkali feldspar megacrysts (with an average diameter of about 5 cm) in a fine-grained tholeiitic matrix (Fig. 18). The alkali feldspar megacrysts are partly resorbed and some of them have plagioclase mantles. Along with the megacrysts, there are quartz xenocrysts as well as country rock xenoliths and rapakivi granite fragments. A conspicuous feature of the rock are pockets of intermingled quartz-feldspar porphyry, alkali feldspar megacrysts, and diabase (Fig. 19).

Two diabase dykes with alkali feldspar megacrysts and quartz xenocrysts are found cutting rapakivi granite at Niemenmaa in the east-central part of the Suomenniemi batholith (Appendix 4). These dykes are 1.5 and 3.5 m wide, and show a more even distribution of alkali feldspar megacrysts and quartz xenocrysts than the Kirkkovouri dyke. The dykes exhibit strongly chilled, xenocryst-free contacts against the

rapakivi granite country rock.

The alkali feldspar diabases probably represent intrusion of diabase magma into partly crystallized rapakivi granite magma chambers in the course of its passage through the Svecofennian crust (Rämö, 1989a).

The Lovasjärvi intrusion

In the southwestern part of the Suomenniemi complex at Lake Lovasjärvi, there occurs a northwest-trending mafic intrusion that is cut by rapakivi granites at both ends (Appendix 4). It has been described by Alviola (1981) and Siivola (1977, 1987). The intrusion is a vertically dipping sheet-like pluton with a length of 5.4 km and width of 150 to 800 m. The northwestern part of it consists of melatroctolite (olivine cumulate with intercumulus plagioclase and clinopyroxene) surrounded by olivine-bearing diabase, while the central and southeastern parts are composed of medium- to coarse-grained olivine-free diabase. The intrusion has caused local melting of the surrounding Svecofennian granites and migmatites (Siivola, 1987).

SAMPLING

A total of 50 whole rock samples (29 silicic, 21 basic) were analysed for Nd and Pb isotopes in the present study. In addition, 20 feldspar fractions (18 alkali feldspars, 2 plagioclases) were analysed for their Pb isotopic composition. 29 of the whole rocks samples (16 silicic, 13 basic) were taken from the Suomenniemi complex in order to gain detailed information on the geochemical evolution of the complex. Furthermore, 21 reference samples (13 silicic, 8 basic) were collected to cover most of the Finnish and Soviet Karelian batholiths and stocks, the gabbroic and anorthositic rocks associated with the

Finnish intrusions, and the Häme diabase dyke swarm.

All the samples analysed for Nd and Pb isotopes were also analysed for their major and trace element contents (except three granite samples for which already published geochemical data is quoted). In order to get a more complete picture of the geochemical evolution of the Suomenniemi batholith and the Suomenniemi diabase dyke swarm, major and trace element contents were determined on an additional 63 samples (42 silicic, 21 basic). The locations (grid coordinates) of the samples collected from the Suomenniemi

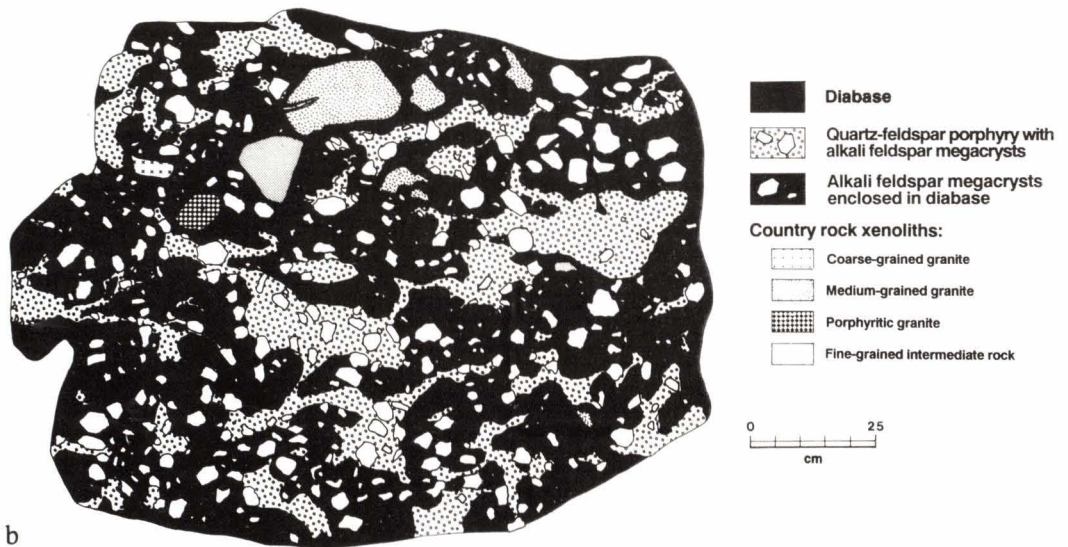
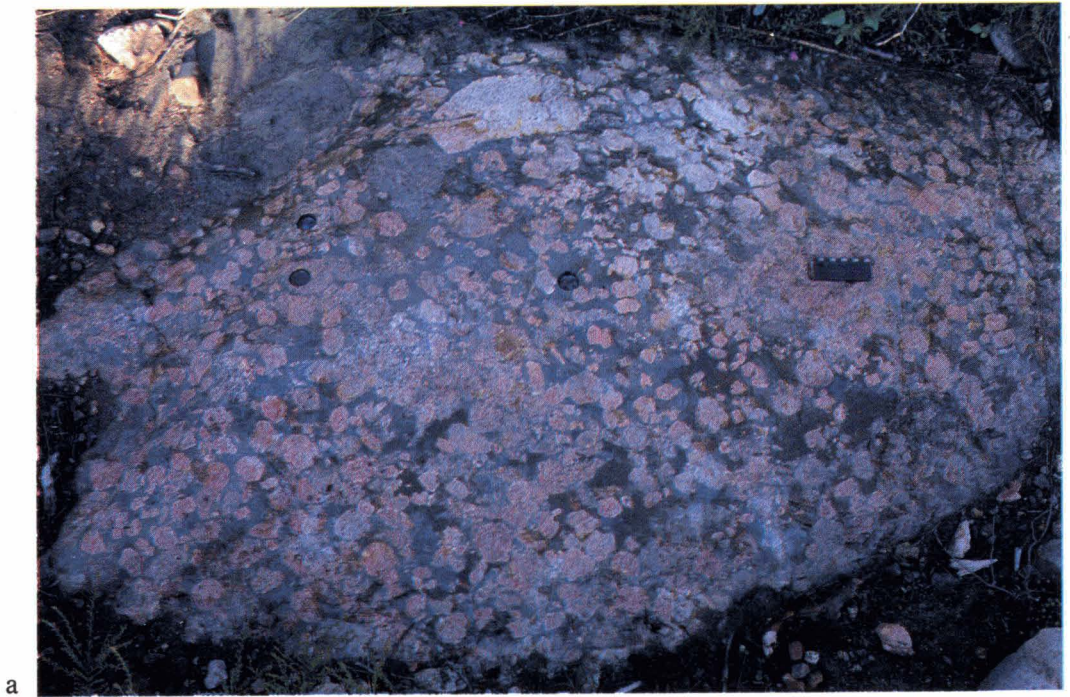


Fig. 19. (a) photograph, (b) sketch of a pocket consisting of intermingled diabase, quartz-feldspar porphyry, and alkali feldspar megacrysts along with country rock xenoliths in the Kirkkovuori diabase dyke. The scale bar in (a) is 10 cm long.

complex are given in Appendices 1 and 2, and they are also indicated in the appended map (Appendix 4). The following sections give short

descriptions of those samples that were analysed for Nd and Pb isotopes as well as for their major and trace element contents.

Rapakivi granites

Altogether 23 granite samples were collected for isotopic studies from the Suomenniemi, Wiborg, Laitila, Vehmaa, Åland, Siipyy, Salmi, and Sotjärvi intrusions. In addition, 32 samples from the Suomenniemi batholith were analysed for their major and trace element contents. Ten of the samples analysed for isotopes are from the Suomenniemi batholith representing the compositional range from the most primitive to the most evolved granite types. The samples from the other intrusions were collected in order to include various granite types with accurate isotopic ages.

Rapakivi granites of the Suomenniemi batholith

Two samples were analysed from the hornblende-clinopyroxene-fayalite granites of the Suomenniemi batholith. Sample **A1130** is from the eastern part of the batholith at Sikolampi. It is a porphyritic, grayish brown rock (Fig. 7) consisting of scattered gray alkali feldspar phenocrysts (diameter 1 to 2 cm) in a medium-grained groundmass of alkali feldspar, quartz, oligoclase, fayalite, ferrohedenbergite, hastingsitic hornblende, ilmenite, fluorite, and zircon. The mafic silicates occur interstitially between the quartz and feldspar grains. The U-Pb zircon age of the sample is 1636 ± 23 Ma (Vaasjoki et al., 1991). Sample **M415.4** is a medium-grained and equigranular grayish brown granite from the southern part of the intrusion. Mineralogically it resembles sample A1130.

Three samples were taken from the hornblende granites. Sample **A1043** is a medium- and even-grained, dark red hornblende granite (Fig. 4) from the southeastern flank of the batholith. A conspicuous feature of this rock is the occurrence of anhedral poikilitic hornblende that encloses

the felsic silicate grains (quartz, feldspars). The granite was dated as 1641 ± 2 Ma old by Vaasjoki et al. (1991). Samples **A1044** and **A1045** were taken farther from the outer contact of the batholith. They are more coarse-grained than sample A1043, show a little more biotite relative to hornblende, and also abundant fayalite relics within the hornblende grains. In addition, one sample, **A1040**, was analysed from the east-central part of the batholith. It is a coarse-grained biotite-hornblende granite also showing idding-site pseudomorphs after fayalite in the cores of the hornblende grains.

Samples **A1041** and **A1042** were analysed from the coarse-grained biotite granite in the northern part of the batholith. They are both slightly porphyritic and show only biotite as the main mafic mineral, which occurs as anhedral crystals filling the interstices between the quartz and feldspar grains. The samples A1041 (equal to sample A98 in Vaasjoki et al., 1991) and A1042 are dated as 1641 ± 1 Ma and 1639 ± 6 Ma old, respectively (U-Pb zircon ages; Vaasjoki et al., 1991).

Two samples were analysed from the topaz-bearing granites in the north-central part of the batholith. Sample **A1097** is a pink, medium-grained aplitic rock with scattered quartz and alkali feldspar phenocrysts (Fig. 10a). The main mafic silicate is a weakly pleochroic mica. Topaz and fluorite amount to 1.8 and 1.0 vol%, respectively. The sample **M664.2** (Fig. 10b) is a coarse-grained porphyritic topaz-bearing biotite granite showing an abundance of miarolitic cavities. A conspicuous feature of the rock are large quartz phenocrysts (diameter 0.5 to 1 cm) that appear to be more abundant than alkali feldspar phenocrysts.

Rapakivi granites from the other intrusions

Four samples were analysed from the Wiborg batholith. Sample **A18** is a dark-coloured clinopyroxene-fayalite-hornblende granite (tirilite) from the northern part of the batholith (Fig. 1). It is medium- to coarse-grained equigranular rock in which the mafic silicates occur as anhedral grains in the interstices of euhedral quartz and feldspar grains. The rock has been dated to be the oldest intrusive phase in the Finnish part of the Wiborg batholith: its U-Pb zircon age is 1646 ± 4 Ma (Vaasjoki et al., 1991). Sample **A29b** is a wiborgite (biotite-hornblende granite with oligoclase-mantled alkali feldspar ovoids) from the central part of the batholith. The wiborgite is younger than the tirilite A18 and has been dated as 1633 ± 1 Ma old (Suominen, 1991). Two samples (A524b, 1/IH/89) were analysed from the Kymi stock in the west-central part of the Wiborg batholith. They are both evolved topaz-bearing granites showing lithian siderophyllite as the main mafic mineral (Haapala, 1988). Sample **A524b** is from the coarse-grained porphyritic granite that forms the bulk of the stock, while sample 1/IH/89 is from the even- and medium-grained granite enclosing the porphyritic central granite. According to Vaasjoki (1977) the U-Pb zircon age of the Kymi stock is about 1640 Ma.

Two samples were analysed from the Laitila batholith. Sample **A606** is a biotite-hornblende granite (Tarkki granite) from the Eurajoki complex in the northern part of the batholith. It is a medium- to coarse-grained and equigranular rock with occasional fayalite (Haapala, 1977a) and has been found to be about 1570 Ma old (Vaasjoki, 1977). Sample **A690** (1-1/AV/66-73 of Vorma, 1976) comes from the marginal Ytö granite representing a young intrusive phase in the southern part of the Laitila batholith. The rock is a porphyritic biotite granite showing well-developed alignment of alkali feldspar phenocrysts (Vorma, 1976, Fig. 21) and is dated as about 1540 Ma old (Vaasjoki, 1977).

One sample, **A710**, was analysed from the Vehmaa batholith. It is a coarse-grained and

equigranular leucocratic muscovite-biotite granite that contains also a little topaz. This rock was used by Vaasjoki (1977) to date the batholith, and was found to be about 1590 Ma old. It should be noted in this context that the U-Pb zircon ages of the Vehmaa and Laitila batholiths and the Kymi stock are based on only a few zircon fractions and on the use of composite discordia lines (Vaasjoki, 1977) and hence they are less accurate than the U-Pb zircon ages of the other granites in this work, which are based on several fractions from each sample (cf. Vaasjoki et al., 1991).

Samples **A295** and **A762** were analysed from the Åland batholith. They are both medium- to coarse-grained, slightly porphyritic biotite-hornblende granites showing a groundmass of graphically intergrown quartz and feldspar. According to Suominen (1991) the U-Pb zircon ages of the samples are 1575 ± 11 Ma (A295) and 1573 ± 6 Ma (A762).

Sample **A373** was taken from the newly discovered Siippy pluton some one hundred km north of the Laitila batholith (Fig. 1). It is a coarse-grained and equigranular biotite granite with a U-Pb zircon age of 1562 ± 14 Ma (Idman, 1989).

Altogether three samples were analysed from the Soviet Karelian intrusions, Salmi and Sotjärvi. The samples from the Salmi batholith are from the collections of the Petrological Museum of the University of Helsinki. Sample **6896** is a slightly porphyritic, medium-grained topaz-bearing biotite granite from Nietjärvi at the western margin of the batholith, while sample **9202** is a coarse-grained porphyritic biotite granite from Kivenkulma also in the western part of the intrusion. In addition to the Salmi samples, a coarse-grained biotite granite **IYL/79** was analysed from the Sotjärvi batholith. This sample is from the collections of I. Laitakari and the exact location of the sample is unknown. In order to calculate the initial Nd isotopic composition of the Soviet Karelian samples, a U-Pb zircon age of 1540 Ma reported for the Salmi batholith by Suominen (1991) was used.

Alkali-feldspar syenites

Of the seven alkali-feldspar syenite samples listed in Appendix 1, two were analysed for their Pb and Nd isotopic composition. Sample **A1111** was taken from the central part of a 6 m wide, northwest-trending, almost horizontal dyke at Heinlahdenniemi in the eastern part of the Suomenniemi batholith. It is a violet red coarse-grained, slightly porphyritic rock consisting mainly of mesoperthite grains (diameter ca. 1 cm) and aggregates of deep-green aegirine-augite. Titanite, oxide, apatite, and zircon are also encountered, as are fine-grained groundmass albite and alkali feldspar (Fig. 12). The sample A1111 has a $^{207}\text{Pb}/^{206}\text{Pb}$ zircon age of 1629 ± 6 Ma (Vaasjoki et al., 1991). Sample **A1164** is from a

northwest-trending, steeply dipping 4 m wide dyke that cuts a dark red biotite-hornblende granite at Kirvessalmi in the east-central part of the batholith. The rock consists of mesoperthite grains (2 to 5 mm in diameter) and interstitial aggregates of aegirine-augite (Fig. 11). Minor amounts of titanite, oxide, zircon, and melanite garnet are present. Intergranular albite is encountered between the mesoperthite grains. In addition to these two samples, the isotopic composition of Pb was analysed for alkali feldspar fraction from sample **M265.1** that is a hydrothermally altered alkali-feldspar quartz syenite at Kirvesniemi (Appendix 4).

Quartz-feldspar porphyry dykes

Nine samples were analysed from the quartz-feldspar porphyry dykes in the Suomenniemi complex, four of them for their Nd and Pb isotopic composition. Sample **A21b** is from the center of a 40 m wide dyke cutting a Svecofenian microcline granite at Mentula, northwest of the Suomenniemi batholith. It shows rounded to angular alkali feldspar and quartz phenocrysts in a medium-grained granophyric groundmass. The U-Pb zircon age of the rock is 1638 ± 32 Ma (Vaasjoki et al., 1991). Sample **A1046** is from the central quartz-feldspar porphyry of the composite dyke at Kuusenhako. It has phenocrysts of alkali feldspar, quartz, and plagioclase, and a fine-grained granitic matrix with biotite as the main mafic constituent. Sample **A1100** is from a more than 15 m wide dyke that cuts hornblende

granite at Nikkari in the eastern part of the Suomenniemi batholith. It has alkali feldspar, quartz, plagioclase, and possible pseudomorphs after hornblende and biotite phenocrysts in a fine-grained granitic groundmass with hornblende and biotite as the mafic silicates. The U-Pb zircon age of the rock is 1635 ± 2 Ma (Vaasjoki et al., 1991). Sample **A1163** is from the quartz-feldspar porphyry in the Korpijärvi composite dyke northwest of the Suomenniemi batholith. It is composed of mainly quartz and alkali feldspar phenocrysts and has a fine-grained groundmass of quartz, feldspar, amphibole, and biotite. This quartz-feldspar porphyry has a U-Pb zircon age of 1636 ± 16 Ma (Vaasjoki et al., 1991).

Diabase dykes and the Lovasjärvi intrusion

Altogether 30 samples were taken from the Suomenniemi diabase dyke swarm, nine of which

were selected for isotopic analyses. From two whole rock samples plagioclase fractions were

separated and their Pb isotopic compositions were measured in order to estimate the initial Pb isotopic composition of the dyke magmas. The samples were selected to cover the anticipated compositional variation in the swarm, and they are believed to represent the average composition of the individual dykes, because the dykes are rather narrow (generally not more than 20 m wide) and usually show no evidence of magmatic layering or other major features of intradyke chemical differentiation.

Sample **A1063** is from a porphyritic diabase dyke at Leppäniemi, 4 km north of the Suomenniemi batholith. The dyke is about 5 m wide, and has tabular plagioclase phenocrysts (5–10 vol%, maximum length 3 cm) in a medium-grained subophitic matrix with plagioclase (An_{60}), clinopyroxene ($Wo_{41}En_{34}Fs_{25}$), olivine (Fo_{50}), and oxide. Sample **A1064** was taken from 40 to 50 m wide, medium to coarse-grained diabase dyke at Marttila, 8 km east-southeast of the Suomenniemi batholith. The groundmass is subophitic with plagioclase (An_{65}), clinopyroxene ($Wo_{36}En_{36}Fs_{28}$), olivine, ilmenomagnetite, and ilmenite and contains scattered plagioclase phenocrysts (≤ 7 cm in length). Sample **A1101** is a medium- to coarse-grained diabase from a 20 m wide dyke at Palvaniemi, 4 km east of the Suomenniemi batholith. It is subophitic with plagioclase, clinopyroxene, olivine, ilmenomagnetite and ilmenite; scattered plagioclase phenocrysts (up to 3 cm in length) also occur. Sample **A1102** is from the groundmass of a 20 m wide diabase dyke at Lehtoniemi, 4.5 km northwest of the Suomenniemi batholith. The sample is coarse-grained and has a subophitic to diabasic texture; plagioclase, clinopyroxene, olivine, oxide, and apatite occur along with interstitial quartz and alkali feldspar. This dyke has scattered plagioclase spherulites (5 to 10 cm in diameter, about six spherulites per m^2 ; see Fig. 15). Sample **A1098** is from a medium to fine-grained, 5 m wide dyke at Ostolahti, 13 km north-northwest of the Suomenniemi batholith. It is subophitic with plagioclase, clinopyroxene,

olivine, and needles of oxide and apatite. Sample **A1118** is from a medium-grained diabase at Tammela 4 km northwest of the Suomenniemi batholith. It is subophitic with plagioclase, olivine, clinopyroxene, and oxide along with some scattered plagioclase phenocrysts (maximum length 2.5 cm). Sample **A1047** is a porphyritic diabase from the composite dyke at Kuusenhako, eastern flank of the Suomenniemi batholith. It has scattered plagioclase phenocrysts (< 5 vol%, 0.5 to 1 cm in length) that are embedded in a fine-grained matrix of plagioclase, uralitic amphibole, biotite, and oxide needles. Sample **A1068** is a plagioclase-phyric diabase from the Leinvihko composite dyke at Savitaipale, 6 km east-southeast of the Suomenniemi batholith. Petrographically it is like A1047. Sample **35.1** is from a ≥ 7 m wide diabase at Vierivänvuori 0.5 km north of the Suomenniemi batholith. It is fine-grained and shows a diabasic texture with plagioclase, clinopyroxene, and oxide; scattered plagioclase phenocrysts (maximum length 5 cm) and quartz xenocrysts mantled by amphibole also occur.

None of the nine diabase samples from the Suomenniemi swarm were dated by U-Pb on zircon or baddeleyite (an attempt was made to separate zircon from sample A1064, but the yield was too low for conventional U-Pb zircon work). Nevertheless, geological evidence coupled with the ages of the Lovasjärvi intrusion and the Korpjärvi composite dyke (Siivola, 1987; Vaasjoki et al., 1991) constrain the age of the dykes to 1640 ± 5 Ma.

Two samples were analysed from the Häme swarm, representing two successive magmatic events (ca. 1665 and 1645 Ma) in this multiple dyke set (Vaasjoki & Sakko, 1989). Sample **A808a** is from a more than 100 m wide diabase dyke at Kasiniemi, Padasjoki (Laitakari, 1969). The sample is subophitic with plagioclase, olivine, clinopyroxene, oxide, and apatite as well as scattered plagioclase phenocrysts (up to 2 cm in length). The U-Pb zircon age of the dyke is 1646 ± 6 Ma (Laitakari, 1987). Sample **A1135** is from a 50 m wide dyke at Virmaila, Padasjoki

belonging to the older magmatic event. It is medium-grained and subophitic with plagioclase, olivine, clinopyroxene, oxide and apatite, and has been dated to be 1667 ± 9 Ma old by Vaasjoki and Sakko (1989).

Two samples were also taken from the Lovasjärvi intrusion. Sample **A1069** is a coarse-grained diabase at Matula in the central part of the intrusion. It is subophitic with plagioclase,

clinopyroxene, oxides, and apatite as primary magmatic minerals. The diabase has been dated as 1643 ± 5 Ma old (Siivola, 1987). Sample **A1129** is a medium-grained melatroctolite at Ojasuo in the northwestern part of the intrusion. It has cumulus olivine (Fo_{58}) with intercumulus plagioclase (An_{43-57}) and clinopyroxene ($\text{Wo}_{42}\text{En}_{40}\text{Fs}_{18}$) (Siivola, 1987; J. Siivola, pers. commun., 1991).

Gabbroic and anorthositic rocks

Eight samples were collected from the Finnish gabbroic and anorthositic rocks in order to cover their temporal range (from 1.65 Ga in southeastern Finland to 1.57 Ga in southwestern Finland) and compositional variation. The gabbroic and anorthositic rocks associated with the Salmi batholith (Fig. 1) were not analysed for the present study. They are the subject of an isotopic study carried out for the Salmi complex by Neymark et al. (in prep.).

Three samples (olivine gabbro **A1110**, leucogabbro **A118**, and anorthosite **MH87a**) were analysed from the Ahvenisto gabbro-anorthosite complex. The olivine gabbro **A1110** is located in the eastern part of the complex, northeast of Lake Sarvilampi. It is an even- and coarse-grained rock consisting of euhedral plagioclase crystals (0.5 to 1 cm in length), poikilitic olivine (Fo_{53}), minor interstitial clinopyroxene, oxide, and a little alkali feldspar. The anorthosite sample **MH87a** was taken from an anorthosite lens (50 by 120 m²) embedded in gabbro in the northern part of the complex, north of Lake Pitkäjärvi. The lens has a sharp contact against the surrounding gabbro and consists of a schistose medium- to coarse-grained plagioclase-dominated matrix and scattered plagioclase megacrysts up to 15 cm in length (cf. Johanson, 1984). Some orthopyroxene and clinopyroxene are also present, the former being more abundant. Interstitial alkali feldspar and

quartz also occur. The leucogabbro **A118** from Nurmaa in the southeastern part of the Ahvenisto complex was originally collected by Vaasjoki (1977) in order to isotopically date the complex. It is a coarse- and even-grained rock with euhedral plagioclase crystals 0.5 to 2 cm in diameter. The main mafic mineral is orthopyroxene; clinopyroxene and a little olivine are present, as are minor amounts of quartz and alkali feldspar. A zircon $^{207}\text{Pb}/^{206}\text{Pb}$ age of 1645 ± 5 Ma was reported for the rock by Vaasjoki et al. (1991).

Two samples (leucogabbro **A1048** and gabbro **A1048b**) were analysed from the Väärälampi gabbro-anorthosite body on the northwestern flank of the Suomenniemi batholith (Appendix 4). The leucogabbro **A1048** is heterogeneous with euhedral plagioclase crystals from 0.5 to several cm in length and interstitial amphibole and chlorite after pyroxene. The gabbro **A1048b** shows scattered plagioclase phenocrysts set in a medium-grained hypidiomorphic matrix of plagioclase (An_{55}), orthopyroxene ($\text{Wo}_2\text{En}_{39}\text{Fs}_{59}$), clinopyroxene ($\text{Wo}_{26}\text{En}_{35}\text{Fs}_{39}$), biotite, amphibole, and oxide. Some interstitial quartz is also found. This sample was used to date the pluton by Vaasjoki et al. (1991) who reported an U-Pb zircon age of 1636 ± 14 Ma for the rock.

Sample **A119** is a leucogabbro from an anorthositic inclusion (1 by 2 km²) in the central part of the Wiborg batholith (Simonen, 1979b).

It is a coarse-grained equigranular rock with euhedral spectrolite (iridescent labradorite) crystals 0.5 to 1 cm in length and interstitial orthopyroxene and clinopyroxene, the former being more abundant than the latter. Minor alkali feldspar and quartz also occur. The U-Pb zircon age of the rock is 1633 ± 1 Ma (Suominen, 1991).

The younger (1.57 to 1.58 Ga old) gabbroic and anorthositic rocks of southwestern Finland were sampled at two sites. The sample **A691b** (31/b/AV/68) is from the Kolinummi intrusion southeast of the Laitila batholith. It is a medium- to coarse-grained, slightly porphyritic gabbro with approximately equal amounts of orthopyroxene and clinopyroxene. A conspicu-

ous feature are interstitial micrographic intergrowths of quartz and alkali feldspar. One sample, **7890**, was analysed from an anorthosite on the island Högggrund in the western part of the Åland rapakivi granite batholith (Sederholm, 1934; Bergman, 1979). The anorthosite body (originally called ossipite-diabase by Sederholm, 1934) is found, together with a Svecofennian foliated granite, in an inclusion that is at least 300 m across and surrounded by rapakivi granite. Sample 7890 is coarse-grained equigranular leucogabbro with euhedral plagioclase crystals (1 to 2 cm in length) and interstitial clinopyroxene, ilmenomagnetite, and quartz.

ANALYTICAL PROCEDURES

General geochemistry

The samples were analysed for major and minor components by XRF at X-Ray Assay Laboratories Ltd (Canada). A few analyses were also made at Rautaruukki Oy (Finland) and at the Geological Survey of Finland. Most of the processed silicic samples weighed several kilograms each, while the basic samples were usually 1 to 2 kg. Most of the basic samples and some of the silicic ones were crushed and milled in agate mill (see specifications in Appendices 1 and 2); the extra SiO_2 thus introduced is estimated

to be $\leq 0.3\%$. Most of the silicic samples (see Appendix 1) were crushed and milled in a chrome steel mill that may have introduced up to 0.15% extra Fe. Ferrous iron was determined by potassium dichromate titration, and fluorine (for the silicic samples) by an ion specific electrode. For the silicic samples, fluorine-free C.I.P.W. norms were calculated. In order to avoid complications arising from variable oxidation states of the basic rocks, their C.I.P.W. norms were calculated after normalizing iron ratios to $\text{Fe}^{2+} = 0.85\text{Fe}_{\text{total}}$.

Nd and Pb isotope geochemistry

Nd and Pb isotopic analyses were performed at the Unit for Isotope Geology, Department of Petrology, Geological Survey of Finland. About 200 g of rock material split into small pieces was washed with clean water in an ultrasonic bath and milled in an iron pan in a swing-mill. 200 to 300 mg of sample powder was dissolved in a

teflon bomb at 180 °C for a few days using a HF — HNO_3 -mixture. After evaporation the sample was dissolved in a second treatment with HCl. The clear solution thus obtained was aliquoted and about one fourth was spiked with ^{235}U , ^{206}Pb , and ^{149}Sm — ^{145}Nd tracers. Pb was purified according to the anion exchange —

anodic electrodeposition procedure of Gulson and Mizon (1979). U was purified by conventional HCl anion exchange (Krogh, 1973), combined with hexone extraction. The alkali feldspar fractions (200 mg) and plagioclase fractions (500 to 700 mg) were first washed with dilute HCl and clean water in an ultrasonic bath. Thereafter they were bathed overnight in a 1:1 mixture of HF and HNO₃ and then digested on a hot plate. The residue was converted to bromide and was purified for lead according to the method of Gulson and Mizon (1979). Chemical separation and purification of Sm and Nd was performed by anion exchange chromatography in methanol-based solutions (the method is described in detail by Huhma, 1986). The measured procedural blanks were generally on the order of 0.5 ng for Nd and 5 ng for Pb.

Isotopic ratios of Sm, Nd, Pb, and U were determined using two non-commercial Nier-type mass spectrometers built at the Geological Survey of Finland. Pb and U were loaded on single Re filaments with silica-gel and Ta₂O₅, respectively. Sm and Nd were loaded on triple or double Re or Ta filaments with H₂O (sometimes, in

search of a more stable emission, also with diluted H₃PO₄). A mass fractionation correction of +0.08‰ per a.m.u. was made to normalize the Pb isotopic ratios to SRM981 Pb standard, and the reported ratios are averages of two mass spectrometer runs (replicate dissolutions were also carried on a few samples). Nd isotopic ratios were normalized to ¹⁴⁶Nd/¹⁴⁴Nd = 0.7219, and 250 to 500 ratios were measured to compute each reported ¹⁴³Nd/¹⁴⁴Nd ratio. The mean ¹⁴³Nd/¹⁴⁴Nd ratio of six runs of La Jolla Nd standard was 0.511854 ± 18 (1 S.D. to the sixth decimal) and the control ¹⁴⁵Nd/¹⁴⁴Nd ratio 0.348404 ± 13 (1 S.D.). The average of the ¹⁴⁵Nd/¹⁴⁴Nd ratios of the analyses given in Tables 3 and 4 is 0.348406 ± 20 (1 S.D.). One measurement of BCR-1 yielded ¹⁴³Nd/¹⁴⁴Nd ratio of 0.512640 ± 21 (2σ_m) and Sm/Nd ratio of 0.2288 (Nd = 28.7 ppm) and one measurement of JB-1 (Geological Survey of Japan Basalt Standard) ¹⁴³Nd/¹⁴⁴Nd ratio of 0.512773 ± 24 (2σ_m) and Sm/Nd ratio of 0.1923 (Nd = 25.7 ppm). The ¹⁴⁷Sm/¹⁴⁴Nd ratios are estimated from duplicate analyses to be correct within 0.4‰.

GENERAL GEOCHEMICAL CHARACTERISTICS OF THE RAPAKIVI GRANITES AND RELATED BASIC ROCKS

Silicic rocks and alkali-feldspar syenites

The rapakivi granites of southeastern Fennoscandia exhibit several compositional features that make them distinct from other granite suites. These include high SiO₂, K₂O, F, Rb, Ga, Zr, Hf, Th, U, and REE (except Eu) abundances as well as high Fe/Mg and K/Na ratios, and low abundances of CaO, MgO, Al₂O₃, P₂O₅, and Sr (Sahama, 1945; Vormaa, 1976; Haapala, 1977a; Nurmi & Haapala, 1986). Furthermore, the youngest intrusive phases are often strongly anomalous topaz-bearing granites showing lowered K/Na ratios, extreme enrichments in F,

Ga, and Rb, elevated Sn abundances, strong depletions in Ba and Sr, and flat normalized REE-patterns (as opposed to the LREE-enriched patterns normally encountered; Haapala, 1977a). In regard to alumina saturation, the rapakivi granites are generally metaluminous or, especially the late-stage granites, slightly peraluminous. They also show alkaline affinities (e.g., relatively high Na₂O + K₂O contents), yet no peralkaline granites have been found in the southeastern Fennoscandian intrusions.

Rapakivi granites and quartz-feldspar porphyry dykes

Compositional data for the rapakivi granites, quartz-feldspar porphyry dykes, as well as the alkali-feldspar syenites dealt with in this study are given in Appendix 1, Table 1, and Figs. 20 through 23. The granites and quartz-feldspar porphyry dykes show the typical compositional features of rapakivi granites outlined above. They have a relatively wide span of SiO₂ contents ranging from 63.0 to 77.0 wt%, and 68.0 to 75.2 wt%, respectively, and have a common average of 71.0 wt% SiO₂. They exhibit high and relatively constant Fe/(Fe + Mg) ratios (Fig. 20a), and relatively high alkali contents (the sums of Na₂O and K₂O are commonly around 8 to 9 wt%,

yet most of the samples plot in the subalkaline field in the alkalis vs. silica diagram in Fig. 20b). On the basis of the NK/A vs. silica diagram (Fig. 20c) they are all subalkaline (molecular (K₂O + Na₂O)/Al₂O₃ ratios are less than one), and the A/CNK diagram (Fig. 20d) shows that they range from metaluminous to peraluminous along with increasing SiO₂ (molecular Al₂O₃/(CaO + Na₂O + K₂O) ratios vary between 0.8 and 1.2). The samples with the highest SiO₂ contents contain up to 2.4 % normative corundum (Appendix 1).

Regarding trace elements in the analysed granites and quartz-feldspar porphyry dykes, F ranges from 0.09 to 1.53 wt%, Sc from 0.8 to 19.1 ppm, Ga from 11 to 61 ppm, Rb from 146 to 974 ppm, Ba from 40 to 2090 ppm, Nb from 21 to

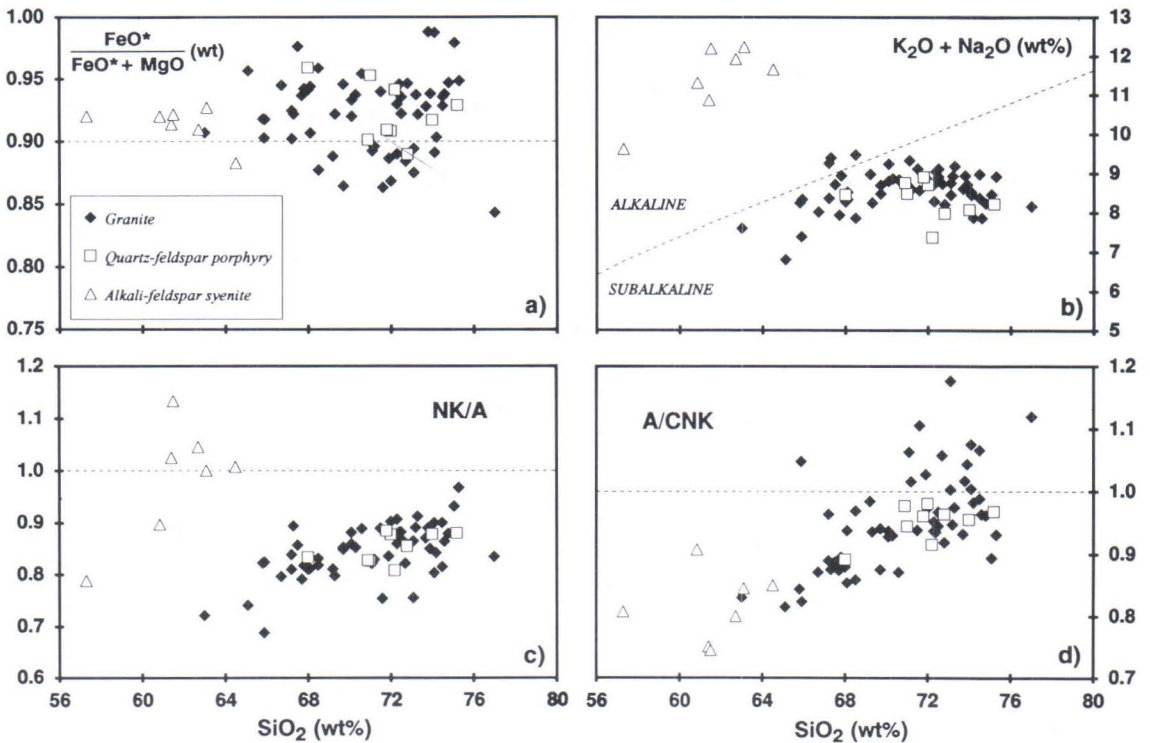


Fig. 20. Analyses of the rapakivi granites, quartz-feldspar porphyry dykes, and alkali-feldspar syenites (Appendix 1) plotted in (a) FeO*/(FeO* + MgO) vs. SiO₂, (b) K₂O + Na₂O vs. SiO₂, (c) NK/A vs. SiO₂, and (d) A/CNK vs. SiO₂ variation diagrams. FeO* denotes total iron as FeO, NK/A molecular (K₂O + Na₂O)/Al₂O₃ ratio, and A/CNK molecular Al₂O₃/(CaO + K₂O + Na₂O) ratio. Line separating the alkaline and subalkaline fields in (b) is from Irvine and Baragar (1971).

100 ppm, Sr from <10 to 233 ppm, Hf from 3 to 28 ppm, Zr from 29 to 1160, and Y from 12 to 164 ppm. Notable also are the relatively high Zn abundances (25 to 181 ppm, average 96 ppm) in the granites and quartz-feldspar porphyry dykes which seem typical of these rocks, as are the enrichments in other incompatible trace elements. Distinctive compositional features of these rocks are also the high Ga/Al ratios (10000*Ga/Al averages 3.69) and high K/Na ratios (average 1.89), as well as large ranges in the Rb/Ba and Rb/Sr ratios (0.08 to 10.93 and 0.65 to 60.08, respectively).

REE abundances in selected granites and quartz-feldspar porphyry dykes are shown in Table 1 and their chondrite-normalized REE-patterns are plotted in Figs. 21a and b, respec-

tively. Three low-silica granites (samples A18, A1130, and A1043) exhibit almost identical patterns that are enriched in the LREE ($La_N=267$ to 299, $[La/Yb]_N=8.47$ to 11.17) and show weak negative Eu anomalies ($[Sm/Eu]_N=1.94$ to 2.15). A biotite granite (sample A1041) from the Suomenniemi batholith shows stronger enrichment in the LREE ($[La/Yb]_N=16.53$, $La_N=648$) and a more distinct negative Eu anomaly ($[Sm/Eu]_N=8.83$). A topaz-bearing granite (sample A1097) from the Suomenniemi batholith has a rather flat REE-pattern ($[La/Yb]_N=1.28$, $La_N=91$) and a very pronounced negative Eu anomaly ($[Sm/Eu]_N=32.23$). This pattern is similar to those of the topaz-bearing Vakkärä granites of the Eurajoki complex in southwestern Finland (Haapala,

Table 1. Rare earth element contents (in ppm) and chondrite-normalized La/Yb and Sm/Eu ratios of selected granites, quartz-feldspar porphyries, and alkali-feldspar syenites.

Sample	Granites					Quartz-feldspar porphyries		Alkali-feldspar syenites	
	A18	A1130	A1043	A1041	A1097	A1100	O62.1	A1111	A1164
La	92.8	82.9	90.7	201	28.1	127	172	72.9	136
Ce	191	177	183	418	73.2	264	319	140	288
Pr	23.8	24.7	21.7	48.2	8.6	32.8	35.2	16.4	37.6
Nd	93.43	95.80	82.64	174.0	30.95	115.6	123.0	60.10	126.2
Sm	18.00	18.11	15.43	30.21	8.55	20.52	18.40	10.80	25.24
Eu	3.16	3.23	3.00	1.29	0.10	2.35	0.92	1.79	3.04
Gd	15.5	15.5	13.5	21.7	7.4	16.7	15.1	8.6	22.9
Tb	2.2	2.3	1.9	3.0	1.6	2.6	2.5	1.3	3.4
Dy	11.9	13.0	12.6	18.0	13.6	15.2	16.6	8.1	20.9
Ho	2.51	2.59	2.32	3.12	3.19	3.02	3.28	1.57	4.42
Er	6.5	7.1	6.4	8.8	10.7	8.9	9.9	4.9	12.5
Tm	0.9	0.9	0.8	1.1	1.8	1.2	1.4	0.5	1.7
Yb	5.6	6.6	6.1	8.2	14.8	8.6	10.8	5.2	12.3
Lu	0.73	0.94	0.95	1.14	2.19	1.20	1.52	0.71	1.70
$(La/Yb)_N^a$	11.17	8.47	10.02	16.53	1.28	9.96	10.74	9.45	7.45
$(Sm/Eu)_N^a$	2.15	2.11	1.94	8.83	32.23	3.29	7.54	2.27	3.13

Note: Nd and Sm by ID (except for sample O62.1) at the Unit for Isotope Geology, Geological Survey of Finland; the other elements (as well as Nd and Sm for sample O62.1) by ICP/MS at X-Ray Assay Laboratories Ltd (Canada).

^a normalizing values are 0.31 for La, 0.209 for Yb, 0.195 for Sm, and 0.0735 for Eu (Boynon, 1984).

1977a, 1988). The REE-patterns of two quartz-feldspar porphyry dykes from the Suomenniemi complex (samples A1100 and O62.1, Fig. 21b) exhibit similar $(La/Yb)_N$ ratios (9.96 and 10.74, respectively) as the low-silica granites in Fig. 21a, but have higher element abundances ($La_N = 410$ and 555) and deeper Eu minima ($[Sm/Eu]_N$ 3.29 and 7.54). These characteristics are rather similar to those reported for the rapakivi-age granite porphyry dykes of Sipoo to the west of the Wiborg batholith (Törnroos, 1984) and a granite porphyry dyke associated with the Laitila batholith (Vorma, 1976).

Alkali-feldspar syenites

Although volumetrically minor, the alkali-feldspar syenite dykes found within the Suomenniemi complex demonstrate that also peralkaline felsic rock types are associated with the south-eastern Fennoscandian rapakivi granite batholiths. The SiO_2 contents of the seven analysed dykes range from 57.3 to 64.5 wt%. Consonant

with the data on the granites and quartz-feldspar porphyry dykes, the alkali-feldspar syenites are strongly enriched in Fe relative to Mg (Fig. 20a). The samples plot clearly in the alkaline field in Fig. 20b and five of them are peralkaline (having molar $(K_2O + Na_2O)/Al_2O_3$ ratios equal to or greater than one; Fig. 20c); those with agpaitic indices less than one are hydrothermally altered and may have lost some of their alkalis in the process. The peralkaline samples show up to 9.1% acmite in the norm (Appendix 1).

Besides showing lower SiO_2 contents, the alkali-feldspar syenites differ from the granites and quartz-feldspar porphyries in showing higher Al, Na, and Fe abundances. Notable are also the higher Fe^{3+}/Fe^{2+} ratios in the alkali-feldspar syenites (Appendix 1). In regard to trace elements, the alkali-feldspar syenites exhibit higher Sc and Zn, and lower F, Sn, and Rb abundances than the silicic rocks. The F in the alkali-feldspar syenites ranges from 0.2 to 0.13 wt%, Sc from 9.5 to 23.1 ppm, Ga from 18 to 27 ppm, Rb from 188 to 288 ppm, Ba from 427 to 1710 ppm, Nb from 30 to 103 ppm, Sr from 46 to 232 ppm, Hf

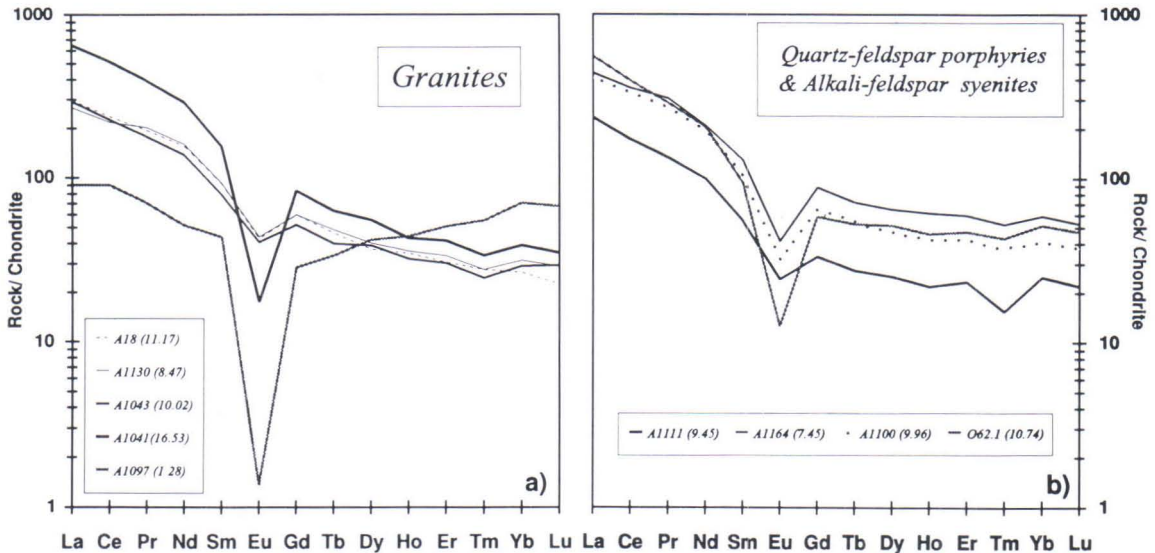


Fig. 21. Rare earth element analyses of (a) rapakivi granites and (b) quartz-feldspar porphyry dykes and alkali-feldspar syenites (solid patterns) listed in Table 1 normalized against chondrite composition. Numbers in parentheses denote normalized La/Yb ratios.

from 16 to 30 ppm, Zr from 433 to 867, Y from 66 to 151 ppm, and Zn from 94 to 207 ppm (Appendix 1).

REE abundances and chondrite-normalized REE-patterns of two alkali-feldspar syenites (samples A1111 and A1064) are shown in Table 1 and in Fig. 21b, respectively. The sample A1111 has a $(La/Yb)_N$ ratio of 9.45 and a $(Sm/Eu)_N$ ratio of 2.27, which are similar to those of the low-silica granites in Fig. 21a, but has somewhat lower element abundances ($La_N = 235$). In con-

trast, sample A1164 is less enriched in the LREE ($[La/Yb]_N = 7.45$) but shows higher element abundances ($La_N = 439$) and a more pronounced negative Eu anomaly ($[Sm/Eu]_N = 3.13$).

Tectonomagmatic affinities and typology

Pearce et al. (1984) presented a set of tectonomagmatic discrimination diagrams purporting to indicate the tectonic setting of granitoid

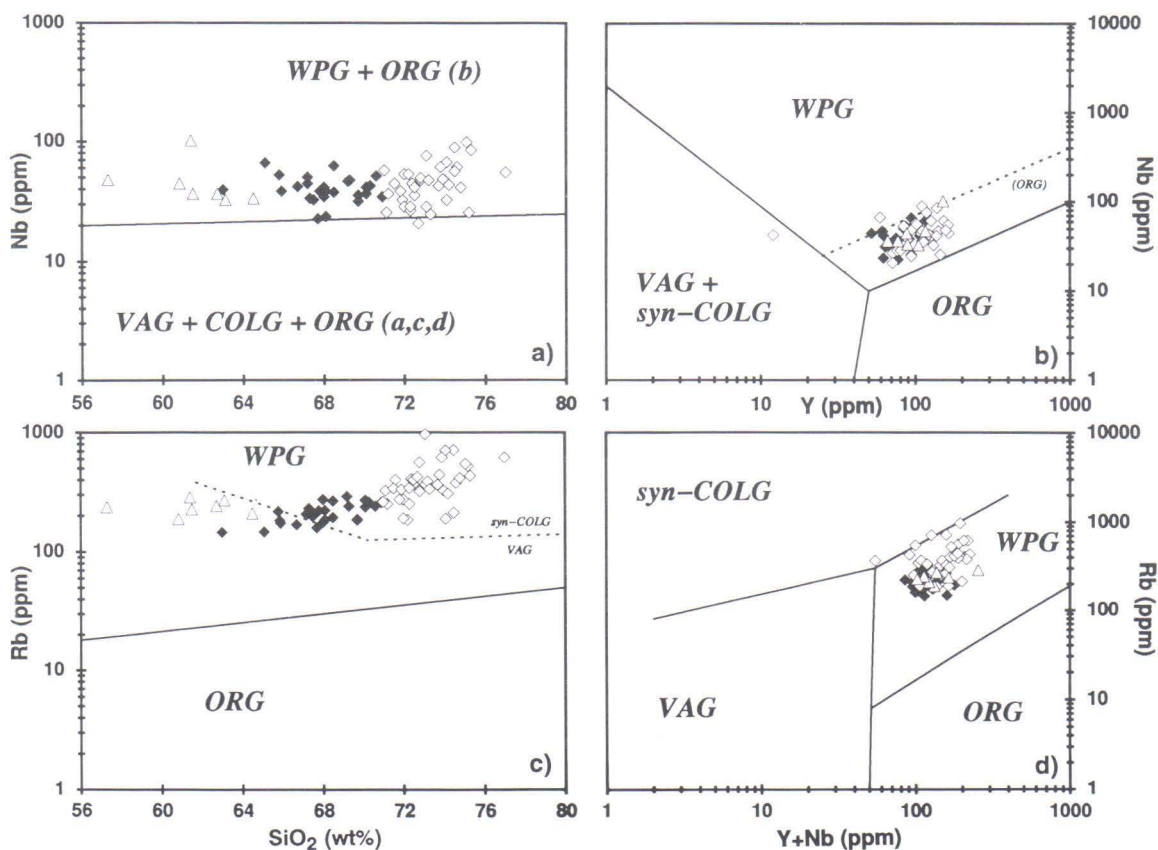


Fig. 22. Analyses of the rapakivi granites, quartz-feldspar porphyry dykes, and alkali-feldspar syenites (Appendix 1) plotted in (a) Nb vs. SiO₂, (b) Nb vs. Y, (c) Rb vs. SiO₂, and (d) Rb vs. Y+Nb tectonomagmatic discrimination diagrams of Pearce et al. (1984). Abbreviations denote ocean ridge granites (ORG), volcanic arc granites (VAG), within plate granites (WPG), and collision granites (COLG). Marked in (b) is also the upper compositional boundary for ocean ridge granites from anomalous ridge segments, and in (c) the discrimination boundary between syn-collision granites and volcanic arc granites (dotted lines; cf. Pearce et al., 1984). Note that post-collision granites can plot in all but the ORG space in (b) and (d) and are transitional between syn-COLG and VAG in (c). Symbols: closed diamonds — silicic rocks with < 71% SiO₂; open diamonds — silicic rocks with ≥ 71% SiO₂; open triangles — alkali-feldspar syenites.

rocks on the basis of their trace element abundances. Utilizing data on Phanerozoic granites of known tectonic settings, they compiled diagrams using the abundances of Y, Nb, Rb, and Ta, and showed that a distinction can be made between ocean ridge granites, volcanic arc granites, within plate granites, and syn-collision granites, but not necessarily between the latter three and post-collision granites. Although the diagrams were constructed on the basis of compositional data on Phanerozoic granites, they can probably be used to gain some indication of the tectonic setting of Proterozoic granitoid rocks as well (Pearce et al., 1984).

Fig. 22 shows the composition of the silicic rocks and the alkali-feldspar syenites of this study plotted in the Nb vs. SiO₂, Nb vs. Y, Rb vs. SiO₂, and Rb vs. Y + Nb discrimination diagrams of Pearce et al. (1984). In each diagram, the silicic rocks plot almost exclusively in the within plate granite space. The alkali-feldspar syenites also plot in the within plate space. It should be noted, however, that as the diagrams were constructed for rocks with more than 5% modal quartz, they may not, in principle, be applicable for these low-silica rocks. Because post-collisional granites plot in all but the ORG space in the Nb vs. Y and Rb vs. Y + Nb diagrams (Figs. 22b and d) and because they are transitional between syn-COLG and VAG in the Rb vs. SiO₂ diagram (Fig. 22c), the tectonic affinity of the rapakivi granites can not be unambiguously discerned by these data.

Whalen et al. (1987) postulated that A-type granites (alkaline, anorogenic, and anhydrous granites possibly derived from residual crustal sources; Collins et al., 1982; see also Loiselle & Wones, 1979) can be differentiated from M-, I-,

and S-type granites (derived by fractionation of mantle-derived magma (M), or by melting of igneous (I) or sedimentary (S) crustal protoliths; see Chappell & White, 1974; White, 1979) on the basis of their high Ga/Al ratios and high contents of large ion lithophile elements such as Y, Ce, Nb, and Zr. Fig. 23 shows the compositions of the silicic rocks and the alkali-feldspar syenites plotted in the (K₂O + Na₂O)/CaO vs. Ga/Al, FeO*/MgO vs. Ga/Al, Agpaitic Index vs. Ga/Al, Zr vs. Ga/Al, Nb vs. Ga/Al, Ce vs. Ga/Al, Y vs. Ga/Al, and Zn vs. Ga/Al diagrams of Whalen et al. (1987). As is evident from these plots, the rapakivi granites and quartz-feldspar porphyries clearly exhibit higher Ga/Al ratios than those observed for the M-, I-, and S-type granites in general. Practically all the granites and quartz-feldspar porphyry dykes plot in the space of A-type granites (one of the more fractionated quartz-feldspar porphyry dykes falls in the space of M-, I-, and S-type granites in Figs. 23a and h). The picture for the alkali-feldspar syenites is not so clear. The bulk of the data plot in the A-type space, but in the (K₂O + Na₂O)/CaO vs. Ga/Al, FeO*/MgO vs. Ga/Al, Y vs. Ga/Al, and Zn vs. Ga/Al diagrams (Figs. 23a, b, g and h) a few of them plot in the space of M-, I-, and S-type granites.

To summarize, the discrimination diagrams of Figs. 22 and 23 suggest that the rapakivi granites (and the quartz-feldspar porphyry dykes and alkali-feldspar syenites) share compositional characteristics with Phanerozoic granites intruded in within plate and post-collisional tectonic settings and that they also exhibit typical compositional features of the Phanerozoic A-type granites (cf. Haapala & Rämö, 1990; Rämö & Haapala, 1991).

Basic rocks

The chemical composition of the diabases, the samples from the Lovasjärvi intrusion, and the gabbroic and anorthositic rocks are presented in Appendix 2, Table 2, and Figs. 24 through 31.

Diabase dykes and the Lovasjärvi intrusion

The diabases of the Suomenniemi and Häme swarms are evolved Fe-rich tholeiites. In

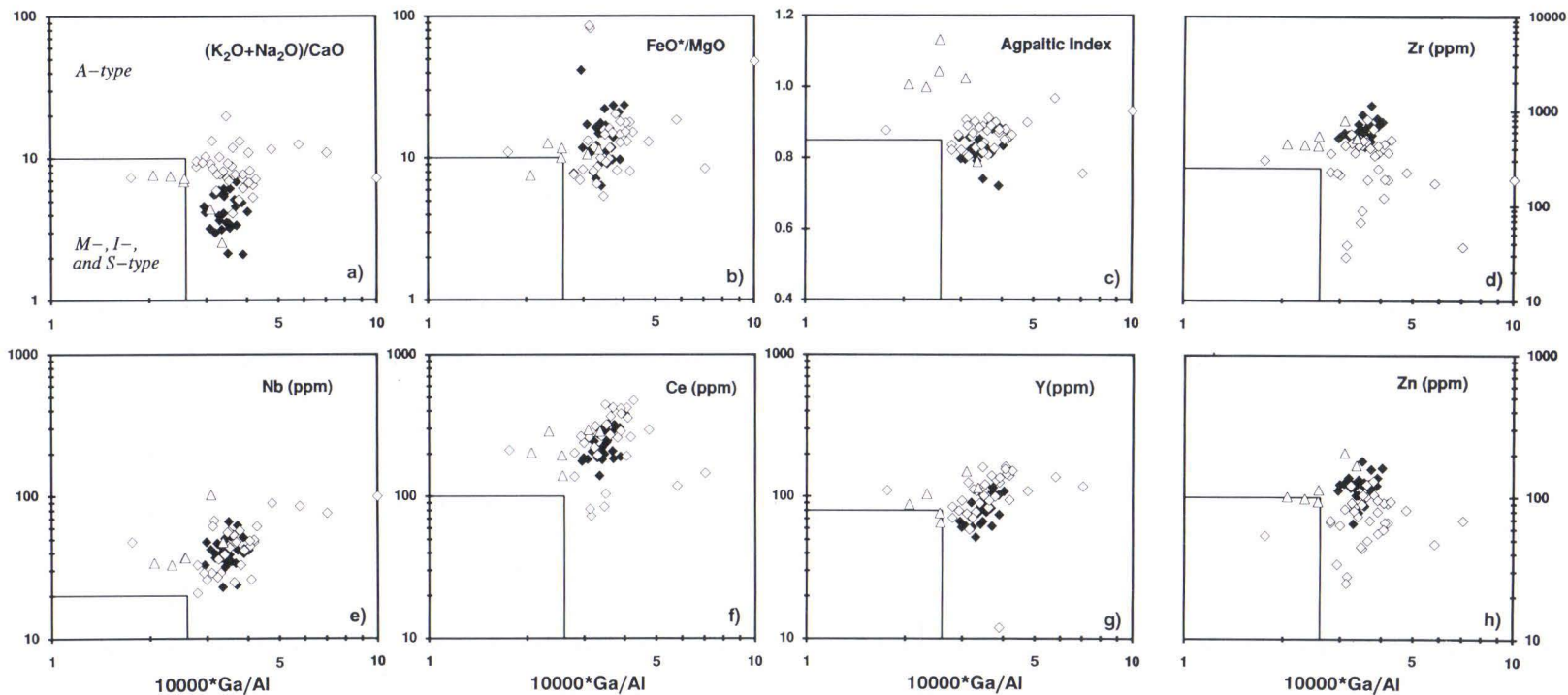


Fig. 23. Analyses of the rapakivi granites, quartz-feldspar porphyry dykes, and alkali-feldspar syenites (Appendix 1) plotted in (a) $(K_2O + Na_2O)/CaO$ vs. Ga/Al , (b) FeO^*/MgO vs. Ga/Al , (c) Agpaitic Index vs. Ga/Al , (d) Zr vs. Ga/Al , (e) Nb vs. Ga/Al , (f) Ce vs. Ga/Al , (g) Y vs. Ga/Al , and (h) Zn vs. Ga/Al diagrams of Whalen et al. (1987). The rectangular boxes denote the joint compositional space of M-, I-, and S-type granites as labeled in (a). Symbols are as in Fig. 22.

$\text{Na}_2\text{O} + \text{K}_2\text{O}$ vs. SiO_2 diagram (Fig. 24) they show transitional character plotting partly in the alkaline and partly in the subalkaline field. Most of the analysed dykes are true basalts; their SiO_2 content ranges from 45.9 to 53.6 wt% and averages 48.9 wt%. All the dykes are hypersthene-normative showing high $\text{Hy}/(\text{Hy} + \text{Di})$ ratios between 0.434 and 0.934 (average 0.746). A distinctive feature of the dykes is their variable silica saturation: the dykes range from olivine tholeiite to quartz tholeiite in normative composition (Fig. 25). This is also reflected in the mineralogy of the dykes, as those with high normative quartz lack modal olivine. Some of the olivine tholeiitic dykes have up to 18.5 wt% Al_2O_3 which may be due to the dykes being slightly cumulus-enriched with respect to plagioclase.

The Fe-enriched character of the dykes cor-

responds with their very low Mg numbers (25.9 to 49.8, average 40.2). Some of the dykes also show evidence of strong postmagmatic oxidation having $\text{Fe}_2\text{O}_3/\text{FeO}$ ratios equalling or even exceeding one (Appendix 2). In $\text{Na}_2\text{O} + \text{K}_2\text{O}$ — FeO — MgO diagram (Fig. 26), they plot in the tholeiitic field and fall far away from the MgO -apex. CaO content of the dykes varies between 5.97 and 8.77 wt% and the relatively low normative $\text{An}/(\text{An} + \text{Ab})$ ratios (0.461 to 0.578, average 0.526) are compatible with the overall evolved character of the dyke magmas. The analysed samples show relatively high TiO_2 (1.83 to 3.17 wt%) and P_2O_5 (0.41 to 1.31 wt%) abundances. In tectonomagmatic diagrams based on major element variations the diabase dykes show a continental character: in the TiO_2 — K_2O — P_2O_5 diagram of Pearce et al. (1975) they plot in

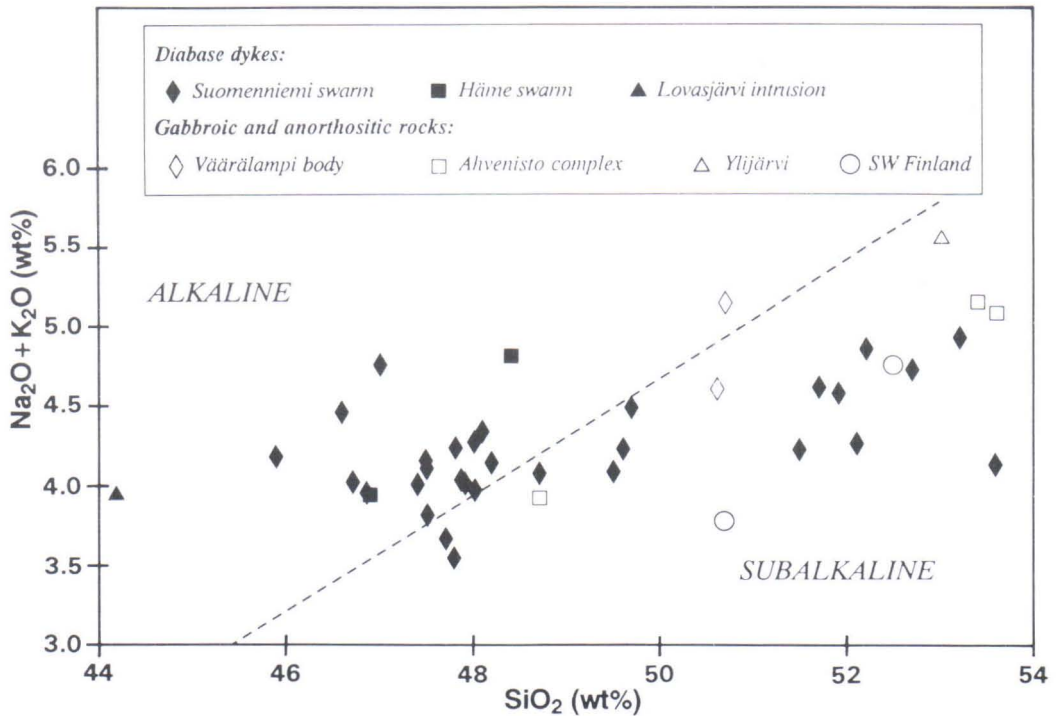


Fig. 24. Chemical analyses (Appendix 2) of the diabase dykes and the Lovasjärvi intrusion (closed symbols) and the gabbroic and anorthositic rocks (open symbols) plotted in $\text{Na}_2\text{O} + \text{K}_2\text{O}$ vs. SiO_2 diagram. Line separating the alkaline and subalkaline fields is from Irvine and Baragar (1971). The sample A1129 (melatroctolite cumulate from the Lovasjärvi intrusion) falls outside the plot area of the diagram.

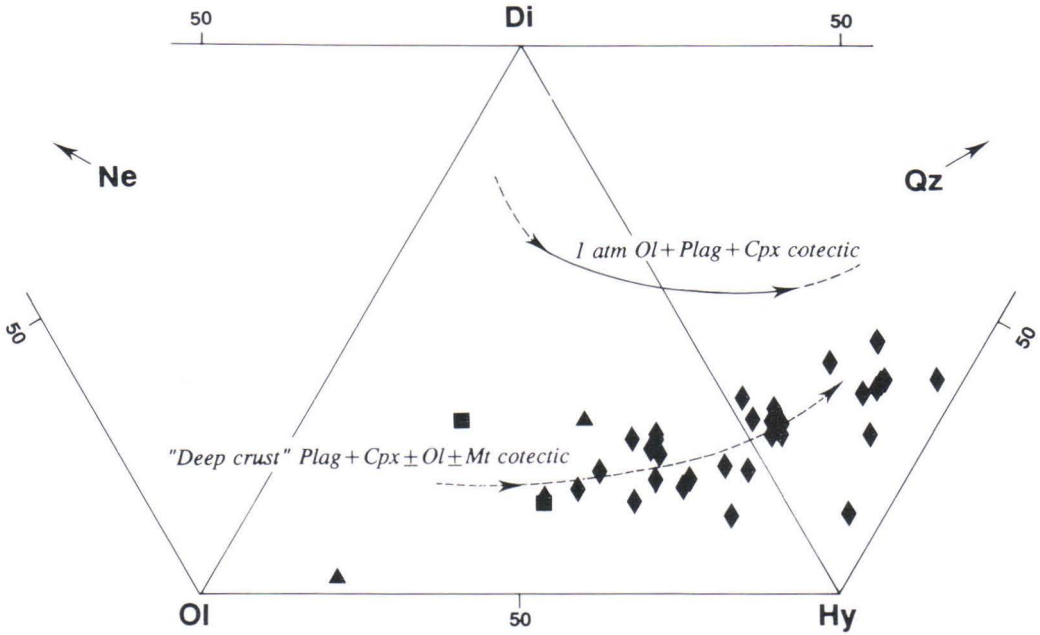
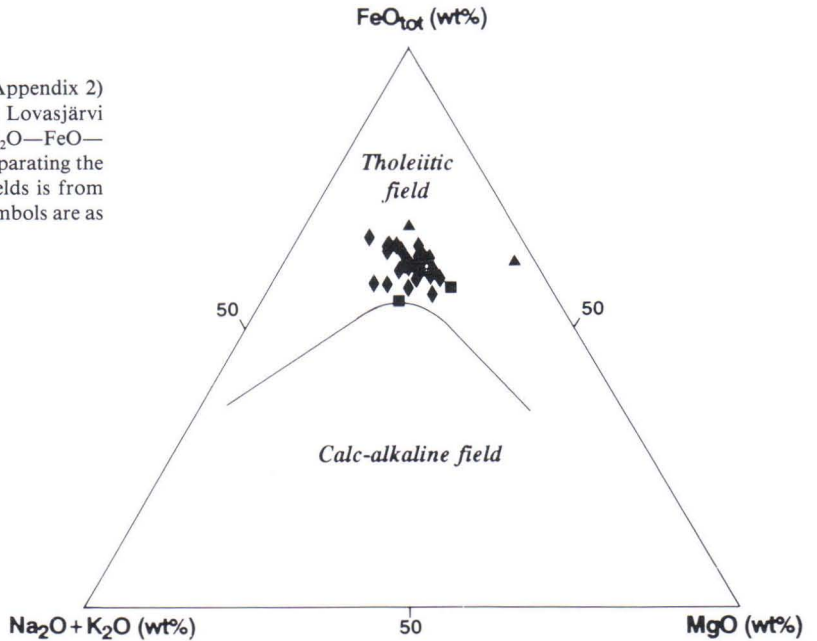


Fig. 25. Normative compositions (Appendix 2) of the diabase dykes and the Lovasjärvi intrusion plotted in a Ol-Hy-Di-Qz-Ne diagram. Also shown is the 1 atm olivine + plagioclase + clinopyroxene cotectic of Walker et al. (1979) and the »Deep crust» plagioclase + clinopyroxene ± olivine ± magnetite cotectic of Thompson et al. (1983). Symbols are as in Fig. 24.

Fig. 26. Chemical analyses (Appendix 2) of the diabase dykes and the Lovasjärvi intrusion plotted in Na₂O + K₂O—FeO—MgO (AFM) diagram. Line separating the tholeiitic and calc-alkaline fields is from Irvine and Baragar (1971). Symbols are as in Fig. 24.



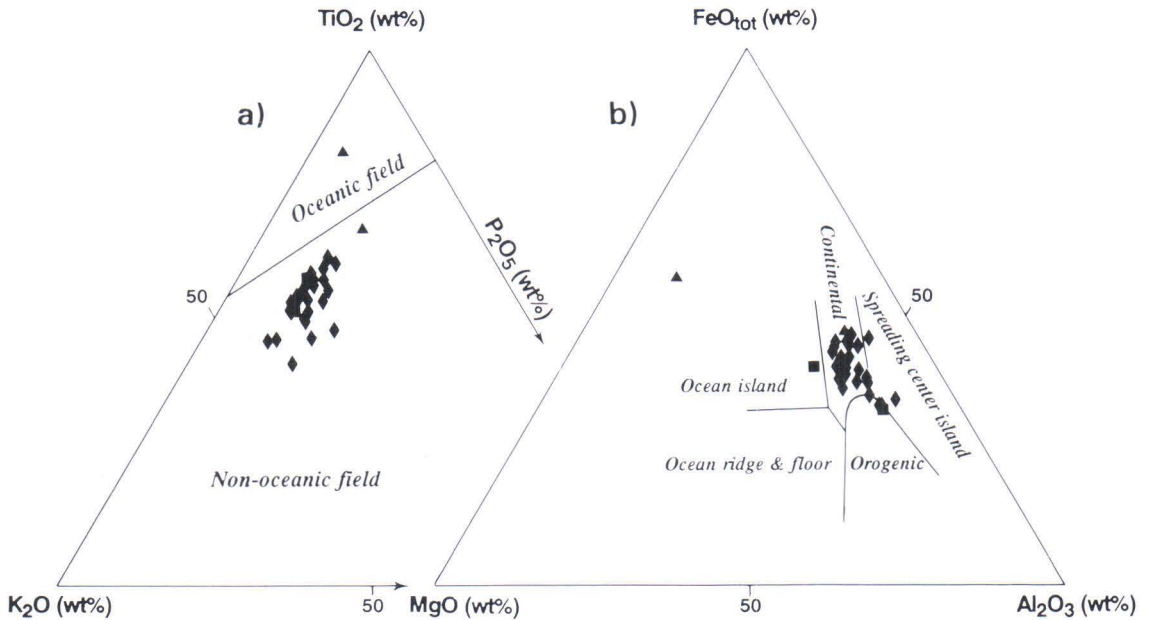


Fig. 27. Chemical analyses (Appendix 2) of the diabase dykes and the Lovasjärvi intrusion plotted in (a) the K_2O — P_2O_5 — TiO_2 diagram of Pearce et al. (1975) and (b) the MgO — FeO — Al_2O_3 diagram of Pearce et al. (1977). Symbols are as in Fig. 24.

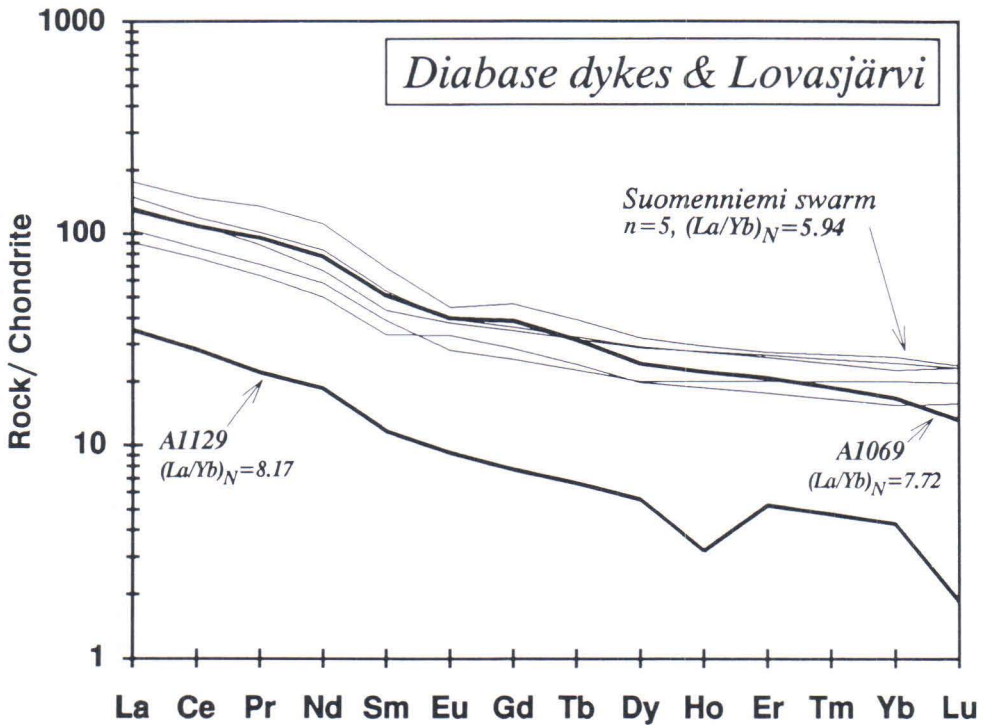


Fig. 28. Rare earth element analyses of the diabase dykes and the Lovasjärvi intrusion listed in Table 2 (excluding Tb and Tm) normalized against chondrite composition.

the non-oceanic field (Fig. 27a) and in the MgO—FeO—Al₂O₃ diagram of Pearce et al. (1977) most of them fall in the continental space (Fig. 27b).

The two samples from the Lovasjärvi intrusion differ from the dykes in having lower SiO₂ and higher TiO₂ abundances. Otherwise, the composition of sample A1069, a coarse-grained diabase from the central part of the intrusion, is rather similar to the more evolved diabases of the Suomenniemi and Häme swarms. Sample A1129, the melatroctolite cumulate from the north-western part of the intrusion, is very low in SiO₂ (37.0 wt%) and very high in Fe and Mg, and shows over 50 % olivine in the norm. In the Mg number of the melatroctolite (53.9) is, however, only slightly higher than those of the Subjotnian dykes.

In accordance with the low Mg numbers of the dykes, their compatible trace element contents are very low (Appendix 2). For example, Ni ranges from 17 to 82 ppm (average 31 ppm) and Cr varies between 13 and 85 ppm (average 41 ppm). In contrast, the melatroctolite cumulate from the Lovasjärvi intrusion has very high contents of Ni (395 ppm) and Cr (1190 ppm), consistent with its cumulate origin. The abundances of incompatible trace elements are high as compared to basalts in general; for example, Rb contents range from 33 to 91 ppm (average 51 ppm) and Zr contents from 146 to 463 ppm (average 252 ppm). The dykes show also relatively high contents of the REE (Table 2, Fig. 28). Chondrite-normalized REE-patterns are moderately enriched in the LREE with a mean (La/Yb)_N ratio of 5.94 and La_N 131 times chondrite (determined for five dykes spanning the compositional range; Table 2). The diabase A1069 from the Lovasjärvi intrusion has La_N of 129, while that for the melatroctolite A1129 is 35.2. On the average, the Lovasjärvi samples have slightly higher (La/Yb)_N ratios than the analysed diabase dykes (Fig. 28).

The chemical features outlined above are roughly similar to those described from Precam-

brian mafic dyke swarms from the U.S.A. (Hammond, 1986; Green et al., 1987), Canada (Condie et al., 1987), Scotland (Weaver and Tarney, 1981), and Australia (Mortimer et al., 1988). They also have much in common with the Phanerozoic continental flood basalts (e.g., Basaltic Volcanism Study Project, 1981). This is shown by the incompatible element plot in Fig. 29 in which the diabase dykes show an overall pattern generally enriched in the more incompatible elements and with negative Nb and Sr anomalies. The pattern is very similar to that of a continental tholeiite average (Holm, 1985); the latter shows, however, lower general levels of element abundances.

Gabbroic and anorthositic rocks

Geochemically, the Finnish rapakivi-related gabbroic and anorthositic rocks are in several respects similar to the Proterozoic massive anorthosites (cf. Emslie, 1980). Their SiO₂ contents are somewhat over 50 wt% on the average, and they have relatively high concentrations of Al₂O₃ (17.3 to 25.5 wt%) as a result of their feldspar-dominated mineralogy. Mg is depleted relative to Fe: the Mg numbers range from 54.6 to 30.3. CaO contents are between 7.22 and 10.10 wt%, and the alkalis are somewhat enriched relative to CaO (e.g., normative An/(An + Ab) ratios range from 0.522 to 0.620). All the samples analysed in the present study are hypersthene-normative and exhibit a large range in normative hypersthene content (from 3.6 wt% in sample A1110 to 18.7 wt% in sample A1048b). As regards silica saturation, the gabbroic and anorthositic rocks show similarities with the diabase dykes: both saturated and oversaturated rocks are encountered, the oversaturated being more abundant in the present data set. One of the samples (the leucogabbro A1048 of the Väärälampi intrusion) also shows a little corundum in the norm. In the Na₂O + K₂O vs. SiO₂ diagram (Fig. 24) the gabbros and anorthosites plot mostly in the subalkaline field.

Table 2. Rare earth element contents (in ppm) and chondrite-normalized La/Yb ratios of selected diabase dykes of the Suomenniemi swarm, the Lovasjärvi intrusion, and the gabbroic and anorthositic rocks.

Sample	Diabase dykes					Lovasjärvi intrusion		Gabbroic and anorthositic rocks						
	A1064	A1101	A1098	A1118	A1068	A1069	A1129	A118	A1110	A1048	A1048b	A119	A691b	7890
La	32.2	28.1	46.3	41.5	54.9	40.1	10.9	32.0	9.2	16.0	24.0	15.5	37.4	14.4
Ce	69	62	96	89	119	88.1	22.9	66.5	18.4	33.8	50.9	32.4	77.0	30.1
Pr	16.4	11.7	2.7	8.3	2.5	4.7	6.9	4.1	10.2	3.9
Nd	34.75	30.00	49.93	39.82	66.29	46.75	11.15	32.89	9.53	18.35	27.8	16.57	42.23	17.05
Sm	7.57	6.5	10.44	8.5	13.38	9.96	2.28	6.37	1.91	3.83	5.79	3.22	8.77	3.96
Eu	2.07	2.43	2.92	2.78	3.29	2.93	0.68	2.19	1.43	1.56	2.11	1.51	2.58	1.31
Gd	12.1	10.1	2.0	5.7	1.5	3.6	5.7	2.9	8.0	4.0
Tb	1.2	0.9	1.5	1.6	1.6	1.4	0.2	0.8	<0.1	0.3	0.6	0.2	1.0	0.5
Dy	6.5	6.4	9.4	9.3	10.4	7.9	1.8	4.1	1.5	3.5	5.0	2.7	7.1	3.6
Ho	2.12	1.6	0.23	0.66	0.33	0.71	1.01	0.58	1.42	0.59
Er	5.8	4.4	1.1	2.4	0.7	1.7	2.7	1.4	3.8	2.2
Tm	0.6	0.5	<0.1	0.2	<0.1	<0.1	0.2	<0.1	0.3	0.1
Yb	4.2	3.25	4.77	5.13	5.5	3.5	0.9	2.0	0.8	1.8	2.6	1.4	3.8	1.8
Lu	0.64	0.51	0.75	0.75	0.77	0.43	0.06	0.16	0.12	0.23	0.41	0.21	0.52	0.19
(La/Yb) _N ^a	5.17	5.83	6.54	5.45	6.73	7.72	8.17	10.79	7.75	5.99	6.22	7.46	6.64	5.39

Note: Nd and Sm by ID at the Unit for Isotope Geology, Geological Survey of Finland; the other elements by NA (samples A1064, A1101, A1068, and A1118) and ICP/MS at X-Ray Assay Laboratories Ltd (Canada).

^a normalizing values are 0.31 for La and 0.209 for Yb (Boynnton, 1984).

The compositional range of the samples analysed in this study is presented in a Mg number vs. normative An/(An + Ab) ratio diagram in Fig. 30; Mg numbers range from 54.7 to 30.3 and normative An/(An + Ab) ratios from 0.620 to 0.522. Excluding the gabbro sample 7890, the normative An content declines consistently with decreasing Mg number. The samples from the Ahvenisto complex range from the high Mg number, high An/(An + Ab) ratio olivine gabbro A1110 down to the leucogabbro A118 that has the lowest values of Mg number and An/(An + Ab) ratio; the anorthosite MH87a is intermediate between the two. The samples from the Väärälampi body (A1048, A1048b) are simi-

lar to each other and plot at lower values relative to the olivine gabbro and anorthosite of the Ahvenisto complex. The gabbro-norites from Ylijärvi (A119) and Kolinummi (A691b) are the most evolved samples of the present data set, and the leucogabbro (7890) from Höggrund exhibits a higher An/(An + Ab) ratio than samples MH87a and A118 from the Ahvenisto complex and the samples from the Väärälampi body.

The analysed gabbroic and anorthositic rocks show, as is also true regarding the diabase dykes, relatively low concentrations of compatible and relatively high concentrations of incompatible trace elements compared with basaltic rocks in general. For example, the Ni and Cr contents are

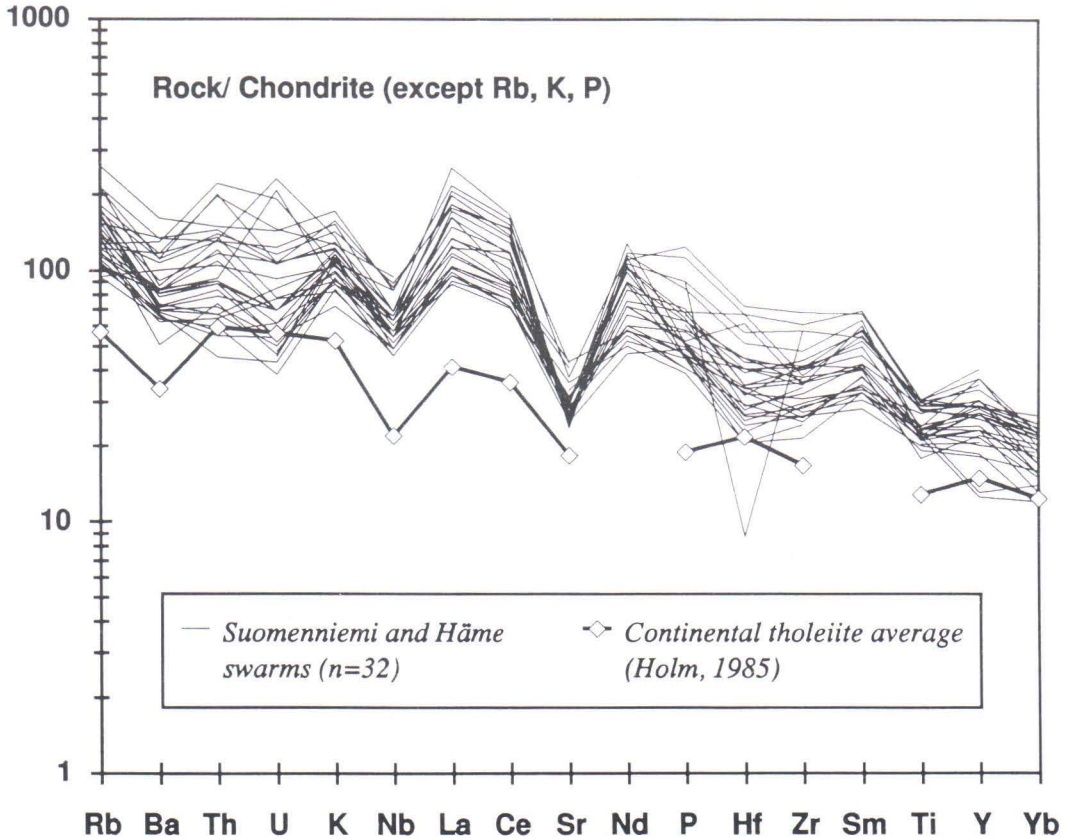


Fig. 29. Incompatible element abundances in the diabase dykes (Appendix 2) compared with the continental tholeiite average of Holm (1985). The data are normalized against chondrite, except Rb, K, and P. Normalizing values for Rb, Ba, Th, K, Nb, Sr, P, Hf, Zr, Ti, and Y are from Thompson et al. (1982), for the REE from Boynton (1984), and for U from Sun (1980).

very low in all samples, ranging from 7 to 56 ppm and 7 to 49 ppm, respectively. Furthermore, the contents of incompatible trace elements such as Rb and Zr show rather wide ranges: 11 to 116 ppm for Rb and 36 to 281 ppm for Zr. The samples from the Väärälampi body differ from those of the other bodies in having higher Rb and Ni contents (Appendix 2).

REE contents of the analysed samples are listed in Table 2, and Fig. 31 shows the chondrite-normalized REE patterns. As were the diabase dykes, the gabbroic and anorthositic rocks are also moderately enriched in the LREE. On the average, the gabbros and anorthosites are slightly more enriched in the LREE than the Subjotnian diabases and the samples from the Lovas-

järvi intrusion: most of the $(La/Yb)_N$ ratios fall in the range from 5.39 to 7.75, excluding sample A118 that shows a higher $(La/Yb)_N$ ratio 10.79. The normalized La contents range from 29.7 (A1110) to 121 (A691b). The anorthosite sample MH87a, which was not analysed for all REE, shows normalized Nd and Sm abundances of 8.20 and 4.25, respectively, indicative of grossly similar overall LREE-enrichment as was observed for the other samples (Fig. 31). A distinctive feature of the gabbroic and anorthositic rocks is that although they are plagioclase-rich rocks, only those that show the lowest contents of total REE exhibit distinct positive Eu-anomalies (samples A1110, A119, and A1048).

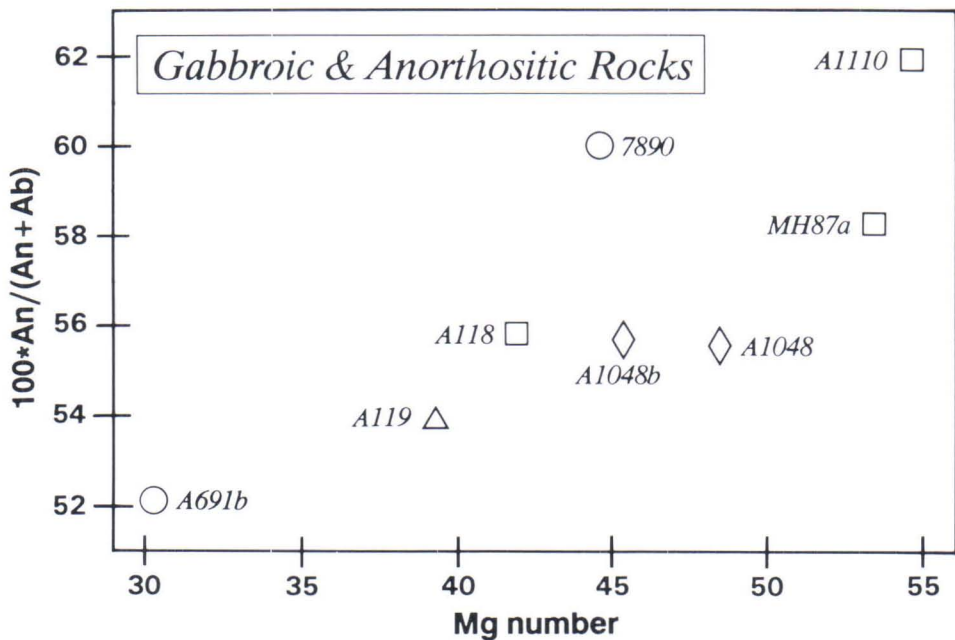


Fig. 30. Composition of the gabbroic and anorthositic rocks (Appendix 2) shown in normative An/(An + Ab) ratio vs. Mg number diagram. Symbols are as in Fig. 24, individual samples are labeled.

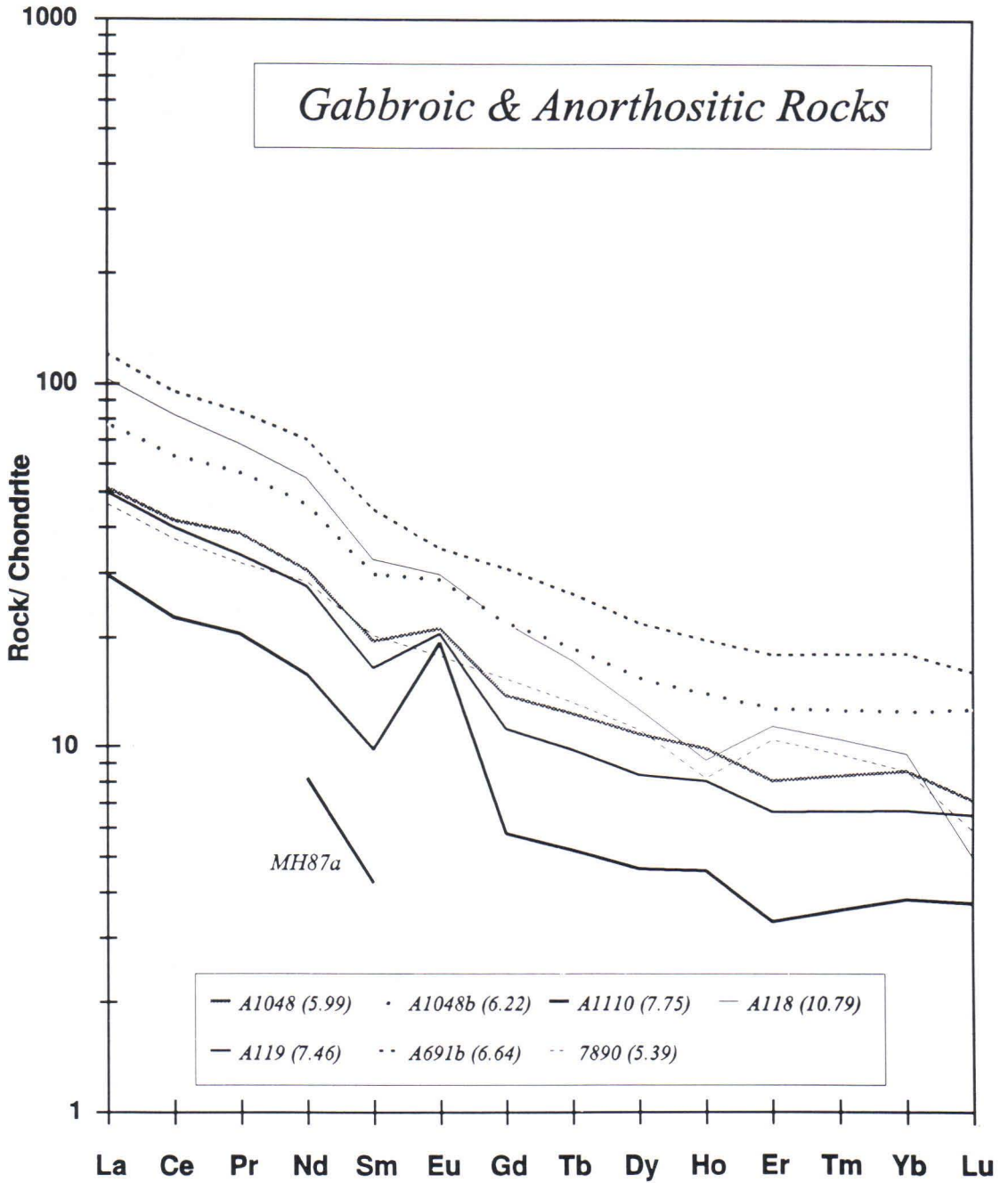


Fig. 31. Rare earth element analyses of the gabbroic and anorthositic rocks listed in Table 2 (excluding Tb and Tm) normalized against chondrite composition. Also shown are the abundances of Nd and Sm in the anorthosite sample MH87a (Table 4). Numbers in parentheses denote normalized La/Yb ratios.

Nd AND Pb ISOTOPE GEOCHEMISTRY

Notes on data presentation

Sm-Nd and Pb-Pb isotopic methods are powerful tools that are widely used in modern petrologic studies. Based on the radioactive decay of ^{147}Sm to ^{144}Nd , ^{238}U to ^{206}Pb , ^{235}U to ^{207}Pb , and ^{232}Th to ^{208}Pb , they can be used to measure the absolute ages of rock samples and to gain information on the origin of the material which the rock samples are composed of. The latter is also their main use in the present work. The basic principles of these isotopic methods are discussed at length by several authors; for the Sm-Nd method see Faure (1986) and DePaolo (1988a), and for the Pb-Pb method Gale and Mussett (1973) and Faure (1986). Some notes regarding data presentation and isotopic modeling are presented below.

Sm-Nd method

The measured $^{143}\text{Nd}/^{144}\text{Nd}$ ratios and the ages of the analysed rock samples are used to calculate the initial $^{143}\text{Nd}/^{144}\text{Nd}$ ratios that the samples probably had at the time of their crystallization. Because different methods are used by isotope laboratories to normalize the measured isotopic ratios of Nd, which thus are not necessarily always compatible with each other (see Faure, 1986, p. 209), the initial $^{143}\text{Nd}/^{144}\text{Nd}$ ratios are reported relative to the Chondritic Uniform Reservoir, CHUR, as $\epsilon_{\text{Nd}}(T)$ values (DePaolo & Wasserburg, 1976):

$$(1) \quad \epsilon_{\text{Nd}}(T) = 10^4 \left[\frac{\frac{^{143}\text{Nd}}{^{144}\text{Nd}}_{\text{SAMPLE}}(T) - \frac{^{143}\text{Nd}}{^{144}\text{Nd}}_{\text{CHUR}}(T)}{\frac{^{143}\text{Nd}}{^{144}\text{Nd}}_{\text{CHUR}}(T)} \right]$$

where $^{143}\text{Nd}/^{144}\text{Nd}_{\text{SAMPLE}}(T)$ and $^{143}\text{Nd}/^{144}\text{Nd}_{\text{CHUR}}(T)$ are the initial ratios in the sample and CHUR, respectively. Rock samples showing long-term

depletion of the LREE relative to CHUR have positive ϵ_{Nd} values, and vice versa. Likewise, the measured $^{147}\text{Sm}/^{144}\text{Nd}$ ratios are compared with that of CHUR using the Sm/Nd fractionation parameter $f_{\text{Sm}/\text{Nd}}$ (DePaolo, 1988a):

$$(2) \quad f_{\text{Sm}/\text{Nd}} = \frac{\frac{^{147}\text{Sm}}{^{144}\text{Nd}}_{\text{SAMPLE}} - \frac{^{147}\text{Sm}}{^{144}\text{Nd}}_{\text{CHUR}}}{\frac{^{147}\text{Sm}}{^{144}\text{Nd}}_{\text{CHUR}}}$$

Samples with positive $f_{\text{Sm}/\text{Nd}}$ parameters are depleted in the LREE relative to CHUR, and those with negative parameters are enriched. Depleted mantle model ages (T_{DM}) of the samples, indicative of the average date when the material (or materials) that constitute the rock sample were differentiated from a postulated LREE-depleted upper mantle source, are calculated in this work according to the model of DePaolo (1981a):

$$(3) \quad \epsilon_{\text{Nd}}(T) = 0.25T_{\text{DM}}^2 - 3T_{\text{DM}} + 8.5$$

where T_{DM} is given in Ga.

Pb-Pb method

Two Pb evolution models are used in the present work to evaluate the significance of the measured Pb isotopic ratios. These are the two-stage model suggested for the evolution of average crustal Pb by Stacey and Kramers (1975) and a two-stage model constructed by Huhma (1986) to fit the Pb isotopic data reported on Finnish 1.9 Ga galenas by Vaasjoki (1981). The main difference between the two models is the timing of the onset of the second stage, which is 3.7 Ga in the former and 3.0 Ga in the latter. The model of Huhma (1986) seems to account better for the evolution of the Svecofennian crust of southern Finland, but the differences between the two

models are very small. For instance, at 3.0 Ga, the $^{206}\text{Pb}/^{204}\text{Pb}$ and $^{207}\text{Pb}/^{204}\text{Pb}$ ratios of the model of Huhma (1986) are 12.90 and 14.340,

respectively, while those of the average crustal Pb model of Stacey and Kramers (1975) are 12.93 and 14.343, respectively.

Nd isotopic results

Nd isotopic data on the analysed 29 silicic rocks and alkali-feldspar syenites and 21 basic rocks are given in Tables 3 and 4, and they are plotted in ϵ_{Nd} vs. age diagrams in Figs. 32 and 33.

Finnish rapakivi granites, quartz-feldspar porphyry dykes, and alkali-feldspar syenites

The Finnish granites (topaz-bearing granites excluded), quartz-feldspar porphyry dykes, and alkali-feldspar syenites all have very similar Nd isotopic characteristics. They exhibit high concentrations of Nd and Sm (generally more than 90 and 15 ppm, respectively) and are strongly enriched in the LREE having $^{147}\text{Sm}/^{144}\text{Nd}$ ratios between 0.1 and 0.12 and $f_{\text{Sm}/\text{Nd}}$ parameters ranging from -0.4 to -0.5. Measured present-day $^{143}\text{Nd}/^{144}\text{Nd}$ ratios vary generally between 0.5115 and 0.5117, and the T_{DM} model ages range from 2.00 to 2.12 Ga, being thus distinctly higher than the U-Pb zircon ages measured for these rocks (Vaasjoki, 1977; Vaasjoki et al., 1991). The topaz-bearing granites (two samples from the Suomenniemi batholith and two from the Kymi stock within the Wiborg batholith) differ from the less fractionated granites in having markedly higher $^{147}\text{Sm}/^{144}\text{Nd}$ ratios (0.146 to 0.167) and $f_{\text{Sm}/\text{Nd}}$ parameters (-0.26 to -0.15), as well as higher present-day $^{143}\text{Nd}/^{144}\text{Nd}$ ratios (0.5120 to 0.5122). Due to the higher Sm/Nd ratios their T_{DM} are meaningless, ranging from 2.18 to 2.83 Ga. Sample A710 from the Vehmaa batholith contains some topaz but does not show an increased Sm/Nd ratio. This sample differs from the rest of the analysed topaz-bearing granites in being less fractionated (Appendix 1).

The ca. 1640 Ma old eastern Finnish samples (those from the Suomenniemi complex and the Wiborg batholith) have slightly negative initial ϵ_{Nd} values that show very little variation: 16 out of the 19 analysed samples fall within the range of -2.2 to -0.9 (Fig. 32). The most fractionated topaz-bearing granite sample A1097 (Sr = 16 ppm) has a measurably more negative $\epsilon_{\text{Nd}}(\text{T})$ value, -2.9 ± 0.4 , while the samples from the Kymi stock (1/IH/89 and M524b) have more positive values (-0.3 ± 0.6 and -0.2 ± 0.5 , respectively). The four analysed quartz-feldspar porphyry dykes have almost identical $\epsilon_{\text{Nd}}(\text{T})$ values that range from -1.3 ± 0.4 to -0.9 ± 0.7 . The two alkali-feldspar syenite samples (A1111 and A1164) have initial $\epsilon_{\text{Nd}}(\text{T})$ values similar to those of the granites (-2.0 ± 0.7 and -1.4 ± 0.5 , respectively).

The ca. 1580 Ma old western Finnish granites (those from the Laitila, Vehmaa, and Åland batholiths and the Siipyy pluton) have slightly more negative $\epsilon_{\text{Nd}}(\text{T})$ values than the eastern Finnish samples, ranging from -3.1 (sample A690, Ytö granite of the Laitila batholith) to -1.4 (sample A295 from the western part of the Åland batholith). The time-integrated Nd isotopic evolution of the eastern and western Finnish samples is, however, very similar (Fig. 32); excluding the topaz-bearing samples, the averages of the T_{DM} model ages of the eastern and western Finnish samples are 2.08 ± 0.05 (1 S.D.) and 2.06 ± 0.03 (1 S.D.) Ga, respectively.

Soviet Karelian rapakivi granites

The three granite samples from Soviet Karelia (biotite granites 9202 and IYL/79, topaz-bearing

Table 3. Sm-Nd isotopic data for the silicic rocks and alkali-feldspar syenites.

Sample	Age ^a (Ma)	Age ^b ref.	Sm (ppm)	Nd (ppm)	$\frac{^{147}\text{Sm}^c}{^{144}\text{Nd}}$	$f_{\text{Sm}/\text{Nd}}^d$	$\frac{^{143}\text{Nd}^e}{^{144}\text{Nd}}$	$\epsilon_{\text{Nd}}(\text{T})^f$	T_{DM}^g (Ga)	$\frac{^{145}\text{Nd}^e}{^{144}\text{Nd}}$
Suomenniemi complex										
Hornblende-clinopyroxene-fayalite granites										
A1130	1636 ± 23	[1]	18.11	95.80	0.1143	-0.42	0.511683 ± 18	-1.4 ± 0.4	2.08	0.348401 ± 12
M415.4	1640		26.90	144.8	0.1123	-0.43	0.511684 ± 18	-1.0 ± 0.4	2.04	0.348405 ± 12
Hornblende granites										
A1043 [§]	1641 ± 2	[1]	15.43	82.64	0.1128	-0.43	0.511636 ± 24	-2.0 ± 0.6	2.12	0.348409 ± 16
A1044	1640		26.26	141.8	0.1119	-0.43	0.511638 ± 24	-1.7 ± 0.6	2.10	0.348414 ± 16
A1045 [§]	1640		18.06	99.78	0.1094	-0.44	0.511629 ± 33	-1.4 ± 0.7	2.06	0.348426 ± 25
Biotite-hornblende granite										
A1040	1640		20.51	112.5	0.1102	-0.44	0.511642 ± 20	-1.3 ± 0.5	2.06	0.348419 ± 11
* §			20.53	112.5	0.1103	-0.44	0.511649 ± 25	-1.2 ± 0.6	2.05	0.348434 ± 18
Biotite granites										
A1041	1641 ± 1	[1]	30.21	174.0	0.1049	-0.47	0.511577 ± 28	-1.4 ± 0.6	2.05	0.348415 ± 22
A1042 [§]	1639 ± 6	[1]	25.84	154.7	0.1009	-0.49	0.511495 ± 25	-2.2 ± 0.6	2.09	0.348382 ± 17
Topaz-bearing granites										
A1097	1640		8.55	30.95	0.1669	-0.15	0.512172 ± 14	-2.9 ± 0.4	2.83	0.348416 ± 16
*			8.41	30.39	0.1672	-0.15	0.512170 ± 36	-3.0 ± 0.8	2.92	0.348427 ± 24
M664.2	1640		16.41	63.28	0.1457	-0.26	0.512017 ± 38	-1.5 ± 0.9	2.30	0.348396 ± 22
Alkali-feldspar syenites										
A1111	1629 ± 6	[1]	10.80	60.10	0.1068	-0.46	0.511575 ± 32	-2.0 ± 0.7	2.09	0.348394 ± 23
A1164	1630		25.24	126.2	0.1209	-0.39	0.511760 ± 19	-1.4 ± 0.5	2.11	0.348403 ± 12
Quartz-feldspar porphyry dykes										
A21b [§]	1638 ± 32	[1]	18.09	105.3	0.1039	-0.47	0.511579 ± 31	-1.2 ± 0.7	2.03	0.348414 ± 25
A1046 [§]	1635		18.84	108.4	0.1050	-0.47	0.511612 ± 31	-0.9 ± 0.7	2.00	0.348392 ± 24
A1100	1635 ± 2	[1]	20.52	115.6	0.1072	-0.45	0.511613 ± 18	-1.3 ± 0.4	2.04	0.348388 ± 14
A1163	1636 ± 17	[1]	18.72	113.5	0.09973	-0.49	0.511548 ± 22	-1.0 ± 0.5	2.00	0.348383 ± 23
Wiborg batholith										
A18 ^{§§}	1646 ± 4	[1]	18.00	93.43	0.1164	-0.41	0.511696 ± 43	-1.5 ± 0.9	2.11	0.348420 ± 23
A29b	1633 ± 1	[2]	19.10	98.20	0.1176	-0.40	0.511731 ± 21	-1.2 ± 0.5	2.08	0.348375 ± 18
A524b	1640	[3]	28.60	115.2	0.1501	-0.24	0.512128 ± 19	-0.2 ± 0.5	2.20	0.348425 ± 14
1/IH/89	1640		8.21	33.78	0.1470	-0.25	0.512091 ± 26	-0.3 ± 0.6	2.18	0.348413 ± 26

Laitila batholith											
A606 ^{§§}	1570	[3]	20.82	110.7	0.1136	-0.42	0.511666±22	-2.3±0.5	2.09	0.348404±16	
A690 ^{§§}	1540	[3]	16.26	90.53	0.1086	-0.45	0.511593±35	-3.1±0.8	2.10	0.348396±21	
Vehmaa batholith											
A710	1590	[3]	14.28	89.68	0.09624	-0.51	0.511485±24	-2.1±0.5	2.02	0.348378±13	
Åland batholith											
A295	1575±11	[2]	13.35	68.50	0.1178	-0.40	0.511751±20	-1.4±0.5	2.05	0.348421±14	
A762	1573±6	[2]	12.20	63.71	0.1158	-0.41	0.511708±19	-1.9±0.5	2.08	0.348407±14	
Siipyy pluton											
A373	1562±14	[4]	16.78	93.93	0.1080	-0.45	0.511609±16	-2.4±0.4	2.07	0.348400±13	
Salmi batholith											
6896 ^{§§}	1540	[2]	11.37	47.74	0.1439	-0.27	0.511764±20	-6.7±0.5	2.82	0.348412±22	
*			11.19	47.08	0.1437	-0.27	0.511798±23	-6.0±0.5	2.73	0.348392±11	
9202 ^{§§}	1540		18.04	102.7	0.1061	-0.46	0.511309±29	-8.1±0.7	2.46	0.348379±17	
Sotjärvi batholith											
IYL/79	1540		22.49	121.3	0.1120	-0.43	0.511494±28	-5.7±0.6	2.32	0.348418±21	

Note: Analyses labeled with superscripts have been published previously by [§] Haapala and Rämö (1990) and ^{§§} Rämö and Haapala (1991). * denotes duplicate analysis.

^a Ages are based on U-Pb zircon data and geological evidence.

^b Age references: [1] Vaasjoki et al. (1991); [2] Suominen (1991); [3] Vaasjoki (1977); [4] Idman (1989).

^c Estimated error is 0.4%.

^d Sm/Nd ratio relative to chondritic ratio (0.1966): $f_{\text{Sm/Nd}} = \frac{^{147}\text{Sm}/^{144}\text{Nd}_{\text{SAMPLE}} - ^{147}\text{Sm}/^{144}\text{Nd}_{\text{CHUR}}}{^{147}\text{Sm}/^{144}\text{Nd}_{\text{CHUR}}}$

^e Normalized to $^{146}\text{Nd}/^{144}\text{Nd} = 0.7219$. Errors are $2\sigma_m$ in last significant digits.

^f $\epsilon_{\text{Nd}}(T) = 10^4 \left[\frac{^{143}\text{Nd}/^{144}\text{Nd}_{\text{SAMPLE}}(T) - ^{143}\text{Nd}/^{144}\text{Nd}_{\text{CHUR}}(T)}{^{143}\text{Nd}/^{144}\text{Nd}_{\text{CHUR}}(T)} \right]$. Chondritic values used for calculation were $^{143}\text{Nd}/^{144}\text{Nd} = 0.51264$ and $^{147}\text{Sm}/^{144}\text{Nd} = 0.1966$.

^g Calculated according to the model of DePaolo (1981a) with $\epsilon_{\text{Nd}}(T) = 0.25T_{\text{DM}}^2 - 3T_{\text{DM}} + 8.5$

Table 4. Sm-Nd isotopic data for the basic rocks and whole rock standards.

Sample	Age ^a (Ma)	Age ^b ref.	Sm (ppm)	Nd (ppm)	$\frac{^{147}\text{Sm}^c}{^{144}\text{Nd}}$	$f_{\text{Sm}/\text{Nd}}^d$	$\frac{^{143}\text{Nd}^e}{^{144}\text{Nd}}$	$\epsilon_{\text{Nd}}(\text{T})^f$	T_{DM}^g (Ga)	$\frac{^{145}\text{Nd}^e}{^{144}\text{Nd}}$
Diabase dykes										
Suomenniemi swarm										
A1063 [§]	1640		7.49	34.56	0.1309	- 0.33	0.511964 ± 28	+ 0.6 ± 0.7	1.98	0.348411 ± 20
A1064 [§]	1640		7.57	34.75	0.1316	- 0.33	0.512018 ± 45	+ 1.6 ± 1.0	1.90	0.348414 ± 22
A1101 [§]	1640		6.50	30.00	0.1311	- 0.33	0.511945 ± 12	+ 0.2 ± 0.3	2.02	0.348436 ± 11
A1102 [§]	1640		11.60	54.19	0.1294	- 0.34	0.511887 ± 24	- 0.6 ± 0.6	2.09	0.348395 ± 28
A1098 [§]	1640		10.44	49.93	0.1264	- 0.36	0.511874 ± 16	- 0.2 ± 0.4	2.04	0.348414 ± 10
A1118 ^{§§§}	1640		8.50	39.82	0.1291	- 0.34	0.511897 ± 36	- 0.3 ± 0.8	2.06	0.348381 ± 27
A1047 [§]	1635		13.77	70.55	0.1180	- 0.40	0.511736 ± 20	- 1.2 ± 0.5	2.08	0.348437 ± 18
A1068 ^{§§§}	1635		13.38	66.29	0.1220	- 0.38	0.511779 ± 29	- 1.2 ± 0.7	2.10	0.348379 ± 18
35.1 ^{§§§}	1640		12.68	69.09	0.1104	- 0.44	0.511659 ± 19	- 1.0 ± 0.5	2.04	0.348467 ± 16
Häme swarm										
A808a ^{§§§}	1646 ± 6	[5]	6.53	31.39	0.1258	- 0.36	0.511864 ± 41	- 0.2 ± 0.9	2.04	0.348405 ± 22
A1135 ^{§§§}	1667 ± 9	[1]	6.88	34.31	0.1212	- 0.38	0.511842 ± 22	+ 0.6 ± 0.5	1.97	0.348417 ± 13
Lovasjärvi intrusion										
A1069 ^{§§§}	1643	[6]	9.96	46.75	0.1287	- 0.35	0.511850 ± 30	- 1.1 ± 0.7	2.14	0.348380 ± 17
*			9.96	46.71	0.1289	- 0.34		- 1.2		
A1129 ^{§§§}	1643		2.28	11.15	0.1239	- 0.37	0.511848 ± 28	- 0.1 ± 0.7	2.02	0.348402 ± 16
Gabbroic and anorthositic rocks										
Suomenniemi complex (Väärälampi body)										
A1048	1636		3.83	18.35	0.1263	- 0.36	0.511879 ± 41	- 0.1 ± 0.9	2.03	0.348339 ± 33
A1048b	1636 ± 14	[1]	5.79	27.80	0.1259	- 0.36	0.511849 ± 34	- 0.6 ± 0.8	2.07	0.348418 ± 28
Ahvenisto complex										
A1110	1645		1.91	9.53	0.1210	- 0.38	0.511865 ± 16	+ 0.8 ± 0.4	1.93	0.348404 ± 12
A118	1645 ± 5	[1]	6.37	32.89	0.1170	- 0.40	0.511749 ± 18	- 0.6 ± 0.5	2.04	0.348396 ± 16
MH87a	1645		0.829	4.92	0.1019	- 0.48	0.511602 ± 16	- 0.3 ± 0.4	1.96	0.348421 ± 11
*			0.809	4.81	0.1017	- 0.48	0.511596 ± 17	- 0.3 ± 0.4	1.96	0.348398 ± 14
Wiborg batholith (Ylijärvi)										
A119	1633 ± 1	[2]	3.22	16.57	0.1210	- 0.38	0.511807 ± 25	- 0.4 ± 0.6	2.03	0.348413 ± 14

Laitila batholith (Kolinummi intrusion)										
A691b	1570	[3]	8.77	42.23	0.1256	- 0.36	0.511819 ± 13	- 1.7 ± 0.4	2.12	0.348388 ± 8
Åland batholith (Höggrund)										
7890	1580	[2]	3.96	17.05	0.1403	- 0.29	0.512023 ± 23	- 0.6 ± 0.6	2.12	0.348430 ± 23
Standards										
Columbia River basalt										
BCR-1			6.57	28.71	0.1384	- 0.30	0.512640 ± 21			0.348437 ± 18
Geological Survey of Japan basalt										
JB-1			4.94	25.69	0.1161	- 0.41	0.512773 ± 24			0.348419 ± 15

Note: Analyses labeled with superscripts have been published previously by [§] Haapala and Rämö (1990) and ^{§§§} Rämö (1990). * denotes duplicate analysis.

^a Ages are based on U-Pb zircon and baddeleyite data and geological evidence.

^b Age references: [1] Vaasjoki et al. (1991); [2] Suominen (1991); [3] Vaasjoki (1977); [5] Laitakari (1987); [6] Siivola (1987).

c, d, e, f, and g as in Table 3.

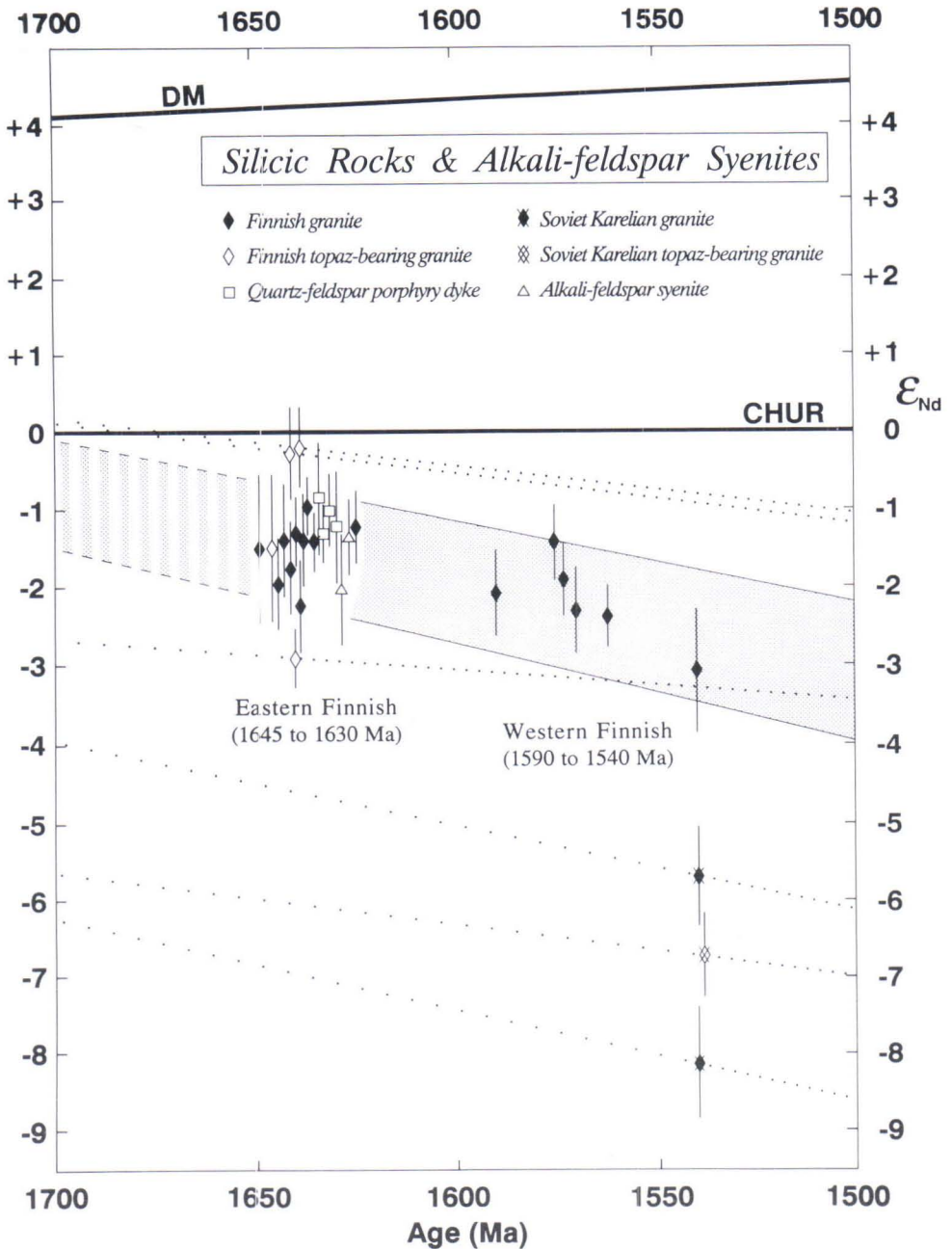


Fig. 32. Nd isotopic data of the rapakivi granites, quartz-feldspar porphyry dykes, and alkali-feldspar syenites (Table 3) plotted in ϵ_{Nd} vs. age diagram. Vertical lines indicate the analytical errors of the individual measurements. Data of the eastern Finnish samples are slightly displaced horizontally in order to show the error bars. CHUR and DM denote the evolution lines of the Chondritic Uniform Reservoir (DePaolo & Wasserburg, 1976) and depleted mantle (DePaolo, 1981a), respectively. The shaded area indicates the evolution path of the Finnish non-topaz-bearing samples, while the dotted lines show the evolution trends of fractionated topaz-bearing granites and Soviet Karelian samples. The ruled shading and the less dense dotting to the left of the data points show extrapolation of the trends toward the depleted mantle evolution line. The average T_{DM} model age of the non-topaz-bearing Finnish granites is 2.06 ± 0.03 (1 S.D.) Ga.

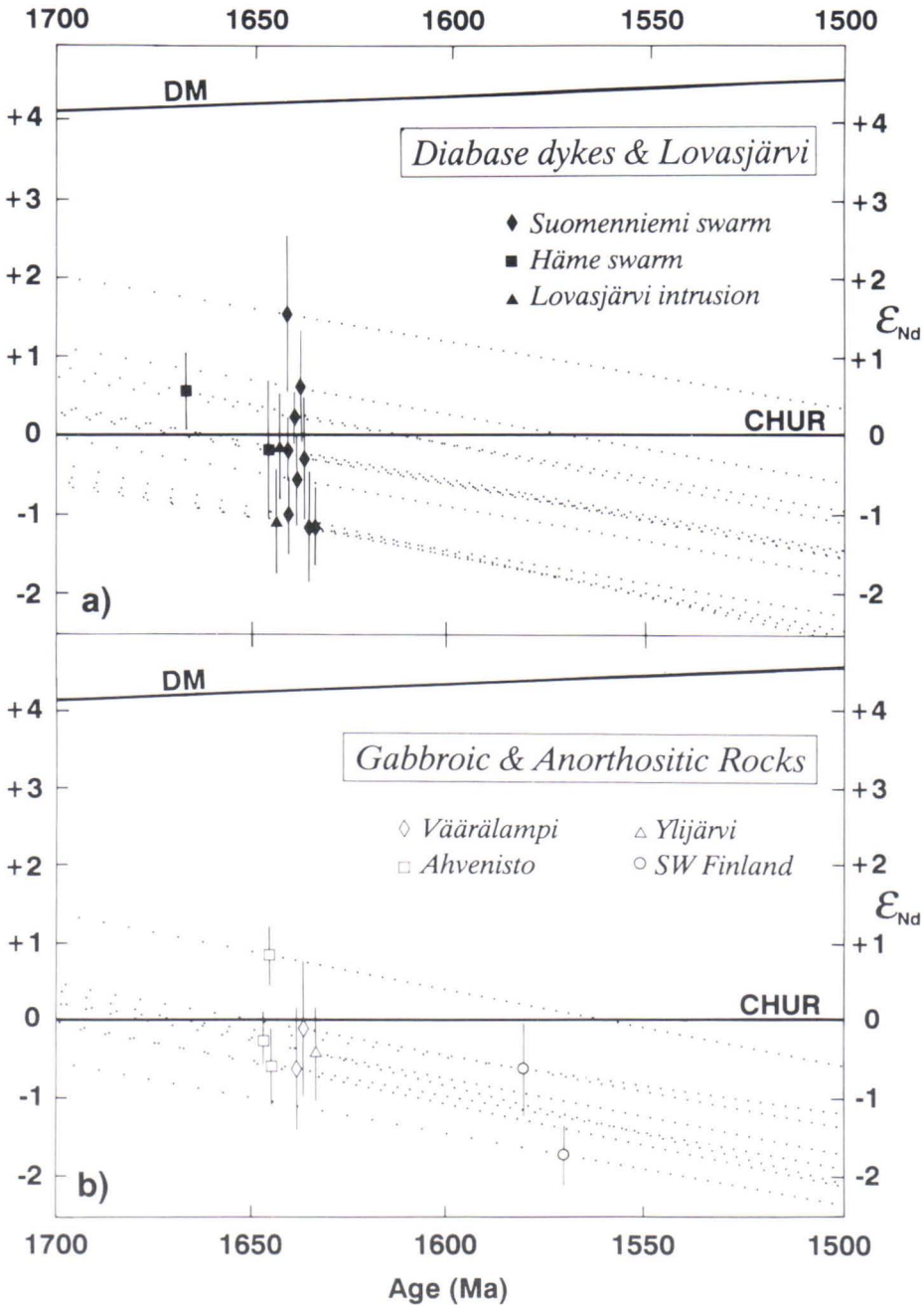


Fig. 33. Nd isotopic data of (a) the diabase dykes and the Lovasjärvi intrusion and (b) the gabbroic and anorthositic rocks (Table 4) plotted in ϵ_{Nd} vs. age diagram. Vertical lines indicate the analytical errors of the individual measurements. Some data points of the 1640 Ma dykes in (a) and the 1645 Ma and 1636 Ma samples in (b) are slightly displaced horizontally to show the error bars. CHUR and DM are as in Fig. 32. The dotted lines show the evolution trends of individual samples; the less dense pattern to the left of the data points shows extrapolation of the trends toward the depleted mantle evolution line. T_{DM} model ages of the samples range from (a) 1.90 to 2.14 Ga and (b) 1.93 to 2.12 Ga.

granite 6896) show similar $^{147}\text{Sm}/^{144}\text{Nd}$ ratios and $f_{\text{Sm}/\text{Nd}}$ parameters as the Finnish non-topaz-bearing and topaz-bearing granites, but their $^{143}\text{Nd}/^{144}\text{Nd}$ ratios are lower, ranging from 0.5113 to 0.5118. This results also in less radiogenic initial isotopic composition: the $\epsilon_{\text{Nd}}(\text{T})$ value of the biotite granite from the Sotjärvi batholith is -5.7 ± 0.6 and the two samples from the Salmi batholith have $\epsilon_{\text{Nd}}(\text{T})$ values of -6.7 ± 0.5 and -8.1 ± 0.7 . Comparable initial Nd isotopic compositions have been measured for the Salmi batholith by Neymark et al. (in prep.). The T_{DM} model ages of the Soviet Karelian samples range from 2.32 to 2.86 Ga. The difference between the initial Nd isotopic composition of the Finnish and Soviet Karelian samples is shown in the ϵ_{Nd} vs. age plot (Fig. 32) in which the Soviet Karelian samples plot considerably below the evolution path of the Finnish samples. It should also be noted that the initial ϵ_{Nd} values of the two samples from the Salmi batholith differ from each other by 1.4 ϵ_{Nd} -units and are not compatible with each other within experimental error; the more fractionated topaz-bearing granite 6896 ($\text{Sr} < 10$ ppm) has a more positive ϵ_{Nd} value than the less fractionated biotite granite 9202 ($\text{Sr} = 76$ ppm).

Diabase dykes and the Lovasjärvi intrusion

Typical of the diabase dykes are the relatively high concentrations of Sm (6.50 to 13.77 ppm) and Nd (30.00 to 70.55 ppm) compared with basaltic rocks in general. Their $^{147}\text{Sm}/^{144}\text{Nd}$ ratios range from 0.1104 to 0.1316, corresponding to $f_{\text{Sm}/\text{Nd}}$ of -0.44 to -0.33. Measured present-day $^{143}\text{Nd}/^{144}\text{Nd}$ ratios are on the order of 0.5117 to 0.5120 and their $\epsilon_{\text{Nd}}(\text{T})$ values range from +1.6 to -1.2. The T_{DM} model ages vary from 1.9 to 2.1 Ga and are, on the average, 0.4 Ga in excess of the true crystallization age of the diabbases determined from zircons and baddeleyites (Laitakari, 1987; Siivola, 1987; Vaasjoki et al., 1991).

The Nd isotopic data on the samples from the Lovasjärvi intrusion are similar to those of the diabase dykes. The coarse-grained diabase (A1069) from the central part of the intrusion shows Sm and Nd concentrations and Sm/Nd ratio close to those in the diabase dykes. The melatroctolite cumulate (A1129) has distinctly lower Sm and Nd concentrations (2.28 and 11.15 ppm, respectively) but the Sm/Nd ratio and isotopic composition of Nd are close to those measured for the diabase dykes. The $f_{\text{Sm}/\text{Nd}}$ fractionation parameters for the Lovasjärvi samples are -0.35 (A1069) and -0.37 (A1129) and their $\epsilon_{\text{Nd}}(\text{T})$ values -1.1 ± 0.7 (sample A1069) and -0.1 ± 0.7 (sample A1129).

The initial Nd isotopic compositions and the evolution paths of individual diabase samples are shown in Fig. 33a. All samples plot clearly below the evolutionary path of the model depleted mantle. The calculated initial isotopic compositions of the dykes are so variable and the range of the Sm/Nd ratios so small that it is not possible to calculate a Sm-Nd whole rock isochron for the diabase dykes.

Gabbroic and anorthositic rocks

The Sm concentrations of the gabbroic and anorthositic rocks range from 0.83 ppm (MH87a anorthosite) to 8.77 ppm (A691b leucogabbro) and the Nd concentrations from 4.92 ppm (MH87a) to 42.23 ppm (A691b). Their $^{147}\text{Sm}/^{144}\text{Nd}$ ratios are generally around 0.12. The anorthosite MH87a of the Mäntyharju complex has the lowest $^{147}\text{Sm}/^{144}\text{Nd}$ ratio of 0.1019 ($f_{\text{Sm}/\text{Nd}} = -0.48$) while the leucogabbro 7890 from the Höggrund anorthosite exhibits the highest $^{147}\text{Sm}/^{144}\text{Nd}$ ratio of 0.1403 ($f_{\text{Sm}/\text{Nd}} = -0.29$) of the rapakivi-age basic rocks analysed in this study. Initial ϵ_{Nd} values of the southeast Finnish samples range from +0.8 to -0.6, while the $\epsilon_{\text{Nd}}(\text{T})$ values of the two analysed western Finnish samples are more negative, -0.6 and -1.7. In the ϵ_{Nd} vs. age diagram (Fig. 33b) the eastern Finnish

samples plot close to the diabase dyke data (showing, however, less variation in ϵ_{Nd} values). Samples from the younger intrusions of south-western Finland plot below the CHUR evolution

line. The T_{DM} model ages of the gabbroic and anorthositic rocks range from 1.93 to 2.12 Ga and are 0.3 to 0.4 Ga in excess of their actual crystallization ages.

Pb isotopic results

Pb isotopic data on the silicic rocks, alkali-feldspar syenites, and the basic rocks are presented in Tables 5, 6, and 7 as well as in Figs. 34, 35, and 36.

Finnish rapakivi granites, quartz-feldspar porphyry dykes, and alkali-feldspar syenites

In addition to the data on the 26 whole rock samples (Table 5), Pb isotopic composition was measured on 16 alkali feldspar fractions (Table 6) separated from 12 granites, a quartz-feldspar porphyry dyke, and three alkali-feldspar syenites. The Finnish whole rock samples show considerable variation in their U and Pb abundances: sample A18 (tirilite from the northern part of the Wiborg batholith) has the lowest abundances (U = 1.29 ppm, Pb = 22 ppm) while the topaz-bearing granites of the Kymi stock exhibit the highest contents (ca. 20 ppm U and 130 ppm Pb). A very high U concentration, 23.6 ppm, was measured for the topaz-bearing granite M664.2 from the Suomenniemi batholith. Furthermore, both topaz-bearing granite samples from the Suomenniemi batholith show higher U/Pb ratios than the rest of the granites.

The Finnish samples show considerable variation also in the isotopic ratios of Pb. For example, the $^{206}\text{Pb}/^{204}\text{Pb}$ ratios range from 17.046 (sample A18) to 20.498 (sample A710). The isotopic ratios measured on the alkali feldspar fractions (Table 6) are relatively radiogenic, showing $^{206}\text{Pb}/^{204}\text{Pb}$, $^{207}\text{Pb}/^{204}\text{Pb}$, and $^{208}\text{Pb}/^{206}\text{Pb}$ ratios higher than 16, 15.35, and 35, respectively. μ_2 values for the Pb in the alkali feldspar fractions calculated according to the two-stage

evolution models of Stacey and Kramers (1975) and Huhma (1986) vary from 9.57 to 9.98 and from 9.27 to 10.43, respectively (Table 6). Compared with the Pb isotopic composition of the granites, the quartz-feldspar porphyry dykes show similar alkali feldspar and whole rock compositions, while the alkali-feldspar syenites have in general somewhat more radiogenic Pb isotopic ratios.

The Pb isotopic composition of the Finnish samples are plotted in $^{207}\text{Pb}/^{204}\text{Pb}$ vs. $^{206}\text{Pb}/^{204}\text{Pb}$ and $^{208}\text{Pb}/^{206}\text{Pb}$ vs. $^{206}\text{Pb}/^{204}\text{Pb}$ diagrams in Fig. 34. In the $^{207}\text{Pb}/^{204}\text{Pb}$ vs. $^{206}\text{Pb}/^{204}\text{Pb}$ plot (Fig. 34a) the data fall along the growth curve of average crustal Pb. The data show moderate scatter and no meaningful Pb-Pb isochrons can be fitted to the data. For example, the samples of the granites of the Suomenniemi batholith define a linear trend of 1391 ± 167 Ma. The topaz-bearing granites have lower $^{207}\text{Pb}/^{206}\text{Pb}$ ratios than the other granites and excluding them from the regression yields a trend with an age of 1631 ± 118 Ma. This is numerically consistent with the ca. 1640 Ma U-Pb zircon age of the batholith (Vaasjoki et al., 1991).

In the $^{208}\text{Pb}/^{206}\text{Pb}$ vs. $^{206}\text{Pb}/^{204}\text{Pb}$ diagram (Fig. 34b), the Finnish samples show considerable scatter, but nevertheless roughly conform to the growth curve of average crustal Pb; most of the alkali feldspar fractions actually plot on or close to the crustal growth curve.

Model ages calculated for the alkali feldspar fractions are shown in Table 6 along with $^{238}\text{U}/^{204}\text{Pb}$ (μ), $^{232}\text{Th}/^{204}\text{Pb}$ (ω), and $^{232}\text{Th}/^{238}\text{U}$ (κ) ratios. The single-stage model ages cluster generally around 1000 Ma, while the two-stage models yield model ages that are closer to the U-

Table 5. U-Pb whole rock isotopic data for the silicic rocks and alkali-feldspar syenites.

Sample	U (ppm) ^a	Pb (ppm) ^a	U/Pb	²⁰⁶ Pb/ ²⁰⁴ Pb	²⁰⁷ Pb/ ²⁰⁴ Pb	²⁰⁸ Pb/ ²⁰⁴ Pb
Suomenniemi complex						
Hornblende-clinopyroxene-fayalite granites						
A1130	1.96	26.95	0.0727	17.456	15.604	37.800
M415.4	3.06	27.09	0.1130	18.350	15.642	39.426
Hornblende granites						
A1043	2.75	27.30	0.1007	17.798	15.630	37.717
A1044	6.80	45.01	0.1511	19.303	15.711	40.198
A1045	4.30	39.74	0.1082	17.798	15.612	38.120
Biotite-hornblende granite						
A1040	4.59	83.15	0.0552	18.805	15.653	40.225
Biotite granites						
A1041	4.94	54.07	0.0914	17.667	15.576	39.065
A1042	5.83	61.32	0.0951	18.193	15.593	40.645
Topaz-bearing granites						
A1097	7.37	31.85	0.2314	19.409	15.656	37.789
M664.2	23.57	41.37	0.5697	19.496	15.653	39.007
Alkali-feldspar syenites						
A1111	3.59	28.05	0.1280	19.428	15.760	41.516
A1164	4.38	29.05	0.1508	19.492	15.757	41.679
Quartz-feldspar porphyry dykes						
A21b	4.80	52.37	0.0917	18.249	15.639	39.977
A1046	6.84	41.38	0.1653	19.457	15.772	41.327
A1100	5.35	39.72	0.1347	18.593	15.649	39.644
A1163	2.83	30.54	0.0927	17.517	15.526	38.003
Wiborg batholith						
A18	1.29	22.74	0.0567	17.046	15.490	36.995
A29b	6.69	34.14	0.1960	20.264	15.833	39.855
A524b	19.26	129.40	0.1488	19.598	15.775	37.205
1/IH/89	19.62	132.60	0.1480	18.111	15.605	36.322
Laitila batholith						
A606	3.77	28.99	0.1300	17.525	15.572	38.178
A690	4.19	39.36	0.1065	20.070	15.810	44.306
Vehmaa batholith						
A710	12.60	45.17	0.2789	20.498	15.792	43.689
Åland batholith						
A295	7.38	28.52	0.2588	19.598	15.771	38.515
A762	7.01	33.58	0.2088	20.065	15.826	39.123
Siipyy pluton						
A373	7.02	50.56	0.1388	17.517	15.517	38.673
Salmi batholith						
6896	6.82	26.14	0.2609	16.729	15.171	37.165
9202	4.71	33.13	0.1422	17.391	15.273	38.500
Sotjärvi batholith						
IYL/79	5.35	42.08	0.1271	16.236	15.139	35.878

Note: The accuracy of the isotopic ratios is $\pm 0.15\%$.

^a all concentrations by isotope dilution.

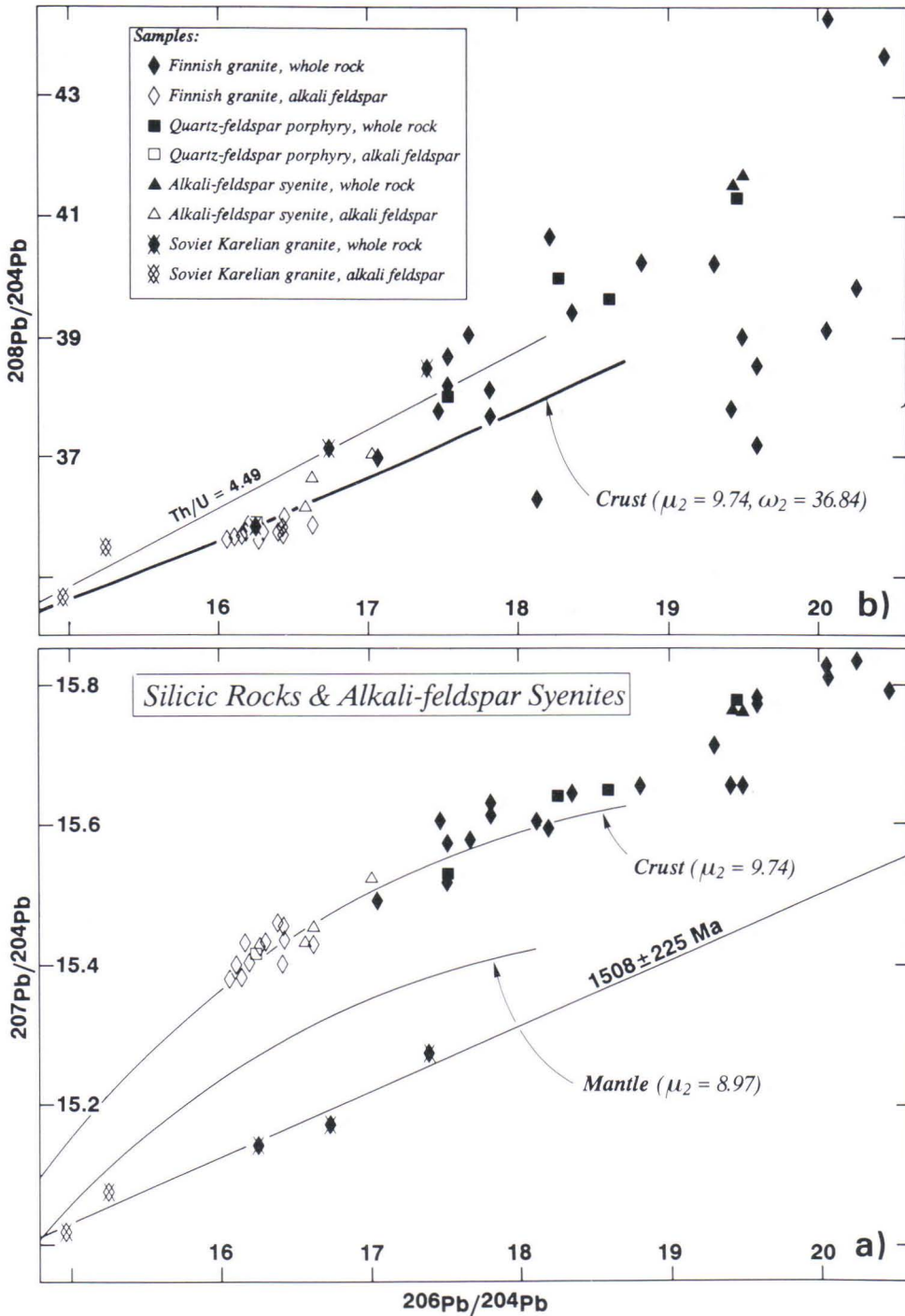


Fig. 34. Pb isotopic composition of the silicic rocks and alkali-feldspar syenites (Tables 5 and 6) plotted in (a) $^{207}\text{Pb}/^{204}\text{Pb}$ vs. $^{206}\text{Pb}/^{204}\text{Pb}$ and (b) $^{208}\text{Pb}/^{206}\text{Pb}$ vs. $^{206}\text{Pb}/^{204}\text{Pb}$ diagrams. Growth curves for average crustal Pb (Stacey & Kramers, 1975) are shown in (a) and (b) and that of the plumbotectonics model mantle (Doe & Zartman, 1979) in (a). Errorchrons for the Soviet Karelian data are shown as well. The size of the symbols in (a) corresponds roughly to the average analytical error.

Table 6. Pb isotopic data for the alkali feldspar fractions.

Sample	^{206}Pb	^{207}Pb	^{208}Pb	Model ages (Ma) ^a			$^{238}\text{U}/^{204}\text{Pb}$ ^a			$^{232}\text{Th}/^{204}\text{Pb}$ ^a			$^{232}\text{Th}/^{238}\text{U}$ ^a		
	^{204}Pb	^{204}Pb	^{204}Pb	1	2	3	1	2	3	1	2	3	1	2	3
Suomenniemi complex															
Hornblende-clinopyroxene-fayalite granites															
A1130/KS	16.152	15.428	35.748	1189	1561	1596	8.32	9.98	10.43	32.69	37.47	32.73	3.93	3.76	3.14
M415.4/KS	16.097	15.399	35.683	1202	1558	1564	8.28	9.85	10.05	32.46	36.87	31.20	3.92	3.74	3.11
Hornblende granites															
A1043/KS	16.415	15.453	35.846	1012	1399	1413	8.31	9.88	10.12	31.67	35.72	30.22	3.81	3.62	2.99
A1044/KS	16.284	15.425	35.776	1084	1454	1455	8.28	9.83	9.97	31.92	35.99	30.19	3.85	3.66	3.03
Biotite-hornblende granite															
A1040/KS	16.420	15.432	36.027	985	1360	1343	8.27	9.75	9.75	32.35	36.54	30.97	3.91	3.75	3.18
Biotite granites															
A1041/KS	16.187	15.401	35.882	1134	1490	1478	8.26	9.77	9.81	32.89	37.40	31.88	3.98	3.83	3.25
A1042/KS	16.138	15.380	35.723	1150	1494	1461	8.23	9.69	9.58	32.22	36.19	29.67	3.92	3.73	3.10
Topaz-bearing granites															
A1097/KS	16.402	15.399	35.731	963	1318	1254	8.21	9.57	9.27	30.72	33.72	26.37	3.74	3.52	2.85
M664.2/KS	16.610	15.426	35.902	829	1203	1138	8.22	9.57	9.29	30.51	33.47	26.47	3.71	3.50	2.85
Alkali-feldspar syenites															
A1111/KS	17.012	15.521	37.061	619	1061	1068	8.33	9.83	9.97	34.27	39.68	36.52	4.11	4.04	3.66
A1164/KS	16.613	15.450	36.654	854	1242	1213	8.27	9.70	9.63	34.29	39.44	35.20	4.15	4.07	3.65
M265.1/KS	16.561	15.430	36.179	872	1248	1199	8.24	9.63	9.43	32.17	36.07	30.12	3.91	3.75	3.19
Quartz-feldspar porphyry dyke															
A1046/KS	16.234	15.414	35.914	1111	1475	1471	8.27	9.81	9.92	32.85	37.42	32.12	3.97	3.82	3.24
Wiborg batholith															
A29b/KS	16.383	15.458	35.774	1042	1432	1459	8.32	9.93	10.29	31.56	35.64	30.23	3.79	3.59	2.94
1/IH/89/KS	16.256	15.424	35.623	1104	1474	1480	8.29	9.85	10.03	31.32	35.08	28.84	3.78	3.56	2.87
Siipyy pluton															
A373/KS	16.047	15.379	35.622	1220	1565	1553	8.25	9.78	9.83	32.31	36.48	30.22	3.92	3.73	3.08
Soviet Karelian batholiths															
9202/KS	15.243	15.073	35.524	1546	1724	1372	7.87	8.73	6.59	34.97	38.39	25.89	4.44	4.40	3.93
IYL/79/KS	14.961	15.018	34.681	1721	1886	1541	7.86	8.75	6.39	31.82	33.48	18.33	4.05	3.83	2.87

Note: The accuracy of the isotopic ratios is $\pm 0.15\%$.

^a Pb-Pb model ages and the model isotopic ratios are calculated according to (1) single-stage model, (2) the two-stage model of Stacey and Kramers (1975), and (3) the two-stage model of Huhma (1986).

Pb zircon ages. As far as the Suomenniemi complex is concerned, the alkali-feldspars of the hornblende-clinopyroxene-fayalite granites have Stacey and Kramers (1975) model ages closest to the true crystallization ages (between 1550 and 1600 Ma), while the alkali-feldspar syenites show the youngest model ages (1061 and 1248 Ma). The alkali feldspar sample A373 from the Siipyy pluton has a Stacey and Kramers (1975) model age of 1565 Ma, which is almost equal to the U-Pb zircon age of the granite (1562 ± 14 Ma; Idman, 1989).

Soviet Karelian rapakivi granites

Compared with the Finnish samples, the three whole rocks and the two alkali feldspar fractions from the Soviet Karelian batholiths have similar U and Pb concentrations but show distinctly less radiogenic Pb isotopic ratios. In $^{207}\text{Pb}/^{204}\text{Pb}$ vs. $^{206}\text{Pb}/^{204}\text{Pb}$ diagram (Fig. 34a) they plot clearly below the average crustal and model mantle growth curves. Single-stage μ values of the alkali feldspar fractions are 7.86 and 7.87, while μ_2 values are 8.73 and 8.75 (model of Stacey & Kramers, 1975) or 6.59 and 6.39 (model of Huhma, 1986). A linear trend with an age of 1508 ± 225 Ma (2σ) and MSWD of 4.1 can be fitted through the Soviet Karelian data. This age, although imprecise, is numerically compatible with U-Pb zircon ages measured for the Salmi batholith (Suominen, 1991; L. Neymark, pers. commun., 1990). The Stacey and Kramers (1975) model ages of the alkali feldspars, 1724 and 1886 Ma (Table 6), are considerably higher than the actual crystallization ages. Using the Pb evolution model of Huhma (1986), lower ages are calculated; the model age for the alkali feldspar from the Sotjärvi batholith (1541 Ma) is very close to the crystallization age of the Salmi batholith. Pb-Pb ages for the individual alkali-feldspar — whole rock pairs are 1491 Ma (sample 9202) and 1527 Ma (sample IYL/79). The age of the sample from the Sotjärvi batholith, 1527 Ma, is consistent with the assumption that the

two Soviet Karelian batholiths are (roughly) coeval.

In the $^{208}\text{Pb}/^{206}\text{Pb}$ vs. $^{206}\text{Pb}/^{204}\text{Pb}$ diagram (Fig. 34b) the Soviet Karelian samples plot toward a slightly higher average Th/U ratio compared with the Finnish samples. A Th/U ratio of 4.49 can be calculated for the Soviet Karelian data.

Diabase dykes and the Lovasjärvi intrusion

The diabase dykes exhibit high concentrations of U (0.56 to 2.71 ppm) and Pb (5.93 to 20.42 ppm) compared with basalts in general, and show relatively radiogenic isotope ratios of Pb (Table 7). The measured U/Pb ratios are generally between 0.07 and 0.13. The two analyzed plagioclase fractions show rather high isotopic ratios as well. The ratios differ from each other considerably, which is probably due to extra radiogenic Pb in the more radiogenic feldspar sample A1064. Compared with the diabase dykes in general, the samples from the Lovasjärvi intrusion have slightly higher uranium isotopic ratios of Pb, and show a similar pattern to that seen in Nd isotopes: the diabase A1069 is similar to the Subjotnian diabases, and the melatroctolite A1129 shows much lower concentrations of U (0.36 ppm) and Pb (2.20 ppm), but has a comparable U/Pb ratio (0.166).

The Pb isotopic ratios of the Subjotnian diabases and the Lovasjärvi intrusion are plotted in $^{207}\text{Pb}/^{204}\text{Pb}$ vs. $^{206}\text{Pb}/^{204}\text{Pb}$ and $^{208}\text{Pb}/^{204}\text{Pb}$ vs. $^{206}\text{Pb}/^{204}\text{Pb}$ diagrams in Fig. 35. In the $^{207}\text{Pb}/^{204}\text{Pb}$ vs. $^{206}\text{Pb}/^{204}\text{Pb}$ diagram (Fig. 35a), the samples plot close to the average crustal Pb growth curve of Stacey and Kramers (1975) and fall along a secondary isochron with an age of 1854 ± 65 Ma (2σ) and MSWD of 1.3. This age is about 200 Ma in excess of the true crystallization age of the dykes determined from zircons and baddeleyites (Laitakari, 1987; Siivola, 1987; Vaasjoki et al., 1991). Sample A1118, which deviates from the other samples, was omitted from

the calculation. The different Pb isotopic composition of this sample could result from the dyke being considerably younger than the other dykes (about 1.1 Ga old, Fig. 35c) or it may indicate that it had a less radiogenic initial Pb isotopic composition. These alternatives are, however, considered improbable as the isotopic systematics of the sample have most probably been affected by later U-gain: the concentration of U is about three times higher in this sample than in the other

diabases with comparable Pb concentrations (Table 7). The Stacey and Kramers (1975) μ_2 values calculated for the plagioclase fractions A1063 and A1064 are 9.69 and 9.62, respectively, which are close to the μ_2 value (9.74) of average crustal Pb (Fig. 35). Stacey and Kramers (1975) second-stage model ages of the plagioclase fractions are 1461 Ma (A1063) and 935 Ma (A1064).

In the $^{208}\text{Pb}/^{204}\text{Pb}$ vs. $^{206}\text{Pb}/^{204}\text{Pb}$ diagram (Fig. 35b), the plagioclases plot close to the

Table 7. U-Pb whole rock and plagioclase isotopic data for the basic rocks.

Sample	U (ppm) ^a	Pb (ppm) ^a	U/Pb	$^{206}\text{Pb}/^{204}\text{Pb}$	$^{207}\text{Pb}/^{204}\text{Pb}$	$^{208}\text{Pb}/^{204}\text{Pb}$
Diabase dykes						
Suomenniemi swarm						
A1063	0.65	6.86	0.0953	17.914	15.562	37.824
A1064	1.00	7.57	0.1320	18.451	15.632	37.962
A1101	0.56	7.73	0.0719	17.527	15.522	37.248
A1102	1.38	13.09	0.1054	18.496	15.640	38.012
A1098	1.01	10.56	0.0956	17.980	15.587	38.012
A1118	2.71	6.64	0.4081	20.285	15.696	37.106
A1047	1.87	15.56	0.1202	18.777	15.702	39.351
A1068	1.51	11.42	0.1322	18.348	15.626	37.966
35.1	1.61	20.42	0.0788	17.482	15.532	37.438
A1063/ plagioclase				16.201	15.390	35.690
A1064/ plagioclase				17.111	15.492	36.442
Häme swarm						
A808a	0.62	6.24	0.0992	17.922	15.595	37.765
A1135	0.59	5.93	0.0993	17.826	15.557	37.765
Lovasjärvi intrusion						
A1069	0.85	7.98	0.1063	18.802	15.680	37.833
A1129	0.36	2.20	0.1655	19.185	15.718	38.215
Gabbroic and anorthositic rocks						
Suomenniemi complex (Väärälampi body)						
A1048	0.66	14.13	0.0469	17.461	15.582	36.763
A1048b	0.93	13.01	0.0715	17.570	15.563	37.190
Ahvenisto complex						
A1110	0.13	2.41	0.0544	17.411	15.483	37.042
A118	0.71	7.15	0.0999	17.681	15.543	37.489
MH87a	0.081	2.79	0.0289	16.504	15.429	36.062
Wiborg batholith (Ylijärvi)						
A119	0.40	5.72	0.0698	17.351	15.540	36.999
Laitila batholith (Kolinummi intrusion)						
A691b	0.66	10.46	0.0627	17.469	15.559	37.775
Åland batholith (Höggrund)						
7890	0.29	3.58	0.0796	17.878	15.566	37.596

Note: The accuracy of the isotopic ratios is $\pm 0.15\%$.

^a all concentrations by isotope dilution.

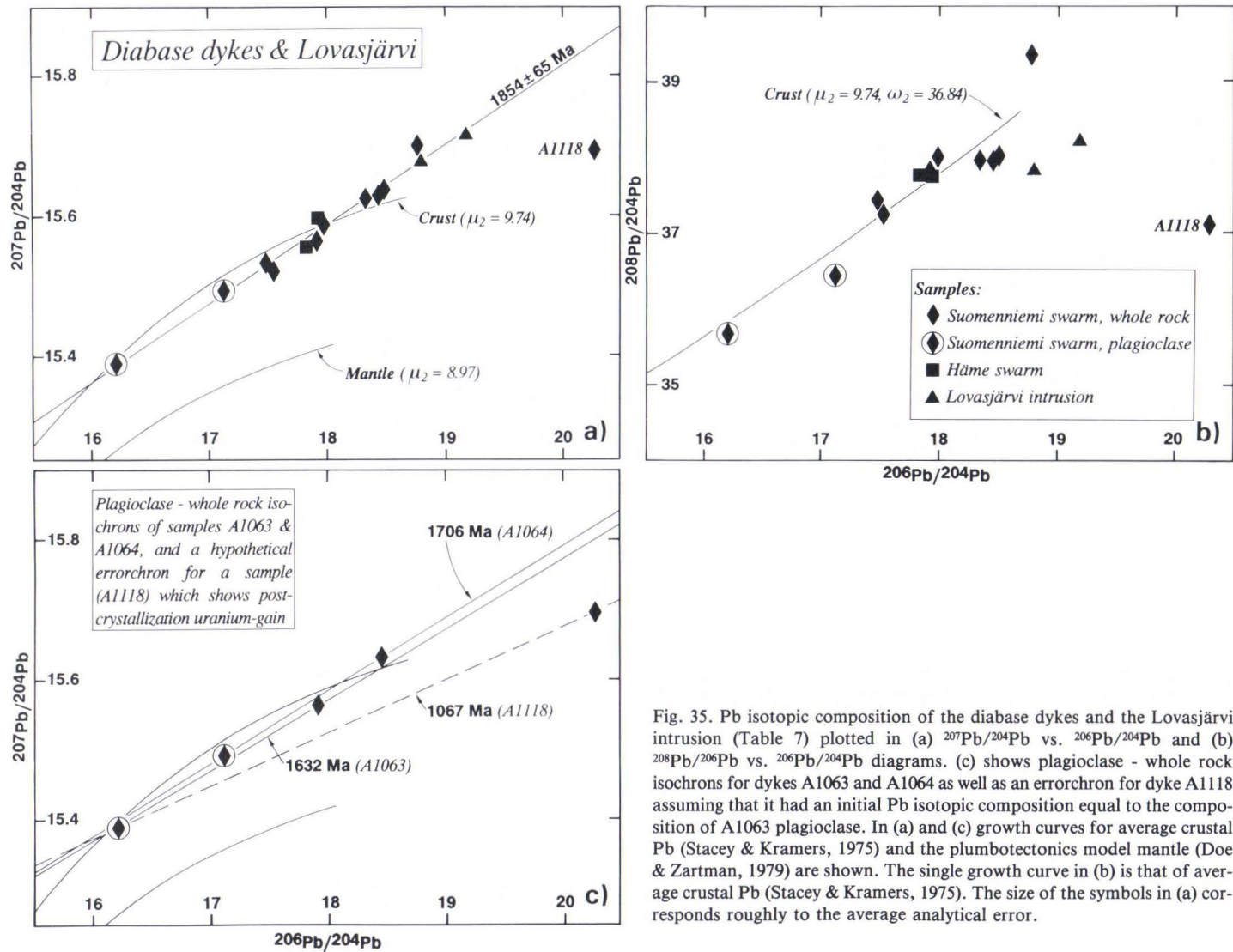


Fig. 35. Pb isotopic composition of the diabase dykes and the Lovasjärvi intrusion (Table 7) plotted in (a) $^{207}\text{Pb}/^{204}\text{Pb}$ vs. $^{206}\text{Pb}/^{204}\text{Pb}$ and (b) $^{208}\text{Pb}/^{206}\text{Pb}$ vs. $^{206}\text{Pb}/^{204}\text{Pb}$ diagrams. (c) shows plagioclase - whole rock isochrons for dykes A1063 and A1064 as well as an errorchron for dyke A1118 assuming that it had an initial Pb isotopic composition equal to the composition of A1063 plagioclase. In (a) and (c) growth curves for average crustal Pb (Stacey & Kramers, 1975) and the plumbotectonics model mantle (Doe & Zartman, 1979) are shown. The single growth curve in (b) is that of average crustal Pb (Stacey & Kramers, 1975). The size of the symbols in (a) corresponds roughly to the average analytical error.

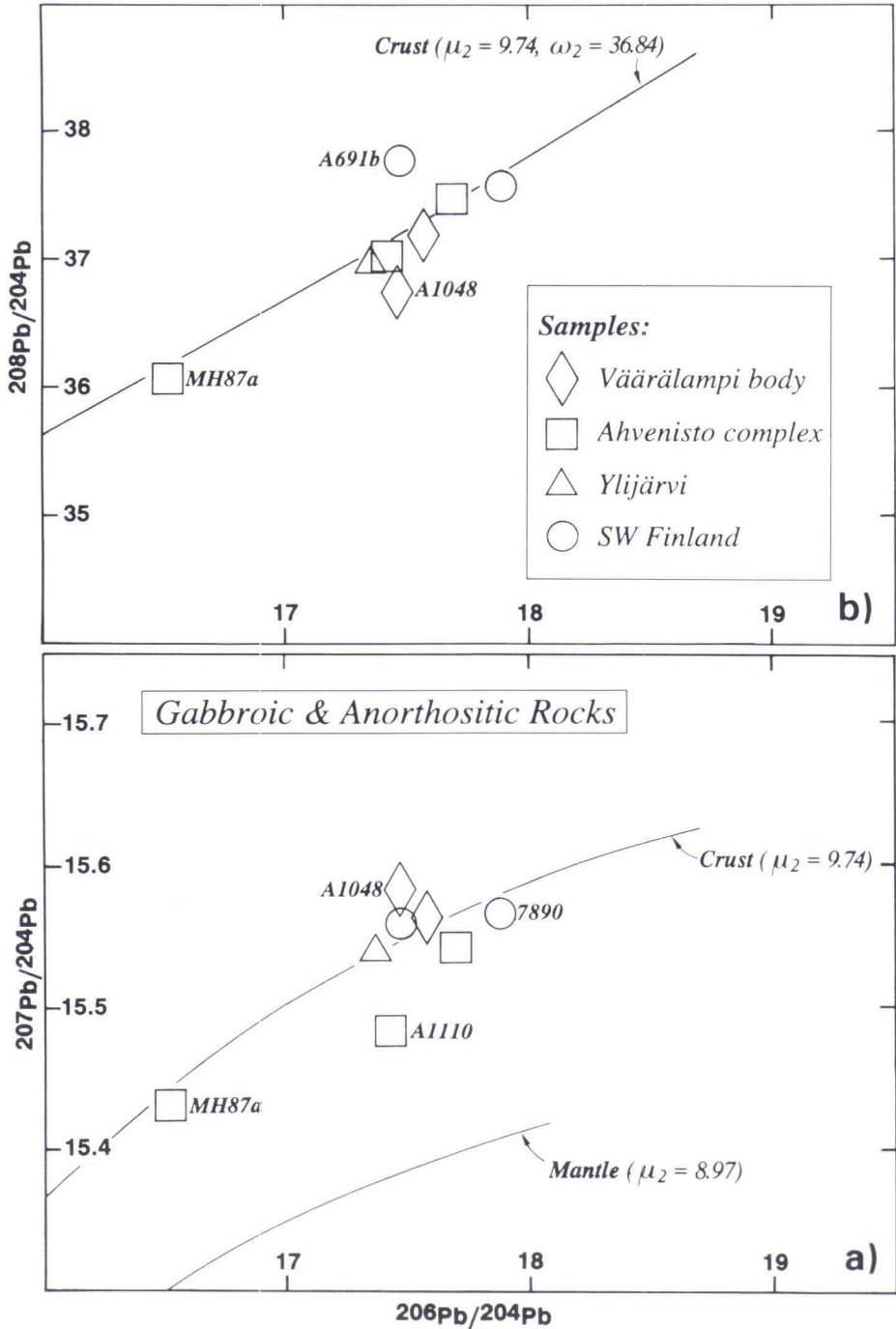


Fig. 36. Pb isotopic compositions of the gabbroic and anorthositic rocks (Table 7) plotted in (a) $^{207}\text{Pb}/^{204}\text{Pb}$ vs. $^{206}\text{Pb}/^{204}\text{Pb}$ and (b) $^{208}\text{Pb}/^{204}\text{Pb}$ vs. $^{206}\text{Pb}/^{204}\text{Pb}$ diagram. Growth curves in (a) and (b) are as in Figs. 35a and b, respectively. The size of the symbols in (a) corresponds roughly to the average analytical error.

growth curve of average crustal Pb, and the somewhat scattered whole rock data cluster around the crustal growth curve as well. The sample A1118 shows a lower Th/U ratio than the other samples, in accord with its high U content. No reasonable regression line can be fitted to the data.

Pb-Pb crystallization ages of 1632 Ma (dyke A1063) and 1706 Ma (dyke A1064) are calculated from the corresponding plagioclase-whole rock pairs (Fig. 35c). Dyke A1063 with the less radiogenic feldspar fraction gives an age that is consistent with the U-Pb zircon and baddeleyite determinations of the diabase dykes and the Lovasjärvi intrusion, which in turn suggests that the Pb isotopic composition measured for this plagioclase is possibly close to that in the dyke at the time of its crystallization. The higher calculated age (1706 Ma) of the sample A1064 could indicate that the dyke is older than the ages measured for the Subjotnian diabases so far. This age should not, however, be considered the actual crystallization age of the dyke, because excess radiogenic Pb in the feldspar fraction may have obscured the actual isochronous relationship of this particular feldspar-whole rock pair.

Gabbroic and anorthositic rocks

The gabbroic and anorthositic rocks show U concentrations from 0.081 ppm (MH87a anorthosite) to 0.93 ppm (A1048b gabbro) and Pb contents from 2.79 ppm (MH87a) to 14.13 ppm (A1048 leucogabbro), and, like the diabase dykes, exhibit relatively radiogenic isotope ratios of Pb. The U/Pb ratios are somewhat

lower than in the diabase dykes ranging from 0.029 to 0.100. The samples from the Väärälampi and Kolinummi intrusions differ from the other samples in having generally higher U and Pb concentrations. The anorthosite sample MH87a has the lowest U/Pb ratio and thus probably the smallest amount of extra radiogenic Pb. A μ_2 value of 9.67 and a second-stage model age of 1290 Ma are calculated for the sample MH87a according to the model of Stacey and Kramers (1975).

The Pb isotopic data of the gabbroic and anorthositic rocks are plotted in $^{207}\text{Pb}/^{204}\text{Pb}$ vs. $^{206}\text{Pb}/^{204}\text{Pb}$ and $^{208}\text{Pb}/^{204}\text{Pb}$ vs. $^{206}\text{Pb}/^{204}\text{Pb}$ diagrams in Fig. 36. In the $^{207}\text{Pb}/^{204}\text{Pb}$ vs. $^{206}\text{Pb}/^{204}\text{Pb}$ plot (Fig. 36a) the data exhibit moderate scatter and plot, like the Pb isotopic data on the diabase dykes, close to the evolution of average crustal Pb. The samples from the Ahvenisto complex have lower U/Pb ratios than the samples from the four other bodies. The olivine gabbro A1110 plots below the crustal growth curve and thus closer to the mantle evolution than the other samples. The anorthosite MH87a plots close to the growth curve of average crustal Pb. No reasonable linear trend can be fitted to the data on the Ahvenisto complex. The samples from the Väärälampi and Kolinummi bodies plot slightly above the average crustal growth curve. Sample A119 from the Ylijärvi anorthosite falls on the crustal growth curve, and the Höggrund leucogabbro 7890 plots slightly below it. In the $^{208}\text{Pb}/^{204}\text{Pb}$ vs. $^{206}\text{Pb}/^{204}\text{Pb}$ diagram (Fig. 36b) the samples plot again along the growth curve of average crustal Pb. The samples of the Ahvenisto complex fall along a regression line (not shown in Fig. 36b) with a calculated Th/U ratio of 3.95.

MAGMA EVOLUTION IN THE SUOMENNIEMI COMPLEX: SILICIC ROCKS AND ALKALI-FELDSPAR SYENITES

As is evident from the discussion above, the Suomenniemi complex comprises two major epi-

sodes of silicic magma intrusion. About 1640 Ma ago the granitic magmas that formed the bulk of

the Suomenniemi batholith were emplaced. This was followed (presumably at about 1635 Ma) by rifting associated with volumetrically minor injections of silicic magma through northwest-trending fissures, producing the quartz-feldspar porphyry dykes that cut the Suomenniemi batholith as well as its country rocks (cf. Appendix 4). In addition to the two episodes of silicic magma intrusion, a small amount of peralkaline intermediate magma was emplaced in the eastern Suomenniemi batholith, and is now observed as roughly northwest-trending syenitic dykes crosscutting the batholith.

The timing of the peralkaline magmatism is somewhat uncertain. As the alkali-feldspar syenite dykes cut the granites of the Suomenniemi batholith, the upper age limit for them is about 1640 Ma. The $^{207}\text{Pb}/^{204}\text{Pb}$ age of a zircon fraction in one of the dykes is 1629 ± 6 Ma (Vaasjoki et al., 1991), and hence on that basis the dyke could be roughly coeval with the quartz-feldspar porphyry dykes, or younger. There are no observations of cross-cutting quartz-feldspar porphyry and peralkaline dykes, but the trend of the dyke sets show that they were possibly emplaced along the same overall fracture system. If the quartz-feldspar porphyries and alkali-feldspar syenites represent two discrete melting episodes in the lower parts of the Svecofennian crust, they probably are not coeval and, in the light of the U-Pb zircon data, the latter may be the younger episode.

Processes producing chemical variation within felsic igneous suites

Chemical variation within felsic igneous suites can result from several processes. These include variable degrees of partial melting of the protolith and/or subsequent fractional crystallization (e.g., McCarthy & Hasty, 1976; Hanson, 1978), restite unmixing (White & Chappell, 1977; Chappell et al., 1987), wall-rock assimilation (Lee & Christiansen, 1983; Reece et al., 1990), magma mixing (Reid et al., 1983; Whalen & Currie, 1990),

A discussion of the magma evolution of the felsic rocks of the Suomenniemi complex thus needs to deal separately with (1) evolution of the granitic rocks constituting the bulk of the Suomenniemi batholith, (2) evolution of the quartz-feldspar porphyry dykes, and (3) evolution of the alkali-feldspar syenites. In order to provide the background to such discussion, selected major element vs. silica, trace element vs. silica, and compatible-incompatible element ratios vs. silica variation diagrams were constructed for the granites of the Suomenniemi batholith (Fig. 37) and for the quartz-feldspar porphyries and alkali-feldspar syenites (Fig. 38). Most of the variation diagrams show distinct compositional trends. In Fig. 37 constituents that generally are considered to behave compatibly in granitic magmas (e.g., Ca, Ti, Ba, Sr, and Sc) show declining trends with increasing silica, while incompatible constituents (Rb, F) exhibit increasing trends. The hornblende-clinopyroxene-fayalite granites form a distinct group in many of the diagrams (Figs. 37c, g, h, j, and n), as do the quartz-feldspar porphyry dykes and alkali-feldspar syenites in Fig. 38.

In the following, various mechanisms causing chemical variability in felsic igneous suites are discussed, methodology of modeling trace element variations in partial melting and crystallization is briefly reviewed, and an attempt is made to explain the compositional variations measured for the granites of the Suomenniemi batholith.

and various processes involving liquid fractionation (liquid immiscibility, fluid separation, thermogravitational diffusion; see Christiansen et al., 1984, and references therein).

The rapakivi granites, in accord with what is suggested for A-type granites in general, probably crystallized from relatively high-temperature, and consequently restite-poor, magmas (cf. Collins et al., 1982; Clemens et al., 1986; Whalen

et al., 1987). Hence the restite unmixing hypothesis can probably be rejected as a potential cause for the observed elemental variations. Incontrovertible petrographic evidence for unmixed restite component (e.g., strongly zoned plagioclase crystals with calcic cores or small aggregates of crystals presumably representing fragments of unmelted protolith; cf. Chappell et al., 1987) has not been found in the felsic rocks of the Suomenniemi complex, and the inflections in the variation diagrams (Figs. 37e, j, and k) are not expected to occur in trends caused by restite unmixing (cf. White & Chappell, 1977, p. 16; Chappell et al., 1987, p. 1125).

Likewise, wall-rock assimilation is not considered to have played a major role in the evolution of the felsic rocks of the Suomenniemi complex. Wall-rock assimilation would result in a variable initial isotopic composition of the radiogenic isotopes, provided that, in this case, differences existed in the isotopic composition of the rapakivi granite magma and the Svecofennian upper crust into which the granites were emplaced. No Nd isotopic data are available of the immediate country rocks of the Suomenniemi batholith, but evidence from the Tampere area some 150 km northwest of the Suomenniemi complex (Huhma, 1987) suggests that the Nd isotopic composition of the Svecofennian upper crust may be slightly less radiogenic than that measured for the felsic rocks of the Suomenniemi complex (see also the discussion on the basic rocks in this work). As regards Pb isotopes, the upper continental crust has in general a relatively high overall U/Pb ratio (e.g., Doe & Zartman, 1979) and it is easy, provided that the crust was differentiated in terms of the U/Pb ratio, to detect incorporation of such material into magmas derived from deeper sources. As will be shown later, incorporation of extra Pb and possibly also Nd are needed to explain differences encountered in initial Pb and Nd isotopic composition of the granites of the Suomenniemi batholith. It is improbable, however, that wall-rock assimilation was a major cause for the compositional varia-

tions observed.

Mixing of mafic mantle magmas and anatectic felsic melts has been invoked as a mechanism for generating chemical variation in certain granitoid suites. For example, in the Topsails A-type igneous suite in western Newfoundland metaluminous granites are considered to represent the result of mixing of a peralkaline magma and mafic magma, coupled with wall-rock assimilation and fractional crystallization (Whalen & Currie, 1990). Evidence for coeval silicic and basic magmas in the Suomenniemi complex are found in the silicic-basic composite dykes. One of the dykes shows the development of intermediate hybrid rocks in the contact zones of the two magmas (Fig. 16), while the other dykes (cf. Fig. 17) show very little silicic-mafic magma interaction, demonstrating the restricted miscibility of these contrasting magma types. Because the granite types in the Suomenniemi batholith are rather felsic and homogeneous throughout and because hardly any intermediate rocks are found in the Suomenniemi complex, it is improbable that mixing of the basic and the silicic anatectic melts alone could be responsible for the chemical variation measured for the granites of the batholith.

Regarding liquid fractionation processes, thermogravitational diffusion is considered to be important at the top of some very silicic magma chambers but is considered to be of minor importance in the evolution of alkali feldspar-rich granitoid rocks in general (Cullers & Graf, 1984). Immiscible fluoride and silicate liquids may form in fluorine-rich magmas, but the concentration of fluorine has to be very high (around 3 to 6 wt% in granitic liquids) for immiscibility to occur (cf. Christiansen et al., 1984, and references therein). Separation of a fluid phase as a major cause of chemical variation in the rapakivi granites is unlikely in the light of the overall dry nature of the bulk of the granites. Variable degrees of partial melting and fractional crystallization thus remain as the major candidates for the cause of the observed chemical variation.

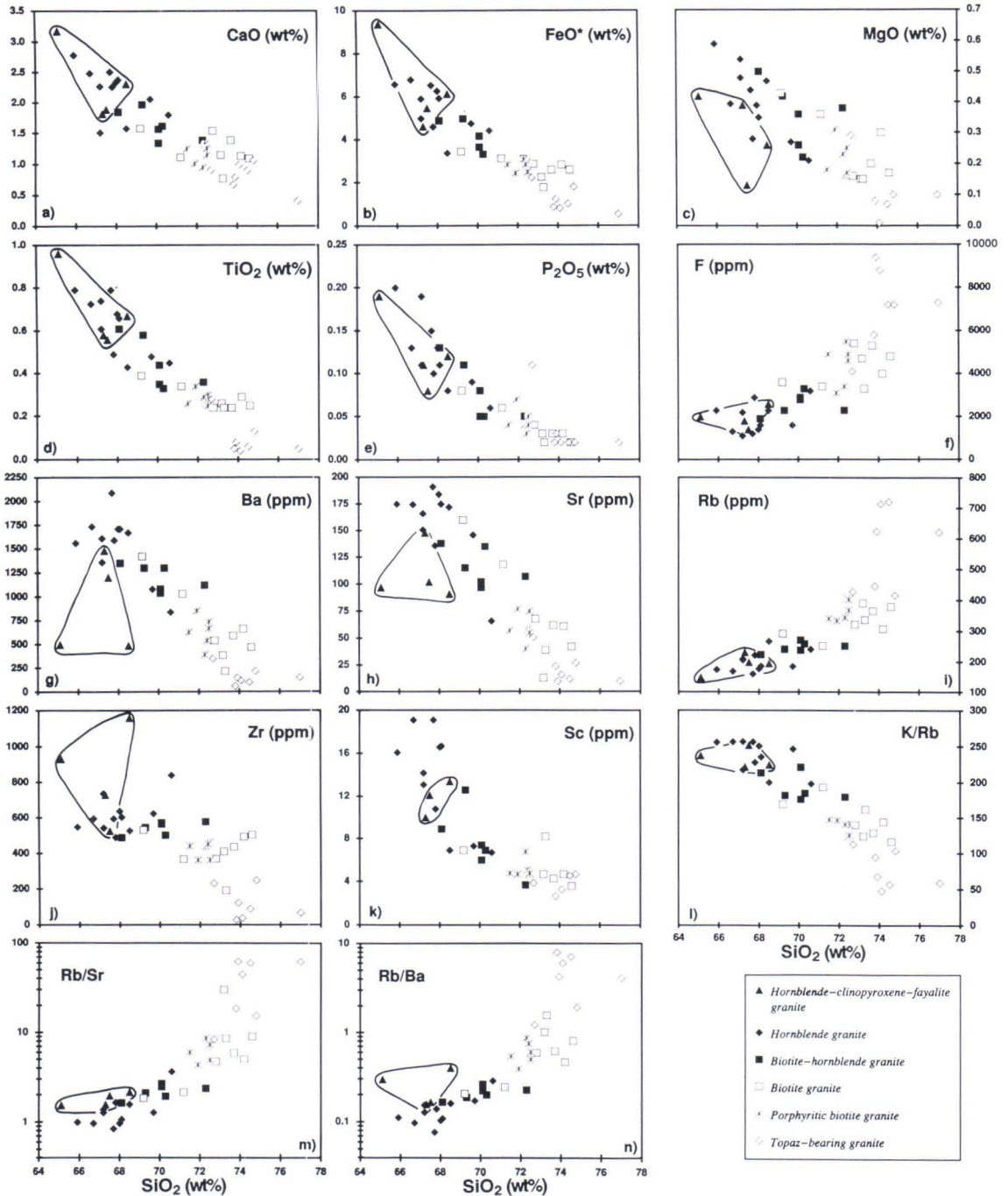


Fig. 37. The analyses of the granites of the Suomenniemi batholith (Appendix 1) plotted in (a) CaO vs. SiO₂, (b) FeO* vs. SiO₂, (c) MgO vs. SiO₂, (d) TiO₂ vs. SiO₂, (e) P₂O₅ vs. SiO₂, (f) F vs. SiO₂, (g) Ba vs. SiO₂, (h) Sr vs. SiO₂, (i) Rb vs. SiO₂, (j) Zr vs. SiO₂, (k) Sc vs. SiO₂, (l) K/Rb vs. SiO₂, (m) Rb/Sr vs. SiO₂, and (n) Rb/Ba vs. SiO₂ variation diagrams. Compositions of the hornblende-clinopyroxene-fayalite granites are enclosed. FeO* denotes total iron as FeO.

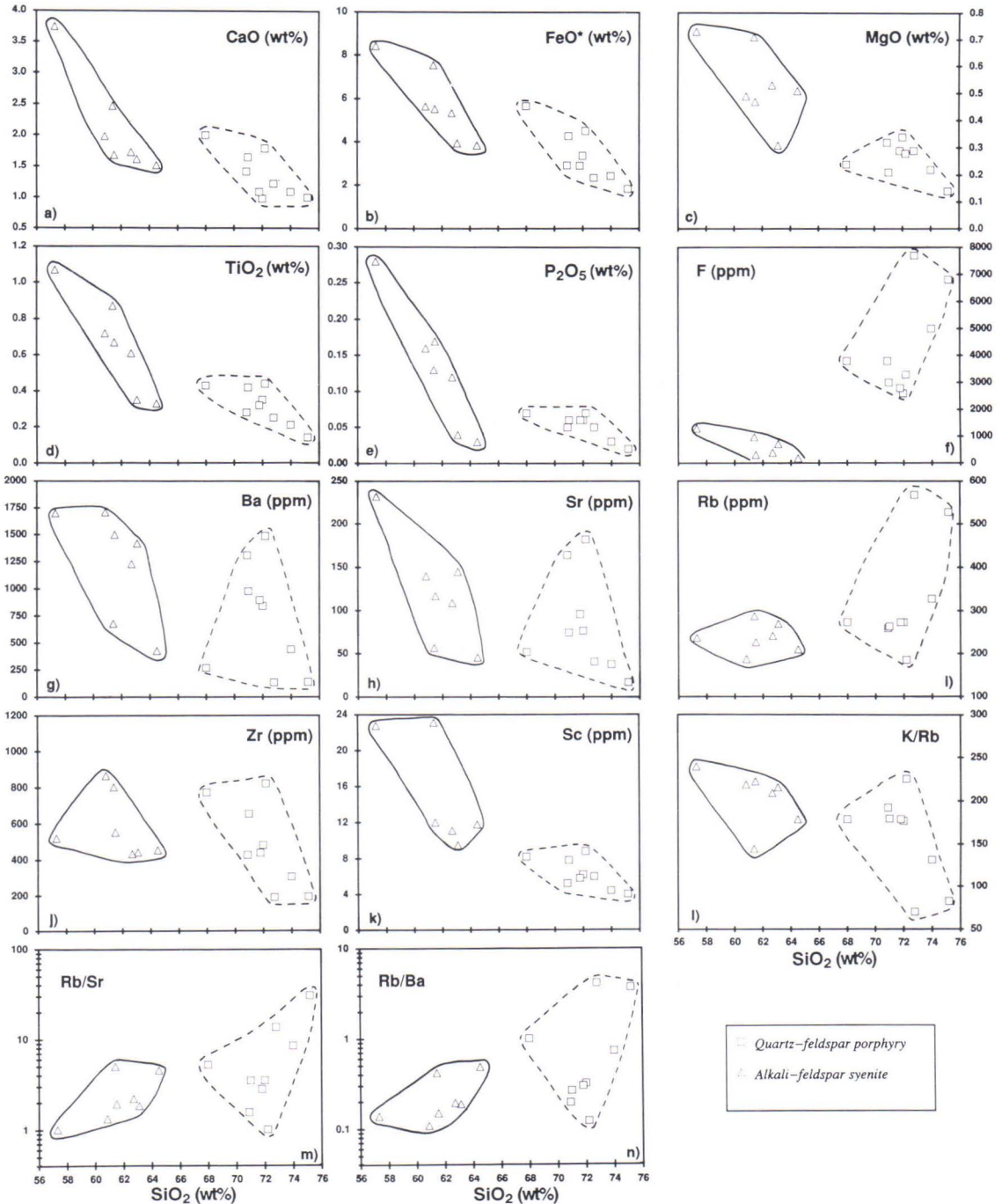


Fig. 38. The analyses of the alkali-feldspar syenites and quartz-feldspar porphyry dykes of the Suomenniemi complex (Appendix 1) plotted in (a) CaO vs. SiO₂, (b) FeO* vs. SiO₂, (c) MgO vs. SiO₂, (d) TiO₂ vs. SiO₂, (e) P₂O₅ vs. SiO₂, (f) F vs. SiO₂, (g) Ba vs. SiO₂, (h) Sr vs. SiO₂, (i) Rb vs. SiO₂, (j) Zr vs. SiO₂, (k) Sc vs. SiO₂, (l) K/Rb vs. SiO₂, (m) Rb/Sr vs. SiO₂, and (n) Rb/Ba vs. SiO₂ variation diagrams. FeO* denotes total iron as FeO.

Methodology of modeling partial melting and fractional crystallization

Several methods have been proposed for modeling the behavior of trace elements during generation and crystallization of silicate melts (cf. Allègre & Minster, 1978; Hanson, 1978). A widely used model to quantify trace element evolution during silicate melt generation is batch melting. In batch melting the trace elements in the melt and solid residue are expected to remain in equilibrium as melting proceeds until the melt is separated from the unmelted residue. Batch melting (Shaw, 1970) is described by the equation

$$(4) \quad C_L^i = \frac{C_o^i}{D_o^i + F(1-P^i)}$$

where C_L^i is the concentration of element i in the melt, C_o^i is the concentration of element i in the original solid, D_o^i is the bulk partition coefficient of element i in the original solid, F is the extent of partial melting, and P^i is the bulk partition coefficient in the mineral assemblage that enters into the liquid. The bulk partition coefficients D_o^i and P^i are the sums of the crystal/liquid partition coefficients of the minerals constituting the appropriate assemblages, weighted according to their weight proportions. If batch melting is modal, i.e. the melting mineral assemblage equals that of the original solid, equation (4) is simply

$$(5) \quad C_L^i = \frac{C_o^i}{D_o^i + F(1-D_o^i)}$$

(Shaw, 1970). Equation (5) shows that the smaller the extent of melting, F , is, the more the concentration ratio C_L^i/C_o^i deviates from unity, and that if the bulk partition coefficient D_o^i is larger than 1, the concentration ratio C_L^i/C_o^i approaches a limiting value of $1/D_o^i$ as F approaches zero (cf. Hanson, 1978, Fig. 1).

The most widely used model to assess trace ele-

ment evolution in crystallizing silicate melts is fractional crystallization that can be described by the equation

$$(6) \quad C_L^i = C_o^i F^{(D^i-1)}$$

where C_L^i is the concentration of element i in the residual melt, C_o^i is the concentration of element i in the initial melt, F is the fraction of melt left, and D^i is the bulk partition coefficient of the crystallizing mineral assemblage for element i . In this model, which is a modification of the Rayleigh distillation law (Rayleigh, 1896), equilibrium is assumed only between the surface of the crystallizing phases and the melt, and the precipitated minerals are assumed to become isolated from the residual melt by, for example, accumulation on the floor or the walls of the magma chamber.

Although batch melting and fractional crystallization models are idealized approximations of the melting and crystallization processes taking place in magma sources and chambers, they provide a reasonable basis on which to model partial melting and fractional crystallization in igneous systems (cf. Allègre & Minster, 1978; Cox et al., 1979). As regards silicic magma evolution, however, the fractional crystallization model may be questioned on the grounds that silicic magmas may be too viscous for the precipitated crystals to become isolated from the evolving magma. Such incomplete separation of the crystals results in compositional trends that consist of bands of variable width, rather than of simple curves, but these can be assessed by calculating the trace element evolution in the precipitated solids (cf. McCarthy & Hasty, 1976; Christiansen et al., 1988). In the high-temperature, largely liquid, F -bearing A-type magmas complications arising from incomplete separation of precipitated solids and liquid are probably of less importance than in other more viscous granitic magmas.

Evolution of the granites of the Suomenniemi batholith

The compositional variations shown in Fig. 37 suggest that the sequence hornblende granite — biotite-hornblende granite — biotite granites — topaz-bearing granite in the Suomenniemi batholith may constitute a single differentiation series, and could register various degrees of protolith partial melting or fractional crystallization. The hornblende-clinopyroxene-fayalite granites are distinct from the main variation sequence in having lower Ba and Sr contents, and higher Zr contents and Fe/Mg ratios than the hornblende granites with comparable SiO₂ (Figs. 37b, c, g, h, and j), indicating that they may belong to a different suite. This interpretation would also be consistent also with the field relations, as the hornblende-clinopyroxene-fayalite granites are found to cut the biotite-hornblende granites and hornblende granites of the batholith (Fig. 8). Because the hornblende-clinopyroxene-fayalite granites show little compositional variation the following discussion will focus on modeling the evolution of the sequence hornblende granite — biotite-hornblende granite — biotite granites — topaz-bearing granite.

Partial melting vs. fractional crystallization

To test whether the compositional variations in the granite sequence of the Suomenniemi batholith could be due to different degrees of partial melting or to fractional crystallization, variations in compatible trace element contents of the granites were used. As can be seen from Figs. 37g and h, Ba and Sr have obviously behaved as compatible elements over the course of differentiation sampled, showing decreasing trends from 2090 to 56 ppm and from 191 to <10 ppm, respectively (Appendix 1). Typical bulk D-values for Ba and Sr in feldspar-dominated rocks of the continental crust are on the order of 2 to 3 (Hanson, 1978; Christiansen et al., 1984), and hence relative variations caused

by different degrees of batch partial melting of such rocks would be 1/2 to 1/3 in terms of the C_L^i/C_0^i ratio (cf. equation [5]). Accordingly, batch melting of a typical crustal source with average abundances of about 250 ppm Ba and Sr (Taylor & McLennan, 1985) would yield maximum ranges of about 250 to 85 ppm for Ba and Sr. These ranges are considerably smaller than those observed in the granites of the Suomenniemi batholith and render variable degrees of partial melting of a feldspar-dominated source improbable as the cause for the observed chemical variations. This is even more true for protoliths with smaller amounts of feldspar due to their lower bulk D-values for Ba and Sr.

Fractional crystallization modeling

On the basis of the preceding discussion it appears that fractional crystallization could be the major cause for the observed chemical variations in the granites of the Suomenniemi batholith. Some indication of the fractionating minerals that could have controlled the magma evolution of the granites is given by the variation trends in Fig. 37. The declining CaO, FeO, MgO, TiO₂, P₂O₅, Ba, Sr, and Zr contents with increasing SiO₂ (Figs. 37a, b, c, d, e, g, h, and j) may have resulted from fractionation of feldspars, biotite, hornblende, pyroxene, Fe-Ti-oxides, apatite, and zircon. The decreasing K/Rb ratios (Fig. 37l) and increasing Rb/Sr and Rb/Ba ratios (Figs. 37m and n), however, suggest that alkali feldspar is needed in the fractionating mineral assemblage and that major biotite fractionation probably did not take place. Furthermore, the distinctive positive correlation in the F vs. SiO₂ diagram (Fig. 37f) suggests that amphibole or biotite may have not been major fractionating phases. If the whole range of differentiation sampled reflects the evolving magma composition, fractionation of zircon may

Table 8. Composition of olivine, clinopyroxenes, amphiboles, alkali feldspar, ilmenite, and garnet in the granites and alkali-feldspar syenites of the Suomenniemi complex.

Sample	Olivine		Clinopyroxenes		Amphiboles		Alkali feldspar	Ilmenite	Garnet
	A1130 [1]	A1130 [3]	A1164 [1]	A1111 [2]	A1130 [2]	A1045 [3]	A1130 [1]	A1130 [1]	A1164 [1]
SiO ₂ (wt%)	29.39	47.47	49.01	52.57	39.97	39.01	68.82	0.03	34.75
TiO ₂	0.00	0.31	0.14	0.04	0.47	2.05	0.04	51.11	1.23
Al ₂ O ₃	0.04	0.85	0.68	0.45	9.60	9.14	20.10	0.00	0.33
FeO ^a	68.87	29.22	29.46	29.92	31.38	30.81	0.08	47.71	31.72
MnO	1.40	0.54	0.55	0.44	0.40	0.33	0.00	0.65	0.67
MgO	0.72	1.45	1.36	1.58	1.55	1.60	0.00	0.02	0.04
CaO	0.00	19.75	14.00	5.98	10.39	10.42	0.11	0.00	31.23
Na ₂ O	0.00	0.27	4.45	8.62	1.77	1.75	1.18	0.05	0.09
K ₂ O	0.00	0.01	0.00	0.02	1.48	1.73	9.18	0.00	0.00
Cr ₂ O ₃	0.00	0.02	0.02	0.00	0.00	0.00	0.00	0.22	0.00
NiO	0.07	0.02	0.11	0.01	0.02	0.08	0.00	0.00	0.08
Total	100.49	99.93	99.78	99.62	97.03	96.92	99.51	99.79	100.14
End-member compositions (mole%):									
	Fo ^b 1.8	Wo ^b 44.3					An 0.8		
	Fa ^b 98.2	En ^b 4.5					Ab 16.2		
		Fs ^b 51.2					Or 83.0		

Note: Electron microprobe analyses by Walter Boyd. Numbers in square brackets denote the number of measurements.

^a Total Fe reported as FeO.

^b Calculated assuming all Fe as Fe²⁺.

have begun relatively late in the crystallization sequence (this is indicated by the marked inflection at about 71 wt% SiO₂ in Fig. 37j), whilst fractionation of apatite could have been more effective at the early stages (less pronounced but yet clear inflection at about 70 wt% SiO₂ in Fig. 37e). As regards fractionation of phases concentrating the LREE (e.g., allanite, monazite), Fig. 21a indicates that they may have been precipitated rather late in the sequence, probably during the interval from the biotite granites to the topaz-bearing granites.

In order to get a more quantitative picture of possible fractional crystallization processes in the Suomenniemi batholith, the least-squares major element approximation method was used to assess possible fractionating mineral assemblages which could have shifted the composition of the evolving magma from an assumed initial magma composition to an assumed evolved composition. These major element constraints were then used to model trace element variations according to the Rayleigh distillation law (equation [6]) using Ba, Sr, and Rb. The calculations were performed using the least-squares approximation program MAGFRAC (Morris, 1984) and the

trace element modeling program MODULUS (Knoper, 1989).

The first premise examined was whether the range of measured compositions (cf. Fig. 37) could represent daughter liquids from a common parent magma. In principle, this might have been possible in the F-rich, relatively low-viscosity rapakivi granite magmas, although incomplete separation of precipitated crystals from residual magma may be a more normal case in silicic magmas (cf. Tindle & Pearce, 1981). For an assumed initial liquid, the composition of hornblende granite O202.1 from the eastern flank of the Suomenniemi batholith (cf. Appendix 4) was used. The rock is a medium-grained, slightly porphyritic granite collected near the outer contact of the batholith. It is relatively low in silica (SiO₂ = 67.7 wt%) and has the highest Ba and Sr contents (2090 and 91 ppm, respectively) as well as the lowest Rb content (160 ppm) of all the analysed granites. The composition of the most siliceous topaz-bearing granite M664.1b from the north-central part of the batholith was used for the assumed most evolved liquid composition. This granite contains 77.0 wt% SiO₂, 151 ppm Ba, and < 10 ppm Sr and has a high abundance

Table 9. Mineral compositions used for major element least-squares approximation calculations of the granites of the Suomenniemi batholith.

	Hornblende	Biotite	Plagioclase	Alkali feldspar	Clinopyroxene	Fayalite	Oxide	Apatite
SiO ₂ (wt%)	40.28	36.18	64.78	66.91	47.53	29.27	0.08	0.00
TiO ₂	2.11	3.27	0.00	0.08	0.31	0.00	26.16	0.00
Al ₂ O ₃	9.79	13.30	20.74	19.96	0.85	0.04	0.15	0.00
FeO	32.19	36.87	0.82	0.06	29.26	68.58	73.14	0.16
MnO	0.29	0.21	0.00	0.01	0.54	1.39	0.38	0.29
MgO	1.51	1.37	0.32	0.00	1.45	0.72	0.04	0.00
CaO	10.36	0.40	2.60	0.10	19.78	0.00	0.02	56.54
Na ₂ O	1.64	0.40	9.33	0.94	0.27	0.00	0.03	0.09
K ₂ O	1.85	8.01	1.40	11.94	0.01	0.00	0.00	0.00
P ₂ O ₅	0.00	0.00	0.00	0.00	0.00	0.00	0.00	42.92
Total	100.00	100.00	100.00	100.00	100.00	100.00	100.00	100.00

Note: Feldspar end-member compositions are An₁₂Ab₈₀Or₈ and An_{0.5}Ab_{10.5}Or₈₉.

Table 10. Least-squares major element modeling of the granites of the Suomenniemi batholith. See text for details.

	MODEL A			MODEL B			MODEL C			MODEL D		
Fractionating assemblage:												
	47%	alkali feldspar		41%	alkali feldspar		67.5%	alkali feldspar		60%	alkali feldspar	
	17%	plagioclase		plagioclase		plagioclase		plagioclase	
	hornblende		53%	hornblende		hornblende		15.5%	hornblende	
	biotite		biotite		biotite		1.5%	biotite	
	quartz		1%	quartz		15.5%	quartz		21.5%	quartz	
	24%	clinopyroxene		clinopyroxene		12.5%	clinopyroxene		clinopyroxene	
	5%	fayalite		fayalite		2%	fayalite		fayalite	
	6.5%	oxide		3%	oxide		2.3%	oxide		0.6%	oxide	
	0.5%	apatite		2%	apatite		0.2%	apatite		0.9%	apatite	
F ^a	0.59			0.68			0.64			0.60		
ΣR ^{2b}	< 0.05			< 0.09			< 0.24			< 0.36		
Model liquid compositions:												
	Initial Assumed	Initial Calculated	Evolved Assumed	Initial Assumed	Initial Calculated	Evolved Assumed	Initial ^d Assumed	Initial Calculated	Evolved Assumed	Initial Assumed	Initial Calculated	Evolved Assumed
SiO ₂	68.25	68.25	77.45	as in A	68.25	as in A	73.38	73.38	as in A	as in C	73.37	as in A
TiO ₂	0.80	0.79	0.05		0.69		0.28	0.28			0.28	
Al ₂ O ₃	13.11	13.09	13.18		13.17		13.06	13.25			13.29	
FeO ^c	6.59	6.60	0.54		6.63		2.79	2.79			2.79	
MnO	0.11	0.11	0.03		0.08		0.04	0.06			0.04	
MgO	0.44	0.24	0.10		0.32		0.22	0.13			0.16	
CaO	2.53	2.54	0.41		2.42		1.21	1.21			1.12	
Na ₂ O	3.03	3.07	3.76		2.94		2.94	2.62			2.56	
K ₂ O	4.98	5.00	4.46		4.89		6.03	5.74			5.67	
P ₂ O ₅	0.15	0.13	0.02		0.30		0.04	0.04			0.16	

Note: The analyses were normalized to 100% total for the modeling.

^a Fraction of residual liquid remaining.

^b Sum of the squares of the residuals.

^c Total Fe reported as FeO.

^d Trace element abundances in the initial assumed magma of model C are (in ppm): Rb 352, Sr 62, Ba 643, Zr 406, La 140, Ce 322, Nd 112, Sm 20.5, Eu 1.8, Tb 2.1, Yb 8, Lu 1, Zn 83, Ga 24, Nb 41, Y 113.

of Rb (622 ppm). It should be noted in this context that several petrographic and geochemical features (e.g., occurrence of primary magmatic topaz and cassiterite; Haapala, 1977a; Haapala & Rämö, 1990) indicate that the topaz-bearing granites of the Finnish rapakivi granite intrusions are an integral part of their magma evolution and hence they need to be included in fractional crystallization models.

In regard to compositions of fractionating minerals, microprobe data shown in Table 8 coupled with published mineral analyses were utilized. The compositions listed in Table 8 were used for clinopyroxene and fayalite. Data from Simonen and Vormaa (1969, Table 6, analysis no. 1) was used for biotite, and the average of the amphibole compositions in Table 8 and in Simonen and Vormaa (1969, Table 4, analysis no. 2) for hornblende. Average of the composition in Table 8 and the mean of the alkali feldspar data of Törnroos (1984, Table 7b) was used for alkali feldspar, while an oligoclase composition reported by Deer et al. (1963a, Table 14, analysis no. 4) was used for plagioclase. The composition of apatite was taken from Deer et al. (1963b, Table 50, analysis no. 3) and a combined composition of ilmenite in Table 8 and magnetite from Haapala & Ojanperä (1972b, Table 2, analysis no. 4) was used for the Fe-Ti-oxide. For trace element modeling, commonly used crystal/liquid distribution coefficients determined for silicic magmas were applied (Appendix 3). Mineral compositions used in the major element calculations are listed in Table 9 normalized to 100% volatile free.

Major element modeling was performed using various permutations of quartz, alkali feldspar, plagioclase, biotite, hornblende, clinopyroxene, fayalite, oxide, and apatite. The best fit was obtained by subtracting 19% alkali feldspar, 10% clinopyroxene, 7% plagioclase, 2.7% oxide, 2% fayalite, and 0.3% apatite from the assumed initial liquid with 59% residual liquid remaining. The sum of the squares of the residuals, ΣR^2 , for this fit is <0.05 , and the calculated model

composition is listed, together with the compositions of the assumed liquids, as model A in Table 10. A somewhat less precise fit ($\Sigma R^2 < 0.09$) was obtained by subtracting 17% hornblende, 13% alkali feldspar, 1% oxide, 0.6% apatite, and 0.4% quartz with 68% residual liquid. This model is shown in Table 10 as B. Other mineral assemblages either turned out to be impossible to subtract or yielded fits with larger ΣR^2 's.

The fractionating mineral assemblage of model A is more compatible with petrographic observations because mafic silicates that could have controlled the composition of the relatively H_2O -poor rapakivi granite magma are more likely to be anhydrous; the hydrous mafic silicate, hornblende, in model B fractionate is invariably found filling the interstices between feldspars and quartz, reflecting its relatively late precipitation from the magma. Furthermore, it has been shown (Clemens et al., 1986) that an early-formed clinopyroxene may react with the residual magma to form hydrous ferromagnesian silicates in A-type melts. In the Suomenniemi batholith, some evidence for such early anhydrous ferromagnesian silicates is provided by amphibole and oxide pseudomorphs and fayalite relics that are commonly found enclosed in the hornblende of the hornblende granites and biotite-hornblende granites.

The major element models A and B were tested in an attempt to model the evolution of Ba, Rb, and Sr. The results are shown in Figs. 39a and b. The suggested values of residual liquid remaining are much too large for the models to account for the measured data ranges. This renders fractional crystallization models A and B difficult to defend. The fact that fractional crystallization using the most primitive sample as the initial liquid results in models with too narrow trace element evolutionary ranges suggests that the low-silica granites (i.e., the hornblende granites and the biotite-hornblende granites) may carry varying amounts of cumulate components in them. Accordingly, composition more silicic than sample O202.1 may represent a more true initial

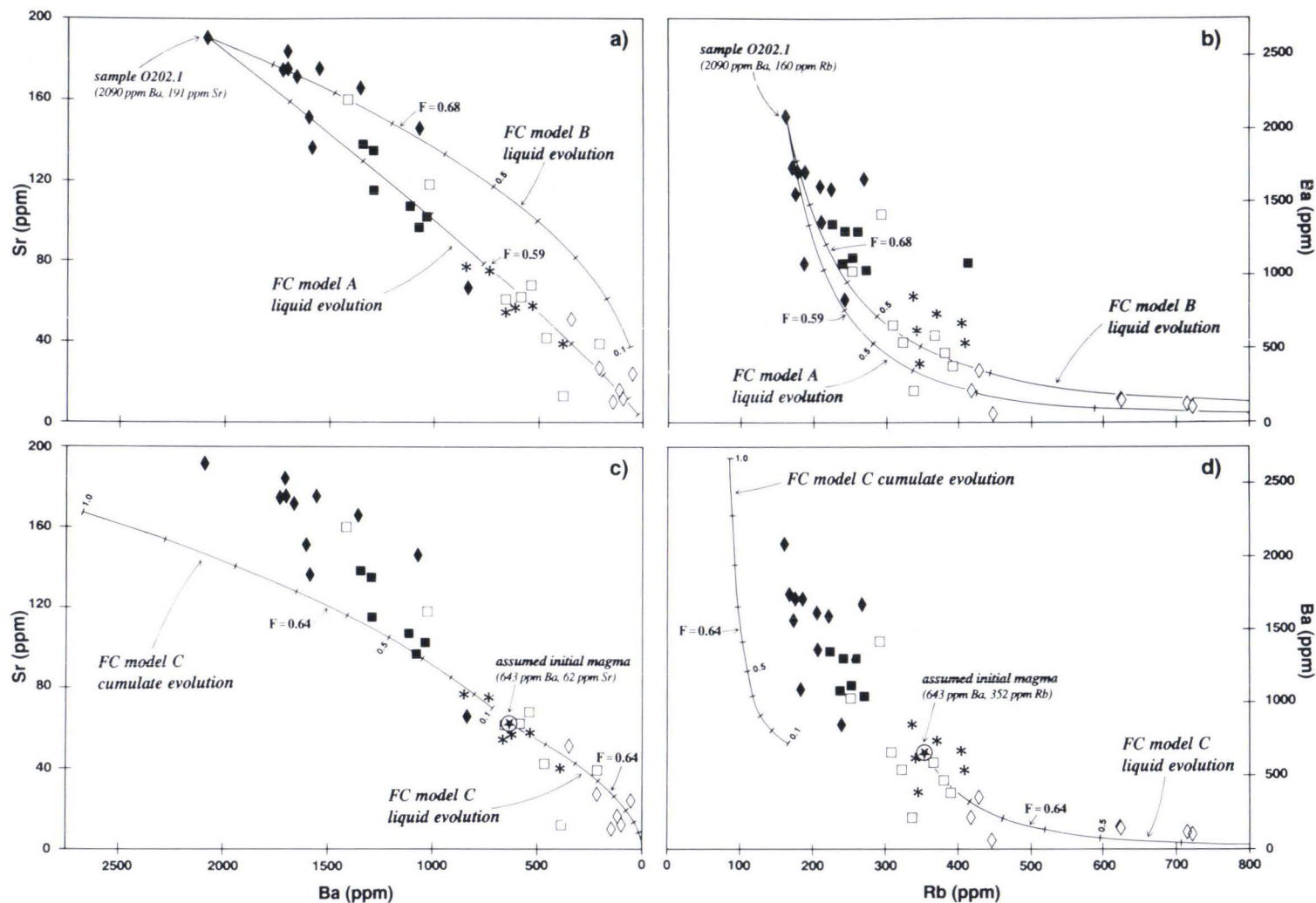


Fig. 39. Fractional crystallization (FC) modeling of the granites of the Suomenniemi batholith shown in Sr vs. Ba (a and c) and Ba vs. Rb (b and d) variation diagrams. (a) and (b) demonstrate liquid evolution for FC models A and B (Table 10) assuming initial magma composition as the most primitive granite O202.1 (68.3% SiO₂, volatile free). (c) and (d) exhibit both liquid and cumulate evolution for FC model C (Table 10) with a more felsic (73.4% SiO₂, volatile free) assumed initial magma. Tick marks along the evolutionary paths indicate the amounts residual liquid remaining (F). The termination point for each model is noted. Symbols as in Fig. 2.

liquid composition.

Selecting an appropriate, more silicic, initial liquid composition is somewhat arbitrary but as the bulk of the exposed parts of the Suomenniemi batholith consists of biotite granite (Appendix 4) this should probably constitute a major component in such a composition. Because most of the biotite-hornblende granites are also relatively low in silica, only the biotite granites were used to estimate an initial magma composition. Rejecting biotite granite L871.1 that is low in SiO_2 and four granites (M114.2, O155.1, O209.2, and O242.1) showing high SiO_2 (see Appendix 1) results in an average composition with 73.38 wt% SiO_2 (normalized to 100% volatile free). Using this as the initial liquid and sample M664.1b for the evolved liquid results in a best-fit assemblage of 24.6% alkali feldspar, 5.7% quartz, 4.5% clinopyroxene, 0.8% oxide, 0.7% fayalite, 0.1% apatite, and 63.6% residual liquid with $\Sigma R^2 < 0.24$. This is shown in Table 10 as model C. Model C differs from model A mainly in showing a lower predicted Na/K ratio, and in having quartz but no plagioclase in the fractionating assemblage. The modeling was performed also using hydrous mafic minerals instead of clinopyroxene and fayalite and this yielded a best-fit of 24% alkali feldspar, 8.5% quartz, 6.3% hornblende, 0.5% biotite, 0.4% apatite, 0.3% oxide, and 60% residual liquid with $\Sigma R^2 < 0.36$. This is shown in Table 10 as model D.

Applying the constraints of the two latter major element models to trace element modeling results in almost identical evolutionary paths of which those of model C are shown in Figs. 39c and d. Model C is preferred as it yields a better major element fit and because the calculated assemblage is more in concert with petrographic observations. In the Sr vs. Ba plot (Fig. 39c) the composition of the residual liquid at $F = 0.64$ is 154 ppm Ba and 29 ppm Sr, which is close to the assumed evolved liquid composition, although Sr is somewhat higher in the modeled liquid. In the Ba vs. Rb plot (Fig. 39d) the modeled liquid

reproduces the trend from the biotite granites to the least fractionated topaz-bearing granites, but is unable to account for the very high Rb contents of the most fractionated topaz-bearing granites (at $F = 0.60$ $\text{Rb} = 496$ ppm). The high Rb contents of these granites may have been caused by post-magmatic autometasomatic processes, which have been suggested as not uncommon in the late topaz-bearing granites of the Finnish rapakivi granite batholiths (cf. Haapala, 1977a). Such secondary processes may also have been responsible for the very low Sr abundances in these granites (Fig. 39c). As regards minor phases, fractionating 0.11% zircon and 0.16% allanite from the model C initial liquid reproduces the low Zr (68 ppm) and Ce (85 ppm) contents in the sample M664.1b used for the assumed evolved liquid composition.

In Fig. 39d the low-silica granites (hornblende granites and biotite-hornblende granites) plot between the evolutionary curves for residual liquid and cumulate. This is consistent with the hypothesis that these granites are cumulus-enriched rocks with variable degrees of precipitated crystals and trapped liquid. In Fig. 39c the hornblende granites and biotite-hornblende granites are somewhat offset from the cumulate evolution curve, but nevertheless identify themselves as cumulates. Due to the approximate nature of the modeling it is impossible to define the proportions of cumulate material and trapped liquid in the low-silica granites.

The hypothetical parental magma of the main granite sequence of the Suomenniemi batholith has 322 ppm Ce and 8.4 ppm Yb. As far as the LREE are concerned, this is between what is measured for the probably cumulate-enriched sample A1043 and for the biotite granite A1041 that shows the highest contents of the REE (Table 1, Appendix 1). The Ce content in the hypothetical parent magma is 0.77 times that in sample A1041. Using this difference also for the other REE and Nd and Sm contents measured for the biotite-hornblende granite sample A1040 yields a hypothetical REE pattern with La/Yb ratio of

11.8 (Fig. 40). Using the fractional crystallization model C major mineral assemblage (Table 10) with 0.17% allanite and 0.13% zircon results in a pattern that matches with the La and Ce measured for one of the most fractionated topaz-bearing granites (sample A1097, Table 1) but is far from being consistent with the middle and heavy REE contents observed. Although being only approximate, this model is consistent with earlier suggestions (e.g., Nurmi & Haapala, 1986) that the characteristic deep Eu minimum and HREE enrichment in the late-stage topaz-bearing granites cannot be the result of fractional crystallization alone. Processes such as postmag-

matic albitization (deep negative Eu anomaly) and greater relative stability of HREE alkali-fluoride complexes in the residual F-rich magmas (higher HREE) have been proposed as responsible for these anomalous features (Nurmi & Haapala, 1986).

In conclusion, the fractional crystallization models indicate that the magma evolution of the main granite sequence (hornblende granite — biotite-hornblende granite - biotite granites — topaz-bearing granite) of the Suomenniemi batholith may have involved a felsic parental magma (73.4 wt% SiO₂, calculated volatile free) precipitating alkali feldspar, quartz, mafic sili-

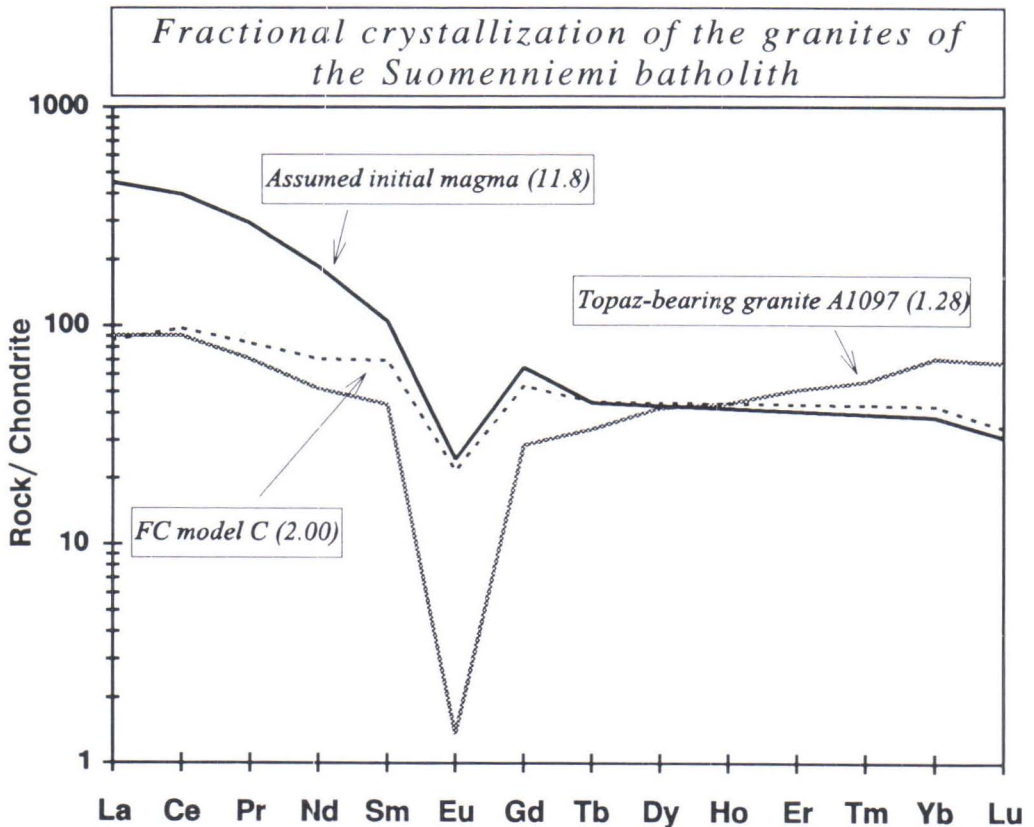


Fig. 40. Rare earth element contents in the assumed initial magma of the Suomenniemi batholith (solid pattern, cf. Table 10) as well as in the topaz-bearing granite A1097 (Table 1) normalized against chondrite composition. Also shown is the fractional crystallization model C (Table 10) product (dashed pattern) from the initial composition with 0.17% allanite and 0.13% zircon in the fractionate. Numbers in parentheses indicate normalized La/Yb ratios.

cates, and Fe-Ti-oxide in the ratio 68/15/15/2, totalling about 35% of the original mass of the magma, as well as minor amounts of apatite, zircon, and a LREE-phase. In this model, the hornblende granites and the biotite-hornblende granites are cumulus-enriched and the biotite granites and the topaz-bearing granites represent liquids. Because the major fractionating mineral is alkali feldspar, the resulting cumulate-bearing rocks should be relative enriched in it. This is consistent with the modal composition of the granites: the alkali feldspar/plagioclase ratio is highest in the hornblende granites and declines in the differentiation sequence toward the topaz-bearing granites (Fig. 2). As the geological map (Appendix 4) shows, those granites identified as cumulates are found in the southern and southeastern parts of the Suomenniemi batholith, while the late-stage topaz-bearing granites are located exclusively in the northern and northwestern parts. If, as is suggested by Vormaa (1972) and Vaasjoki et al. (1991), the Suomenniemi batholith predates the Wiborg batholith, this could mean that the intrusion of the latter tilted the Suomenniemi batholith to the north-northwest, and thus the present-day erosional section is deeper in the southern and southeastern parts of the batholith.

Isotopic implications

The initial Nd isotopic compositions of the granites of the Suomenniemi batholith do not correlate with the chemical composition of the samples, except for the most fractionated topaz-bearing granite A1097 that has a somewhat lower $\epsilon_{Nd}(T)$ value than the bulk of the granites (Table 3, Fig. 32). The more negative ϵ_{Nd} value is consistent with assimilation of unradiogenic upper crustal material during the evolution of the batholith. As regards the Salmi batholith, the different (in this case more positive) ϵ_{Nd} value of the topaz-bearing granite 6896 compared with the more negative ϵ_{Nd} value of the less fractionated biotite granite 9202 could also be explained by high-level contamination by Proterozoic crustal

material that in this case is more radiogenic than the parental magma from the lower crust. This would, however, require a more radiogenic source for the magma of the Sotjärvi batholith, and imply that the two Soviet Karelian batholiths were derived from sources with distinct Nd isotopic compositions.

Because all but one of the granites of the Suomenniemi batholith show a random ϵ_{Nd} -compositional distribution, combined assimilation—fractional crystallization modeling was not applied to them. The average $\epsilon_{Nd}(T)$ value of the non-topaz-bearing granites is considered as indicative of the average Nd isotopic composition of the source of the magma from which the granites of the Suomenniemi batholith were crystallized, and, provided that the source was crustal, also of the isotopic composition of the lower continental crust in that area.

In contrast to the Nd data, the Pb isotopic compositions of the various granite types show isotopic-compositional correlations. In Fig. 41 the Pb isotopic data on the hornblende granites, biotite-hornblende granites and biotite granites, and topaz-bearing granites are shown along with the data on the hornblende-clinopyroxene-fayalite granites. In the $^{207}\text{Pb}/^{204}\text{Pb}$ vs. $^{206}\text{Pb}/^{204}\text{Pb}$ diagram (Fig. 41a), the hornblende granites and the hornblende-clinopyroxene-fayalite granites show the highest relative $^{207}\text{Pb}/^{206}\text{Pb}$ ratios (the average μ_2 values for the Pb in the alkali feldspars are 9.85 and 9.91, respectively), the topaz-bearing granites have the lowest ratios (average μ_2 value 9.57), and the biotite-hornblende granites and the biotite granites are intermediate between these two extremes (μ_2 averages 9.74). Moreover, the data on the non-topaz-bearing granites define linear trends yielding rough age estimates that are consistent with U-Pb zircon determinations, but the linear trend of the topaz-bearing granites has an age (1250 ± 58 Ma) that cannot be matched with the actual crystallization age of the batholith. A comparable difference between the rock types is established also in the $^{208}\text{Pb}/^{206}\text{Pb}$ vs. $^{206}\text{Pb}/^{204}\text{Pb}$ diagram (Fig. 41b) in

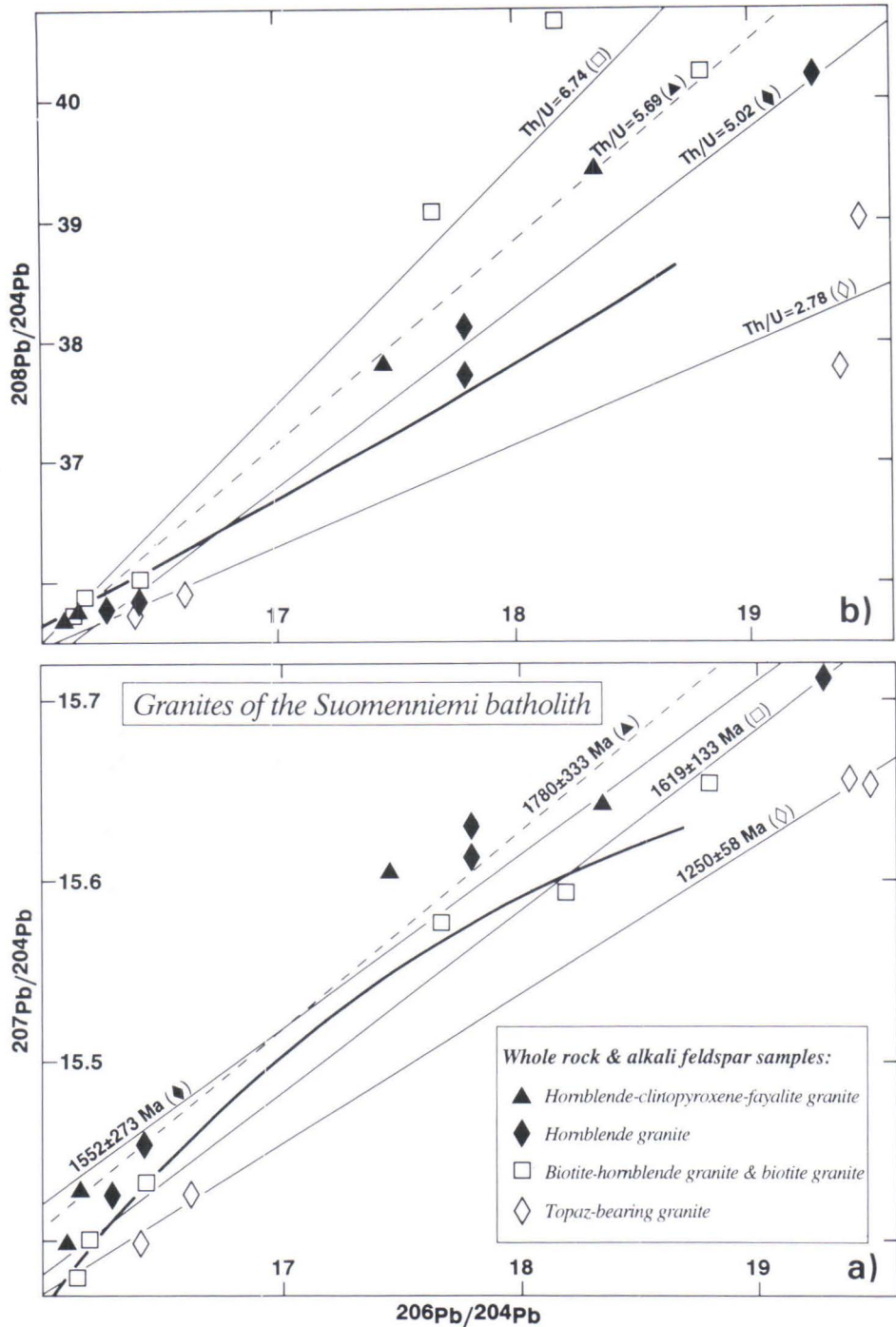


Fig. 41. Pb isotopic composition (Tables 5 and 6) of the granites of the Suomenniemi batholith plotted in (a) $^{207}\text{Pb}/^{204}\text{Pb}$ vs. $^{206}\text{Pb}/^{204}\text{Pb}$ and (b) $^{208}\text{Pb}/^{206}\text{Pb}$ vs. $^{206}\text{Pb}/^{204}\text{Pb}$ diagrams. Individual errorchrons are shown for the hornblende-clinopyroxene-fayalite granites ($1780 \pm 333\text{Ma}$, $\text{Th}/\text{U} = 5.69$), hornblende granites ($1552 \pm 273\text{Ma}$, $\text{Th}/\text{U} = 5.02$), biotite-hornblende granites and biotite granites ($1619 \pm 133\text{Ma}$, $\text{Th}/\text{U} = 6.74$), and topaz-bearing granites ($1250 \pm 58\text{Ma}$, $\text{Th}/\text{U} = 2.78$). Thick curves denote evolution of average crustal Pb (Stacey & Kramers, 1975).

which the data on the topaz-bearing granites have a considerably lower calculated Th/U ratio.

The declining alkali feldspar $^{207}\text{Pb}/^{206}\text{Pb}$ ratios in the sequence hornblende granite — biotite-hornblende granite — biotite granite — topaz-bearing granite can not be explained by closed-system fractional crystallization but require incorporation of extra Pb with a lower $^{207}\text{Pb}/^{206}\text{Pb}$ ratio than that in the initial magma. In terms of the fractional crystallization model C (Table 10) this implies that the cumulus-enriched granites may have initial $^{207}\text{Pb}/^{206}\text{Pb}$ ratios close to those of the initial magma and that the more felsic granites (especially the topaz-bearing ones) have ratios affected by extra Pb incorporated into the evolving magma, reflecting the earlier separation of the cumulus-enriched granites from the melt.

The unexpectedly young age, 1250 ± 58 Ma, of the topaz-bearing granite whole-rock—alkali feldspar linear trend suggests that these granites have not remained as closed systems after crystallization, and is indicative of post-crystallization U-gain. Linear trends with abnormally

young ages and variable alkali feldspar $^{207}\text{Pb}/^{206}\text{Pb}$ ratios have been measured also for the fractionated topaz-bearing granites of the Eurajoki complex (Vaasjoki, 1977). According to Vaasjoki (1977), the extremely variable alkali feldspar Pb isotopic ratios were probably caused by differentiation processes. It is interesting to note that the samples from the topaz-bearing granites in the Kymi stock do not show such low relative $^{207}\text{Pb}/^{206}\text{Pb}$ ratios (the μ_2 value for the one analysed alkali feldspar fraction is 9.85, Table 6) and also give a reasonable estimate of age of the stock (the alkali feldspar - whole rock pair of sample 1/IH/89 yields an age of 1579 Ma). Hence, compared with the data on the granites of the Suomenniemi batholith, the Kymi stock may consist of granites less affected by open-system processes. The samples from the Kymi stock have, however, a very low calculated Th/U ratio of 1.61. This suggests that the relative Th/U ratio in the topaz-bearing granites might also be a primary feature inherited, possibly at least in the case of the Kymi stock, from the protolith.

Quartz-feldspar porphyry dykes and alkali-feldspar syenites

Compared with the granites of the Suomenniemi batholith, the quartz-feldspar porphyry dykes have somewhat less pronounced, but yet otherwise grossly similar compositional trends in the silica variation diagrams (Figs. 37 and 38). Like the granites, they also show considerable ranges in Ba and Sr abundances indicative of feldspar fractionation; these ranges are large enough to render variable degrees of partial melting incapable to account for the variations. The dykes also show a considerable range in SiO_2 content (from ca. 68 to 75 wt%) and exhibit evidence for fractionation of mafic silicates (Figs. 38a, c, and k), Fe-Ti-oxide (Figs. 38b and d), apatite (Fig. 38e), and zircon (Fig. 38j).

Besides being lower in silica, the alkali-feldspar syenites differ markedly from the silicic rocks in showing no enrichment in F and Rb with increas-

ing SiO_2 (Figs. 38f and i). Feldspar fractionation has possibly controlled the evolution of the syenitic magma, as the Ba vs. SiO_2 and Sr vs. SiO_2 diagrams (Figs. 38g and h) exhibit clear declining trends along with increasing SiO_2 . The feldspar was probably relatively low in potassium because there is no marked change in the K/Rb ratio (Fig. 38l). This is consistent with the hypersolvus character of the alkali-feldspar syenites. Other possible fractionating phases comprise Fe-Ti-oxide (Figs. 38b and d), titanite (Figs. 38a and d), and apatite (Fig. 38e). Because the data on the quartz-feldspar porphyry dykes and the alkali-feldspar syenites are relatively few, no attempt of quantitative modeling was made. The origin of these rocks will, however, be briefly discussed in the chapter that follows.

PROTOLITH OF THE FINNISH RAPAKIVI GRANITES

The basic question regarding the origin of the rapakivi granites is whether they were ultimately derived from the mantle and represent the end product of a complex series of evolutionary events (partial melting in the mantle, fractionation of the mantle-derived melts, incorporation of and reaction with crustal materials etc.; cf. Barker et al., 1975) or whether they are anatectic melts extracted exclusively from the continental crust (cf. Vormaa, 1976; Anderson & Cullers, 1978). The mantle and continental crust have, in general, different Nd and Pb isotopic composi-

tions (DePaolo, 1981a; Doe & Zartman, 1979) and hence isotopic data on these elements are useful in assessing the origin of a particular igneous rock supposedly derived from either source. Independent Nd and Pb isotopic evidence regarding the origin of the Finnish rapakivi granites are discussed below, and, together with the general geochemical data, they are used to construct batch melting models to define a possible protolith composition for the Suomenniemi batholith.

Nd isotopic evidence

Recent isotopic studies (Patchett et al., 1981; Huhma, 1986; Patchett & Kouvo, 1986; Patchett et al., 1987; Hanski et al., 1990; Huhma et al., 1990; Rämö, 1990) indicate that a time-integrated LREE-depleted mantle existed beneath the Fennoscandian shield during the Proterozoic. As far as the Sm-Nd isotopic system is concerned, the degree of depletion roughly conforms to the depleted mantle evolution suggested by DePaolo (1981a). Evidence for heterogeneity in the Fennoscandian mantle is, however, provided by some primitive mantle-derived rocks that show $\epsilon_{Nd}(T)$ values that are higher (+4.2 at 2090 Ma; Huhma, 1986; Huhma et al., 1990) and lower (+1.6 at 1990 Ma; Hanski et al., 1990) than those in the penecontemporaneous model depleted mantle.

The juvenile 1.9 Ga Svecofennian crust hosting the Finnish rapakivi granites shows a restricted range of $\epsilon_{Nd}(T)$ values lying between the evolution of the depleted mantle and CHUR, and is considered to have formed largely of material newly derived from the depleted mantle (Huhma, 1986; Patchett & Kouvo, 1986). This is reflected in the T_{DM} model ages of samples from the Svecofennian crust: the average T_{DM} model age of the data of Huhma (1986) and Patchett and Kouvo (1986) is 2.12 ± 0.14 (1 S.D.) Ga. It should be noted that this figure does not

indicate the time of differentiation of the juvenile crust from the mantle, but results from addition of a minor amount (ca. 10%, Patchett & Kouvo, 1986; Huhma, 1986) of Archean material to the mantle component.

The Finnish rapakivi granites show a narrow range of $\epsilon_{Nd}(T)$ values and have, excluding the topaz-bearing granites that have Sm/Nd ratios affected by crystal fractionation, a very well-defined average T_{DM} model age of 2.06 ± 0.03 (1 S.D.) Ga. This is almost equal to the average T_{DM} model age of the Svecofennian crust. In the light of these isotopic data, the rapakivi granites could have originated (1) by mixing of material from depleted mantle and Archean crust in the same proportion in which these components were mixed during the formation of the Svecofennian crust (cf. Patchett & Arndt, 1986), (2) by mixing of depleted mantle material and the Svecofennian crust, (3) by partial melting of the Svecofennian crust in a process that did not result in any significant fractionation of the Sm/Nd ratio, or (4) allowing a change in the Sm/Nd ratio, by partial melting of Svecofennian material with $\epsilon_{Nd}(T)$ values lower than the average ϵ_{Nd} value of the Svecofennian crust (cf. Nelson & DePaolo, 1985). These different possibilities are schematically presented in Fig. 42. The first (Fig. 42a) is considered improbable due to the very narrow

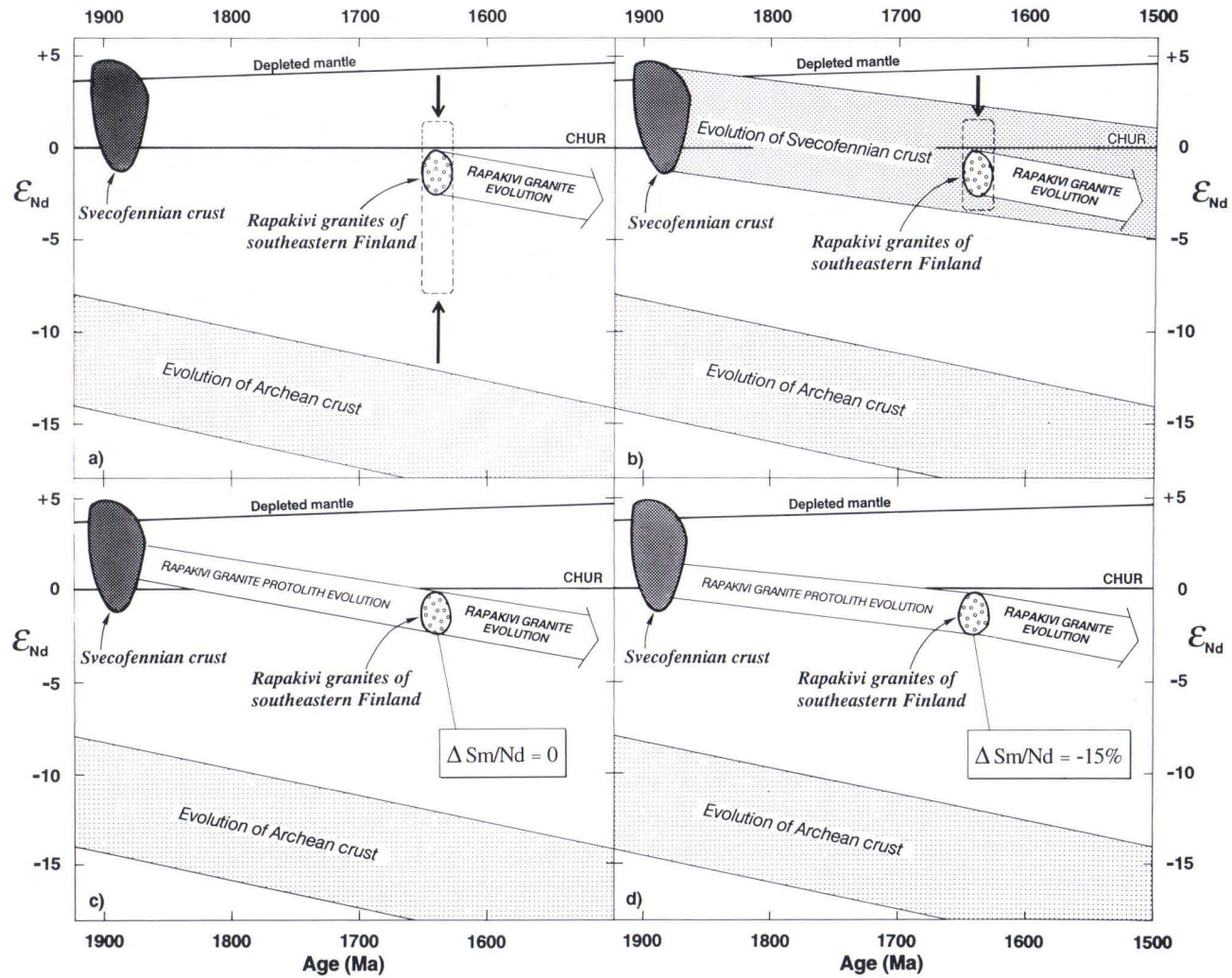


Fig. 42. Alternatives regarding the origin of the Finnish rapakivi granites based on their initial Nd isotopic composition. The ϵ_{Nd} vs. age diagrams denote origin by (a) mixing of Archean crustal material and depleted mantle, (b) mixing of Svecofennian crustal material and depleted mantle, (c) reworking of the Svecofennian crust with no change in the Sm/Nd ratio of the rapakivi granite protolith, (d) reworking of the Svecofennian crust with a 15% decrease in the protolith Sm/Nd ratio. See text for further discussion.

range of the $\epsilon_{Nd}(T)$ values of the rapakivi granites. Mixing of such extreme components (depleted mantle and average Archean crust differ from each other by about 20 ϵ_{Nd} units at 1.6 Ga) would have resulted in substantial scatter of ϵ_{Nd} values of the rapakivi granites, as denoted by the hypothetical dashed space in Fig.

42a. The second alternative may be more feasible than the first, but again would probably have resulted in a larger range of ϵ_{Nd} values than that observed (dashed space in Fig. 42b). The third and fourth alternatives (Figs. 42c and d) involving only crustal reworking are considered the most plausible.

Pb isotopic evidence

Like initial Nd isotopic composition, initial Pb isotopic ratios are commonly used to constrain the origin of igneous rocks. A conventional procedure for determining the initial Pb isotopic ratios of granitic rocks is to analyse alkali feldspar fractions extracted from them. Because the U/Pb and Th/Pb ratios in alkali feldspar are very low, it contains only a marginal amount of extra radiogenic Pb formed in the rock subsequent to crystallization, and thus preserves a record of the Pb isotopic composition of the magma from which is crystallized (cf. Faure, 1986). This in turn facilitates inferences to be made on the ultimate origin of the magma. It is also common practice to calculate model ages for alkali feldspars, that, if the evolution of the Pb in the particular feldspar followed the evolution model used, can be considered as the crystallization age of the rock. Complications rendering the alkali feldspar common Pb method somewhat suspect may result from a multi-stage history of the Pb, from introduction of extra Pb with different isotopic composition into the system, or from metamorphic open-system processes subsequent to crystallization (cf. Faure, 1986).

The alkali feldspar analyses of the rapakivi granites and alkali-feldspar syenites listed in Table 6 are plotted in $^{207}\text{Pb}/^{204}\text{Pb}$ vs. $^{206}\text{Pb}/^{204}\text{Pb}$ diagram in Fig. 43. Also shown in Fig. 43 is the growth curve of the Svecofennian crust, constructed on the basis of galena Pb isotopic data from the central Finnish batholith area and Svecofennian supracrustal rocks (Vaasjoki, 1981), as well as six Stacey and Kramers (1975) model isochrons. As can be seen from Fig. 43,

the Pb isotopic composition of alkali feldspars from the Finnish granites (topaz-bearing granites A1097 and M664.2 excluded) fall precisely on the growth curve of the Svecofennian crust. The average μ_2 value for the alkali feldspars of the non-topaz-bearing rapakivi granites is 9.83 ± 0.08 (1 S.D.), while the average for the Svecofennian crust is 9.81 ± 0.22 (1 S.D.). This indicates that the Pb in the rapakivi granites originated from an environment that had the same overall U/Pb ratio as the Svecofennian crust. This in turn is consistent with the hypothesis that the rapakivi granites derive from the 1.9 Ga crust. It should also be noted that, in Fig. 43, the alkali feldspars plot in an area which is almost equal to the compositional range measured for galenas associated with the Finnish rapakivi granites (Vaasjoki, 1981).

Some of the Stacey and Kramers (1975) model ages of the rapakivi granite alkali feldspars (Table 6) are almost 200 Ma younger than the actual crystallization ages of the granites, which, provided that Pb in these rocks followed a two-stage evolution, could result from minor amounts of radiogenic Pb (the exact amount of radiogenic Pb in the alkali feldspars is not known because they were not analysed for their U and Th abundances). As noted earlier, the topaz-bearing granites of the Suomenniemi batholith have probably acquired some extra Pb during the magma evolution in the batholith: they fall below the data for the other granites in Fig. 43. It should also be noted that the alkali feldspar fraction from the Siipyy pluton has a model age equal to the U-Pb zircon age of the pluton, suggesting that

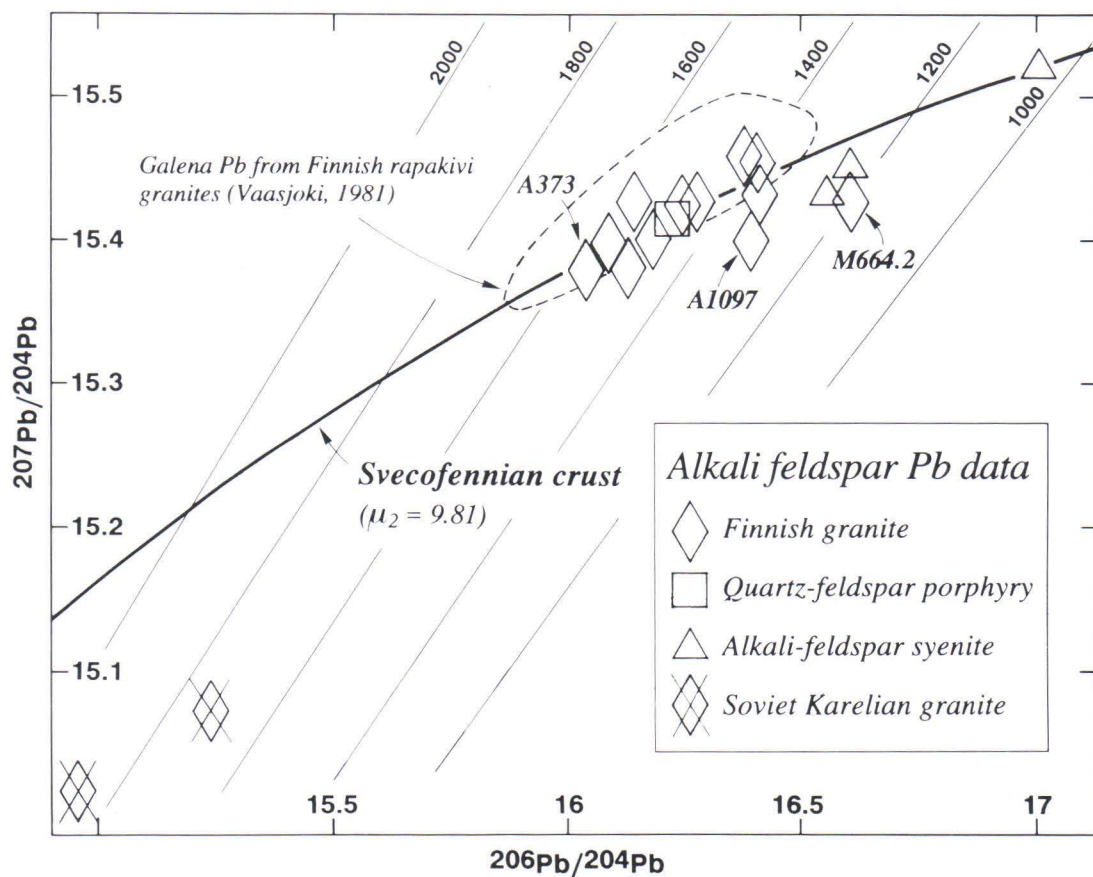


Fig. 43. Alkali feldspar analyses (Table 6) of the silicic rocks and alkali-feldspar syenites plotted in $^{207}\text{Pb}/^{204}\text{Pb}$ vs. $^{206}\text{Pb}/^{204}\text{Pb}$ diagram. Also shown is the growth curve of the Svecofennian crust (approximated from the data of Vaasjoki, 1981) and Stacey and Kramers (1975) model isochrons for 1000, 1200, 1400, 1600, 1800, and 2000 Ma. Dashed space denotes the composition of galenas associated with Finnish rapakivi granites (Vaasjoki, 1981).

the Pb in this sample could conform to the two-stage model of Stacey and Kramers (1975). This might result from the fact that the Siipyy pluton is a small intrusion (cf. Idman, 1989) and crystallized more rapidly than the large rapakivi granite

batholiths that have alkali feldspars with younger model ages, and hence was not exposed to prolonged fractionation processes that could have introduced extra upper crustal Pb into the magma.

Partial melting modeling: the main granite sequence of the Suomenniemi batholith

The Nd and Pb isotopic data are strongly in favor of a crustal origin for the rapakivi granites. Using the major and trace element data on the main granite sequence (hornblende granite — biotite-hornblende granite — biotite granites — topaz-bearing granite) of the Suomenniemi

batholith it is possible to gain some indication of the depth of magma generation, protolith composition, and also of the amount of fractionation of the Sm/Nd ratio during the anatexis of the Svecofennian crust.

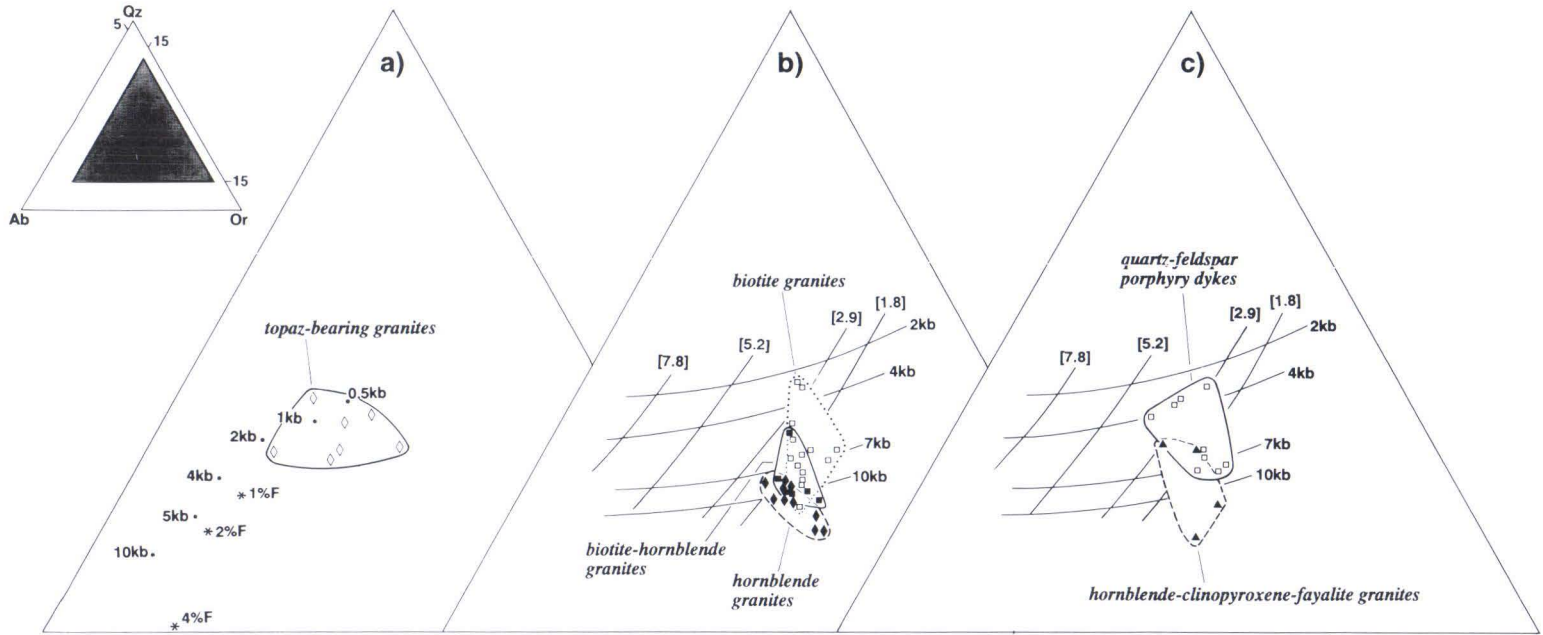


Fig. 44. Normative Ab-Or-Qz diagrams showing the compositions (Appendix 1) of (a) topaz-bearing granites, (b) hornblende granites, biotite-hornblende granites, and biotite granites, and (c) hornblende-clinopyroxene-fayalite granites and quartz-feldspar porphyry dykes of the Suomenniemi complex. Dots in (a) indicate minimum melting compositions in the system $\text{KAlSi}_3\text{O}_8\text{—NaAlSi}_3\text{O}_8\text{—SiO}_2\text{—H}_2\text{O}$ for $P_{\text{H}_2\text{O}} = P_{\text{total}} = 0.5, 1, 2, 4, 5,$ and 10 kb (Winkler et al., 1975) and stars show minimum melting compositions at 1 kb with excess H_2O and 1, 2, and 4% F (Manning, 1981). In (b) and (c) a $P_{\text{H}_2\text{O}} = P_{\text{total}}$ vs. Ab/An ratio grid, adopted from Anderson and Cullers (1978), is shown for 2, 4, 7, and 10 kb $P_{\text{H}_2\text{O}}$ and Ab/An ratios of 1.8, 2.9, 5.2, and 7.8.

Depth of magma generation

In Fig. 44, the compositions of the granites of the Suomenniemi batholith are plotted in the normative Ab-Or-Qz diagram and compared with experimental work in the Qz-Or-Ab-H₂O and Qz-Or-Ab-An-H₂O systems. The topaz-bearing granites plot rather close to the experimentally determined minimum melt compositions in the system Qz-Or-Ab-H₂O at 0.5 to 1 kb total water pressure (Fig. 44a), but also show a slight overall shift toward lower relative Qz contents, a feature in part probably resulting from the increased F content in the residual magmas. This feature is more pronounced in the topaz-bearing granites of the Eurajoki complex and the Kymi stock (Haapala, 1977a; Haapala & Rämö, 1990).

When the anorthite component is taken into account in melting experiments in the granite system, the minimum melt composition is observed to move, with decreasing Ab/An ratio, along the quaternary univariant line toward the An-Or-Qz-plane of the Qz-Or-Ab-An(+H₂O) tetrahedron (James & Hamilton, 1969; von Platen & Höller, 1966). The effect of protolith anorthite component on the composition of the resulting minimum melts has been compiled in the form of a grid projected on the Ab-Or-Qz diagram by Anderson and Cullers (1978), and is reproduced in Figs. 44b and c. As noted by Anderson and Cullers (1978), this pressure - Ab/An ratio grid is in principle applicable only for H₂O-saturated melting. However, the displacement of minimum melt compositions caused by H₂O-undersaturated melting is possibly along the isobaric surfaces in Figs. 44b and c (cf. Luth, 1969) and hence qualitative pressure estimates based on the H₂O-saturated melting experiments may apply to H₂O-undersaturated melting (Anderson & Cullers, 1978).

As can be seen from Fig. 44b, the normative compositions of the granites of the Suomenniemi batholith correspond to a range of pressures from > 10 kb to < 3 kb and an Ab/An ratio from < 1 to about 3. Moreover, the corresponding overall pressure estimate decreases from the

hornblende granites through the biotite-hornblende granites to the biotite granites. Qualitatively, this could mean that the hornblende granites represent primitive melts from a deep crustal source with the high-pressure melt generation signature preserved (10 kb equals 36 km), and that the shift toward lower apparent pressure in the sequence hornblende granite — biotite-hornblende granite — biotite granites indicates progressive adjustment of the evolving magma to near-surface conditions. However, because the low-silica hornblende granites, as suggested by the fractional crystallization modeling, presumably are mixtures of cumulate crystals and trapped liquid, they may yield invalid pressure estimates in Fig. 44b.

The bulk of the granite data in Fig. 44b plot between the 7 and 10 kb contours indicating an overall magma generation depth of 25 to 36 km. This is close to the pressure estimate of magma generation for the Proterozoic Wolf River batholith in north-central U.S.A. (Anderson & Cullers, 1978). As the present total thickness of the Svecofennian crust under the Wiborg and Suomenniemi batholiths is estimated at about 40 km (Korja & Elo, 1990; see also Luosto, 1990) and as the rapakivi granites were obviously emplaced at shallow levels in the crust (≤ 3 km; cf. Vorma, 1976), this pressure estimate corresponds to the lower and middle crust. The normative composition of the hornblende-clinopyroxene-fayalite granites show considerable scatter but nevertheless falls in the high-pressure area in Fig. 44c. Hence this discrete group of rocks could represent another melting event in the lower/middle crust.

It should be noted that normative compositions of dark rapakivi granites (tirilites) and wiborgites from the Wiborg batholith and a biotite-hornblende granite from the Eurajoki complex have been interpreted in accordance with the 1 kb system of James and Hamilton (1969) as lying within the plagioclase field and reflecting relatively early crystallization of plagioclase in these rocks (Vorma, 1971; Haapala, 1977a). The compositions of these granites plot in

approximately the same area as the compositions of the granites of the Suomenniemi batholith in Fig. 44 (see Fig. 23 in Vormaa, 1971, and Fig. 100 in Haapala, 1977a), and hence also probably reflect the pressures at which the melts for these granites were generated in the lower parts of the crust. This scheme also applies to most of the rapakivi-age granite porphyry dykes west of the Wiborg batholith (see Fig. 20 in Törnroos, 1984).

Assessment of a possible protolith composition

Trace element modeling of partial melting processes in order to find suitable candidates for the source composition of an igneous suite involves several assumptions which render any derived model at best a probable solution but never a unique one. In modeling the protolith of the Finnish rapakivi granites the set of assumptions include, in addition to those made regarding the actual melting model and the crystal/liquid partition coefficients, (1) the mineralogy of the source, (2) the mineral assemblage that enters into the melt, and (3) the relative amount of partial melting.

Because the rapakivi granites are largely restite-free, there is little direct evidence for possible source rock compositions. One way to get around this problem is to use model compositions suggested for common rock types of the continental crust and see whether they can yield the assumed parental magma composition with reasonable melt modes and degrees of partial melting. The concept of rheologically critical melt percentage (RCMP) has been developed to distinguish anatectic systems that may yield restite-free mobile magmas from those that behave as migmatites (cf. Clemens & Vielzeuf, 1987, and references therein). Usually RCMP is considered to be of the order of 20 to 35 vol% melt, but it is strongly dependent on the rock type undergoing partial melting and may even be less than 15 vol% (Clemens & Vielzeuf, 1987). Important factors controlling crustal anatexis are the type and amount of hydrous silicates in the

rocks that undergo melting. For example, if temperature in a water-deficient system rises high enough, breakdown of any biotite or hornblende may result in relative amounts of melt exceeding the appropriate RCMP (Clemens & Vielzeuf, 1987). As far as magma generation for large granitic bodies is concerned, a melt fraction of 30 to 50 % may be needed to facilitate convective motion in anatectic regions that eventually results in segregation of large homogeneous, high crystal fraction magma bodies (Wickham, 1987). Substantially lower melt percentages (<10%) have been, however, proposed for some voluminously minor A-type granite magmas (cf. Christiansen et al., 1988). In summary, feasible melt percentages in crustal anatexis may range from <15 to >50%.

The fractional crystallization model for the evolution of the granites of the Suomenniemi batholith yields an estimate of a possible initial composition of the rapakivi granite magma. This model composition (Table 10) can be used in search of possible protolith compositions for the batholith. Because partial melting modeling is based on a considerable amount of assumptions, the relevance of it here is to differentiate between sources that yield feasible melt compositions from those that do not.

The initial magma composition proposed by the fractional crystallization modeling suggests a prominent biotite control on the partial melting process. The Rb/Sr and Ba/Sr ratios in this model composition are very high, 5.7 and 10.4, respectively, and indicate that the relative contribution of biotite to the melt was larger than that of feldspars (high Rb and Ba vs. low Sr). This would be consistent with partial melting caused by fluid-absent breakdown of biotite in response to a substantial amount of extra heat introduced into the lower parts of the continental crust (cf. Clemens et al., 1986). The role suggested for feldspars in the partial melting process is also consistent with the prominent negative Eu anomaly in the assumed initial magma composition (Fig. 40).

In order to get a rough idea of the nature of

Table 11. Source rock compositions used in the batch melting modeling of the granites of the Suomenniemi batholith.

Mineral	Average lower crust		Tonalite		Granodiorite		Granite		Granulite		Garnet-bearing granulite	
	Source ^a Mode	Melt ^f Mode	Source ^b Mode	Melt ^f Mode	Source ^c Mode	Melt ^f Mode	Source ^d Mode	Melt ^f Mode	Source ^e Mode	Melt ^f Mode	Source ^e Mode	Melt ^f Mode
Hornblende	0.05	0.06	0.09	0.11	0.045	0.06
Biotite	0.1	0.13	0.125	0.16	0.108	0.13	0.045	0.06	0.16	0.2	0.16	0.2
Plagioclase	0.29	0.32	0.59	0.22	0.402	0.2	0.315	0.2	0.53	0.31	0.53	0.31
Alkali feldspar	0.007	0.02	0.045	0.16	0.199	0.25	0.29	0.34
Clinopyroxene	0.05	0.03
Orthopyroxene	0.29	0.16	0.058	0.039	0.016	0.004
Quartz	0.17	0.24	0.13	0.34	0.246	0.36	0.348	0.4	0.25	0.45	0.25	0.45
Oxide	0.04	0.03	0.02	0.01	0.002	0.001	0.002	0.001
Zircon	0.0001	0.0005	0.0001	0.0005	0.0002	0.001	0.0003	0.0015	0.0002	0.001	0.0002	0.001
Apatite	0.0005	0.001	0.0005	0.001	0.0005	0.001	0.0005	0.001	0.0005	0.001	0.0005	0.001
Allanite	0.0001	0.0005	0.0001	0.0005	0.0002	0.001	0.0003	0.0015	0.0002	0.001	0.0002	0.001
Garnet	0.042	0.035
Trace element abundances (in ppm):												
Rb	53		130		170		209		58			as in
Sr	230		620		372		123		285			granulite
Ba	150		1450		938		426		483			
Zr	70		150		191		232		241			
La	11		26		36		45.9		31			
Ce	23		57		74		91		72			
Nd	12.7		30		37		44		36			
Sm	3.17		5.17		6.41		7.65		9.75			
Eu	1.17		1.76		1.75		1.73		4.13			
Tb	0.59		0.92		0.97		1.01		1.18			
Yb	2.2		2.8		3.22		3.63		3.73			
Lu	0.29		0.39		0.65		0.9		0.9			
(La/Yb) _N ^g	3.37		6.26		7.54		8.52		5.60			

^a Source mode as the molecular normative composition of the average lower crust of Taylor and McLennan (1985), trace element abundances from Taylor and McLennan (1985, Table 4.4).

^b Source mode from Wyllie (1977, Table I), trace element abundances as mean values from Cullers et al. (1981, Table A3) except Zr and Nd that were estimated on the basis of the other element abundances.

^c Source mode from Wyllie (1977, Table I), trace element abundances intermediate between tonalite and granite.

^d Source mode from Wyllie (1977, Table I), trace element abundances are the average of collision granite and within plate granite compositions represented by Pearce et al. (1984, Table 2).

^e Source mode modified from Meriläinen (1976, Table 18), trace element abundances are mean values reported for post-Archean granulite facies terrains by Rudnic and Presper (1990, Table II).

^f Melt modes listed are those used to derive the models shown in Figs. 45 and 46.

^g Chondrite-normalized ratios.

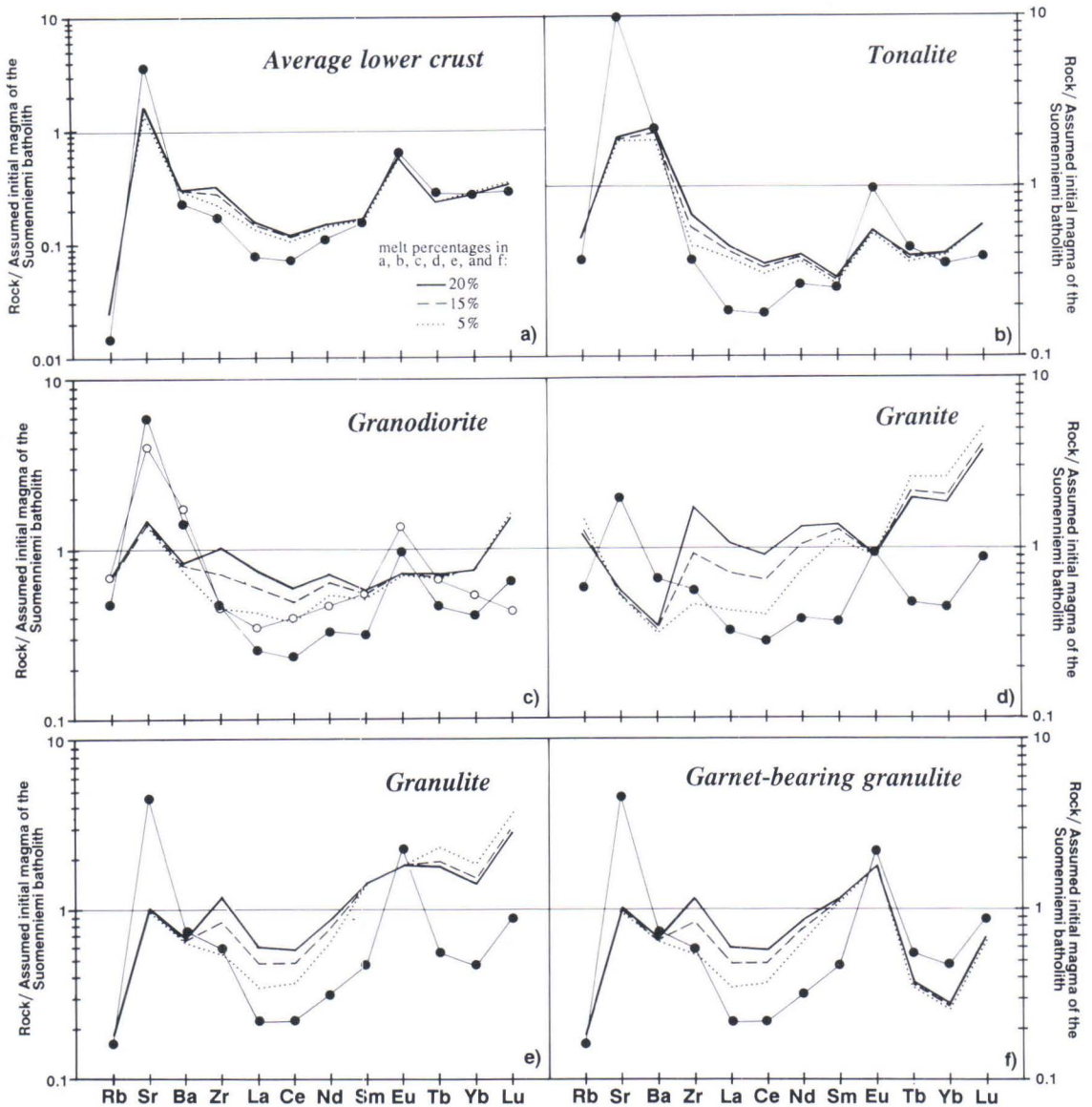


Fig. 45. Batch melting models of (a) average lower crust composition, (b) tonalite, (c) granodiorite, (d) granite, (e) granulite, and (f) garnet-bearing granulite with zircon, allanite, and apatite in the residue, normalized against the assumed initial magma composition of the Suomenniemi batholith (cf. Table 10). Dotted, dashed, and solid lines indicate melt compositions at 5%, 15%, and 20% of melting, respectively. Patterns with closed circles indicate the appropriate source compositions and the one with open circles in (c) is a composition calculated back from the hypothetical initial magma composition of the Suomenniemi batholith at $F=0.20$. Source and melt modes are listed in Table 11.

the protolith of the granites of the Suomenniemi batholith, batch melting trace element modeling was performed on several common crustal rock compositions that were considered to be

possible as sources for these granites, including a global average lower crust composition, tonalite, granodiorite, granite, granulite, and garnet-bearing granulite. Elements used for modeling

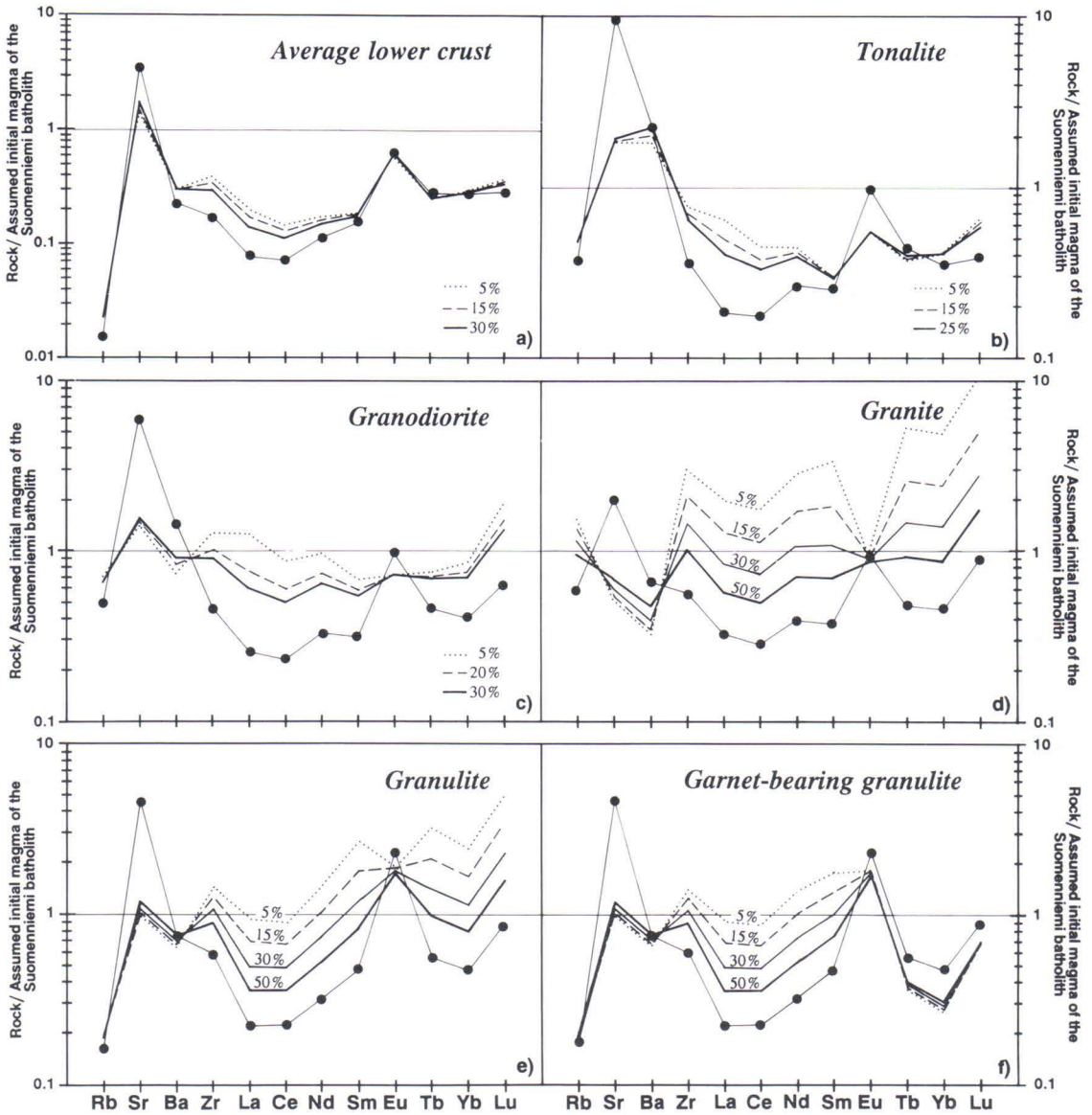


Fig. 46. Batch melting models of (a) average lower crust composition, (b) tonalite, (c) granodiorite, (d) granite, (e) granulite, and (f) garnet-bearing granulite with no zircon, allanite, and apatite in the residue, normalized against the assumed initial magma composition of the Suomenniemi batholith (cf. Table 10). Dotted, dashed, and solid lines indicate melt compositions at the denoted percentages of melting. Patterns with closed circles are as in Fig. 45. Source and melt modes are listed in Table 11.

were Rb, Sr, Ba, Zr, and the REE, and the source modes and trace element abundances applied were those listed in Table 11. The degree of melting was varied between 5 and 50% and melt

modes (Table 11) were estimated by allocating a dominant role for quartz, alkali feldspar, and the sodic component of plagioclase in the melting process (cf. Wyllie, 1977). Crystal/liquid parti-

tion coefficients used in the calculations were those listed in Appendix 3. The results of the batch melting calculations, normalized against the assumed initial magma composition of the Suomenniemi batholith, are shown in Figs. 45 and 46.

The batch melting calculations were done both with (Fig. 45) and without (Fig. 46) zircon, allanite, and apatite in the residue. In the former case, in order to satisfy the the high Zr and LREE contents of the assumed initial rapakivi granite magma, zircon and allanite are required to enter the melt with a melt mode/source mode ratio of approximately 5:1. This high ratio restricts the relative amount of partial melting in this model to $\leq 20\%$. With no zircon, allanite, and apatite in the residue larger melt percentages are possible.

It is evident from Figs. 45a and 46a that the average mafic (54% SiO₂) lower crust composition is improbable as the source for the rapakivi granite magma. There is far too little biotite (i.e., Rb) in the modeled melts, and also the total REE content in the source is too low. The tonalite also appears to be unlikely as the rapakivi granite protolith (Figs. 45b and 46b). The biotite component in the melt is again too low, feldspar components (Sr, Ba) too high, and the REE abundances in the source too low.

The batch melting modeling also renders the average granite improbable as a source for the rapakivi granite magma. It can be seen from Figs. 45d and 46d that there is clearly too much feldspar left in the residue in the partial melting processes (Sr and Ba are too low in the model melts) and that the HREE/LREE ratios in the calculated melts are too high. In granulites (Figs. 45e and f, 46e and f), the feldspar-controlled components Sr and Ba are reproduced well but the biotite component in the melts is clearly too low. Moreover, the REE pattern of the granulites is much too depleted in the LREE to yield an acceptable melt composition. Garnet in the source (Figs. 45f and 46f) renders the HREE contents in the model melts too low to be consistent with the assumed initial magma composition.

As is evident from Figs. 45c and 46c, granodiorite is a viable candidate for the protolith of the assumed initial magma of the Suomenniemi batholith. With zircon, allanite, and apatite in the residue (Fig. 45c), the biotite and feldspar components in the model melt are consistent with the assumed initial melt composition at $F = 0.20$. The REE patterns of the assumed initial magma and the model melt at $F = 0.20$ are roughly parallel with each other, although the abundances reached at $F = 0.20$ are somewhat below those in the assumed initial magma. With no zircon, allanite, and apatite in the residue (Fig. 46c), Zr and the REE are also best reproduced by melting to $F = 0.20$, which results in identical pattern with that in Fig. 45c because the minor components are exhausted at $F = 0.20$. The models imply that the source may have had higher REE contents than that assumed for the average granodiorite (cf. Table 11). A protolith composition calculated for 20% melting using the element contents in the assumed initial magma of the Suomenniemi batholith is also shown in Fig. 45c. Although showing somewhat higher REE abundances, the pattern of the calculated initial composition is similar to that used for the granodiorite.

In conclusion, the batch melting modeling suggests an intermediate to acid (granodioritic) igneous source that presumably underwent a relatively restricted amount of partial melting (ca. 20%) to produce the initial magma of the Suomenniemi batholith. At $F = 0.20$, it is impossible to distinguish between the two models (Figs. 45c and 46c), but as the melting of the protolith presumably started by water-absent breakdown of biotite at a relatively high temperature (cf. Clemens et al., 1986; Creaser & White, 1991), zircon could probably have been melted if it was present in the protolith.

Melting of the model granodiorite to $F = 0.20$ produces a melt with a Sm/Nd ratio that is ca. 15% smaller than that in the original granodiorite source. This amount of fractionation of the Sm/Nd ratio of the Svecofennian crust in the partial melting process would suggest a protolith

composition in the lower part of the compositional space of the Svecofennian crust (Fig. 42d). This is consistent with the relatively felsic nature proposed for the protolith by the batch melting modeling: the lower part of the compositional space of the Svecofennian crust in the ϵ_{Nd} vs.

age diagram (Fig. 42) is dominated by analyses of intermediate and acid rocks, while those of basic rocks plot close to the evolution of the depleted mantle (cf. Huhma, 1986; Patchett & Kouvo, 1986).

Insights into the origin of the minor felsic intrusive phases in the Suomenniemi complex

Although the geochemical data on the minor felsic intrusive phases (hornblende-clinopyroxene-fayalite granite, quartz-feldspar porphyry, alkali-feldspar syenite) of Suomenniemi complex are few, some suggestions can be made about their origin.

The hornblende-clinopyroxene-fayalite granites that intrude the main granites of the batholith differ in trace elements from the latter mainly in having lower Sr and Ba and higher Zr contents (Fig. 37). In the normative Ab-Or-Qz diagram

(Fig. 44c) they show wide scatter but plot approximately in the same area as the hornblende granites. Accordingly, if the hornblende-clinopyroxene-fayalite granites represent a separate melt phase, the melting may have taken place at a slightly higher pressure than the melting that generated the initial magma for the Suomenniemi batholith. In Fig. 47, the average composition of the four hornblende-clinopyroxene-fayalite granites is normalized against the assumed initial magma of the granites of the

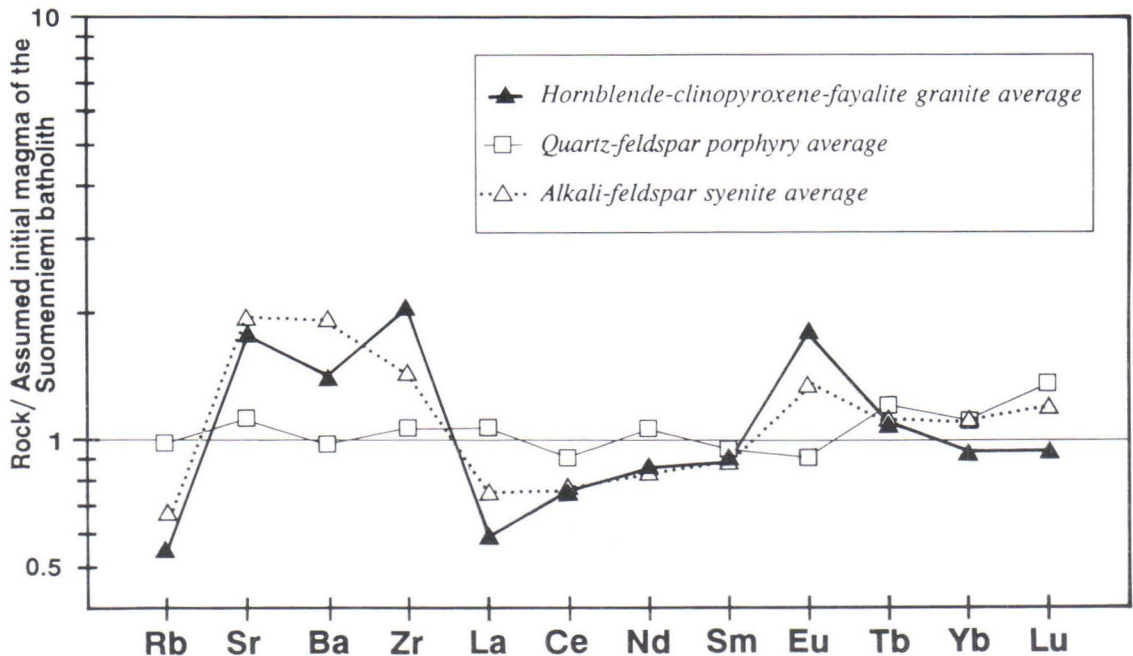


Fig. 47. Average chemical composition of the hornblende-clinopyroxene-fayalite granites (pattern with closed triangles), quartz-feldspar porphyry dykes (open squares), and alkali-feldspar syenites (open triangles) of the Suomenniemi complex normalized against the assumed initial magma composition of the Suomenniemi batholith (cf. Table 10).

Suomenniemi batholith. The hornblende-clinopyroxene-fayalite granites have higher Sr, Ba, and Zr contents, lower Rb abundance, and are depleted in the LREE relative to the normalizing composition. The higher Sr and Ba as well as lower Rb and the REE pattern could be explained by involving a more mafic protolith (cf. Figs. 45a and b, 46a and b). The high Zr content, however, is more in favor of a cumulate origin for these rocks, as is their normative composition (Fig. 44c).

Fayalite-bearing, relatively low-silica granites that are also late in the intrusion sequence of a granite complex have been described from central North America (cf. Barker et al., 1975; Bickford et al., 1981). In the St. Francois Mountains (Missouri) they have been interpreted as being the parental magma from deeper crustal sources, emplaced along ring fractures after formation and resurgent doming of a caldera (Bickford et al., 1981). In the Pikes Peak batholith of central Colorado these rocks occur as irregular small bodies (1.6 km in maximum diameter) lying scattered along an arc with a radius of 4 km, and have been interpreted as fragmented foundered roots of a ring dyke (Barker et al., 1975, p. 114–115). The hornblende-clinopyroxene-fayalite granite bodies in the Suomenniemi complex show similarities with these North American lithologies, and their emplacement may have been related to such processes as cauldron subsidence and ring dyke injection which are not hard to envision for the Finnish high-level rapakivi granite batholiths (cf. Bergman, 1986). The hornblende-clinopyroxene-fayalite granites could represent cumulate liquids initially trapped in the hotter lower parts of the Suomenniemi batholith, but obviously more data are needed to resolve the origin of these granites.

As can be seen from Fig. 47, the average composition of the quartz-feldspar porphyry dykes is very close to the composition of the assumed initial magma of the Suomenniemi batholith. Moreover, in the normative Ab-Or-Qz diagram (Fig. 44c) the less silicic quartz-feldspar porphyries plot along the 7kb contour. These obser-

vations are consistent with a roughly similar origin for the granites and the quartz-feldspar porphyry dykes.

The average composition of the alkali-feldspar syenites is similar to the average composition of the hornblende-clinopyroxene-fayalite granites in Fig. 47. There are, however, fundamental differences such as the low F content which is found to decrease with increasing SiO₂ (Fig. 38f), the opposite to what is observed for the granites and quartz-feldspar porphyry dykes (Figs. 37f and 38f, respectively). In the normative Ab-Or-Qz diagram they plot close to the Ab-Or side which, if taken directly as indicative of the pressure of melt-generation within a quartz-feldspathic source, indicates pressures on the order of 30 kb (cf. Huang & Wyllie, 1975) and hence well within the subcontinental mantle where such lithologies are absent.

The not infrequent association of peralkaline and subalkaline rock types within A-type granite complexes has been explained in a variety of ways. Whalen and Currie (1990) suggest that metaluminous magmas may form from peralkaline magmas through fractional crystallization and mixing with basic magma. Harris and Mariner (1980) relate the differences to different partial melting conditions in the lower crust, melting in the presence of halide-rich volatiles generating the peralkaline magma and further melting under volatile conditions the subalkaline magma. Collerson (1982) suggests that peralkaline magmas form from mantle-derived basic magma via contamination by the continental crust, and that the temporally associated subalkaline rocks are crustal melts. According to Clemens et al. (1986) peralkaline granite magmas might form from A-type low-Ca subalkaline magmas through early fractionation of plagioclase. This plagioclase effect of Bowen (1928) may be aided by high relative Cl content in the magma: Cl forms complexes with Na and hence reduces its activity in the melt resulting in the precipitation of a calcic plagioclase and consequently leading to a peralkaline trend for the residual liquid (Christiansen et al., 1983).

As far as the alkali-feldspar syenites in the Suomenniemi complex are concerned, their origin by fractional crystallization from the subalkaline magma seems improbable as the differentiation of the granites implies a peraluminous trend for the residual liquid (Fig. 20d). In the light of the

field, age, and geochemical data it seems more probable that the alkali-feldspar syenites represent the product of a later, localised partial melting event that probably tapped a source relatively low in F. It is possible that this was a source from which the granites were previously extracted.

SOVIET KARELIAN RAPAKIVI GRANITES: A MIXED SOURCE

The strongly negative initial ϵ_{Nd} values of the Soviet Karelian batholiths suggest that old crustal material, separated from the mantle a long time before the juvenile 1.9 Ga Svecofennian crust formed, was involved in the genesis of these batholiths. This is not surprising, as the Salmi and Sotjärvi batholiths are located at the eastern edge of the Proterozoic crust immediately adjacent to the Archean craton of eastern Fennoscandia (Fig. 1). Because the $\epsilon_{Nd}(T)$ values of the Soviet Karelian batholiths plot considerably below the evolution of the Finnish granites and thus toward distinctly negative ϵ_{Nd} values characteristic of ancient continental crust (cf. Huhma, 1986; Fig. 42), a logical conclusion is that both Svecofennian and Archean crustal material were fused to generate the Soviet Karelian batholiths and that they are mixtures of these two components.

Assuming such a mixed source for the Soviet Karelian granites, the relative amounts of Svecofennian and Archean contribution can be evaluated by using a two-component mixing equation (Pushkar et al., 1972). Mixing x parts of Archean and one part of Svecofennian crustal material to yield the Nd isotopic composition of the samples from the Soviet Karelian batholiths is described by the equation

$$(7) \quad x = \frac{C_{Nd}(SVEC)[\epsilon_{Nd}(SOV) - \epsilon_{Nd}(SVEC)]}{C_{Nd}(ARCH)[\epsilon_{Nd}(ARCH) - \epsilon_{Nd}(SOV)]}$$

(cf. Patchett & Bridgwater, 1984) where $C_{Nd}(i)$ is the concentration of Nd in component i , $\epsilon_{Nd}(i)$ is the ϵ_{Nd} value of component i , SVEC and ARCH denote Svecofennian and Archean com-

ponents, respectively, and SOV the Soviet Karelian batholiths. Because both of the anticipated sources are crustal and because the magmas for the Finnish and Soviet Karelian rapakivi granites were probably generated by similar processes in the lower parts of the crust, the Nd concentrations of the two sources can be approximated as equal. This reduces the right-hand side of equation (7) to $[\epsilon_{Nd}(SOV) - \epsilon_{Nd}(SVEC)] / [\epsilon_{Nd}(ARCH) - \epsilon_{Nd}(SOV)]$.

The average initial ϵ_{Nd} value of the Svecofennian source can be approximated by calculating the average ϵ_{Nd} value of the Finnish rapakivi granites at the time of the crystallization of the Soviet Karelian batholiths. Excluding the topaz-bearing granites from the calculation (ϵ_{Nd} values, other than initial, of such highly fractionated rocks may be subject to error, cf. Miller & Mittelfehldt, 1982), an average of $\epsilon_{Nd}(1540 \text{ Ma}) = -2.52 \pm 0.40$ (1 S.D.) is obtained. This well-defined figure is considered to be what would have been the average initial composition of the Soviet Karelian plutons if no Archean crust was involved in their genesis, and thus is also an estimate of the composition of the Svecofennian lower crust component at that time.

The Nd isotopic composition of the Archean crustal source is more controversial. The main problem is whether the data measured for samples from the upper exposed parts of the Archean crust can be used as such to model the lower crust as well. Several workers (e.g., Weaver & Tarney, 1980; Ben Othman et al., 1984; DePaolo, 1988b; Zartman & Haines, 1988) suggest that there may not be any significant

difference in the overall Sm/Nd ratio between the upper and lower continental crust. Recent studies on granulite xenoliths assumed to sample the lower parts of the continental crust suggest, however, that the lower crust may be more mafic and consequently exhibit a higher Sm/Nd ratio than the upper crust (Rudnick & Taylor, 1987; Kempton et al., 1990; see also Taylor & McLennan, 1985). Nd isotopic data on the Fennoscandian Archean craton have been published by Martin et al. (1983), Jahn et al. (1984), Huhma (1986), and Öhlander et al. (1987). The 19 analysed Archean gneiss and mafic meta-igneous samples have, as is typical of samples from Archean continental crust, very unradiogenic Nd isotopic ratios, and their average ϵ_{Nd} value at 1540 Ma is -17.2 ± 3.6 (1. S.D.). This is somewhat lower than the $\epsilon_{Nd}(1540 \text{ Ma}) = -15$ of the Post-Archean average Australian Shale (PAAS) that has been considered as a global average of Archean continental crust (cf. Nance & Taylor, 1976). Assuming that the Fennoscandian Archean craton is homogeneous with respect to its long-term Sm/Nd ratio, the average ($\epsilon_{Nd} = -16$ at 1540 Ma) of the analysed samples and PAAS can be used to model the Archean lower crustal source. If, however, the lower parts of the Fennoscandian Archean craton were substantially more mafic than its upper exposed parts (i.e., had a distinctly higher average Sm/Nd ratio), a less negative ϵ_{Nd} value should be used for the Archean component. Some indication of such a more radiogenic lower crust Nd isotopic composition may be provided by post-tectonic ca. 1.8 Ga old granites from northern Finland analysed for Nd isotopes by Huhma (1986), Hf isotopes by Patchett et al. (1981), and Pb isotopes by Kouvo et al. (1983). These granites were emplaced within or close to the Archean craton, show distinctly negative $\epsilon_{Nd}(T)$ values of -9.1 and -7.9 (Huhma, 1986) as well as negative $\epsilon_{Hf}(T)$ values and low alkali feldspar $^{207}\text{Pb}/^{206}\text{Pb}$ ratios, and have been suggested as being derived largely from the Archean crust (Patchett et al., 1981; Kouvo et al., 1983; Huhma, 1986; Haapala et al., 1987). The $\epsilon_{Nd}(1540 \text{ Ma})$ values of these granites are -12.6

and -11.8, and thus about five ϵ_{Nd} units higher than the average $\epsilon_{Nd}(1540 \text{ Ma})$ value of the samples from the Archean upper crust. Accordingly, they might reflect the composition of a more radiogenic Archean lower crustal source.

Using the $\epsilon_{Nd}(1540 \text{ Ma}) = -16$ for the Archean component and the average (-6.9) of the initial ϵ_{Nd} values of the Soviet Karelian biotite granites, a figure of 32% is calculated as the Archean contribution from equation (7) (Table 12). When the average $\epsilon_{Nd}(1540 \text{ Ma})$ value of the two northern Finnish granites is used, the result is 45%. This suggests that the Archean component in the Soviet Karelian rapakivi granite batholiths may amount to 30 to 45%, the remaining 70 to 55% being reworked 1.9 Ga Svecofennian material that is considered to be the sole source for the Finnish rapakivi granites.

Table 12. Mixing of Archean and Svecofennian crustal material to yield the Nd isotopic composition of the Soviet Karelian batholiths. See text for details.

Mixture	ϵ_{Nd} at 1.54 Ga		Archean contribution	
	Archean component	Svecofennian ^c component	x	%
-6.9	-16 ^a	-2.52	0.481	32
-6.9	-12.2 ^b	-2.52	0.826	45

^a average of data on the exposed parts of the Fennoscandian Archean craton (19 gneiss and mafic meta-igneous samples analysed by Martin et al., 1983, Jahn et al., 1984; Huhma, 1986, and Öhlander et al., 1987) and the Post-Archean average Australian Shale (PAAS) of Nance and Taylor (1976) (see also Patchett & Bridgwater, 1984).

^b assumed composition of a postulated more mafic Archean lower crust, derived from the data of Huhma (1986) on two post-tectonic 1.8 Ga granites from northern Finland.

^c average of the Finnish rapakivi granites (fractionated topaz-bearing granites excluded).

An alternative to the two-component mixing origin is that the Soviet Karelian batholiths were derived from a single crustal source that had differentiated from the mantle roughly 2.4 Ga ago (the T_{DM} model ages of the two unfractionated Soviet Karelian samples are 2.46 and 2.32

Ga, Table 3). There is, however, no indisputable evidence for such a source in the Fennoscandian shield; indeed, new ion microprobe U-Pb zircon data on Svecofennian early Proterozoic sedimen-

tary rocks seem to preclude the existence of crustal segments in the Fennoscandian shield intermediate in age between Archean and Svecofennian (Huhma et al., 1991).

RAPAKIVI GRANITES AS PROBES INTO THE LOWER CONTINENTAL CRUST: IMPLICATIONS OF THE Nd AND Pb ISOTOPIC DATA

A generally held view is that granites reflect the isotopic character of their source regions deep in the continental crust and that they may, when subsequent melt evolution effects are filtered out, yield statistical regional averages of the isotopic composition of those parts of the crust from which they derive (cf. Chappell, 1979; Ben Othman et al., 1984; DePaolo, 1988b). The Nd and Pb isotopic composition of the Finnish rapakivi granites does not markedly deviate from those measured for the samples from the exposed parts of the juvenile 1.9 Ga Svecofennian crust. Provided that the Finnish granites actually are pure crustal melts, this means that the juvenile crust was not differentiated to any substantial degree in terms of Nd and Pb isotopes by the time of emplacement of the rapakivi granites.

The very unradiogenic Pb isotopic ratios measured for the Soviet Karelian samples indicate that a source (or sources) with retarded Pb isotopic evolution contributed to the Soviet Karelian rapakivi granite magmas. The interpretation of the Soviet Karelian Nd data by the two-component mixing model implies that this source with the low U/Pb ratio is the Archean lower crust. Such depletion of U in the lower continental crust during intra-crustal differentiation processes (metamorphism, partial melting) has been documented by several authors (e.g., Heier & Adams, 1965; Gray & Oversby, 1972) and has been suggested to be a direct function of the tectonothermal age of the crust (Rudnick & Goldstein, 1990).

In constructing the two-stage evolution model for the Svecofennian galena Pb data, Huhma

(1986) suggested that a high U/Pb Archean upper crustal source and a low U/Pb mantle had the major roles in contributing to the resulting mixing line («orogenic trend» of Vaasjoki, 1981), but that Archean lower crustal sources with low U/Pb ratio probably also contributed. Some indication of the unradiogenic Pb isotopic character of the Fennoscandian Archean lower crust is provided by the alkali feldspar Pb data on the two 1.8 Ga old post-tectonic granites in northern Finland (Kouvo et al., 1983). The initial Pb isotopic ratios measured for the alkali feldspars correspond to μ_2 values of 7.7 and 8.9 (calculated according to the two-stage model of Stacey & Kramers, 1975), with the sample with the lower μ_2 value also having the lower $\epsilon_{Nd}(T)$ value. The average μ_2 value of the northern Finnish granites is somewhat lower than that of the Soviet Karelian rapakivi granites.

Using the constraints of the Nd mixing calculations for the contribution of Archean crust to the Soviet Karelian batholiths, a crude estimate of the overall U/Pb ratio of the Archean lower crust can be accomplished. Moreover, it appears that the alkali feldspar Pb data can be used to refine the Nd mixing model. The two-component mixing equation (7) and the least radiogenic alkali feldspar Pb isotopic ratios of the Finnish and Soviet Karelian batholiths (samples A373/KS and IYL/79/KS in Table 6) can be used to evaluate the $^{206}\text{Pb}/^{204}\text{Pb}$ and $^{207}\text{Pb}/^{204}\text{Pb}$ ratios in the Archean lower crustal source. On the basis of the the Nd isotopic data it was calculated that the proportion of the Archean component relative to the Svecofennian one, x (cf. equation [7]), could

be 0.481 (using data on the samples of the exposed parts of the Archean craton) or 0.826 (assuming that the two northern Finnish post-tectonic granites tapped a higher Sm/Nd Archean lower crust source). Assuming that the Pb concentrations in the Svecofennian and Archean lower crustal sources were equal, the $^{206}\text{Pb}/^{204}\text{Pb}$ ratio of the Archean source is obtained from the equation

$$(8) \quad \frac{^{206}\text{Pb}}{^{204}\text{Pb}}(\text{ARCH}) = \frac{\frac{^{206}\text{Pb}}{^{204}\text{Pb}}(\text{SOV}) - \frac{^{206}\text{Pb}}{^{204}\text{Pb}}(\text{SVEC})}{x} + \frac{^{206}\text{Pb}}{^{204}\text{Pb}}(\text{SOV})$$

where $^{206}\text{Pb}/^{204}\text{Pb}(i)$ is the Pb isotopic ratio in component i , x is the relative proportion of Archean component as defined by equation (7), and ARCH, SOV, and SVEC denote Archean, Soviet Karelian, and Svecofennian components, respectively. An identical equation can be written for the $^{207}\text{Pb}/^{204}\text{Pb}$ ratios. Inserting the least radiogenic alkali feldspar $^{206}\text{Pb}/^{204}\text{Pb}$ ratio of the Finnish granites (16.047) as $^{206}\text{Pb}/^{204}\text{Pb}(\text{SVEC})$ and that of the Soviet Karelian granites (14.961) as $^{206}\text{Pb}/^{204}\text{Pb}(\text{SOV})$ in the equation (8) results in $^{206}\text{Pb}/^{204}\text{Pb}(\text{ARCH}) = 12.703$ for $x = 0.481$ and $^{206}\text{Pb}/^{204}\text{Pb}(\text{ARCH}) = 13.646$ for $x = 0.826$. The corresponding $^{207}\text{Pb}/^{204}\text{Pb}$ ratios are 14.267 ($x = 0.481$) and 14.581 ($x = 0.826$). The Stacey and Kramers (1975) second-stage model ages of these isotopic compositions are 3.21 Ga ($x = 0.481$) and 2.49 Ga ($x = 0.826$), whilst the μ_2 values are 12.0 ($x = 0.481$) and 8.2 ($x = 0.826$). The high apparent μ_2 value of 12.0 calculated assuming the smaller Archean contribution (32%, Table 12) probably indicates that this figure is not valid and suggests a larger amount of Archean contribution in the Soviet Karelian rapakivi granites, and, by implication, that the Archean lower crust has a higher Sm/Nd ratio than the Archean upper crust. The μ_2 value, 8.2, corresponding to the larger value of x , is close to the average μ_2 value, 8.3, calculated for the Pb in the alkali feldspars of the two post-tectonic granites in northern Finland. If the

post-tectonic granites actually represent melts generated from the Archean lower crust (cf. Patchett et al., 1981; Kouvo et al., 1983; Huhma, 1986; Haapala et al., 1987), the calculations imply that the Archean component in the Soviet Karelian batholiths amounts to the higher value suggested by the Nd mixing model (45%, Table 12) and that the Archean lower crust may have an apparent μ_2 value of the order of 8.

The U/Pb evolution of the main postulated sources for Pb in the Fennoscandian shield are shown in Fig. 48. Growth curves for Archean upper crust with $\mu_2 = 11.8$, depleted mantle with $\mu_2 = 9.17$, and average Svecofennian juvenile crust with $\mu_2 = 9.81$ (all approximated from the galena Pb data of Vaasjoki, 1981) as well as for the hypothetical Archean lower crust ($\mu_2 = 8$) are shown along with the calculated composition of the Archean lower crust (using $x = 0.826$). Data on the alkali feldspars of the two post-tectonic granites of northern Finland (Kouvo et al., 1983) and Stacey and Kramers (1975) model isochrons for 1000, 1540, and 1900 Ma are shown as well. In contrast to the data for the Finnish samples, the alkali feldspars from the Soviet Karelian plutons plot to the left of the second-stage model isochron at 1540 Ma (the model ages of the two samples are 1886 and 1724 Ma; Table 6). This implies that the Pb evolution of the Archean source cannot be assessed by this kind of simple two-stage model. It is possible that the Fennoscandian Archean lower crust consists of several different reservoirs with variable, but low, U/Pb ratios, and that more than one of these reservoirs were tapped by the processes that generated the Soviet Karelian rapakivi granite magmas. For example, several reworking events between 3.5 and 2.4 Ga ago, that could also have given rise to such distinct environments with low U/Pb ratios have been identified in the Archean of northern Finland (Jahn et al., 1984).

As can be seen from Fig. 34b, the Soviet Karelian data show, on the average, a slightly higher overall Th/U ratio (4.49) compared to the Finnish data. The κ_2 values ($^{232}\text{Th}/^{238}\text{U}$ ratios) calculated for the Pb in the Soviet Karelian alkali

feldspar fractions are 4.40 and 3.83 (Table 6) while the average for the Pb in the Finnish alkali feldspars is 3.73 ± 0.16 (1 S.D.). This suggests that the Archean lower crustal source (or sources) had a slightly higher average Th/U ratio than the Svecofennian lower crust, a feature presumably resulting from a longer interval of U depletion in the Archean lower crust environment.

While discussing preliminary Nd isotopic data on the Soviet Karelian batholiths, Rämö and Haapala (1991) found it impossible to decide conclusively whether the Archean signature in the

Salmi batholith was inherited from the Archean tonalite-trondhjemite-granodiorite basement itself or from Proterozoic sedimentary rocks carrying a major Archean component. The present data, however, resolve this controversy, because partial melting of such sedimentary source rocks, carrying at least some detritus from the high U/Pb Archean upper crust (cf. Fig. 48), would have produced crustal melts with relatively radiogenic Pb isotopic ratios and thus very different from the unradiogenic Soviet Karelian magmas.

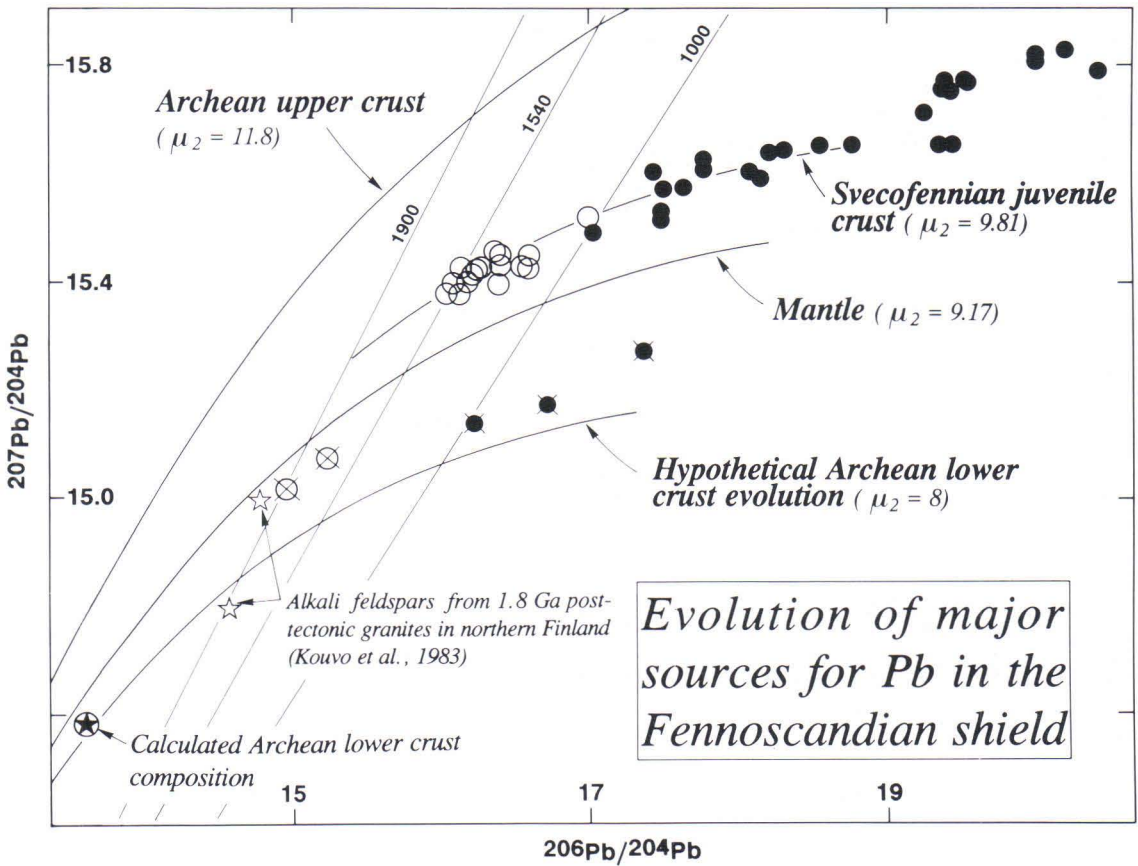


Fig. 48. Pb isotopic data of the Finnish and Soviet Karelian rapakivi granites (Tables 5 and 6) plotted in $^{207}\text{Pb}/^{204}\text{Pb}$ vs. $^{206}\text{Pb}/^{204}\text{Pb}$ diagram showing the growth curves of major sources for Pb in the Fennoscandian shield. The latter comprise Archean upper crust ($\mu_2 = 11.8$), mantle ($\mu_2 = 9.17$), juvenile 1.9 Ga Svecofennian crust ($\mu_2 = 9.81$), and hypothetical Archean lower crust (apparent $\mu_2 = 8$). Stacey and Kramers (1975) model isochrons for 1000, 1540, and 1900 Ma are also shown. Rapakivi samples: open circles — Finnish alkali feldspars; closed circles — Finnish whole rocks; crossed open circles — Soviet Karelian alkali feldspars; crossed closed circles — Soviet Karelian whole rocks. Composition of alkali feldspars from two 1.8 Ga post-tectonic granites in northern Finland (Kouvo et al., 1983) and a calculated Archean lower crust composition are also shown. See text for further details.

RAPAKIVI-AGE BASIC ROCKS: MANTLE SOURCE CHARACTERISTICS AND MAGMA EVOLUTION

Evolution of the diabase dyke magmas

The Subjotnian diabbases were crystallized from basic liquids that were rapidly quenched at shallow levels near the surface of the Earth. This is manifested by the observation of Lindqvist and Laitakari (1980) who reported basaltic glass from a dyke belonging to the Häme swarm proper. Accordingly, the analysed dyke samples are considered to give a reasonable indication of the composition of the actual liquids from which the dykes crystallized. Some qualitative aspects of diabase magma evolution are discussed below along with quantitative modeling based on major and trace element as well as isotopic data. The discussion is based on the data of the Suomenniemi swarm and the Lovasjärvi intrusion that geographically constitute relatively restricted sampling. This minimizes complications arising from possible lateral compositional heterogeneity in the lithosphere (i.e., continental crust and lithospheric mantle) from which the diabase dykes are thought to have inherited their compositional features.

Primitive melts from a LIL-enriched mantle?

One possible explanation for the incompatible trace element enriched character, unradiogenic Nd isotopic compositions, and the radiogenic Pb isotopic compositions of the Subjotnian diabbases is that they were derived from an enriched mantle source in the subcontinental lithosphere. Studies of ultramafic xenoliths in alkali basalts and kimberlites suggest variable relative enrichment or depletion of the lithophile trace elements (the LREE, K, U, Th, Rb etc.) in the uppermost parts of the subcontinental mantle (e.g., Menzies, 1983; Nixon & Davies, 1987; McDonough, 1990). The xenoliths have been grouped into different categories on the basis of their time-integrated isotopic ratios and element contents. Enriched

compositions have been attributed to enrichment processes caused by silicate melts or CO₂-H₂O fluids enriched in these elements (cf. Bailey, 1982; Menzies, 1983; Hawkesworth et al., 1984; Le Roex, 1987). One geological environment in which these enrichment processes can occur is the subcontinental lithosphere above a subduction zone where the lithospheric mantle is affected by LIL-element enriched fluids derived from the down-going slab (Wittke et al., 1989). Partial melting of the enriched parts of the subcontinental lithospheric mantle can produce primitive mafic melts with a LREE-enriched character.

In order to discern whether the REE patterns of the diabase dykes of the Suomenniemi swarm could have been produced by partial melting of a LREE-enriched mantle source, two modal batch melting models were devised. These involved spinel lherzolite from the upper parts of the lithospheric mantle and garnet lherzolite representing higher pressure (cf. McDonough et al., 1985). Modal compositions used were 80% olivine, 10% orthopyroxene, 8% clinopyroxene, and 2% spinel for the former (Menzies, 1983) and 50% olivine, 30% orthopyroxene, 10% clinopyroxene, and 10% garnet for the latter (Cox, 1983). REE contents used were those suggested for post-Archean subcontinental lithospheric mantle by McDonough (1990). The models were derived using the trace element modeling program MODULUS (Knoper, 1989), with the crystal/liquid distribution coefficients listed in Appendix 3. Both the average ($La_N = 8.39$, $[La/Yb]_N = 6.74$) and maximum ($La_N = 26.8$, $[La/Yb]_N = 14.0$) REE contents given by McDonough (1990) were used in the calculations.

The results of the calculations are shown in Fig. 49. It is evident from Figs. 49a and b that batch melting of garnet lherzolite does not yield the REE pattern of the diabase dykes: the resulting patterns are much too enriched in the LREE.

Moreover, as garnet peridotites in general are somewhat more enriched in the LREE than spinel peridotites (McDonough, 1990), these melt patterns may indicate the minimum LREE-enrichments produced by melting garnet-bearing peridotites. Patterns more in accordance with the diabase data are obtained by melting of spinel

lherzolite (Fig. 49c and d). At the relatively large degrees of partial melting (10 to 30%) that are generally believed to produce tholeiitic melts from mantle peridotite (e.g., Jaques & Green, 1980; Basaltic Volcanism Study Project, 1981), LREE-enrichments similar to those measured for the samples of the Lovasjärvi intrusion are

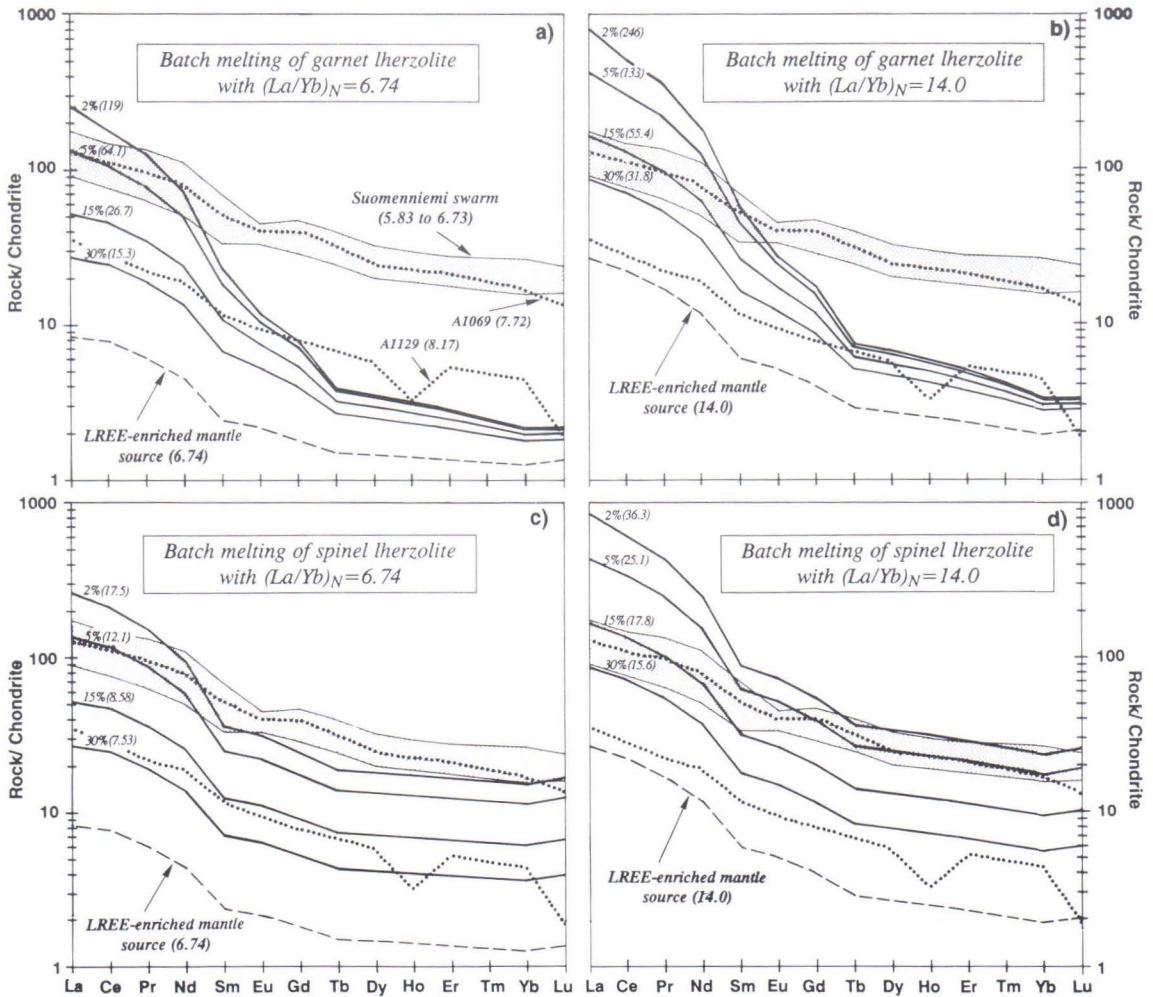


Fig. 49. Batch melting models of various postulated upper mantle compositions enriched in the light rare earth elements. (a) and (b) demonstrate the results of batch melting calculations of garnet lherzolite (50% olivine, 30% orthopyroxene, 10% clinopyroxene, 10% garnet), (c) and (d) those of spinel lherzolite (80% olivine, 10% orthopyroxene, 8% clinopyroxene, 2% spinel), with REE contents as those suggested for post-Archean subcontinental lithospheric mantle by McDonough (1990). Thick solid lines indicate 2, 5, 15, and 30 % melting of the lherzolites (dashed patterns) with the average (a and c) and maximum (b and d) REE abundances of McDonough (1990). The compositional band of the diabase dykes of the Suomenniemi swarm (shaded area) and the patterns of the two samples of the Lovasjärvi intrusion (stippled) are also shown. Numbers in parentheses indicate chondrite-normalized La/Yb ratios.

produced by partial melting of spinel lherzolite with the average REE contents of McDonough (1990). 10 to 30% batch melting of spinel lherzolite with 2690 ppm Cr (McDonough, 1990) would, however, produce tholeiitic melts with 960 to 1120 ppm Cr, which is very different from what is observed for the Subjotnian diabases (i.e., 13 to 85 ppm Cr; Appendix 2). The liquid line of descent followed by such primitive mafic melts to more evolved compositions such as the Subjotnian diabases requires pyroxene and/or spinel fractionation, further increasing the level of LREE-enrichment, in excess of those measured for the diabase dykes and the Lovasjärvi intrusion.

In the light of the batch melting models it seems unlikely that the Suomenniemi diabases represent unmodified melts from LREE-enriched lithospheric mantle sources. Considering the uncertainties involved in choosing the source compositions and crystal/liquid partition coeffi-

cients, conclusive evidence against such an origin is lacking, however. It is nevertheless worthwhile to seek other causes for the LREE-enriched character of the diabase dykes.

Qualitative constraints from petrography and major and trace element variations

Nearly all of the diabases from the Suomenniemi area have plagioclase as a liquidus phase — either being conspicuously plagioclase-phyric, or showing at least some scattered plagioclase phenocrysts or megacrysts. The olivine phenocryst pseudomorphs found in the chilled margins of some dykes, and the melatroctolite cumulate of the Lovasjärvi intrusion further suggest that olivine has probably been cotectic with plagioclase. Because tholeiitic basalts in general are expected to precipitate few phenocrysts during their ascent from magma chambers (Huppert &

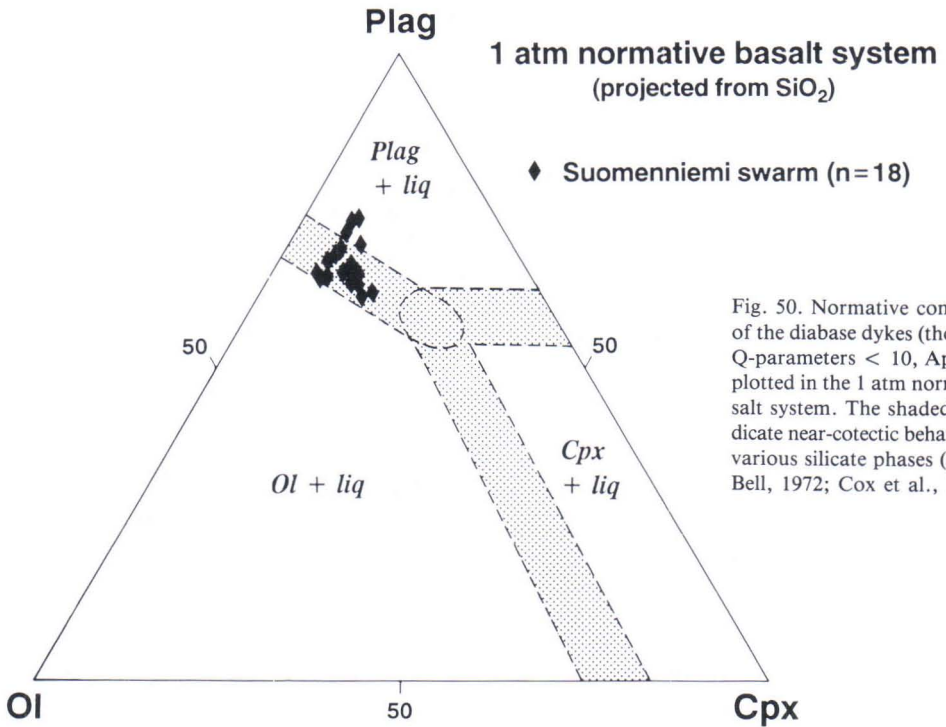


Fig. 50. Normative compositions of the diabase dykes (those having Q-parameters < 10, Appendix 2) plotted in the 1 atm normative basalt system. The shaded areas indicate near-cotectic behavior of the various silicate phases (cf. Cox & Bell, 1972; Cox et al., 1979).

Sparks, 1985), the observed phenocryst assemblages are probably the result of magma evolution that took place at depth, i.e., within intracrustal chambers.

The fact that plagioclase and olivine are found as liquidus phases in the diabases of the Suomenniemi complex can be used to place constraints on the overall pressure regime in which the dyke magmas developed. The composition of the dia-

base dykes is plotted in the simple normative basalt (Ol-Cpx-Plag-Qz) system in Fig. 50 (cf. Cox et al., 1979, p. 230). Most of the dykes plot on the 1 atm olivine + plagioclase cotectic as expected from petrographic observations. Those having high Al_2O_3 (samples A1063, A1064, A1101, and O239.1) are slightly displaced from the cotectic, falling in the plagioclase + liquid field, which is consistent with them possibly being somewhat cumulus-enriched with respect to plagioclase. Qualitatively, these observations suggest that the diabase magmas last equilibrated in a low-pressure environment.

In Fig. 51, the Ni, Cr, and Sr abundances in the diabases of the Suomenniemi swarm are plotted against their MgO content. Positive correlations exist between Ni and MgO as well as Cr and MgO, while Sr is relatively constant though scattered relative to MgO. These trace element patterns are typical of low-pressure gabbro (plagioclase + olivine + clinopyroxene) fractionation: declining Ni with MgO caused by olivine removal, declining Cr by clinopyroxene removal or by fractionation of Cr spinel at slightly higher pressure, and nearly constant Sr maintained by plagioclase fractionation (cf. Cox, 1980; Cox & Hawkesworth, 1985).

Gabbro fractionation results in specific major element patterns, including sympathetic behavior of CaO and MgO, relatively constant though variable Al_2O_3 , and Fe enrichment relative to Mg (Cox, 1980). The data on the Subjotnian diabases show a rough positive CaO vs. MgO correlation (Fig. 52a) and scattered Al_2O_3 with respect to MgO (Fig. 52b). Fe is not, however, enriched relative to Mg (Fig. 52c). This may, at least in part, result from the combined effects of the high overall degree of Fe-enrichment of the dykes (see Fig. 26) and the apparent dominant role of plagioclase in the fractionating assemblage (olivine phenocrysts, although present, are very rare compared to plagioclase phenocrysts). That clinopyroxene was fractionated is suggested by the decreasing Cr (Fig. 51b) and is further supported by the declining CaO/ Al_2O_3 ratio relative

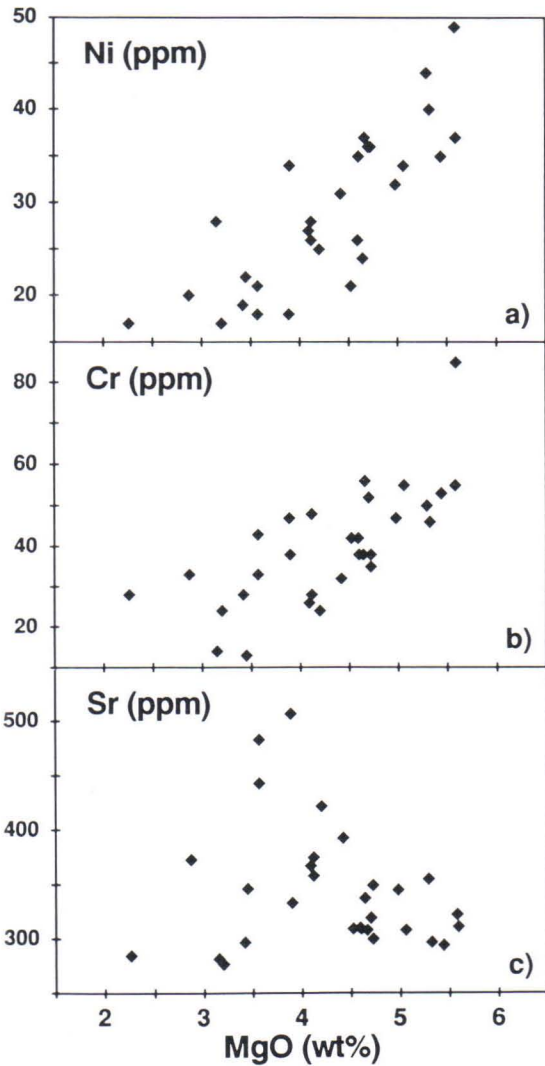


Fig. 51. The chemical analyses of the diabase dykes of the Suomenniemi swarm (Appendix 2) plotted in (a) Ni vs. MgO, (b) Cr vs. MgO, and (c) Sr vs. MgO variation diagrams.

to MgO (Fig. 52d; cf. Basaltic Volcanism Study Project, 1981, p. 153). No clinopyroxene phenocrysts are present in the dykes, however. This conflict of major and trace element variations invoking clinopyroxene fractionation, and lack of clinopyroxene as a phenocryst phase, has been reported elsewhere in association with continental basalts (Cox, 1980; Basaltic Volcanism Study Project, 1981, and references therein; Lightfoot et al., 1990). It may indicate precipitation of clinopyroxene at higher pressure, with resorption of the phenocrysts, possibly due to certain polybaric effects within the low-pressure regime, as suggested by Cox (1980).

In the conventional normative Ol-Hy-Di-Qz-Ne diagram (Fig. 25), the diabase dykes show a range from silica-saturated to silica-oversaturated compositions and plot rather close to the Hy corner.

They fall clearly below the 1 atm olivine + plagioclase + clinopyroxene cotectic of Walker et al. (1979), close to the tentative lower crust plagioclase + clinopyroxene \pm olivine \pm magnetite cotectic of Thompson et al. (1983). This projection also implies clinopyroxene fractionation taking place at a higher pressure.

In conclusion, petrographic features (plagioclase and olivine on the liquidus) and the compositional patterns shown in Figs. 25 and 50 suggest that the evolution of the diabase magmas of the Suomenniemi swarm was to a considerable extent controlled by fractionation in a crustal pressure regime. This involved plagioclase, olivine, and probably clinopyroxene fractionation that took place while the mafic magmas were evolving in intra-crustal magma chambers. The Lovasjärvi mafic intrusion possibly represents

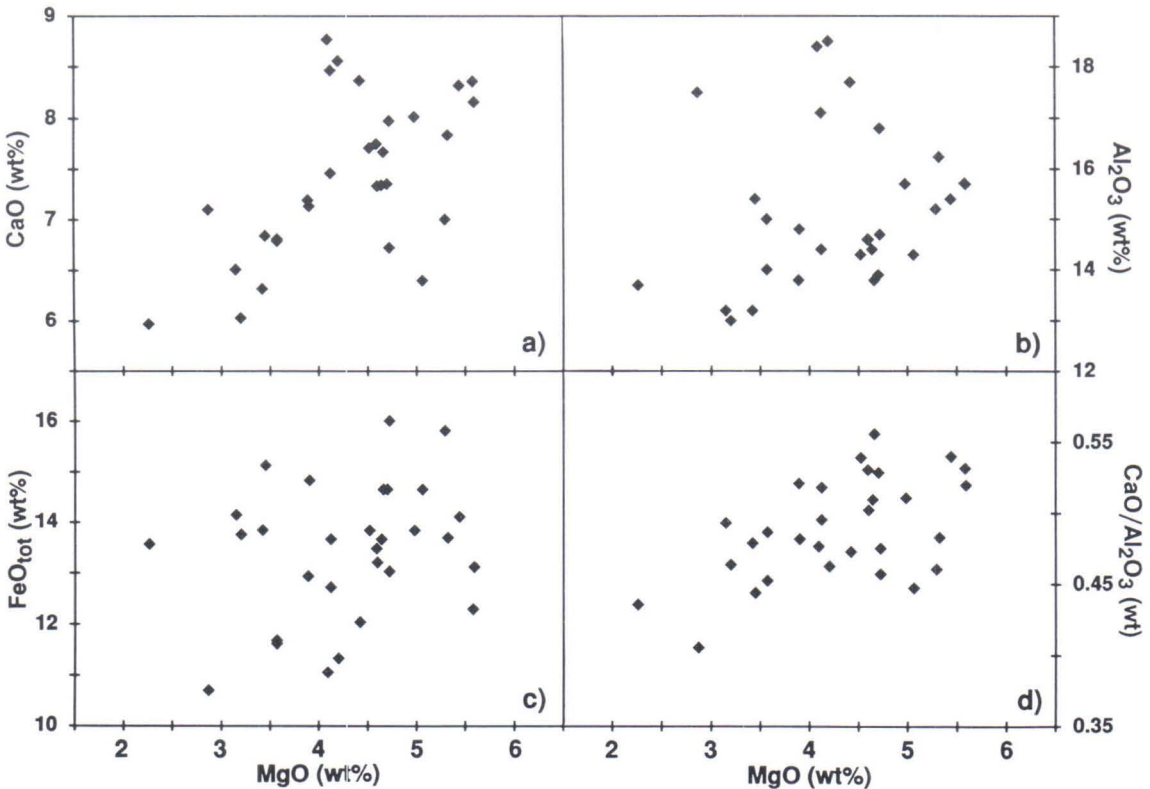


Fig. 52. The chemical analyses of the diabase dykes of the Suomenniemi swarm (Appendix 2) plotted in (a) CaO vs. MgO, (b) Al₂O₃ vs. MgO, (c) FeO vs. MgO, and (d) CaO/Al₂O₃ vs. MgO variation diagrams.

such a chamber, and provides evidence for the fractionation processes. The conclusions above confirm those of Boyd (1972) who considered the chemical characteristics of the Häme swarm to be products of extensive near-surface fractionation.

Closed-system fractional crystallization modeling

In order to find out whether closed-system fractional crystallization could account for the compositional variation in the Suomenniemi swarm, major element fractional crystallization

modeling was used to assess possible fractionation assemblages and degrees of fractionation over the range of observed dyke compositions. The least-squares approximation program MAGFRAC (Morris, 1984) was used to calculate assemblages and degrees of fractionation consistent with assumed initial and evolved liquid compositions.

Because the major element compositions of the analysed dyke samples show pronounced scatter at any one level of SiO₂ and MgO contents (Figs. 24 and 52), averages of several analyses were used as end-member compositions in the modeling. For the initial liquid, the average com-

Table 13. Least-squares major element modeling of the diabase dykes of the Suomenniemi swarm. See text for details.

	MODEL I			MODEL II		
Fractionating assemblage:						
	65%	plagioclase		60%	plagioclase	
	20%	olivine		23%	olivine	
	11%	clinopyroxene		16%	clinopyroxene	
	3%	magnetite		0.2%	magnetite	
	1%	ilmenite		0.8%	ilmenite	
F ^a	0.46			0.47		
ΣR ^{2b}	< 0.25			< 0.33		
Model liquid compositions:						
	Initial Assumed	Initial Calculated	Evolved Assumed	Initial Assumed	Initial Calculated	Evolved Assumed
SiO ₂	49.14	49.16	53.50	49.66	49.71	as in I
TiO ₂	2.23	2.23	3.21	1.90	1.90	
Al ₂ O ₃	17.29	17.31	13.66	16.32	16.31	
FeO ^c	12.97	12.97	14.21	12.78	12.78	
MnO	0.19	0.16	0.18	0.19	0.16	
MgO	5.06	5.03	2.95	5.79	5.73	
CaO	8.53	8.49	6.34	8.68	8.60	
Na ₂ O	2.75	2.27	2.43	2.45	2.19	
K ₂ O	1.35	1.24	2.34	1.74	1.25	
P ₂ O ₅	0.50	0.54	1.18	0.49	0.56	

Note: The analyses were normalized to 100% total for the modeling.

^a Fraction of residual liquid remaining.

^b Sum of the squares of the residuals.

^c Total Fe reported as FeO.

Table 14. Composition of olivines, clinopyroxenes, and plagioclases from the diabase dykes of the Suomenniemi swarm and olivines from the melatroctolite cumulate of the Lovasjärvi intrusion.

Sample	Olivines						Clinopyroxenes						Plagioclases				
	A1063	O30.1	O30.1 (margin)	O138.1	Lovasjärvi intrusion		A1063	A1063 (margin)	O30.1	A1064	O138.1	O138.1 (margin)	A1063	O30.1	O30.1 (margin)	A1064	O138.1
					A1129	18396											
SiO ₂ (wt%)	34.22	33.01	32.50	33.20	35.30	36.56	47.70	48.21	49.09	49.52	48.92	50.00	53.30	51.98	51.45	52.89	53.13
TiO ₂	0.07	0.03	0.03	0.02	0.02	0.04	1.84	1.60	1.06	0.97	1.28	0.60	0.13	0.13	0.08	0.03	0.08
Al ₂ O ₃	0.05	0.02	0.04	0.05	0.22	0.00	3.80	3.11	2.31	1.93	2.46	1.42	29.17	30.55	30.91	29.68	29.36
FeO ^a	41.51	42.48	49.25	48.46	36.76	35.84	14.92	15.20	14.31	16.99	15.54	16.17	0.60	0.60	0.52	0.51	0.42
MnO	0.56	0.63	0.77	0.79	0.40	0.37	0.32	0.32	0.30	0.40	0.40	0.34	0.03	0.00	0.00	0.00	0.02
MgO	23.29	24.16	17.93	17.50	27.99	26.74	11.49	11.81	13.43	12.58	11.88	11.24	0.06	0.06	0.07	0.05	0.06
CaO	0.26	0.00	0.00	0.06	0.07	0.15	19.29	19.01	18.78	17.15	18.63	19.25	11.70	13.05	12.89	12.78	12.76
Na ₂ O	0.00	0.00	0.00	0.00	0.10	0.00	0.33	0.30	0.27	0.27	0.22	0.30	4.09	3.42	3.25	3.67	3.91
K ₂ O	0.00	0.00	0.00	0.00	0.00	0.00	0.02	0.03	0.02	0.02	0.00	0.02	0.39	0.36	0.47	0.33	0.00
Cr ₂ O ₃	0.00	0.00	0.00	0.00	0.04	0.03	0.00	0.06	0.22	0.22	0.00	0.00	0.00	0.00	0.00
NiO	0.07	0.07	0.03	0.06	0.00	0.00	0.04	0.04	0.00	0.00	0.00
ZnO	0.20	0.05
BaO	0.04
Total	100.03	100.40	100.55	100.14	100.86	99.70	99.75	99.62	99.61	99.93	99.79	99.61	99.47	100.15	99.64	99.94	99.74
End-member compositions (mole%):																	
	Fo ^b 50.0	50.3	39.4	39.2	57.6	57.1	Wo ^b 41.1	40.2	38.6	35.8	39.4	40.5	An 59.8	66.7	66.4	64.5	64.3
	Fa ^b 50.0	49.7	60.6	60.8	42.4	42.9	En ^b 34.1	34.7	38.4	36.5	35.0	32.9	Ab 37.8	30.4	31.5	33.5	35.7
							Fs ^b 24.8	25.1	23.0	27.7	25.7	26.6	Or 2.4	2.9	2.2	2.0	0.0

Note: Electron microprobe analyses by Walter Boyd (Suomenniemi swarm) and Jaakko Siivola (Lovasjärvi intrusion).

^a Total Fe reported as FeO.

^b Calculated assuming all Fe as Fe²⁺.

position of eight of the most primitive samples listed in Appendix 2 was used (see Table 13). These exhibit a range of Mg numbers from 48.7 (sample 133.2) to 43.1 (sample 145.1) and normative An/(An + Or) ratios from 0.578 (sample A1064) to 0.556 (sample 136.2), including also some of the high-Al compositions. The average composition of three of the most evolved samples (A1047, A1068, and O176.1, with Mg numbers 25.9, 31.8, and 32.8, respectively) was used for the derived liquid (Table 13).

Microprobe data on olivine, clinopyroxene, and plagioclase of the diabase dykes and the Lovasjärvi intrusion (Table 14) were used as compositions of the fractionating phases. Because the olivine phenocrysts found in the chilled margins of some of the dykes are completely altered, the compositions of the cumulus olivines in the melatroctolite of the Lovasjärvi intrusion were used. The average Mg/Fe ratio of the Lovasjärvi olivines, Fo_{57.4} (Table 14), is almost identical to the Mg/Fe ratio of olivine that would be in equilibrium with the assumed primitive liquid according to the model of Roeder and Emslie (1970), that is Fo_{56.8}. This olivine composition was used throughout the modeling, as the precipitation of olivine probably took place only at relatively early stages of the fractionation (the more evolved dykes lack olivine in the mode and in the norm). The plagioclase composition (An_{59.8}, sample A1063) listed in Table 14 is from a phenocryst, and is less basic than the other four compositions measured in groundmass plagioclase. This could mean that the composition of the plagioclases that precipitated in the magma chambers possibly ranged from more basic, say An₇₀, down to at least An₆₀. It is thus probably justified to use the most basic measured plagioclase composition, An_{66.7}, to model plagioclase fractionation in this context. Because no clinopyroxene phenocrysts are found in the diabase dykes, an average of the non-margin groundmass clinopyroxene analyses listed in Table 14 was used. This involves some uncertainty, but is not considered to result in any substantial error

Table 15. Mineral compositions (in wt%) used for major element least-squares approximation calculations of the diabase dykes of the Suomenniemi swarm.

	Plagioclase	Olivine	Clinopyr.	Magnetite	Ilmenite
SiO ₂	51.64	35.83	49.00	0.52	0.51
TiO ₂	0.08	0.03	1.29	21.88	51.28
Al ₂ O ₃	31.02	0.11	2.64	2.60	0.00
FeO	0.52	36.20	15.50	72.92	45.13
MnO	0.00	0.38	0.36	0.52	0.51
MgO	0.07	27.29	12.39	1.56	2.56
CaO	12.94	0.11	18.53	0.00	0.00
Na ₂ O	3.26	0.05	0.27	0.00	0.00
K ₂ O	0.47	0.00	0.02	0.00	0.00
Total	100.00	100.00	100.00	100.00	100.00

Note: Silicate end-member compositions are An₆₇Ab₃₀Or₃, Fo₅₇, and Wo₃₉En₃₆Fs₂₅.

as the amounts of clinopyroxene fractionation required are relatively small. This is also true with minor amounts of oxides required for modeling; they were assumed to have compositions similar to those measured for a tholeiitic dyke in southwestern Finland by Haapala and Ojanperä (1972b, analysis no. 1 in Tables 2 and 3). The mineral compositions used in the calculations are listed in Table 15 normalized to 100% total.

Calculations show that it is impossible to produce the assumed evolved liquid composition from the assumed initial liquid by fractionating plagioclase alone: the sums of the squares of the residuals, ΣR^2 , are >10 for the assemblages plagioclase ± magnetite ± ilmenite. Better fits are obtained with the observed silicate phenocryst assemblage olivine + plagioclase ± magnetite ± ilmenite, for which ΣR^2 's are >1.0. However, an acceptable result also requires clinopyroxene as a fractionating phase. The best fit with the smallest ΣR^2 (<0.25), is obtained fractionating 35% plagioclase, 11% olivine, 5.5% clinopyroxene, 2% magnetite, and 0.5% ilmenite from the assumed initial liquid with 46% residual liquid. The result of this approximation is shown in Table 13 as model I. The composition of the calculat-

ed initial liquid is close to that of the assumed initial liquid, except for the alkalis which are somewhat higher in the latter.

The modeling supports a dominant role for plagioclase in the evolution of the Suomenniemi swarm. Because some of the dykes constituting the hypothetical initial liquid composition possibly are slightly cumulus-enriched with respect to plagioclase (e.g., sample A1064 with 18.40 wt% Al_2O_3 contains 56 vol% plagioclase), the figure arrived at above for the amount of plagioclase fractionation should be considered a maximum. The most primitive dyke (sample 133.2) with the highest Mg number has lower Al_2O_3 content and higher SiO_2 content (Table 13) than the eight sample average. Using this composition as the assumed initial liquid results in a fractionate of 31% plagioclase, 12% olivine, 8.5% clinopyroxene, 0.1% magnetite, and 0.4% ilmenite with 47% residual liquid remaining (model I in Table 13). The degree of fit is, however, somewhat poorer ($\Sigma R^2 < 0.33$) than in model I. The assemblages olivine + plagioclase \pm magnetite \pm ilmenite yield still poorer fits, with ΣR^2 's > 2.2 .

The closed-system major element fractional crystallization modeling requires that (1) plagioclase had a dominant role in controlling the fractionation of the dykes, (2) clinopyroxene, along with plagioclase and olivine, belongs to the fractionating assemblage, although it has not been encountered as a phenocryst phase in the dykes, and that (3) a relatively large amount of crystallization, about 55%, is needed to yield the evolved liquid composition, assuming the fractionation actually took place in a closed system.

The validity of the closed-system fractional crystallization modeling was tested in an attempt to produce the REE pattern of one of the most evolved dykes (A1068) from that of one of the most primitive dykes (A1101). In the modeling, crystal/liquid distribution coefficients listed in Appendix 3 were used. They were compiled from various studies of trace element partitioning between mafic melts (preferably tholeiitic basalt)

and precipitating mineral phases (Hanski, 1983, and references therein). Using the calculated gabbroic assemblage of model I (Table 13) and $F = 0.46$ for closed-system FC modeling of REE with concentrations for the primitive liquid being those measured for the sample A1101 that has the lowest total abundances of REE except Eu ($\text{La}_N = 91$, $(\text{La}/\text{Yb})_N = 5.83$), ends up with similar contents of the LREE ($\text{La}_N = 182$) than those measured for sample A1068 ($\text{La}_N = 177$; see Fig. 53). Closed-system fractional crystallization of this assemblage does not, however, produce the observed LREE-enrichment: the modeled evolved liquid has a $(\text{La}/\text{Yb})_N$ ratio of 5.89 while that for the sample A1068 is 6.73. This is also true for the model II FC assemblage (Table 13) that results in $\text{La}_N = 179$ and $(\text{La}/\text{Yb})_N = 6.02$ at $F = 0.47$.

The fact that closed-system fractional crystallization modeling does not seem to account for the within-swarm LREE-enrichment suggests that the fractionation of the dyke magmas took place in an open system. This is further suggested by Nd isotopic-compositional correlations.

Nd isotopic-compositional correlations

The Nd isotopic composition of the diabase dykes shows a consistent correlation with the chemical composition of the dykes. Generally, the higher the Sm and Nd concentrations, the lower the $^{147}\text{Sm}/^{144}\text{Nd}$ ratios, $^{143}\text{Nd}/^{144}\text{Nd}$ ratios, and $\epsilon_{\text{Nd}}(T)$ values, and the higher the T_{DM} model ages (Table 4).

Correlations also exist among Nd isotopic composition and fractionation indicators. Fig. 54 shows the $\epsilon_{\text{Nd}}(T)$ values of the diabase dykes plotted against Mg number and normative $\text{An}/(\text{An} + \text{Ab})$ ratio as well as Rb and Zr concentrations. For the Suomenniemi swarm, logarithmic correlations can be seen, $\epsilon_{\text{Nd}}(T)$ values showing positive correlation with Mg number (Fig. 54b) and normative $\text{An}/(\text{An} + \text{Ab})$ ratio (Fig. 54d), and negative correlation with Rb and Zr concentrations (Figs. 54a and c). Sample

A808a from the Häme swarm deviates from the trend of the Suomenniemi data in the Mg number vs. ϵ_{Nd} plot (Fig. 54b). This may be due to the dyke A808a being rather wide (> 100 m) and possibly having been modified by intra-dyke differentiation. The diabase from the Lovasjär-

vi intrusion (A1069) plots on the Mg number vs. ϵ_{Nd} correlation trend in Fig. 54b and the melatroctolite cumulate (A1129) deviates from it considerably. In the Rb and Zr vs. ϵ_{Nd} value diagrams (Figs. 54a and c) the Lovasjärvi samples deviate from the dyke samples of the Suomen-

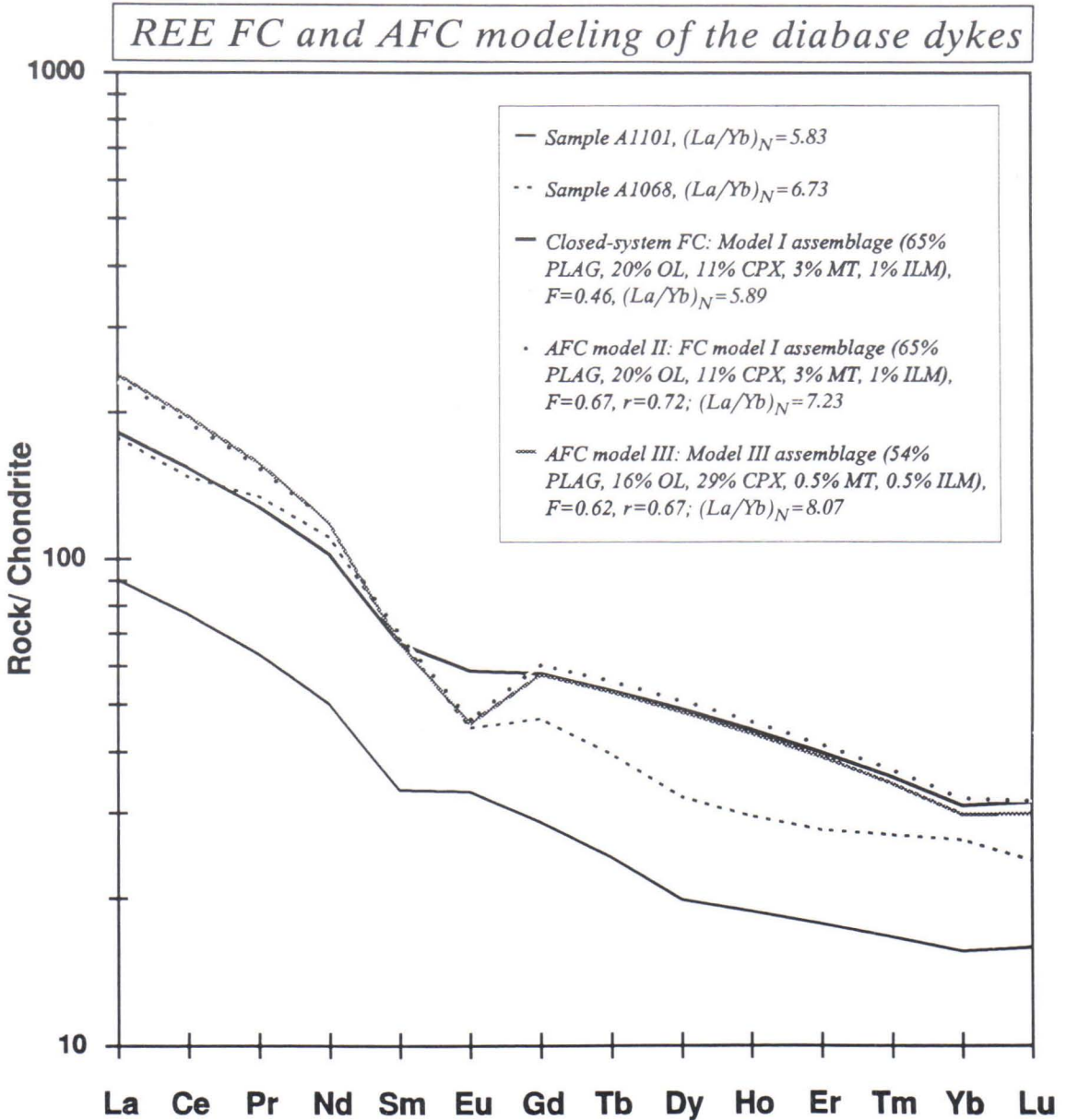


Fig. 53. Rare earth element fractional crystallization (FC) and combined assimilation-fractional crystallization (AFC) modeling of the Suomenniemi diabase dyke swarm. See text for details.

niemi swarm and plot toward lower ϵ_{Nd} values and element concentrations.

These isotopic-compositional correlations favor open-system processes in the evolution of the diabase magmas, as fractional crystallization alone is not capable of fractionating radiogenic isotopic ratios such as those of Nd. The shift of ϵ_{Nd} values from positive to negative with declining Mg number and normative An/(An + Ab) ratio as well as increasing incompatible element concentrations suggests that incorporation of materials with relatively unradiogenic Nd isotopic composition and relatively high contents of incompatible elements has occurred concomitantly with fractional crystallization.

Combined assimilation-fractional crystallization modeling

It has been shown by various workers (e.g., Patchett, 1980; Watson, 1982; Farmer & DePaolo, 1983) that basic magmas intruded into the continental crust can be contaminated with crustal materials. Two different models of contamination have been proposed: assimilation in intra-crustal magma chambers in association with fractional crystallization (DePaolo, 1981b) and assimilation while flowing through dykes (Huppert & Sparks, 1985). The latter is applicable for high-temperature mafic magmas (e.g., komatiites and picritic basalts), but is considered of less im-

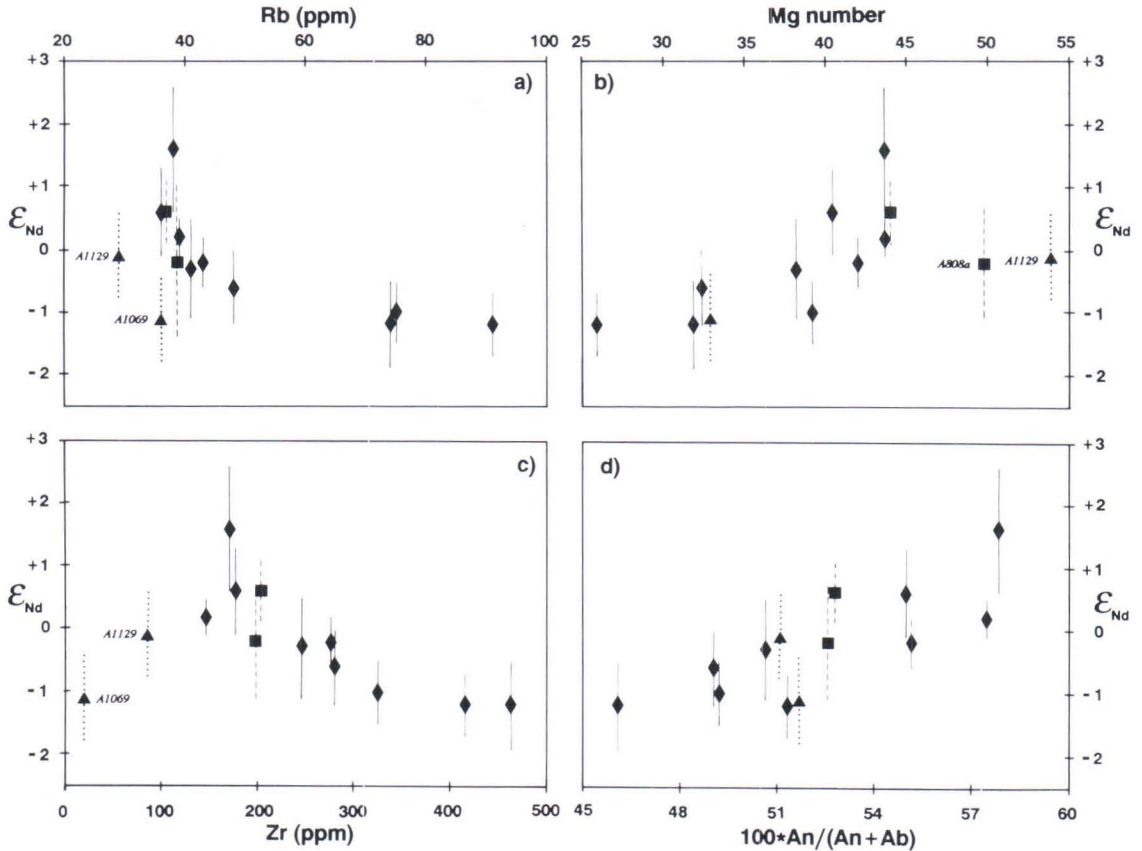


Fig. 54. Initial Nd isotopic composition of the diabase dykes and the Lovasjärvi intrusion (Table 4), expressed as $\epsilon_{Nd}(T)$ values, plotted against their (a) Rb and (c) Zr concentrations, (b) Mg numbers, and (d) normative An/(An + Ab) ratios (Appendix 2). Vertical lines indicate analytical errors of the ϵ_{Nd} values. Symbols are as in Fig. 24.

portance for cooler and more viscous basaltic liquids (Huppert & Sparks, 1985).

It is probable that the primitive mantle-derived magmas (presumably with a time-integrated LREE-depleted character), from which the Subjotnian diabbases eventually crystallized, were subject to contamination. The diabase dykes provide information on late evolutionary stages of these magmas, and it is possible that incorporation of crustal materials concomitantly with fractional crystallization in the low-pressure crustal environment resulted in the intra-swarm variation in LREE-enrichment (Fig. 53) and variable initial Nd isotopic compositions (Fig. 33a). An attempt is made below to assess the validity of the latter hypothesis using combined assimilation-fractional crystallization (AFC) modeling.

Assimilation occurring concurrently with fractional crystallization was considered a viable petrological process by Bowen (1928) who discussed assimilation of granitic fragments incorporated into fractionating basaltic magma, driven by the liberation of latent heat of crystallization from the latter. Mathematical formulation of AFC processes involving a magma body that is assimilating chamber wallrock at a certain rate and simultaneously precipitating crystals at a rate that may or may not be equal to the rate of assimilation was developed by DePaolo (1981b). In recent studies of layered basic intrusions (DePaolo, 1985; Stewart & DePaolo, 1990) the model has been extended to take into account such processes as magma replenishment and extrusion as well. According to DePaolo (1981b), the concentration of element *m*, C_m , in a fractionating and assimilating magma is described by the equation

$$(9) \quad C_m = C_m^0 \left[F^{-z} + \left(\frac{r}{r-1} \right) \frac{C_a}{zC_m^0} (1-F^{-z}) \right]$$

for *r* values not equal to one, where C_m^0 is the initial concentration of element *m* in the magma, *F* is the amount of residual liquid remaining, *r* is the ratio of mass assimilation rate (\dot{M}_a) to

the fractional crystallization rate (\dot{M}_c), *z* is given by $z = (r + D - 1)/(r - 1)$ where *D* is the bulk *D*-value of element *m* in the magma, and C_a is the concentration of element *m* in the assimilate. The relative amount of assimilate, M_a , to the mass of the original magma, M_m^0 , is given by

$$(10) \quad M_a = M_m^0 \left(\frac{r}{r-1} \right) (F-1)$$

(cf. Farmer & DePaolo, 1983).

AFC evolution paths differ from simple closed-system fractional crystallization paths particularly for elements that have bulk *D*-values much smaller than one, i.e. the strongly incompatible elements. These are enriched in the residual magma more effectively by AFC processes than by fractional crystallization alone. This applies to the REE in basaltic magmas.

To model changes in the isotopic composition of radiogenic elements in magmas evolving by AFC processes, DePaolo (1981b) showed that, for *r* values not equal to one, the resulting isotopic ratio ϵ_m of an assimilating and crystallizing magma can be written as

$$(11) \quad \epsilon_a = (\epsilon_a - \epsilon_m^0) \left[1 - \left(\frac{C_m^0}{C_m} \right) F^{-z} \right] + \epsilon_m^0$$

where ϵ_m^0 is the initial isotopic ratio of the magma and ϵ_a is the isotopic ratio in the assimilate.

The Subjotnian diabase dykes were emplaced in an environment in which large volumes of silicic magmas were produced within the continental crust that the dyke magmas penetrated. Such partially molten crust is expected to be an effective density barrier for basic melts (e.g., Perry et al., 1987; Huppert & Sparks, 1988). Besides rendering the passage of the basic melts through the crust slower, it also provides a high-temperature environment in which contamination of the basic melts by crustal materials is more likely than if they were intruded into cooler non-anatectic crust.

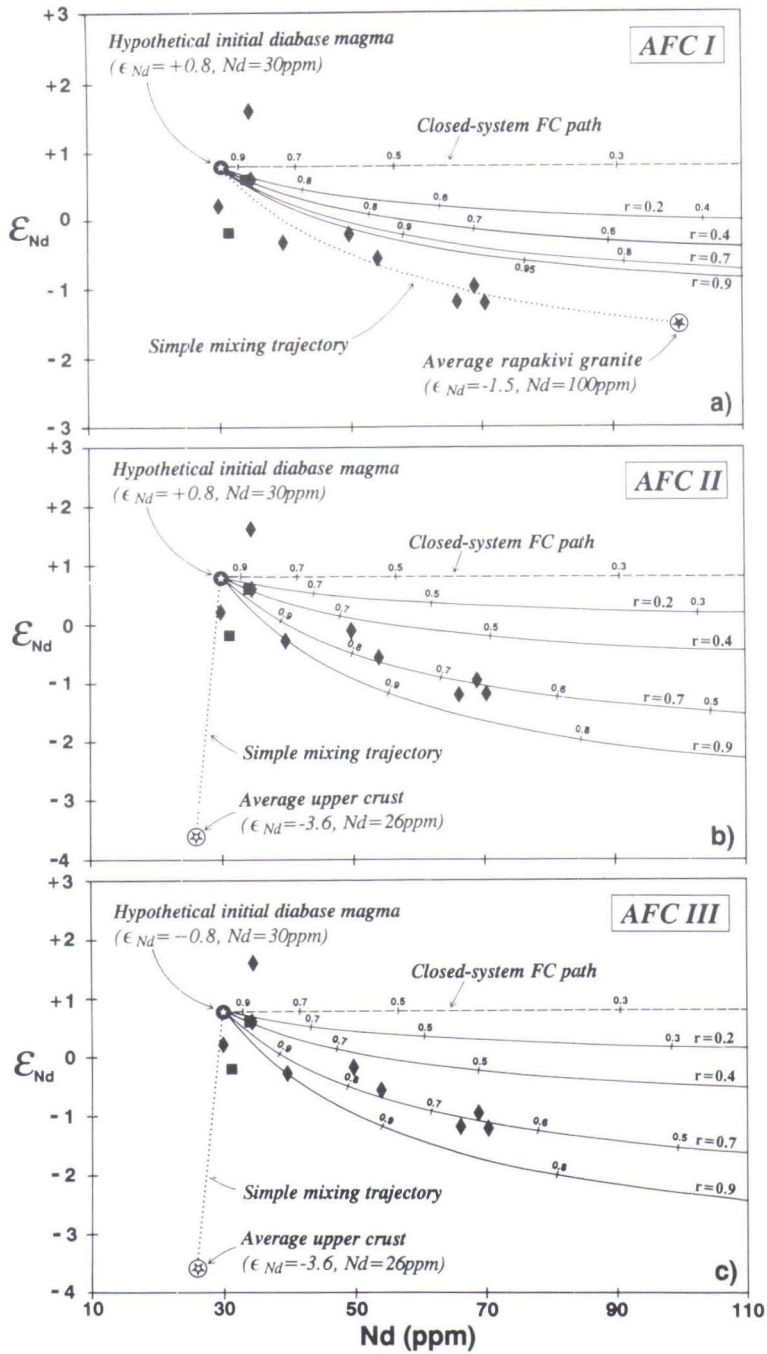


Fig. 55. ϵ_{Nd} vs. Nd concentration of the diabase dykes of the Suomenniemi (diamonds) and Häme (squares) swarms and curves (solid lines) denoting possible shifts in ϵ_{Nd} and Nd content at r values of 0.2, 0.4, 0.7, and 0.9 for a hypothetical initial diabase magma ($\epsilon_{Nd} = +0.8$, $Nd = 30$ ppm) undergoing concomitant fractional crystallization of a gabbro assemblage (a and b: 65% plagioclase, 20% olivine, 11% clinopyroxene, 3% magnetite, 1% ilmenite; c: 54% plagioclase, 16% olivine, 29% clinopyroxene, 0.5% magnetite, 0.5% ilmenite) and assimilation of (a) average rapakivi granite ($\epsilon_{Nd} = -1.5$, $Nd = 100$ ppm) and (b and c) average upper continental crust ($\epsilon_{Nd} = -3.6$, $Nd = 26$ ppm). Closed-system fractional crystallization paths (dashed) and simple mixing lines (dotted) between the end-member compositions are shown as well. Tick marks along the paths denote fractions of residual liquid remaining (F).

To model open-system evolution of the diabase dyke magmas, an intra-crustal magma chamber was assumed in which the basaltic magma fractionates and incorporates materials from the chamber wall rocks or anatectic melts. The individual diabase dykes are assumed to sample this evolving chamber at different stages of its evolution. This is considered justified as tholeiitic magmas are expected to be little modified by contamination and/or fractionation during flowage through dykes (Huppert & Sparks, 1985). Moreover, such a model of magma evolution in an intra-crustal chamber(s) is consistent with the overall low-pressure major element signature of the diabase dykes (Figs. 25 and 50). One may argue about the validity of assuming a single intra-crustal magma chamber for the diabase dykes of the Suomenniemi swarm that are exposed over an area of more than 500 km². The model, however, is probably applicable for one or more discrete intra-crustal reservoirs in which the magmas evolve by similar processes (low-pressure fractionation, assimilation of grossly similar crustal compositions).

Because the Svecofennian crust was loaded with anatectic rapakivi granite magma at the time of emplacement of the diabase dykes, it was first considered whether such felsic melts could have acted as the contaminant during the low-pressure fractionation of the diabase magmas. The rapakivi granites and associated silicic dyke rocks analysed in the present study have high contents of Nd and other LREE, and the magmas from which they crystallized most probably had these characteristics too. The average Nd abundance measured for the felsic rocks is 99 ppm and the average initial ϵ_{Nd} value of the silicic rocks and alkali-feldspar syenites of the Suomenniemi complex is -1.54 (cf. Table 3).

To determine whether or not a melt with such characteristics (Nd = 100 ppm, ϵ_{Nd} = -1.5) could have been a contaminant responsible for the variation in the initial Nd isotopic composition measured for the Suomenniemi swarm, AFC model I (Fig. 55a) was devised. The initial diabase magma was assumed to have a Nd content

of 30 ppm, and, because the highest measured ϵ_{Nd} value, $+1.6 \pm 1.0$, has a rather large error on it, an ϵ_{Nd} value of +0.8 (i.e., the average of the three positive ϵ_{Nd} values) was used. The plagioclase-dominated gabbro assemblage of the closed-system FC modeling (with a bulk D-value of 0.080 for Nd) was used as the fractionate; this is considered justified as a first approximation because the observed compatible trace element variations are consistent with such an assemblage, and because the bulk D-value of Nd is actually rather insensitive to modest variations in the relative proportions of the precipitating silicate phases.

As can be seen from Fig. 55a, AFC processes with a contaminant such as the average rapakivi granite cannot account for the measured data pattern, i.e. the shift in the initial Nd isotopic composition from slightly positive (ca. +1) to slightly negative (ca. -1). This is due largely to the relatively high average ϵ_{Nd} value (-1.5) of the rapakivi granites. It should also be noted that although the simple mixing curve in Fig. 55a fits the measured data well, major element constraints render such mixing unlikely. Assuming simple mixing, the most evolved diabase dykes are ca. 4:6 mixtures of the initial diabase magma and the average rapakivi granite. With SiO₂ contents of 49% and 73%, respectively, this mixture would have a SiO₂ content of 63.4% which is clearly too high a figure for the evolved dykes (cf. Table 13).

Because assimilation of the average rapakivi granite, thought to indicate the average ϵ_{Nd} value of the lower parts of the Svecofennian crust, can not explain the changes in the initial Nd isotopic composition of the Suomenniemi swarm, a model upper crustal contaminant with a slightly lower ϵ_{Nd} value was considered next. It has been suggested (e.g., Taylor & McLennan, 1985) that fine grained clastic sediments (shales) represent the average composition of the upper continental crust, at least regarding those elements (e.g., the REE) that are not much fractionated during sedimentary processes. Taylor and McLennan (1985, p. 46) provide an average

Table 16. Major element abundances (in wt%) and selected trace element abundances (in ppm) suggested for average upper continental crust by Taylor and McLennan (1985, p. 46).

SiO ₂	66.0	Zr	190	Nd	26
TiO ₂	0.5	Nb	25	Sm	4.5
Al ₂ O ₃	15.2	Rb	112	Eu	0.88
FeO	4.5	Th	10.7	Tb	0.64
MnO	0.08	U	2.8	Yb	2.2
MgO	2.2	Sr	350	Lu	0.32
CaO	4.2	Cr	35	Ba	550
Na ₂ O	3.9	Ni	20	Hf	5.8
K ₂ O	3.4	La	30	Ce	64

Chondrite-normalized La/Yb ratio 9.2

upper crustal composition, the essentials of which are shown in Table 16. Nd isotopic data on Svecofennian clastic metasedimentary rocks that could represent estimates of average Svecofennian upper crust, are few. Huhma (1987) published Nd data on four metagreywackes and an interbedded intermediate metavolcanite from the Tampere schist belt in central Finland. These supracrustal rocks are enriched in the LREE showing Sm/Nd ratios around 0.18. This is close to the Sm/Nd = 0.173 estimated for the upper continental crust by Taylor and McLennan (1985). The average Nd concentration of the samples analyzed by Huhma (1987) is 32 ppm, while that for the global average of Taylor and McLennan (1985) is 26 ppm.

The initial (1.9 Ga) ϵ_{Nd} values of the supracrustal rocks of the Tampere area average -0.9 (Huhma, 1987). This is similar to the ϵ_{Nd} values of many Svecofennian synorogenic granitoid rocks (Huhma, 1986; Patchett & Kouvo, 1986). Unpublished data on Svecofennian sedimentary rocks indicate generally somewhat lower ϵ_{Nd} values than the data from the Tampere schist belt (H. Huhma, pers. commun., 1990). Calculated at 1.64 Ga, the supracrustal rocks of the Tampere area have ϵ_{Nd} values ranging from -3.1 to -4.0 and averaging -3.6, which is lower than the rapakivi average by about two units (the lowest ϵ_{Nd} value measured for the

Suomenniemi complex is -2.9 ± 0.4 , though). Using the ϵ_{Nd} value -3.6 of the Finnish supracrustal rocks and a Nd concentration of 26 ppm estimated for the average upper continental crust by Taylor and McLennan (1985) as the assimilant, the AFC model II shown in Fig. 55b was generated. The overall trend measured for the Suomenniemi swarm is produced with $r = 0.72$ at $F = 0.67$ which yield $\epsilon_{Nd} = -1.12$ and $Nd = 70.93$ ppm. The r value (assimilation rate/crystallization rate) of 0.72 is relatively large, but probably realistic in a crust with elevated temperatures, locally even close to its fusion temperature (cf. DePaolo, 1981b; Wittke et al., 1989). The amount of crystallization required by the AFC model II, $F = 0.67$, is distinctly smaller than that predicted by the closed-system FC modeling (Table 13).

The $(La/Yb)_N$ ratio of the model upper continental crust of Taylor and McLennan (1985) is 9.2 (Table 16). This is clearly higher than the $(La/Yb)_N$ ratios of the two extreme patterns of the diabase dykes (i.e., 5.83 and 6.73). Using the AFC constraints above ($F = 0.67$, $r = 0.72$) and the Taylor and McLennan (1985) average REE pattern for the upper continental crust for the assimilant results in the AFC model II shown in Fig. 53. The modeled REE pattern exhibits somewhat higher absolute element concentrations than the pattern of the evolved sample A1068 (except for Nd and Sm which are about the same), and a deeper Eu minimum. However, the $(La/Yb)_N$ ratio, 7.23, is now distinctly higher than in the closed-system fractionation modeling.

The AFC modeling outlined here is obviously sensitive to the values chosen for the element concentrations in the assimilant. Nevertheless, it shows that such within-swarm LREE-enrichment as observed in the Suomenniemi diabbases can probably be produced by an AFC process with an average upper crustal composition as the assimilant. More importantly, it also allows for the observed shift in the initial Nd isotopic composition of the dykes.

Major element constraints on assimilation

For the AFC model II outlined above ($r = 0.72$, $F = 0.67$), the mass of the assimilant relative to the mass of the assumed initial magma is calculated from equation (10) to be 0.85. This means that with the average upper crustal composition (66.00 wt% SiO₂) listed in column C in Table 17, assimilation alone would shift the assumed initial basaltic magma composition A (49.14 wt% SiO₂) to an andesite D (56.89 wt% SiO₂); moreover, the SiO₂ content of the final AFC product would be even higher due to the fractionation of a gabbro assemblage.

It is clear that bulk contamination of the diabase magmas with the average upper crustal contaminant is not a feasible solution. Instead, assimilation of only the most easily-fusible (i.e. the most incompatible) elements from such a source may have occurred. Such selective assimilation processes have been experimentally studied by Watson (1982) who modeled basalt contamination by continental crust concluding that selective incorporation of REE and other highly-charged trace cations into basaltic melts is likely under conditions of basalt-induced crustal melting (see also Patchett, 1980). As the continental crust is enriched for example in the LREE and such elements as Th and U relative to the mantle, these elements would be enriched in contaminated mantle-derived mafic melts.

In order to more quantitatively assess possible assimilation processes in the diabase dyke magmas it is instructive to consider the major element effects of the AFC model II outlined above. Considering only fractional crystallization, fractionation of the mineral assemblage calculated in the FC modeling (model I, Table 13) results, at $F = 0.67$, in the composition in column E in Table 17. Comparing the composition E with the proposed assimilant C and the assumed evolved liquid B shows that it is impossible to produce the high TiO₂ (3.21 wt%) and FeO (14.21 wt%) contents of B from E by assimilation of C that has only 0.50 wt% TiO₂ and 4.50 wt% FeO. TiO₂ and FeO are refractory components in the

continental crust (i.e., they are not expected to enter in substantial amounts into partial melts of a felsic crust), and thus fractional crystallization is required to produce the total enrichment of these elements from the assumed initial liquid composition A to the assumed evolved liquid composition B. This is probably also true with MgO and CaO that are refractory constituents as well. Qualitatively, these observations indicate larger relative amount of clinopyroxene fractionation and smaller relative amount of Fe-Ti-oxide precipitation than that suggested by the closed-system FC modeling. Column G in Table 17 shows a composition that is roughly compatible with the requirement that the TiO₂, FeO, MgO, and CaO contents in the evolved liquid B are developed from A by fractional crystallization alone. The composition G is produced from A by fractionating 54% plagioclase, 16% olivine, 29% clinopyroxene, 0.5% magnetite, and 0.5% ilmenite at $F = 0.62$. This model III assemblage has a bulk D-value of 0.109 for Nd, which is somewhat larger than the 0.080 of the closed-system FC model I assemblage. Using this larger bulk D-value for ϵ_{Nd} vs. Nd AFC modeling results in the AFC model III paths shown in Fig. 55c. These are not much different from the paths in Fig. 55b; at $F = 0.62$ and $r = 0.67$, $\epsilon_{Nd} = -1.04$ is fixed for Nd = 71.06 ppm. The REE pattern produced by the AFC model III is also close to the pattern resulting from the AFC model II, showing, however, slightly stronger enrichment in the LREE (Fig. 53).

To change the SiO₂ abundance of composition G (49.94 wt%) to the evolved liquid SiO₂ content of composition B (53.50 wt%) by simple mixing of G with composition C (66.00 wt% SiO₂) would mean 22% contamination of the basaltic magma with the upper crust composition. In order to keep the model self-consistent, however, the relative proportions of Al₂O₃ and Na₂O in the contaminant must be assumed smaller than in the average crustal composition of Taylor and McLennan (1985). This in turn would probably mean larger relative proportion of SiO₂ in the contaminant and hence a compo-

Table 17. Hypothetical major element variations introduced by assimilation and fractional crystallization processes in the diabase magmas of the Suomenniemi swarm. See text for details.

	A	B	C	D	E	G
	Assumed initial liquid	Assumed evolved liquid	Crustal assimilant (Upper crust of Taylor & McLennan, 1985)	Product of bulk assimilation of C by A with $r=0.72$ at $F=0.67$	Product of fractional crystallization of FC model I gabbro assemblage ^a from A at $F=0.67$	Product of fractional crystallization of model III gabbro assemblage ^b (includes larger proportion of clinopyroxene and less oxides than FC model I) from A at $F=0.62$
SiO ₂	49.14	53.50	66.00	56.89	50.62	49.94
TiO ₂	2.23	3.21	0.50	1.43	2.65	3.11
Al ₂ O ₃	17.29	13.66	15.20	16.33	15.68	17.14
FeO ^c	12.97	14.21	4.50	9.08	13.48	14.07
MnO	0.19	0.18	0.08	0.14	0.21	0.20
MgO	5.06	2.95	2.20	3.75	4.14	3.25
CaO	8.53	6.34	4.20	6.54	7.58	6.18
Na ₂ O	2.75	2.43	3.90	3.28	3.03	3.30
K ₂ O	1.35	2.34	3.40	2.29	1.86	2.01
P ₂ O ₅	0.50	1.18	0.27	0.74	0.80

Note: The analyses were normalized to 100% total for the modeling.

^a FC model I assemblage: 65% plagioclase, 20% olivine, 11% clinopyroxene, 3% magnetite, and 1% ilmenite.

^b Model III assemblage: 54% plagioclase, 16% olivine, 29% clinopyroxene, 0.5% magnetite, and 0.5% ilmenite.

^c Total Fe reported as FeO.

sition approaching that of a minimum melt extracted from a quartz-feldspathic source.

Trace element variations

Fig. 56 shows the contents of various incompatible trace elements measured for the dykes of the Suomenniemi swarm plotted against their Zr contents. Each plot shows one of the closed-system FC models (model I assemblage, end at $F=0.46$, Table 13) and two AFC models: AFC model II (FC model I assemblage, $r=0.72$, end at $F=0.67$) and AFC model III (model III assemblage listed in Table 17, $r=0.67$, end at $F=0.62$). All the plots suggest that closed-system fractional crystallization (indicated by the stippled paths) cannot account for the measured incompatible element variations. The $F=0.46$ required by the FC modeling results in paths that span only a half (Figs. 56a, c, and d) or about two-thirds (Figs. 56e, f, and g) of the compositional trends, or are offset from the observed data (Figs. 56b and h). In contrast, the two AFC models produce paths that are consistent with the measured data. The Ba vs. Zr, Hf vs. Zr, La vs. Zr, and Yb vs. Zr plots (Figs. 56a, c, e, and g) show that combined assimilation-fractional crystallization with element concentrations in the assimilant such as those of Taylor and McLennan (1985) model upper crust produces the observed trends at the required stages of fractionation (dashed and solid paths). The trends in the Th vs. Zr, U vs. Zr, Rb vs. Zr, and Nb vs. Zr plots (Figs. 56b, d, f, and h) require an assimilant with concentrations 1/4 to 1/2 times those in the model upper crust (thick solid paths).

The trace element variations are compatible with assimilation of upper crustal materials in which, when normalized against Zr, the REE, Ba, and Hf are most readily entered into the assimilating magma and in which 1/4 to 1/2 of the concentrations of Th, U, Nb, and Rb in the model upper crust are required to construct the best-fit AFC paths. An important point to note is that the data also require assimilation of Zr

and Hf. Zr and Hf are usually considered refractory components during crustal contamination, i.e. they are expected to remain largely in residual zircon during partial melting of the crust (cf. Thirlwall & Jones, 1983). The suggested incorporation of extra crustally derived Zr and Hf in the mafic magmas probably reflects the high overall temperature of the melt-loaded Svecofenian crust during the Subjotnian time.

Compatible trace element vs. Zr variation diagrams for the Suomenniemi swarm are shown in Fig. 57. The data are scattered (largely due to variable Zr), but it is clear that the closed-system FC model fails to produce the overall measured trends. The FC paths (stippled) in the Sr vs. Zr and Cr vs. Zr plots (Figs. 57a and b) follow roughly the observed data, but the degree of fractionation (0.46) is much too small to fit the whole data ranges which would require a F value of about 0.3. The latter is also true regarding the Ni vs. Zr plot (Fig. 57c), which also shows that the bulk D -value of the FC model I assemblage for Ni (3.81) is clearly too large. The AFC model II (dashed path) reproduces almost the whole data range in the Sr vs. Zr plot (Fig. 57a), while the AFC model III (solid line) gives a trend with too small a slope. However, assuming a smaller concentration, 250 ppm, for Sr in the assimilant produces an AFC model III (thick solid path) consistent with the observed data. In the Cr vs. Zr plot (Fig. 57b) AFC model II (dashed path) is roughly consistent with the measured data, while the AFC model III fails to produce an acceptable path, as the melt is too rapidly depleted in Cr. In the Ni vs. Zr plot (Fig. 57c) both AFC models are inconsistent with the measured data: Ni declines much too rapidly in the modeled melts.

Ni and Cr are trace elements that are largely concentrated in refractory minerals (e.g., olivine, pyroxene, and spinel) that are not abundant constituents of the average continental crust. It is thus probable that little Cr and Ni is incorporated into anatectic melts extracted from a typical continental crust, and therefore also into basic melts assimilating such a source. This also seems to be

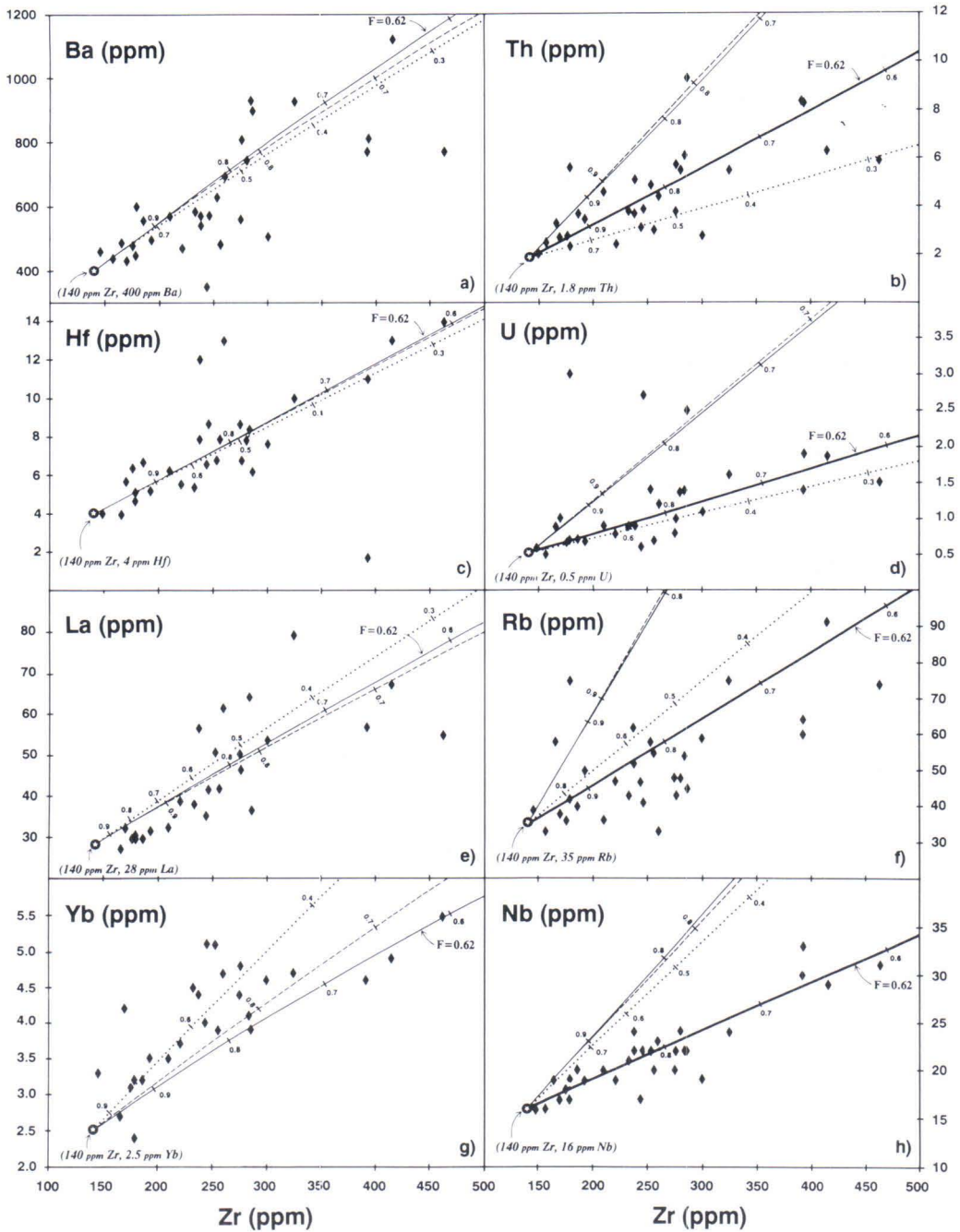


Fig. 56. Incompatible trace element contents in the diabase dykes of the Suomenniemi swarm (diamonds; Appendix 2) plotted in (a) Ba vs. Zr, (b) Th vs. Zr, (c) Hf vs. Zr, (d) U vs. Zr, (e) La vs. Zr, (f) Rb vs. Zr, (g) Yb vs. Zr, and (h) Nb vs. Zr variation diagrams. Each plot shows evolutionary paths for closed-system fractional crystallization of FC model I (Table 13) gabbro assemblage (dotted lines), as well as combined assimilation-fractional crystallization paths with FC model I assemblage (AFC model II, dashed lines) and model III (Table 17) assemblage (AFC model III, solid lines) assuming element abundances in the assimilant as those listed in Table 16. (b), (d), (f), and (h) also show AFC model III paths with assimilant concentrations less than those shown in Table 16, i.e. Th = 5 ppm, U = 0.9 ppm, Rb = 30 ppm, and Nb = 6 ppm (thick solid lines). Tick marks along the paths denote fractions of residual liquid remaining (F). Termination points for AFC model III are shown. Bulk D-values for the model III assemblage (54% plagioclase, 16% olivine, 29% clinopyroxene, 0.5% magnetite, 0.5% ilmenite) are: Ba 0.151, Th 0.016, Hf 0.040, U 0.018, La 0.094, Rb 0.029, Yb 0.209, Nb 0.045, and Zr 0.038.

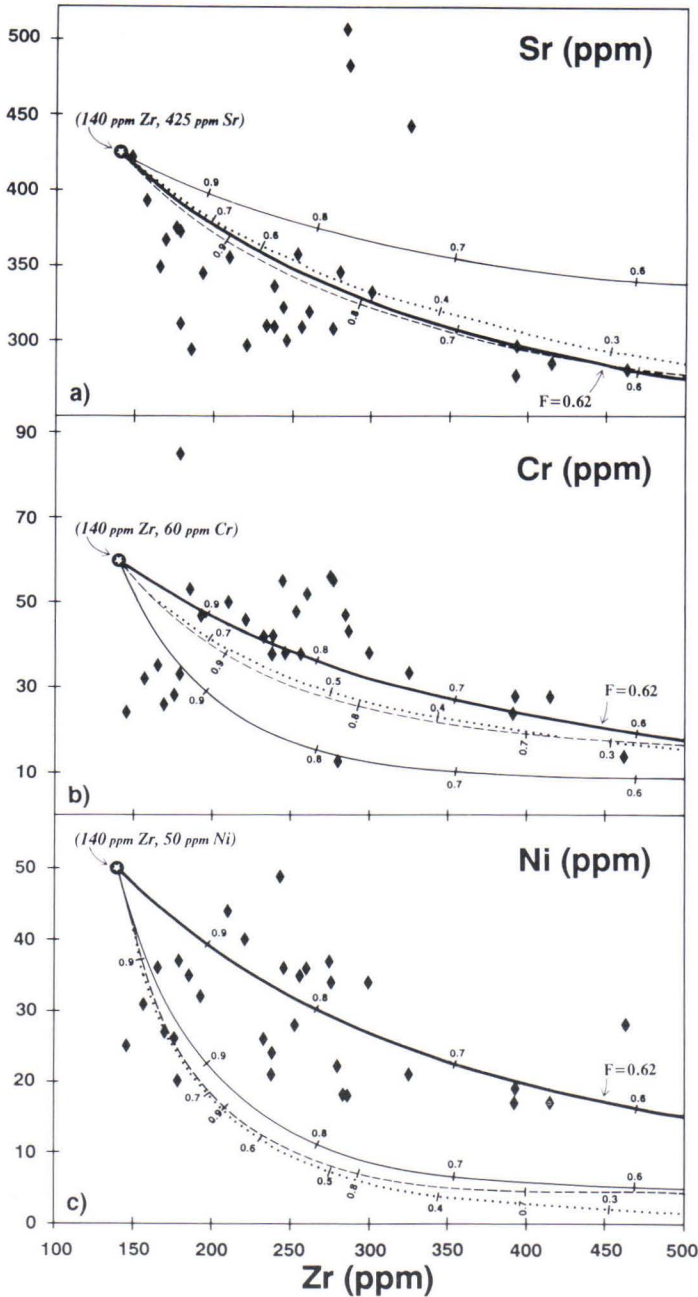


Fig. 57. Compatible trace element contents in the diabase dykes of the Suomenniemi swarm (diamonds; Appendix 2) plotted in (a) Sr vs. Zr, (b) Cr vs. Zr, and (c) Ni vs. Zr variation diagrams. Each plot shows evolutionary paths for closed-system fractional crystallization of FC model I (Table 13) gabbro assemblage (dotted lines), as well as combined assimilation-fractional crystallization paths with FC model I assemblage (AFC model II, dashed lines) and model III (Table 17) assemblage (AFC model III, solid lines) assuming element abundances in the assimilant as those listed in Table 16. (a) also shows an AFC model III path with assimilant Sr concentration less than that in Table 16, i.e. 250 ppm (thick solid line). In (b) and (c) the thick solid lines indicate composite evolution paths calculated assuming closed-system fractional crystallization (model III assemblage) for (b) Cr and (c) Ni and combined assimilation-fractional crystallization (model III assemblage) for Zr. Tick marks along the paths denote fractions of residual liquid remaining (F). Termination points for model III are shown. Bulk D-values for the model III assemblage are: Sr 1.10, Cr 3.24, Ni 3.24, and Zr 0.038.

the case for the diabase dykes of the Suomenniemi swarm, as the observed trends in the Cr vs. Zr and Ni vs. Zr plots (Figs. 57b and c) are produced assuming closed-system fractional crystallization (model III assemblage, $F = 0.62$) for Ni and Cr and AFC model III (model III assemblage, $F = 0.62$) for Zr (thick solid paths in Figs. 57b and c). These composite evolutionary paths would show somewhat deeper slopes if the dilution effect due to the open-system evolution was taken into account, but would, however, probably still be consistent with the measured data. 20% dilution of the basic magma, for instance, would lower the Cr and Ni contents in the modeled melts by about 4 ppm at $F = 0.62$.

In conclusion, the models show that the evolution of the basaltic magma(s) from which the

diabase dykes of the Suomenniemi swarm crystallized most probably took place in an open system. The magma evolution can be assessed by standard AFC modeling (DePaolo, 1981b). The proposed rate of assimilation (assimilation rate relative to crystallization rate of 0.67) is large enough to render the bulk assimilation of the average upper crust composition (Taylor & McLennan, 1985) impossible. Nevertheless, the measured trace element and Nd isotopic trends can be produced by incorporation of the more incompatible constituents from the model upper crust composition concurrently with fractionation of a plagioclase-rich gabbro assemblage in which the amount of clinopyroxene exceeds that of olivine.

Model for the origin of uranogenic Pb in the diabases

The Pb isotopic systematics of the diabase dykes are consistent with a major incorporation of crustal Pb into the mafic magmas. In Fig. 58, a model for the origin of the uranogenic Pb in the Subjotnian diabases is presented. The scheme is based on the two-stage Pb evolution model proposed for the Svecofennian crust by Huhma (1986). Huhma (1986) based his model on the data of Vaasjoki (1981) who analysed the Pb isotopic composition of galenas from various Svecofennian formations, ending up with an »orogenic trend» shown in Fig. 58. The trend was explained by Huhma (1986) as a mixing line between an Archean high U/Pb upper crustal source and a low U/Pb depleted mantle source, with some contribution probably also from low U/Pb Archean lower crustal sources. According to Huhma (1986), these sources had differentiated from the mantle about 3.0 Ga ago, when the system had a Pb isotopic composition of $^{206}\text{Pb}/^{204}\text{Pb} = 12.9$ and $^{207}\text{Pb}/^{204}\text{Pb} = 14.34$. In this model, mantle evolution since 3.0 Ga was characterized by a low overall U/Pb ratio ($^{206}\text{Pb}/^{204}\text{Pb}$ ca. 14.8 at 1.9 Ga, corresponding to

a μ_2 value of 7.6 between 3.0 and 1.9 Ga). The present-day Pb isotopic composition of this model mantle source is substantially less radiogenic than the Pb isotopic ratios measured for present-day mid-ocean ridge basalts (cf. Church & Tatsumoto, 1975; Sun, 1980), and it also plots very close to the Geochron (Fig. 57).

According to the model presented in Fig. 58, the isotopic composition of uranogenic Pb in the Subjotnian mafic rocks (initial model $^{206}\text{Pb}/^{204}\text{Pb} = 15.802$, calculated using the μ_2 value 9.58 of the less radiogenic plagioclase sample A1063) is derived by mixing a melt from the mantle ($\mu_2 = 7.6$, $^{206}\text{Pb}/^{204}\text{Pb} = 15.202$ at 1.64 Ga) and average Svecofennian crust ($\mu_2 = 9.94$, $^{206}\text{Pb}/^{204}\text{Pb} = 15.911$ at 1.64 Ga) in the proportion 4:1. This is obtained by inserting the appropriate $^{206}\text{Pb}/^{204}\text{Pb}$ ratios in equation (7) and assuming a concentration ratio of 1:20 for the Pb concentrations in the mantle-derived melt and crust, respectively (cf. Sun, 1980; Weaver and Tarney, 1980; Taylor & McLennan, 1985; Zartman & Haines, 1988). The process led to almost complete obliteration of the original lead isotopic

composition of the mantle magmas and the age of the secondary isochron probably gives the date of the final homogenization of the isotope ratios of the crustal Pb that took place during the Svecofennian orogeny.

The model requires that in the orogenic Svecofennian crust U/Pb fractionation at about 1.9 Ga had generated various subsystems with specific U/Pb ratios, and that these subsystems

were subsequently sampled by the Subjotnian diabase magmas during the contamination processes. The preservation of the approximate age of the orogeny (i.e. the secondary 1854 ± 65 Ma isochron) requires that the contamination event at 1640 Ma did not result in any substantial U/Pb fractionation, because otherwise the isochronous relationship of the individual samples would have been destroyed. This implies,

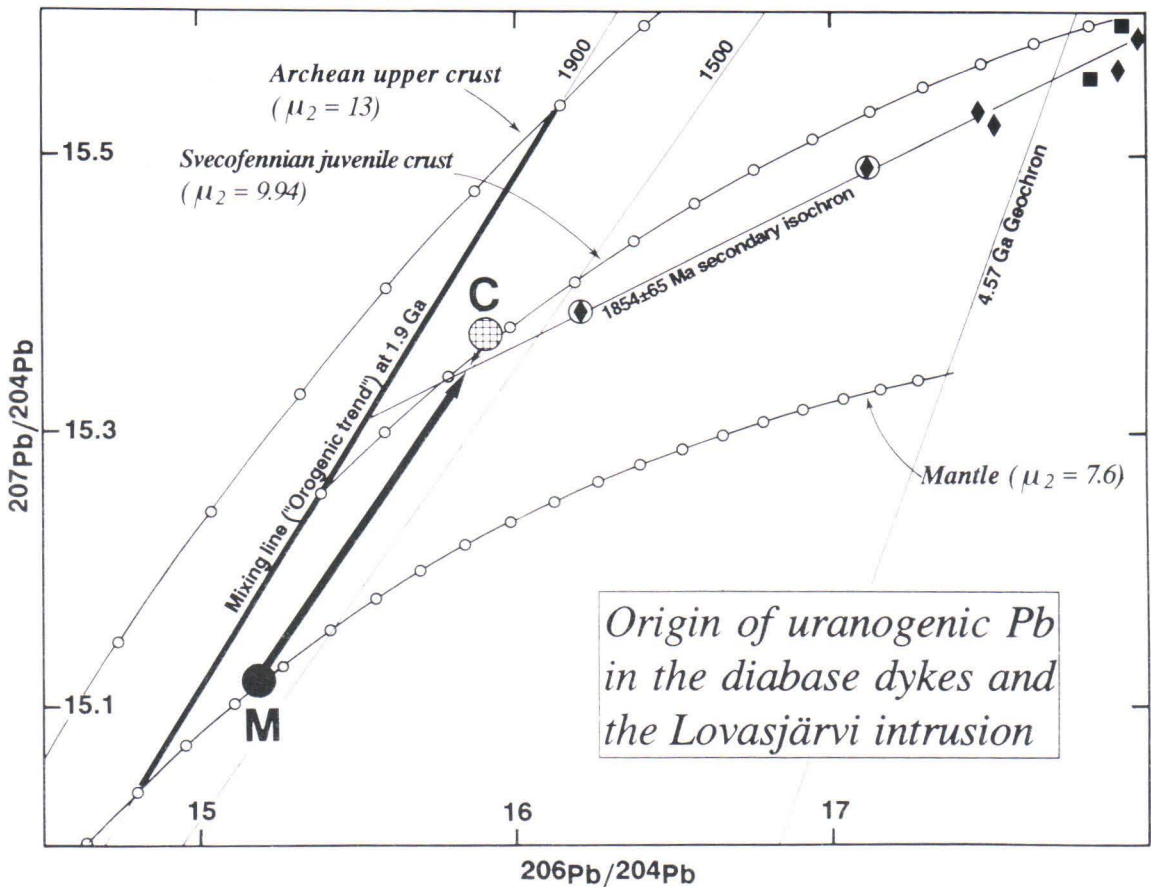


Fig. 58. $^{207}\text{Pb}/^{204}\text{Pb}$ vs. $^{206}\text{Pb}/^{204}\text{Pb}$ diagram illustrating the origin of uranogenic Pb in the diabase dykes and the Lovasjärvi intrusion. The sources of Pb are the Outokumpu-type mantle (M) and the juvenile 1.9 Ga Svecofennian crust (C). The mantle-derived diabase magmas have incorporated a considerable amount of crustal Pb resulting in obliteration of their original isotopic composition. Marked in the figure is the mixing line («orogenic trend») for Svecofennian leads (cf. Vaasjoki, 1981; Huhma, 1986), growth curves for Archean high U/Pb upper crust and low U/Pb mantle (Huhma, 1986), average growth curve for the Svecofennian crust (approximated by the average μ_2 value, 9.94, of the Pb in the galenas from Svecofennian supracrustal rocks and the central Finnish batholith area; Vaasjoki, 1981), second-stage 1500 and 1900 Ma model isochrons, and the 4.57 Ga Geochron calculated from the Canyon Diablo primordial Pb (Tatsumoto et al., 1973). The model is constructed according to the two-stage evolution model of Huhma (1986), with the second stage commencing 3.0 Ga ago at $^{206}\text{Pb}/^{204}\text{Pb} = 12.9$ and $^{207}\text{Pb}/^{206}\text{Pb} = 14.34$. Samples are as in Fig. 35a.

for example, that no major mineral phases significantly fractionating the U/Pb ratio were involved in the evolution of the diabase magmas after the commencement of the contamination processes. This is consistent with the proposed

gabbroic fractionation assemblage (plagioclase, clinopyroxene, and olivine all have D-values for U and Pb less than 1; cf. e.g. Larsen, 1979; Kogarko et al., 1980; Dostal et al., 1976, 1983; McKay & Weill, 1976).

Diabase whole rock U-Pb errorchrons

U-Pb whole rock isotopic systems are not frequently utilized to date magmatic events. This is mainly due to the fact that U is a mobile element under oxidizing conditions and rock samples that have been exposed to chemical weathering normally lose a fraction of their U, which leads to destruction of their U-Pb isotopic systems (Faure, 1986). Nevertheless, it turns out that the Subjotnian diabase dykes can be dated and some aspects of the evolution of the diabase magmas evaluated using isotopic U-Pb whole rock data.

The U-Pb whole rock data of the Subjotnian diabases are shown in $^{206}\text{Pb}/^{204}\text{Pb}$ vs. $^{238}\text{U}/^{204}\text{Pb}$ and $^{207}\text{Pb}/^{204}\text{Pb}$ vs. $^{235}\text{U}/^{204}\text{Pb}$ diagrams in Fig. 59. A linear trend with an age of 1516 ± 73 Ma can be fitted to the data in the $^{206}\text{Pb}/^{204}\text{Pb}$ vs. $^{238}\text{U}/^{204}\text{Pb}$ diagram (Fig. 59a). Samples A1047, A1069, and A1102 that show elevated $\text{Fe}^{3+}/\text{Fe}^{2+}$ ratios (Appendix 2) plot distinctly to the left of the calculated trend and have obviously been affected by U-loss during weathering. These were omitted from the calculation, as was sample A1118 which was probably affected by earlier U-gain. The data regression for the $^{207}\text{Pb}/^{204}\text{Pb}$ vs. $^{235}\text{U}/^{204}\text{Pb}$ diagram (Fig. 59b) was performed likewise. The age of the $^{207}\text{Pb}/^{204}\text{Pb}$ vs. $^{235}\text{U}/^{204}\text{Pb}$ trend, 1669 ± 56 Ma, differs substantially from the age of the $^{206}\text{Pb}/^{204}\text{Pb}$ vs. $^{238}\text{U}/^{204}\text{Pb}$ trend, and is close to what is considered to be the true crystallization age of the Subjotnian diabases of southeastern Finland, determined from zircons and baddeleyites to range from 1665 to 1635 Ma (Vaasjoki et al., 1991).

How can these different dates be explained? The conditions that a rock suite must fulfill in order to be reliably dated by whole rock parent-daughter type isotopic methods are (1) that all the rock samples analyzed are of the same age, (2) that they had the same initial isotopic composition, and (3) that they remained as closed systems after crystallization. There is no obvious reason why the Subjotnian data would not fulfill the first condition. Even if the analysed samples spanned the entire 30 Ma time interval discovered for the emplacement of the Subjotnian diabase dykes in southeastern Finland (Vaasjoki et al., 1991), it would not have any substantial effect on the U-Pb whole rock data (U decay during 30 Ma would result in a change in the isotopic ratios that, at maximum, would be of the order of the analytical accuracy for the $^{206}\text{Pb}/^{204}\text{Pb}$ ratios and about 1/4 times the analytical accuracy for the $^{207}\text{Pb}/^{204}\text{Pb}$ ratios). Condition (3) is largely fulfilled by omitting the samples with clearly disturbed U/Pb systematics from the calculations. The Pb evolution model (Fig. 58) suggests that the analysed dyke samples had variable initial Pb isotopic ratios and that relative variation in the $^{206}\text{Pb}/^{204}\text{Pb}$ ratio of the dyke magmas was higher than that in the $^{207}\text{Pb}/^{204}\text{Pb}$ ratio. These variable initial Pb isotopic ratios (condition 2) are probably one reason for the discrepancy in the ages of the two linear trends in Fig. 59, with the $^{206}\text{Pb}/^{204}\text{Pb}$ vs. $^{238}\text{U}/^{204}\text{Pb}$ system being more affected by incorporation of extra crustal Pb into the mafic magmas.

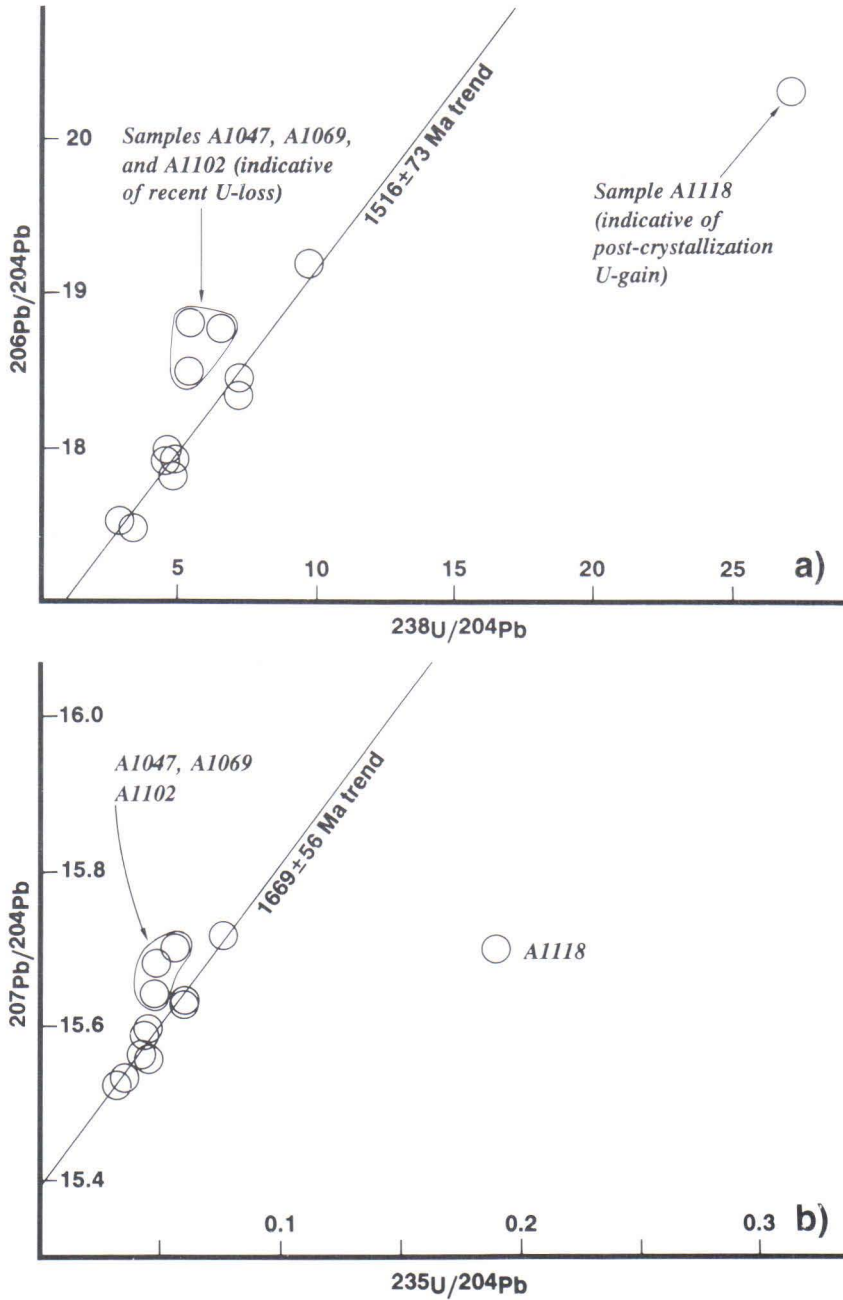


Fig. 59. Whole-rock U-Pb isotopic data (Table 7) of the diabase dykes and the Lovasjärvi intrusion plotted in (a) $^{206}\text{Pb}/^{204}\text{Pb}$ vs. $^{238}\text{U}/^{204}\text{Pb}$ and (b) $^{207}\text{Pb}/^{204}\text{Pb}$ vs. $^{235}\text{U}/^{204}\text{Pb}$ diagrams. Samples showing recent U-loss are enclosed.

Origin of the gabbroic and anorthositic rocks

Nd isotopic constraints

The general compositional trend of the gabbroic and anorthositic rocks shown in the Mg number vs. normative An/(An + Ab) ratio diagram (Fig. 30) can be attributed to fractionation of plagioclase and a mafic phase (cf. Wiebe, 1990), but the limited data available precludes detailed evaluation of the crystallization history of these basic rocks in this context. Because compositional-isotopic correlations, indicative of open-system magmatic processes, were found for the diabase dykes, it was considered reasonable to study whether the initial Nd isotopic composition of the gabbroic and anorthositic rocks vary in a similar manner with the bulk composition of the samples. Most of the gabbroic and anorthositic rocks analysed in the present study are probably cumulates and as such do not represent liquid compositions. Combined with fractionation indicators the trace element contents of these rocks should, however, give some indication of the evolution of the magmas from which the rocks were crystallized.

In Fig. 60, the Rb and Zr concentrations as well as Mg numbers and normative An/(An + Ab) ratios of the analysed gabbroic and anorthositic rocks are plotted against their ϵ_{Nd} values. In the Rb vs. ϵ_{Nd} plot (Fig. 60a) the samples show, excluding the Väärälampi data, a negative correlation; the samples of the Väärälampi body differ from the other samples in having distinctly higher concentrations of Rb. In the Zr vs. ϵ_{Nd} plot (Fig. 60c) there is no such difference between the Väärälampi and the other plutons, and the samples show an overall negative correlation. The variation of initial Nd isotopic composition with the fractionation indicators (Figs. 60b and d) establish slight positive correlations.

A distinctive feature of the Nd data on the gabbroic and anorthositic rocks is that all samples except one (i.e., the olivine gabbro A1110) show negative $\epsilon_{Nd}(T)$ values. The

samples from the ca. 1640 Ma old plutons of southeastern Finland (Ahvenisto, Väärälampi, Ylijärvi) exhibit slightly negative $\epsilon_{Nd}(T)$ values ranging from -0.1 to -0.6 (excluding the sample A1110 that has $\epsilon_{Nd}(T)$ value of $+0.8 \pm 0.4$), while the samples from the 60 to 70 Ma younger intrusions of southwestern Finland show, on the average, more negative $\epsilon_{Nd}(T)$ values (-0.6 and -1.7). If the Nd isotopic composition of the gabbroic and anorthositic rocks represents source compositions in the subcontinental mantle, it means that the gabbroic and anorthositic rocks of southeastern Finland were derived from an approximately chondritic source, and those of southwestern Finland from a source more enriched in the LREE. This would imply that upper mantle domains with different time-integrated LREE compositions exist beneath the continental crust in southwestern and southeastern Finland. This is, however, inconsistent with Nd isotopic data from the 1260 Ma old tholeiitic dykes (Jotnian or Postjotnian diabases) of southwestern Finland that indicate a clear time-integrated LREE-depleted character for the upper mantle (the Jotnian dykes have initial ϵ_{Nd} values between +1.6 and +3.2; Rämö, 1990). It is very difficult to envisage a petrological process that would change such a long-term LREE-enriched character ($\epsilon_{Nd} = -1.7$) of the mantle source to distinctly LREE-depleted ($\epsilon_{Nd} \geq +3.2$) within just 300 Ma.

Because the gabbroic and anorthositic rocks were intruded through the Svecofennian crust and because they obviously did not crystallize from primitive mantle melts (all have very low concentrations of Ni and Cr as well as low Mg numbers and normative An/(An + Ab) ratios), their LREE-enriched character can possibly be explained by invoking crustal contamination of the mantle-derived melts. This scheme would involve a LREE-depleted mantle as the source for the mafic magmas (perhaps similar to that postulated for the Subjotnian diabase dykes) and

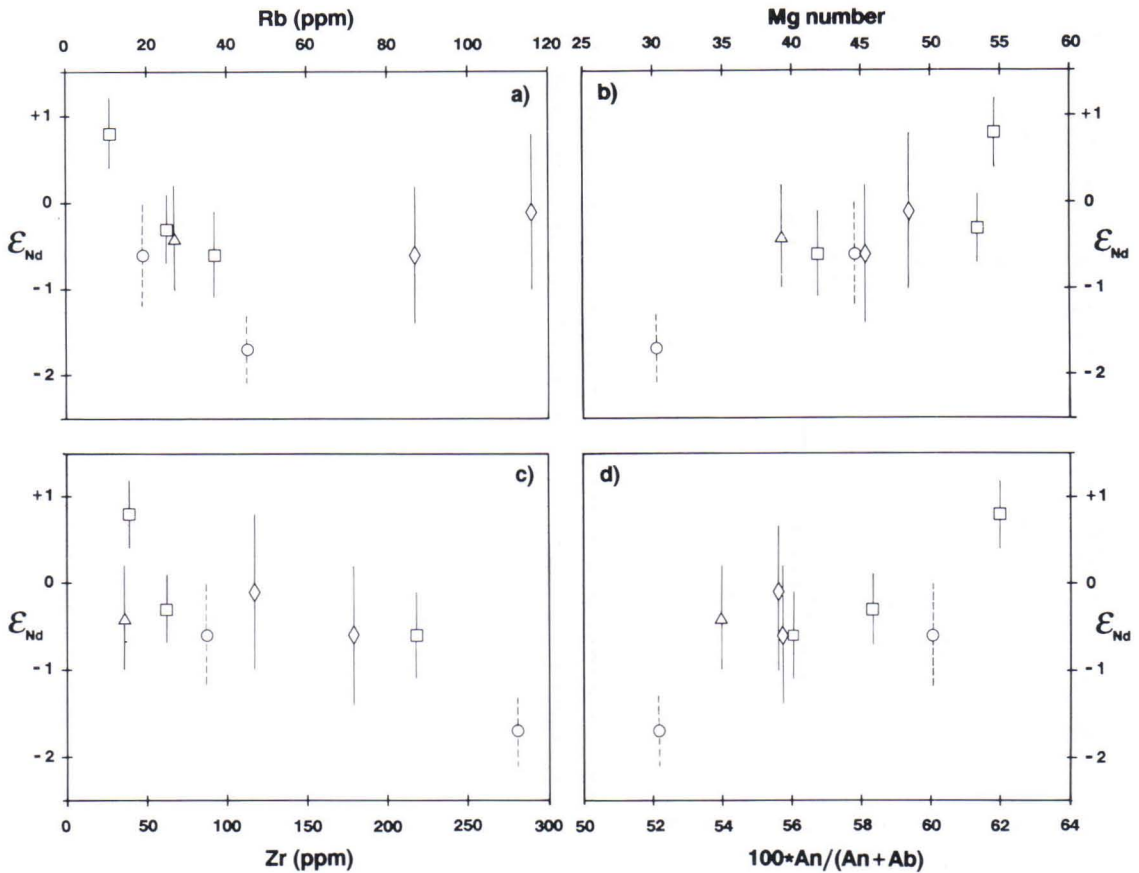


Fig. 60. Initial Nd isotopic compositions of the gabbroic and anorthositic rocks (Table 4), expressed as $\epsilon_{Nd}(T)$ values, plotted against their (a) Rb and (c) Zr concentrations, (b) Mg numbers, and (d) normative An/(An + Ab) ratios (Appendix 2). Vertical lines indicate analytical errors of the ϵ_{Nd} values. Symbols are as in Fig. 24.

a Svecofennian crustal contaminant. The contamination model would allow similar Nd isotopic compositions for the mantle beneath south-eastern and southwestern Finland, and the overall integrated Sm/Nd evolution of the Svecofennian crustal contaminant along a path with negative slope in the $\epsilon_{Nd}(T)$ vs. age plot (Fig. 42b) would cause the more negative $\epsilon_{Nd}(T)$ values of the southwest Finnish samples.

Anorthosite lenses within the gabbro-anorthosite complexes, ubiquitous occurrence of plagioclase phenocrysts in the gabbroic rocks, and the correlation trend in Fig. 30 suggest that

plagioclase fractionation was an important controlling factor of the evolution of the magmas from which the gabbroic and anorthositic rocks crystallized. Plagioclase is considered a stable phase at depths less than 40 km (Cox et al., 1979), that is, within the continental crust. Thus by analogy with the evolution of the diabase dyke magmas, the shift of the initial Nd isotopic composition of the gabbroic and anorthositic rocks toward more unradiogenic isotopic ratios along with fractionation (Fig. 60) suggests that crustal contamination may also have had a role in the evolution of these basic rocks.

Pb isotopic constraints

The Pb isotopic composition of the gabbroic and anorthositic rocks is consistent with a major contribution of crustal Pb to the mantle-derived magmas from which these rocks were eventually crystallized. The Pb isotopic composition of the anorthosite sample MH87a is possibly rather close to the initial Pb isotopic composition of the magma from which the plagioclases were precipitated. It falls close to the evolution of average crustal Pb in the $^{207}\text{Pb}/^{204}\text{Pb}$ vs. $^{206}\text{Pb}/^{204}\text{Pb}$ diagram (Fig. 36), and actually also rather close to the plagioclase of the diabase sample A1063 (cf. Fig. 35a). The olivine gabbro A1110, that has the highest $\epsilon_{\text{Nd}}(\text{T})$ value of +0.8, plots closest to mantle evolution curve, and probably has Pb isotopic ratios least affected by radiogenic crustal Pb, a scheme consistent with the crustal contamination hypothesis. It is also worth noting that this feature is not observed in the diabase dyke data: the dykes with positive ϵ_{Nd} values do not plot toward lower U/Pb ratio in the $^{207}\text{Pb}/^{204}\text{Pb}$ vs. $^{206}\text{Pb}/^{204}\text{Pb}$ diagram, when compared with the rest of the dykes.

The gabbroic and anorthositic rocks exhibit lower Pb isotopic ratios than most of the diabasites, in line with their lower U/Pb ratios. They also show larger scatter in the $^{207}\text{Pb}/^{204}\text{Pb}$ vs.

$^{206}\text{Pb}/^{204}\text{Pb}$ diagram and do not conform to a reasonable isochron, as the Subjotnian diabasites do. Moreover, there are differences between the different plutons (e.g., low U/Pb Ahvenisto vs. high U/Pb Väärälampi). This indicates that the Pb in the basic magmas from which the individual plutons were crystallized originated from slightly different U/Pb environments. In the light of the crustal contamination hypothesis, this would mean that the mafic magmas tapped distinctive Pb sources during their transit through, and residence in, the continental crust.

In the $^{208}\text{Pb}/^{204}\text{Pb}$ vs. $^{206}\text{Pb}/^{204}\text{Pb}$ diagram (Fig. 36b), six gabbroic samples out of eight conform closely to the evolution line of average crustal Pb. The samples from the Ahvenisto complex plot along a regression line (not shown in Fig. 36b) that has a Th/U ratio of 3.95. The two samples that fall off the crustal evolution line plot toward higher (A691c) and lower (A1048) Th/U ratio, but show less overall scatter compared with the diabase Pb data (Fig. 35c). That the gabbroic and anorthositic rocks show less scatter in their Th/U ratios could be the result of a more homogeneous source of the thorogenic Pb in the magmas from which these rocks crystallized, and may indicate a larger relative amount of contamination by lower crust.

DISCUSSION

The petrogenesis of the southeastern Fennoscandian rapakivi granites and associated gabbroic and anorthositic rocks and diabase dykes is relevant to a number of petrological and geochemical problems. These include the origin of the Proterozoic anorogenic (or post-orogenic) granites and massive anorthosites, genetic connection between these two contrasting rock groups, processes controlling magma evolution of continental basalts, relation between gabbroic and anorthositic bodies and diabase dykes, nature and

evolution of the Proterozoic subcontinental mantle, and the role of juvenile early Proterozoic crust and Archean crustal material in Proterozoic intra-cratonic magma generation.

Rapakivi granites and related Proterozoic anorogenic (or post-orogenic) granites have been the subject of active research during the last two decades, especially focusing on North American and Finnish occurrences. Several studies (e.g., Kranck, 1969; Bridgwater & Windley, 1973; Bridgwater et al., 1974; Vormaa, 1976; Emslie,

1978; Anderson & Cullers, 1978; Bickford et al., 1981; Cullers et al., 1981; Haapala, 1988; Wyborn et al., 1988; Rogers & Greenberg, 1990) consider them to represent anatectic melts from pre-existing continental crust, yet in others (e.g., Barker et al., 1975) they are interpreted as products of the interaction of mantle-derived mafic magma and crust-derived anatectic magma. The Phanerozoic A-type granites, with which the rapakivi granites share many compositional and petrographic characteristics, were originally interpreted as being derived from the mantle, either by simple fractionation of mantle magma or fractionation combined with incorporation of granulitic lower crustal material (Loiselle & Wones, 1979). Those in favor of an anatectic origin for these rocks invoke either a residual (granulitic) protolith the composition of which had been affected by a previous extraction of a granitic melt (e.g., Collins et al., 1982; Whalen et al., 1987; Clemens et al., 1986; Christiansen et al., 1988) or a non-residual yet otherwise relatively anhydrous intermediate (tonalitic to granodioritic) source (Anderson & Cullers, 1978; Cullers et al., 1981; Anderson & Bender, 1989; Emslie & Hunt, 1990; Creaser et al., 1991). The important condition for the source is that it is water-deficient so that the partial melting begins at high temperature by decomposition of hydrous silicates (biotite, hornblende) that are enriched in F to derive the characteristic high F content in these rocks.

The Nd and Pb isotopic data presented in this study on the Finnish rapakivi granites are strongly in favor of a crustal origin for these rocks and render major incorporation of mantle materials in the rapakivi granites improbable. The relatively high (i.e., only slightly negative) ϵ_{Nd} values of the Finnish rapakivi granites reflect the juvenile character of their source that was formed during the Svecokarelian orogeny by mixing of a small amount of Archean crustal material with depleted mantle material 200 to 250 Ma before the oldest (eastern Finnish) rapakivi granites were emplaced (Huhma, 1986; Patchett & Kouvo,

1986). A comparable parent-daughter relationship between a juvenile crust and the rapakivi granites is found in the Ketilidian terrain of South Greenland where the ca. 1750 Ma old rapakivi granites register ϵ_{Nd} values between -1.4 and +1.2 (Patchett & Bridgwater, 1984). The juvenile Ketilidian crust was formed only about 50 Ma before the intrusion of the rapakivi granites (Gulson & Krogh, 1975) which is probably why the ϵ_{Nd} values of these granites are more positive than those of the Finnish rapakivi granites. It should be noted that such positive ϵ_{Nd} values have also been considered as possible evidence for mantle component in certain anorogenic granites (e.g., the 1100 Ma old Pikes Peak batholith in Colorado, DePaolo, 1981a; cf. also Barker et al., 1975) but in the case of the Finnish rapakivi granites a crustal origin is considered the most probable one. The reaction melting model proposed for the combined mantle-crust origin of the Pikes Peak batholith suggests syenitic rocks as precursors of the rapakivi granites proper (Barker et al., 1975). In the Suomenniemi complex, however, the peralkaline alkali-feldspar syenites constitute a later, separate intrusive phase and hence do not fit the model of Barker et al. (1975).

Considerable controversy regarding the origin of the Finnish rapakivi granites and the penecontemporaneous basic rocks was brought up by the Hf isotopic studies of Patchett et al. (1981) which demonstrated similar ϵ_{Hf} values ranging from 0 to +3 for the granites and the basic rocks. This implied that the silicic and basic rocks were derived from the same source, which was more probably the mantle than the crust. In the light of the Nd data presented in this study, this controversy may have been due to sampling, as the rapakivi-age basic rocks analysed by Patchett et al. (1981) were those that show negative ϵ_{Nd} values (samples A118, A119, and A1069 collected from the same rock type as the sample A573 of Patchett et al., 1981) not much different from the ϵ_{Nd} values of the rapakivi granites.

The partial melting and fractional crystalliza-

tion modeling of the granites of the Suomenniemi batholith suggest that an intermediate to acid igneous rock (granodiorite) could have acted as a protolith for the initial magma of the batholith. The hypothetical initial magma is relatively high in silica (73.4% SiO₂, calculated volatile free) and is rather similar to the average composition of the Laitila batholith, except for Zr which is considerably lower in the latter (Vorma, 1976, Appendix 2, col. 53). In discussing the geochemistry of the Finnish rapakivi granites, Vorma (1976) noted that the rapakivi granites show lower K/Rb ratios and Sr contents as well as higher Zr, Ba, and F contents than granitic rocks in general. The geochemical modeling performed for the Suomenniemi batholith demonstrates that the low-silica granites in that intrusion are probably cumulus-enriched, and hence the relatively high Ba and Zr encountered may be due to cumulus alkali feldspar and zircon, respectively. The relatively low K/Rb ratios and high F contents are probably due to magma generation processes within the lower/middle crust initiated by decomposition of a F-bearing biotite (and amphibole). The overall enrichment in the LREE can also be explained by melting of a LREE-enriched protolith.

The isotopic data on the whole rock samples and alkali feldspar fractions suggest that the crystallization of the Suomenniemi batholith took place in an open system with some incorporation of Pb (and possibly also Nd) from the country rocks into the evolving magma. Although this is a more likely process in mafic magma systems, such contamination has also been documented for A-type granite melts (Reece et al., 1990). In the case of the Suomenniemi batholith, the more primitive granites (other than the topaz-bearing granites) appear to show largely unaffected isotope ratios and hence are considered as registering the isotopic composition of their source.

The Proterozoic massive anorthosites constitute a distinct group of igneous rocks that has long been the subject of active discussion (cf. Morse, 1982a, for a review). The association of

rapakivi granites with Proterozoic anorthosites is well documented in North America (e.g., Anderson & Cullers, 1978; Emslie, 1978) where the anorthositic rocks are much more abundant at the present level of exposure than in southeastern Fennoscandia. The gabbroic and anorthositic rocks associated with the Finnish rapakivi granites are, however, geochemically and petrographically akin to the lithologies encountered in the Proterozoic massive anorthosites and hence the data in the present work may place constraints on the origin of massive anorthosites as well. Controversy exists as to whether the parental magmas for the anorthosites were hyperfeldspathic themselves (Wiebe, 1980, 1990) or whether they crystallized from more normal basaltic liquids (Emslie, 1980), or whether they have in common a unique parental magma at all (Duchesne, 1984). Isotopic studies are generally in favor of a mantle origin for these rocks (e.g., Basu & Pettingill, 1983; Ashwall et al., 1986; Demaiffe et al., 1986; Menuge, 1988) and contamination of the mafic magmas with crustal components has often been invoked as a controlling factor in the chemical and isotopic evolution of the anorthosites (Ashwall et al., 1986; Gray, 1987; Menuge, 1988; Geist et al., 1990; Wiebe, 1990). Enriched subcontinental mantle may have, however, contributed to the composition of these rocks as well (cf. Morse, 1982a).

The gabbroic and anorthositic rocks of the Ahvenisto complex were interpreted by Savolahti (1956) to be considerably older than the associated rapakivi granites, but recent isotopic studies (Vaasjoki, 1977; Vaasjoki et al., 1991) have confirmed the close temporal relationship of these contrasted rock types. The Nd isotopic data in the present work indicate that the Finnish rapakivi granites and associated gabbroic and anorthositic rocks are probably not comagmatic. The ϵ_{Nd} values of the gabbroic and anorthositic rocks are higher than those of the penecontemporaneous granites by about one ϵ_{Nd} unit. Because the gabbroic and anorthositic rocks presumably were contaminated by unradiogenic crustal Nd, the original ϵ_{Nd} value of the basic

magmas from which these rocks precipitated may have been around +1 or even larger. Hence the overall difference in the ϵ_{Nd} value of the silicic and basic magmas may have been at least two ϵ_{Nd} units. One further line of evidence against a comagmatic origin is the fact that the olivine gabbro A1110 has a distinctly lower (i.e., more mantle-like) $^{207}Pb/^{206}Pb$ ratio than the rapakivi granites. It should also be noted that the origin of the gabbroic and anorthositic rocks by early accumulation of plagioclase from a primitive rapakivi granite magma (see the discussion in Vormaa, 1976, p. 89) is inconsistent with the fractional crystallization model for the granites of the Suomenniemi batholith that indicates cumulates enriched in alkali feldspar.

The diabase dykes associated with the rapakivi granites and gabbroic and anorthositic rocks of southern Finland constitute typical Precambrian mafic dyke swarms that are common in cratonic areas throughout the world (cf. Halls & Fahrig, 1987; Parker et al., 1990) and have been considered to represent feeder conduits for continental flood basalts that were subsequently eroded exposing the underlying dyke systems (Basaltic Volcanism Study Project, 1981; Thompson et al., 1983). Considerable debate has focused on the interaction of flood basalt and mafic dyke magmas with continental materials during their passage through, and residence in, the continental crust. The main problems are whether the generally encountered incompatible element enriched character of these mafic magmas reflects a source in the subcontinental mantle (e.g., Sheraton & Black, 1981; Weaver & Tarney, 1981; Menzies et al., 1983; McDonough et al., 1985; Condie et al., 1987; Ellam & Cox, 1989) or whether it is a result of the magmas being contaminated with continental crustal materials (e.g., Carlson et al., 1981; Allègre et al., 1982; Thirlwall & Jones, 1983; Dupuy & Dostal, 1984; Cox & Hawkesworth, 1985; Chiesa et al., 1989).

The Nd and Pb isotopic and general geochemical data presented for the rapakivi-age Subjotnian diabases in this work are consistent with a crustal contamination origin for the

within-swarm enrichment in incompatible elements. Thus it appears that, at least when intruded through a crust concurrently in the process of anatectic melting, continental basalts are prone to contamination with these elements. As regards the Svecofennian crust in the Subjotnian time, it is quite understandable that mafic magmas passing through the hot, partially molten crust were contaminated with incompatible trace elements that partition into anatectic melts. A contributing factor may have been the lowered average density of the partially molten crust which possibly decreased the overall velocity with which the mafic magmas penetrated the crust, thus allowing them more time to interact with crustal components (cf. Perry et al., 1987; Huppert & Sparks, 1988). It is important to note in this context that the 1260 Ma old Jotnian diabase dykes of southwestern Finland which are not associated with coeval silicic magmatism exhibit much less radiogenic Pb and more radiogenic Nd isotopic compositions as well as lower abundances of incompatible elements than the Subjotnian dykes (Rämö, 1990). The magma evolution of the Jotnian and Subjotnian diabases probably followed a grossly similar path (melt generation at approximately equal level in the subcontinental mantle, subsequent crystal fractionation in intra-crustal magma chambers). By the Jotnian time at 1260 Ma, however, the Svecofennian crust had cooled down, and that could be one reason why the Jotnian dykes appear to be less affected by crustal components (cf. Rämö, 1990).

An item subject to a certain amount of controversy is the relationship of the gabbroic and anorthositic bodies with the Subjotnian diabase dykes. It has been suggested (Laitakari & Leino, 1989) that the Ahvenisto gabbro-anorthosite complex (Fig. 1) probably acted as a magma chamber for the dykes of the Häme swarm. In the light of recent isotopic age determinations (Vaasjoki et al., 1991), however, the overall setting may have been more complex, as the age of the Ahvenisto complex is defined at about 1645 ± 5 Ma, while the diabase dykes comprise at least three magmatic events aged at about

1665, 1645, and 1635 Ma. There are no known contact exposures of gabbroic and anorthositic rocks and Subjotnian diabbases, as, in, for example Labrador where tholeiitic dykes are found to cut anorthosite complexes and associated granitic rocks (Ashwall et al., 1986), but the fundamental difference in the mode of occurrence of the Finnish gabbroic and anorthositic rocks and diabase dykes is that the former are intruded by the rapakivi granites while for the latter also the opposite relationship is encountered. It may be that the gabbroic and anorthositic rocks were derived from mantle magmas associated with relatively early stages of the generation of the rapakivi granite magmas, and that the diabase dykes, which in part were emplaced later than the gabbroic and anorthositic rocks, were associated with evolutionary stages when magmatic underplating had resulted in rupturing of the Svecofennian crust facilitating intrusion of mantle magmas through fissures.

Both the gabbroic and anorthositic rocks exhibit compositional characteristics indicative of crustal contamination but also show some differences in this respect. A distinctive feature of the gabbroic and anorthositic rocks is the presence of orthopyroxene in almost all of the analysed samples (only the olivine gabbro A1110 with the highest ϵ_{Nd} value and lowest $^{207}Pb/^{206}Pb$ ratio is devoid of it). According to Gray (1987) progressive crustal contamination of magmas precipitating anorthositic rocks is registered by the gradation from olivine anorthosite to orthopyroxene anorthosite. In mantle-derived mafic magmas the normal sequence of low-pressure crystallization is olivine-clinopyroxene-orthopyroxene but if extra SiO_2 is incorporated in substantial amounts, orthopyroxene may precipitate before clinopyroxene (Schiffries, 1990). This is what may have happened in the Ahvenisto complex, and is indicative of wall-rock assimilation during crystallization of the complex. Orthopyroxene is, however, rare or absent in the diabase dykes. The reason for the dykes not showing orthopyroxene, although they exhibit positive evidence for incor-

poration of crustal (silica-rich) material, is not known. One explanation might be that the dyke magmas developed at a lower overall pressure than the magmas from which the gabbroic and anorthositic rocks crystallized, or that the amount of silica introduced was not large enough to bring about the change in the order of pyroxene precipitation.

As regards the nature of the mantle beneath the Fennoscandian shield, the Nd isotopic data of the basic rocks suggest that it was one with at least a slight time-integrated LREE-depleted character. The most depleted diabase ($\epsilon_{Nd} = +1.6$) and olivine gabbro ($\epsilon_{Nd} = +0.8$) are themselves rather evolved and may have originated from magmas that originally were more depleted in the LREE (i.e., had more positive ϵ_{Nd} values) than that measured for these two samples. The nature of such primitive magmas is speculative but may have been olivine tholeiitic (cf. Emslie, 1978) or picritic (cf. Sparks, 1986).

Studies dealing with the genesis of the Proterozoic anorogenic granites (including the rapakivi granites) have suggested that a juvenile crustal source, differentiated from the mantle shortly before the emplacement of the anorogenic granites, is a characteristic environment for these granites (Anderson, 1983; Anderson & Bender, 1989). The data on the Soviet Karelian rapakivi batholiths indicate, however, that substantial incorporation (about 45%) of considerably older material may also yield typical rapakivi granite melts. The isotopic contrast between the Finnish and Soviet Karelian rapakivi granites also demonstrates the sensitivity with which these rocks reflect the isotopic composition of the lower/middle crust from which they derive.

The overall tectonic environment of emplacement of the rapakivi granites and the associated basic rocks of southeastern Fennoscandia was obviously an extensional one, as is demonstrated by the diabase and quartz-feldspar porphyry dykes. A fundamental question is whether the igneous activity was anorogenic or whether it had a causal relationship with orogeny. The former line of

thought relates the generation of these rocks to partial melting and magma production in the mantle, followed by fusion of lower parts of the continental crust due to heat provided by the mantle magmatism, and generation of anatectic granitic liquids that finally emplace at upper crustal levels as rapakivi granite complexes (Kranck, 1969; Bridgwater & Windley, 1973; Bridgwater et al., 1974; Emslie, 1978; Anderson, 1983; Haapala, 1988). In contrast, the latter line of thought considers the partial melting of the lower parts of the crust as a result of tectonical thickening of the orogenic crust (Vorma, 1976; Van Schmus & Bickford, 1981; Nelson & DePaolo, 1985). While discussing the origin of the Finnish rapakivi granites Vorma (1976) suggested that the formation of the rapakivi granite magma took place during the compressional stage of the Svecokarelian orogeny, and that it was emplaced into the upper crust during the subsequent distensional post-orogenic stage. A relation to orogeny for the Finnish rapakivi granites has also been invoked by Hubbard and Branigan (1987) and Gaál (1990). In contrast, Nurmi and Haapala (1986), Haapala (1988), and Haapala and Rämö (1990), among others, consider the Finnish rapakivi granites as anorogenic, being generated by heat derived from mantle-derived mafic magmas, now represented by the gabbroic and anorthositic rocks and the diabase dykes.

There are several lines of evidence in favor of an anorogenic origin for the rapakivi granites of southeastern Fennoscandia:

- There exists a considerable time-interval of 200 to 300 Ma between the Svecokarelian orogeny and the emplacement of the rapakivi granites. It is considered improbable that a silicic melt generated during this orogeny could have prevailed within the lower crust for hundreds of millions years and later intrude in the upper parts of the continental lithosphere.
- Melting of a water-deficient lower crustal source requires elevated temperatures and hence a considerable amount of thermal

energy. This can be introduced by mafic mantle magmas.

- Active, convecting mantle, rather than a passive mantle in which melting takes place by simple adiabatic decompression, is a more viable source for the energy required for the anatexis and generation of the magmas for the voluminous silicic intrusions. It also accounts better for the LREE-depleted (asthenospheric) Nd isotopic character suggested for the parental magmas of the diabase dykes and the gabbroic and anorthositic rocks.
- The prolonged nature of the basic igneous activity related to the rapakivi granites (Vaasjoki et al., 1991) fits well active rifting associated with thermal upwelling of the asthenosphere (cf. Şengör & Burke, 1978; Basaltic Volcanism Study Project, 1981). Furthermore, the fact that the juvenile 1.9 Ga Svecofennian crust was already deeply eroded at the time when the rapakivi granites were emplaced may have been partly due to doming of the lithosphere in association with the onset of active rifting (cf. Basaltic Volcanism Study Project, 1981, p. 842).
- Recent geophysical studies (Luosto, 1990; Korja & Elo, 1991) have shown that the Finnish rapakivi granites are located in areas of thin crust. This is consistent with mafic underplating but does not fit a model implying a thickened continental crust.

Various global causes have been proposed to have controlled the generation of the Proterozoic rapakivi granites. The profuse nature of this magmatism during the Proterozoic has resulted in the concept of a »single» event that is unique in the geological history. For example, Bridgwater and Windley (1973) suggested that the emplacement of these rocks was due to global-scale mantle activity and crustal rifting and coined the expression »anorthosite event». Anderson and Bender (1989) formulated a crustal overturn model and related the genesis of the anorogenic granites to chemical unstability of the newly generated and

vertically undifferentiated juvenile crust — mantle system, and suggested that the unstable setting will eventually result in considerable crustal reorganization leading to the emplacement of anatectic granitic magmas within the upper parts of the juvenile crust. Hoffman (1989) suggested a model involving the generation of an early Proterozoic supercontinent (Laurentia-Baltica) that affected the thermal state of the underlying mantle and promoted large-scale mantle upwellings (superswells) and extensive partial melting in the upper mantle (see also Gurnis, 1988), eventually leading to anatectic melt-

ing in the continental crust and generation of the anorogenic granites.

The generation of the rapakivi granites and related basic rocks of southeastern Fennoscandia may have been related to the formation of the early Proterozoic supercontinent and subsequent magmatic activity in the subcontinental mantle and continental crust, consonant with the hypothesis of Hoffman (1989). In Subjotnian time, the southeastern part of the Fennoscandian shield presumably was the site of incipient rifting that eventually, however, was aborted and failed to integrate into a world-wide plate system.

CONCLUSIONS

The Nd and Pb isotopic and general geochemical data presented in this work lead to the following conclusions:

- 1) The rapakivi granites of eastern Fennoscandia are typical Proterozoic A-type granites with a metaluminous to slightly peraluminous chemistry, intimate temporal and spatial association with basic rocks, and the occurrence of a minor volume of peralkaline felsic rocks.
- 2) The nature of the basic magmatism associated with the rapakivi granites is tholeiitic and includes mafic dykes geochemically akin to continental flood basalts, as well as gabbroic and anorthositic rocks typical of the Proterozoic massive anorthosites.
- 3) The Finnish rapakivi granites were derived from the lower parts of the juvenile 1.9 Ga Svecofennian crust that was formed during the Svecokarelian orogeny some 200 to 300 Ma before the emplacement of the rapakivi granites.
- 4) The Soviet Karelian rapakivi granites are probably about one-to-one mixtures of juvenile (1.9 Ga) and Archean lower crustal materials.
- 5) The initial magma of the Suomenniemi batholith was presumably silicic (ca. 73% SiO₂,

calculated volatile free) and may have been formed by ca. 20% partial melting of an intermediate to acid (granodioritic) source. This magma underwent fractionation of alkali feldspar, quartz, mafic silicates, oxide, apatite, zircon, and a LREE-phase resulting in cumulates (hornblende granite, biotite-hornblende granite) and rocks precipitated from residual liquids (biotite granite, topaz-bearing granite). Some indication of open-system processes is provided by the Pb and Nd isotopic data.

- 6) The lower part of the Fennoscandian Archean craton has a very low overall U/Pb ratio. The isotopic composition of the Finnish and Soviet Karelian rapakivi granites imply an apparent Stacey and Kramers (1975) μ_2 value of 8 for the Archean lower crustal regime, which is in sharp contrast to the high U/Pb character of the Archean upper crust.

- 7) The diabase dykes and the gabbroic and anorthositic rocks were derived from a time-integrated LREE-depleted mantle source with a minimum ϵ_{Nd} value of ca. +1 at 1640 Ma. The magma evolution of the diabase dykes of the Suomenniemi complex can be assessed by AFC

modeling involving fractionation of a gabbroic assemblage and incorporation of the more incompatible constituents from an average upper crustal composition. The magmas from which the

gabbroic and anorthositic rocks crystallized were presumably also affected by crustal contamination.

ACKNOWLEDGEMENTS

My warmest thanks go to Professor Ilmari Haapala, my superior, who directed my interest to rapakivi granites. He also devised the idea for this study, initiated it, and shared his encouragement and experience as a granite petrologist throughout the work.

An essential part of the data presented in this work was acquired at the Unit for Isotope Geology, Department of Petrology, Geological Survey of Finland. I am grateful to Professor Atso Vormaa, head of the Department, for the permit to work at the Unit. My sincere thanks go to the staff of the Unit: Matti Vaasjoki, Hannu Huhma, Olavi Kouvo, and Matti Sakko introduced me into the realm of isotope geology and gave invaluable advice and help throughout the study, Tuula Hokkanen and Marita Niemelä were never too busy to assist me at the chemistry lab, and Lasse Heikkinen and Arto Pulkkinen skillfully kept the mass spectrometers running. I am also grateful to Matti Karhunen for careful milling of the isotopic samples and to the laboratory staff of the Unit for Mineralogy of the Geological Survey for mineral separations.

Much of the mapping of the Suomensieniemi batholith was done by the late Mervi Tähtinen, whose accidental death was an irreplaceable loss to our working team. In the field I was also assisted by Lassi Pakkanen and Tuure Rämö, my father, who did a considerable job in exposing and cleaning outcrops.

I am grateful to Professor Jaakko Siivola for providing me with unpublished microprobe data and Aimo Tyrväinen for putting unpublished field data from the northern part of the Suomen-

niemi complex at my disposal. Reijo Alviola, Ilmari Haapala, Hannu Idman, Olavi Kouvo, Ilkka Laitakari, Martti Lehtinen, Jaakko Siivola, Veli Suominen, and Atso Vormaa provided me with samples from the Wiborg, western Finnish, and Soviet Karelian batholiths and the Lovasjärvi intrusion, which is gratefully acknowledged.

In particular, I would like to thank Walter Boyd who ran the microprobe for me, critically reviewed the manuscript and corrected its English, and continuously improved my knowledge of basic igneous rocks through many stirring discussions. Discussions with Hannu Huhma, Matti Vaasjoki, Hugh O'Brien, Atso Vormaa, Olavi Kouvo, Ilkka Laitakari, Mikko Niironen, Fredrik Pipping, and Nils Gustavsson are also highly appreciated, as are authoritative reviews of the manuscript by Ilmari Haapala, Hannu Huhma, Hugh O'Brien, and Atso Vormaa.

I express my cordial thanks to Professor Kauko Korpela, acting Director of the Geological Survey, for approving publication of this paper as a Bulletin of the Geological Survey of Finland.

I am thankful also to Lassi Pakkanen and Iris Pasternack for point counting work, Pirjo Hainonen, Elsa Järvimäki, Jukka Päivärinta, Marja Tiihonen, and Riitta Virtanen for making the figures, and Liisa Sirén, Marja Tiihonen, Elsa Järvimäki, and Riitta Virtanen for drawing the appended map.

Financial support from the Academy of Finland, the University of Helsinki, and Suomen Kulttuurirahasto (The Cultural Foundation of Finland) is gratefully acknowledged.

REFERENCES

- Allègre, C.J. & Minster, J.F., 1978.** Quantitative models of trace element behavior in magmatic processes. *Earth and Planetary Science Letters* 38, 1—25.
- Allègre, C.J., Treuil, M., Minster, J.F., Minster, B. & Albarède, F., 1977.** Systematic use of trace elements in igneous processes. Part I: Fractional crystallization processes in volcanic suites. *Contributions to Mineralogy and Petrology* 60, 57—75.
- Allègre, C.J., Dupré, B., Richard, P. & Rousseau, D., 1982.** Subcontinental versus suboceanic mantle, II. Nd-Sr-Pb isotopic comparison of continental tholeiites with mid-ocean ridge tholeiites, and the structure of the continental lithosphere. *Earth and Planetary Science Letters* 57, 25—34.
- Alviola, R., 1981.** Selostus Mäntyharjun Lovasjärven intruusiota koskevasta teollisuusmineraalitutkimuksista vv. 1976—1978. Unpublished report M 19/3132/-81/80, Geological Survey of Finland, 91 p.
- Anderson, J.L., 1983.** Proterozoic anorogenic granite plutonism of North America. *In* L.G. Madaris, Jr., C.W. Byers, D.M. Mickelson & W.C. Shanks (Editors), *Proterozoic geology*. Geological Society of America Memoir 161, 133—154.
- Anderson, J.L. & Bender, E.E., 1989.** Nature and origin of Proterozoic A-type granitic magmatism in the south-western United States of America. *Lithos* 23, 19—52.
- Anderson, J.L. & Cullers, R.L., 1978.** Geochemistry and evolution of the Wolf River batholith, a late Precambrian rapakivi massif in North Wisconsin, U.S.A. *Precambrian Research* 7, 287—324.
- Arth, J.G., 1976.** Behavior of trace elements during magmatic processes — a summary of theoretical models and their applications. *U.S. Geological Survey Journal of Research* 4, 41—47.
- Ashwall, L.D., Wooden, J.L. & Emslie, R.F., 1986.** Sr, Nd, and Pb isotopes in Proterozoic intrusives astride the Grenville Front in Labrador: Implications for crustal contamination and basement mapping. *Geochimica et Cosmochimica Acta* 50, 2571—2585.
- Bailey, D.K., 1982.** Mantle metasomatism — continuing chemical change within the Earth. *Nature* 296, 525—530.
- Barker, F., Wones, D.R., Sharp, W.N. & Desborough, G.A., 1975.** The Pikes Peak batholith, Colorado Front Range, and a model for the origin of the gabbro-anorthosite-syenite-potassic granite suite. *Precambrian Research* 2, 97—160.
- Basaltic Volcanism Study Project, 1981.** Basaltic volcanism on terrestrial planets. Pergamon, New York, 1286 p.
- Basu, A.R. & Pettingill, H.S., 1983.** Origin and age of Adirondack anorthosites re-evaluated with Nd isotopes. *Geology* 11, 514—518.
- Ben Othman, D., Polvé, M. & Allègre, C.J., 1984.** Nd-Sr isotopic composition of granulites and constraints on the evolution of the lower continental crust. *Nature* 307, 510—515.
- Bergman, L., 1979.** Geological map of Finland, 1:100 000, pre-Quaternary rocks, Sheet 1012 Mariehamn. Geological Survey of Finland.
- Bergman, L., 1986.** Structure and mechanism of intrusion of postorogenic granites in the archipelago of southwestern Finland. *Acta Academiae Aboensis, Series B*, 46 (5), 74 p.
- Bickford, M.E., Sides, J.R. & Cullers, R.L., 1981.** Chemical evolution of magmas in the Proterozoic terrane of the St. Francois Mountains, southeastern Missouri. 1. Field, petrographic, and major element data. *Journal of Geophysical Research* 86, B11, 10365—10386.
- Bickle, M.J., Ford, C.E. & Nisbet, E.G., 1977.** The petrogenesis of peridotitic komatiites: Evidence from high-pressure melting experiments. *Earth and Planetary Science Letters* 37, 97—106.
- Bowen, N.L., 1928.** The evolution of the igneous rocks. Princeton University Press, 332 p.
- Boyd, W.W., Jr., 1972.** Diabase variation and genesis. *Bulletin of the Geological Society of Finland* 44, 21—34.
- Boynton, W.V., 1984.** Cosmochemistry of the Rare Earth Elements: Meteorite studies. *In* P. Henderson (Editor), *Rare earth element geochemistry, Developments in geochemistry* 2. Elsevier, Amsterdam, Oxford, New York, Tokyo, 63—114.
- Bridgwater, D. & Windley, B.F., 1973.** Anorthosites, post-orogenic granites, acid volcanic rocks and crustal development in the North Atlantic Shield during the mid-Proterozoic. *Geological Society of South Africa Special Publication* 3, 307—317.
- Bridgwater, D., Sutton, J. and Watterson, J., 1974.** Crustal down-folding associated with igneous activity. *Tectonophysics* 21, 57—77.
- Carlson, R.W., Lugmair, G.W. & MacDougall, J.D., 1981.** Columbia River volcanism: the question of mantle heterogeneity or crustal contamination. *Geochimica et Cosmochimica Acta* 45, 2483—2499.
- Chappell, B.W., 1979.** Granites as images of their source rocks. *Geological Society of America Abstracts with Programs* 11, 400.
- Chappell, B.W., & White, A.J.R., 1974.** Two contrasting granite types. *Pacific Geology* 8, 173—174.
- Chappell, B.W., White, A.J.R. & Wyborn, D., 1987.** The importance of residual source material (restite) in granite petrogenesis. *Journal of Petrology* 28, 1111—1138.
- Chiesa, S., Civetta, L., De Fino, M., La Volpe, L. & Orsi, G., 1989.** The Yemen Trap series: genesis and evolution of a continental flood basalt province. *Journal of Volcanology and Geothermal Research* 36, 337—350.
- Christiansen, E.H., Burt, D.M., Sheridan, M.F. & Wilson, R.T., 1983.** The petrogenesis of topaz rhyolites from the western United States. *Contributions to Mineralogy and Petrology* 83, 16—30.
- Christiansen, E.H., Bikun, J.V., Sheridan, M.F., & Burt, D.M., 1984.** Geochemical evolution of topaz rhyolites from the Thomas Range and Spor Mountain, Utah.

- American Mineralogist 69, 223—236.
- Christiansen, E.H., Stuckless, J.S., Funkhouser-Marolf, M.J. & Howell, K.H., 1988.** Petrogenesis of rare-metal granites from depleted crustal sources: an example from the Cenozoic of western Utah, U.S.A. *In* R.P. Taylor & D.F. Strong (Editors), Recent advances in the geology of granite-related mineral deposits. Canadian Institute of Mining and Metallurgy Special Volume 39, 307—321.
- Church, S.E. & Tatsumoto, M., 1975.** Lead isotope relations in oceanic ridge basalts from the Juan de Fuca-Gorda Ridge area, N.E. Pacific Ocean. *Contributions to Mineralogy and Petrology* 53, 253—279.
- Clemens, J.D. & Vielzeuf, D., 1987.** Constraints on melting and magma production in the crust. *Earth and Planetary Science Letters* 86, 287—306.
- Clemens, J.D., Holloway, J.R. & White, A.J.R., 1986.** Origin of an A-type granite: experimental constraints. *American Mineralogist* 71, 317—324.
- Collerson, K.D., 1982.** Geochemistry and Rb-Sr geochronology of associated Proterozoic peralkaline and subalkaline anorthositic granites from Labrador. *Contributions to Mineralogy and Petrology* 81, 126—147.
- Collins, W.J., Beams, S.D., White, A.J.R. & Chappell, B.W., 1982.** Nature and origin of A-type granites with particular reference to southeastern Australia. *Contributions to Mineralogy and Petrology* 80, 189—200.
- Condie, K.C., Bobrow, D.J. & Card, K.D., 1987.** Geochemistry of Precambrian mafic dykes from the Southern Superior Province. *In* H.C. Halls & W.F. Fahrig (Editors), Mafic dyke swarms. Geological Association of Canada, Special Paper 34, 95—108.
- Cox, K.G., 1980.** A model for flood basalt vulcanism. *Journal of Petrology* 21, 629—650.
- Cox, K.G., 1983.** The Karoo Province of southern Africa: Origin of trace element enrichment patterns. *In* C.J. Hawkesworth & M.J. Norry (Editors), Continental basalts and mantle xenoliths. Shiva, Nantwich, Cheshire, 139—157.
- Cox, K.G. & Bell, J.D., 1972.** A crystal fractionation model for basaltic rocks of the New Georgia Group, British Solomon Islands. *Contributions to Mineralogy and Petrology* 37, 1—13.
- Cox, K.G. & Hawkesworth, C.J., 1985.** Geochemical stratigraphy of the Deccan Traps at Mahabaleshwar, western Chats, India, with implications for open system magmatic processes. *Journal of Petrology* 26, 355—377.
- Cox, K.G., Bell, J.D. & Pankhurst, R.J., 1979.** The interpretation of igneous rocks. George Allen & Unwin, London, Boston, Sydney, 450 p.
- Creaser, R.A. & White, A.J.R., 1991.** Yardea dacite — large-volume, high-temperature felsic volcanism from the middle Proterozoic of South Australia. *Geology* 19, 48—51.
- Creaser, R.A., Price, R.C. & Wormald, R.J., 1991.** A-type granites revisited: assessment of a residual-source model. *Geology* 19, 163—166.
- Cullers, R.L. & Graf, J.L., 1984.** Rare earth elements in igneous rocks of the continental crust: intermediate and silicic rocks — ore petrogenesis. *In* P. Henderson (Editor), Rare earth element geochemistry, Developments in geochemistry 2. Elsevier, Amsterdam, Oxford, New York, Tokyo, 275—316.
- Cullers, R.L., Koch, R.J. & Bickford, M.E., 1981.** Chemical evolution of magmas in the Proterozoic terrane of the St. Francois Mountains, southeastern Missouri 2. Trace element data. *Journal of Geophysical Research* 86, B11, 10388—10401.
- Deer, W.A., Howie, R.A. & Zussman, J., 1963a.** Rock-forming minerals volume 4, framework silicates. Longmans, Great Britain, 435 p.
- Deer, W.A., Howie, R.A. & Zussman, J., 1963b.** Rock-forming minerals volume 5, non-silicates. Longmans, Great Britain, 371 p.
- Demaiffe, D., Weis, D., Michot, J. & Duchesne, J.C., 1986.** Isotopic constraints on the genesis of the Rogaland anorthositic suite (Southwest Norway). *Chemical Geology* 57, 167—179.
- DePaolo, D.J., 1981a.** Neodymium isotopes in the Colorado Front range and crust-mantle evolution in the Proterozoic. *Nature* 291, 193—196.
- DePaolo, D.J., 1981b.** Trace element and isotopic effects of combined wallrock assimilation and fractional crystallization. *Earth and Planetary Science Letters* 53, 189—202.
- DePaolo, D.J., 1985.** Isotopic studies of processes in mafic magma chambers: I. The Kiglapait intrusion, Labrador. *Journal of Petrology* 26, 925—951.
- DePaolo, D.J., 1988a.** Neodymium isotope geochemistry: An introduction. Springer-Verlag, Berlin, Heidelberg, New York, London, Paris, Tokyo, 187 p.
- DePaolo, D.J., 1988b.** Age dependence of the composition of continental crust: evidence from Nd isotopic variations in granitic rocks. *Earth and Planetary Science Letters* 90, 263—271.
- DePaolo, D.J. & Wasserburg, G.J., 1976.** Nd isotopic variations and petrogenetic models. *Geophysical Research Letters* 3, 249—252.
- Doe, B.R. & Zartman, R.E., 1979.** Plumbotectonics, The Phanerozoic. *In* H.L. Barnes (Editor), Geochemistry of hydrothermal ore deposits, 2nd edition. John Wiley & Sons, New York, 22—70.
- Dostal, J., Capedri, S. & Dupuy, C., 1976.** Uranium and potassium in calc-alkaline volcanic rocks from Sardinia. *Lithos* 9, 179—183.
- Dostal, J., Dupuy, C., Carron, J.P., La Guen de Kerneizon, M. & Maury, R.C., 1983.** Partition coefficients of trace elements: application to volcanic rocks of St. Vincent, West Indies. *Geochimica et Cosmochimica Acta* 47, 525—533.
- Duchesne, J.C., 1984.** Massif anorthosites: another partisan review. *In* W.L. Brown (Editor), Feldspars and feldspathoids. D. Reidel Publishing Company, 411—433.
- Dupuy, C. & Dostal, J., 1984.** Trace element geochemistry of some continental tholeiites. *Earth and Planetary Science Letters* 67, 61—69.
- Ehlers, C. & Ehlers, M., 1977.** Shearing and multiple intrusion in the diabases of Åland archipelago, SW Finland. *Geological Survey of Finland, Bulletin* 289, 31p.
- Ehlers, C. & Ehlers, M., 1978.** Geological map of Finland, 1:100 000, pre-Quaternary rocks, Sheet 1023 Kumlinge. Geological Survey of Finland.

- Ellam, R.M. & Cox, K.G., 1989.** A Proterozoic lithospheric source for Karoo magmatism: evidence from the Nuanetsi picrites. *Earth and Planetary Science Letters* 92, 207—218.
- Emslie, R. F., 1978.** Anorthosite massifs, rapakivi granites, and late Proterozoic rifting of North America. *Precambrian Research* 7, 61—98.
- Emslie, R.F., 1980.** Geology and petrology of the Harp Lake complex, central Labrador: an example of Elsonian magmatism. *Geological Survey of Canada, Bulletin* 293, 136 p.
- Emslie, R.F. & Hunt, P.A., 1990.** Ages and petrogenetic significance of igneous mangerite-charnockite suites associated with massif anorthosites, Grenville province. *Journal of Geology* 98, 213—231.
- Eskola, P., 1928.** On rapakivi rocks from the bottom of the Gulf of Bothnia. *Fennia* 50 (27), 29 p.
- Eskola, P., 1930.** On the disintegration of rapakivi. *Bulletin de la Commission Géologique de Finlande* 92, 96—105.
- Eskola, P., 1949.** The mica of the moro. *Bulletin de la Commission Géologique de Finlande* 144, 113—116.
- Farmer, G.L. & DePaolo, D.J., 1983.** Origin of Mesozoic and Tertiary granite in the western U.S. and implications for pre-Mesozoic crustal structure. I. Nd and Sr isotopic studies in the geocline of the northern Great Basin. *Journal of Geophysical Research* 88, 3379—3401.
- Faure, G., 1986.** Principles of isotope geology, 2nd edition. John Wiley & Sons, New York, Chichester, Brisbane, Toronto, Singapore, 589 p.
- Frosterus, B., 1903.** Vuorilajikartan selitys, C2, Mikkelin. Suomen geologinen yleiskartta, 1:400 000. Geologinen toimisto, 102 p.
- Gaál, G., 1990.** Tectonic styles of early Proterozoic ore deposition in the Fennoscandian shield. *Precambrian Research* 46, 83—114.
- Gale, N.H. & Mussett, A.E., 1973.** Episodic uranium-lead models and the interpretation of variations in the isotopic composition of lead in rocks. *Reviews of Geophysics and Space Physics* 11, 37—86.
- Gaudette, H.E., Mendoza, V., Hurley, P.M. & Fairbairn, H.W., 1978.** Geology and age of the Parguaza rapakivi granite, Venezuela. *Geological Society of America, Bulletin* 89, 1335—1340.
- Geist, D.J., Frost, C.D. & Kolker, A., 1990.** Sr and Nd isotopic constraints on the origin of the Laramie Anorthosite Complex, Wyoming. *American Mineralogist* 75, 13—20.
- Goni, J.C., 1961.** O Rapakivi Lauras — Jaridas metalíferas associadas — Lauras do Sul — Rio Grande do Sul — Brasil. Universidade do Rio Grande do Sul Escola de Geologia, Boletim 7, 71 p.
- Gray, C.M., 1987.** Strontium isotopic constraints on the origin of Proterozoic anorthosites. *Precambrian Research* 37, 173—189.
- Gray, C.M. & Oversby, V.M., 1972.** The behavior of lead isotopes during granulite facies metamorphism. *Geochimica et Cosmochimica Acta* 36, 939—952.
- Green, J.C., Bornhorst, T.J., Chandler, V.W., Mudrey, M.G., Jr., Myers, P.E., Pesonen, L.J. & Wilband, J.T., 1987.** Keweenaw dykes of the Lake Superior region: evidence for evolution of the Middle Proterozoic Mid-continent Rift of North America. *In* H.C. Halls & W.F. Fahrig (Editors), Mafic dyke swarms. Geological Association of Canada, Special Paper 34, 289—302.
- Gulson, B.L. & Krogh, T.E., 1975.** Evidence of multiple intrusion, possible resetting of U-Pb ages, and new crystallization of zircons in the post-tectonic intrusions ('Rapakivi granites') and gneisses from South Greenland. *Geochimica et Cosmochimica Acta* 39, 65—82.
- Gulson, B.L. & Mizon, K.J., 1979.** Lead isotopes as a tool for gossan assessment in base metal exploration. *Journal of Geochemical Exploration* 11, 299—320.
- Gurnis, M., 1988.** Large-scale mantle convection and the aggregation and dispersal of supercontinents. *Nature* 332, 695—699.
- Haapala, I., 1974.** Some petrological and geochemical characteristics of rapakivi granite varieties associated with greisen-type Sn, Be, and W mineralization in the Eurajoki and Kymi areas, southern Finland. *In* M. Štemprok (Editor), Metallization associated with acid magmatism I. Praha, Ústředni ústav geolický, 159—169.
- Haapala, I., 1977a.** Petrography and geochemistry of the Eurajoki stock, a rapakivi-granite complex with greisen-type mineralization in southwestern Finland. *Geological Survey of Finland, Bulletin* 286, 128 p.
- Haapala, I., 1977b.** The controls of tin and related mineralizations in the rapakivi-granite areas of southeastern Fennoscandia. *Geologiska Föreningens i Stockholm Förhandlingar* 99, 130—142.
- Haapala, I., 1988.** Metallogeny of the Proterozoic rapakivi granites of Finland. *In* R.P. Taylor & D.F. Strong (Editors), Recent advances in the geology of granite-related mineral deposits. Canadian Institute of Mining and Metallurgy, Special Volume 39, 124—132.
- Haapala, I. & Ojanperä, P., 1969.** Triplite and wolframite from a greisen-bordered veinlet in Eurajoki, SW Finland. *Bulletin of the Geological Society of Finland* 41, 99—105.
- Haapala, I. & Ojanperä, P., 1972a.** Genthelvit-bearing greisens in southern Finland. *Geological Survey of Finland, Bulletin* 259, 22 p.
- Haapala, I. & Ojanperä, P., 1972b.** Magnetite and ilmenite from some Finnish rocks. *Bulletin of the Geological Society of Finland* 44, 13—20.
- Haapala, I.J. & Rämö, O.T., 1987.** Petrogenesis of the rapakivi granites of Finland. *Geological Society of America, Abstracts with Programs* 19 (7), 689.
- Haapala, I.J. & Rämö, O.T., 1988.** The rapakivi granites of Finland. *Geological Association of Canada, Mineralogical Association of Canada, Canadian Society of Petroleum, Geologists Joint Annual Meeting Program with Abstracts* 13, A49.
- Haapala, I. & Rämö, O.T., 1990.** Petrogenesis of the Proterozoic rapakivi granites of Finland. *In* H.J. Stein & J.L. Hannah (Editors), Ore-bearing granite systems; Petrogenesis and mineralizing processes. *Geological Society of America, Special Paper* 246, 275—286.
- Haapala, I., Front, K., Rantala, E. & Vaarma, M., 1987.** Petrology of Nattanen-type granite complexes, northern Finland. *Precambrian Research* 35, 225—240.
- Hackman, V., 1934.** Das Rapakiwirandgebiet der gegend von Lappeenranta (Willmanstrand). *Bulletin de la Commission Géologique de Finlande* 106, 87 p.

- Häkli, T.A. & Wright, T.L., 1967.** The fractionation of nickel between olivine and augite as a geothermometer. *Geochimica et Cosmochimica Acta* 31, 877—884.
- Halls, H.C. & Fahrig, W.F. (Editors), 1987.** Mafic dyke swarms. Geological Association of Canada, Special Paper 34, 503 p.
- Hammond, J.G., 1986.** Geochemistry and petrogenesis of Proterozoic diabase in the southern Death Valley region of California. *Contributions to Mineralogy and Petrology* 93, 312—321.
- Hanski, E.J., 1983.** Alkuaineiden jakautuminen mineraalien ja silikattisulan kesken: jakautumiskertoimet. Unpublished compilation of mineral-silicate melt distribution coefficients, University of Oulu, 179 p.
- Hanski, E., Huhma, H., Smolkin, V.F. & Vaasjoki, M., 1990.** The age of the ferropicritic volcanics and comagmatic Ni-bearing intrusions at Pehenga, Kola Peninsula, U.S.S.R. *Bulletin of the Geological Society of Finland* 62, 123—133.
- Hanson, G.N., 1978.** The application of trace elements to the petrogenesis of igneous rocks of granitic composition. *Earth and Planetary Science Letters* 38, 26—43.
- Harris, N.B.W. & Marriner, G.F., 1980.** Geochemistry and petrogenesis of a peralkaline granite complex from the Midian mountains, Saudi Arabia. *Lithos* 13, 325—337.
- Haskin, L.A. & Korotev, R.L., 1977.** Test of a model for trace element partitioning during closed-system solidification of silicate liquid. *Geochimica et Cosmochimica Acta* 47, 525—533.
- Hawkesworth, C.J., Rogers, N.W., van Calsteren, P.W.C. & Menzies, M.A., 1984.** Mantle enrichment processes. *Nature* 311, 331—335.
- Heier, K.S. & Adams, J.A.S., 1965.** Concentration of radioactive elements in deep crustal material. *Geochimica et Cosmochimica Acta* 29, 53—61.
- Henderson, P., 1984.** General geochemical properties and abundances of the rare earth elements. *In* P. Henderson (Editor), *Developments in geochemistry 2: Rare earth element geochemistry*. Elsevier, Amsterdam, Oxford, New York, Tokyo, 1—32.
- Higuchi, H. & Nagasawa, H., 1969.** Partition of trace elements between rock-forming minerals and the host volcanic rocks. *Earth and Planetary Science Letters* 7, 281—287.
- Hoffman, P.F., 1989.** Speculations on Laurentia's first gigayear (2.0 to 1.0 Ga). *Geology* 17, 135—138.
- Holm, P.E., 1985.** The geochemical fingerprints of different tectonomagmatic environments using hygromagmatophile element abundances of tholeiitic basalts and basaltic andesites. *Chemical Geology* 51, 303—323.
- Huang, W.-L. & Wyllie, P.J., 1975.** Melting reactions in the system $\text{NaAlSi}_3\text{O}_8\text{-KAlSi}_3\text{O}_8\text{-SiO}_2$ to 35 kilobars, dry and with excess water. *Journal of Geology* 83, 737—748.
- Hubbard, F. & Branigan, N., 1987.** Late Svecofennian magmatism and tectonism, Åland, Southwest Finland. *Precambrian Research* 35, 241—256.
- Huhma, H., 1986.** Sm-Nd, U-Pb and Pb-Pb isotopic evidence for the origin of the Early Proterozoic Svecofennian crust in Finland. Geological Survey of Finland, Bulletin 337, 48 p.
- Huhma, H., 1987.** Provenance of Early Proterozoic and Archaean metasediments in Finland: a Sm-Nd isotopic study. *Precambrian Research* 35, 127—143.
- Huhma, H., Cliff, R.A., Perttunen, V. & Sakko, M., 1990.** Sm-Nd and Pb isotopic study of mafic rocks associated with early Proterozoic continental rifting: the Peräpohja schist belt in northern Finland. *Contributions to Mineralogy and Petrology* 104, 369—379.
- Huhma, H., Claesson, S., Kinny, P.D. & Williams, I.S., 1991.** The growth of early Proterozoic crust: new evidence from Svecofennian detrital zircons. *Terra Nova* 3, 175—178.
- Huppert, H.E. & Sparks, R.S.J., 1985.** Cooling and contamination of mafic and ultramafic magmas during ascent through continental crust. *Earth and Planetary Science Letters* 74, 371—386.
- Huppert, H.E. & Sparks, S.J., 1988.** The generation of granitic magmas by intrusion of basalt into continental crust. *Journal of Petrology* 29, 599—624.
- Idman, H., 1989.** The Siipyy granite — a new rapakivi occurrence in Finland. *Bulletin of the Geological Society of Finland* 61, 123—127.
- Irvine, T.N. & Baragar, W.R.A., 1971.** A guide to the chemical classification of the common volcanic rocks. *Canadian Journal of Earth Sciences* 8, 523—548.
- Irving, A.J., 1978.** A review of experimental studies of crystal/liquid trace element partitioning. *Geochimica et Cosmochimica Acta* 42, 743—770.
- Irving, A.J., 1980.** Petrology and geochemistry of composite ultramafic xenoliths in alkalic basalts and implications for magmatic processes within the mantle. *American Journal of Science* 280, 389—426.
- Irving, A.J. & Frey, F.A., 1978.** Distribution of trace elements between garnet megacrysts and host volcanic liquids of kimberlitic to rhyolitic composition. *Geochimica et Cosmochimica Acta* 42, 771—787.
- Irving, A.J. & Frey, F.A., 1984.** Trace element abundances in megacrysts and their host basalts: Constraints on partition coefficients and megacryst genesis. *Geochimica et Cosmochimica Acta* 48, 1201—1221.
- Irving, A.J., Merril, R.B. & Singleton, D.E., 1978.** Experimental partitioning of rare earth elements and scandium among armalcolite, ilmenite, olivine and mare basalt liquid. *Proceedings of the 9th Lunar and Planetary Science Conference*, 601—612.
- Jahn, B., Vidal, P. & Kröner, A., 1984.** Multi-chronometric ages and origin of Archaean tonalitic gneisses in Finnish Lapland: a case for long crustal residence time. *Contributions to Mineralogy and Petrology* 86, 398—408.
- James, R.S. & Hamilton, D.L., 1969.** Phase relations in the system $\text{NaAlSi}_3\text{O}_8\text{-KAlSi}_3\text{O}_8\text{-CaAl}_2\text{Si}_2\text{O}_8\text{-SiO}_2$ at 1 kilobar water vapour pressure. *Contributions to Mineralogy and Petrology* 21, 111—141.
- Jaques, A.L. & Green, D.H., 1980.** Anhydrous melting of peridotite at 0—15 kb pressure and the genesis of tholeiitic basalts. *Contributions to Mineralogy and Petrology* 73, 287—310.
- Johanson, B.S., 1984.** Ahvenisto Gabbro-anortositkomplex — en petrografisk och mineralogisk undersökning. Unpublished M.Sc. thesis, University of Helsinki, Department of Geology, 85 p.
- Johanson, B.S., 1989.** Monzodioritic rocks of the gabbro-

- anorthosite complex associated with the Ahvenisto rapakivi granite batholith, southern Finland. *In* I. Haapala & Y. Kähkönen (Editors), Symposium Precambrian granitoids abstracts. Geological Survey of Finland, Special Paper 8, 74.
- Kempton, P.D., Harmon, R.S., Hawkesworth, C.J. & Moorbath, S., 1990.** Petrology and geochemistry of lower crustal granulites from the Geronimo Volcanic Field, southeastern Arizona. *Geochimica et Cosmochimica Acta* 54, 3401—3426.
- Knoper, M.W., 1989.** MODULUS: a spreadsheet program for modeling the petrogenesis of igneous rocks. Computers and Geosciences, submitted manuscript.
- Kogarko, L.N., Ramendik, G.I., Romanchev, B.P. & Trofimov, V.A., 1980.** Trace-element fractionation by minerals of alkalic basalt. *Doklady Earth Science Section* 254, 213—215.
- Korja, A. & Elo, S., 1990.** Crustal and upper mantle structure of the Wiborg batholith, SE Finland. Abstracts of the second symposium on the Baltic shield held in Lund, Sweden, June 5—7, 1990, 57.
- Korja, A. & Elo, S., 1991.** Geophysical evidence for a mantle plume in the middle Proterozoic of southeastern Finland. Geological Association of Canada, Mineralogical Association of Canada, Joint Annual Meeting with Society of Economic Geologists Program with Abstracts 16, A68.
- Kouvo, O., Huhma, H. & Sakko, M., 1983.** Isotopic evidence for old crustal involvement in the genesis of two granites from northern Finland. *Terra cognita* 3, 135.
- Kranck, E.H., 1969.** Anorthosites and rapakivi, magmas from the lower crust. *In* Y.W. Isachsen (Editor), Origin of anorthosites and related rocks. New York State Museum and Science Service Memoir 18, 93—97.
- Krogh, T.E., 1973.** A low-contamination method for hydrothermal decomposition of zircon and extraction of U and Pb for isotopic age determinations. *Geochimica et Cosmochimica Acta* 37, 485—494.
- Kushiro, I., Shimizu, N., Nakamura, Y. & Akimoto, S., 1972.** Compositions of coexisting liquid and solid phases formed on melting of natural garnet and spinel lherzolites at high pressures: A preliminary report. *Earth and Planetary Science Letters* 14, 19—25.
- Laitakari, I., 1969.** On the set of olivine diabase dikes in Häme, Finland. *Bulletin de la Commission Géologique de Finlande* 241, 65 p.
- Laitakari, I., 1987.** Hämeen subjotuninen diabaasijoniparvi, English abstract: The Subjotnian diabase dyke swarm of Häme. *In* K. Aro & I. Laitakari (Editors), Suomen diabaasit ja muut mafiset juonikivilajit (Diabases and other mafic dyke rocks in Finland). Geological Survey of Finland, Report of Investigation 76, 99—116.
- Laitakari, I. & Leino, H., 1989.** A new model for the emplacement of the Häme diabase dyke swarm, central Finland. *In* S. Autio (Editor), Geological Survey of Finland current research 1988. Geological Survey of Finland, Special Paper 10, 7—8.
- Laitala, M., 1984.** Pellingin ja Porvoon kartta-alueiden kallioperä, English summary: Pre-Quaternary rocks of the Pellinki and Porvoo map-sheet areas, Geological map of Finland 1:100 000, Explanation to the maps of Pre-Quaternary rocks, Sheets 3012 and 3021. Geological Survey of Finland, 53 p.
- Larsen, L.M., 1979.** Distribution of REE and other trace elements between phenocrysts and peralkaline undersaturated magmas, exemplified by rocks from the Gardar igneous province, South Greenland. *Lithos* 12, 303—315.
- Laurén, L., 1970.** An interpretation of the negative gravity anomalies associated with the rapakivi granites and the Jotnian sandstone in southern Finland. *Geologiska Föreningens i Stockholm Förhandlingar* 92, 21—34.
- Le Roex, A.P., 1987.** Source regions of mid-ocean ridge basalts: Evidence for enrichment processes. *In* M.A. Menzies & C.J. Hawkesworth (Editors), Mantle metasomatism. Academic Press, London, 389—422.
- Lee, D.E. & Christiansen, E.H., 1983.** The granite problem as exposed in the Southern Snake Range, Nevada. *Contributions to Mineralogy and Petrology* 83, 99—116.
- Lehijärvi, M. & Tyrväinen, A., 1969.** Geological map of Finland, 1:100 000, pre-Quaternary rocks, Sheet 3114 Vuohijärvi. Geological Survey of Finland.
- Lightfoot, P.C., Hawkesworth, C.J., Devey, C.W., Rogers, N.W. & van Calsteren, P.W.C., 1990.** Source and differentiation of Deccan Trap lavas: implications of geochemical and mineral chemical variations. *Journal of Petrology* 31, 1165—1200.
- Lindberg, B. & Eklund, O., 1989.** The rapakivi granite — diabase association in southwestern Finland. *In* I. Haapala & Y. Kähkönen (Editors), Symposium Precambrian granitoids abstracts. Geological Survey of Finland, Special Paper 8, 82 p.
- Lindqvist, K. & Laitakari, I., 1980.** Glass and amygdules in Precambrian diabases from Orivesi, southern Finland. *Bulletin of the Geological Society of Finland* 52, 221—229.
- Loiselle, M.C. & Wones, D.R., 1979.** Characteristics and origin of anorogenic granites. Geological Society of America, Abstracts with Programs 11, 468.
- Lopez-Escobar, L., Vergara, M. & Frey, F., 1981.** Petrology and geochemistry of lavas from Antuco volcano, a basaltic volcano of the southern Andes (37°25' S). *Journal of Volcanology and Geothermal Research* 11, 329—352.
- Luosto, U., 1990.** Seismic data from the northern segment of the EGT and from the nearby profiles. *In* R. Freeman & St. Mueller (Editors), Proceedings of the sixth workshop of the geotraverse (EGT) project. European Science Foundation, Strasbourg, 53—61.
- Luth, W.C., 1969.** The systems $\text{NaAlSi}_3\text{O}_8\text{-SiO}_2$ and $\text{KAlSi}_3\text{O}_8\text{-SiO}_2$ to 20 kb and the relationship between H_2O content, $P_{\text{H}_2\text{O}}$, and P_{total} in granitic magmas. *American Journal of Science* 267A, 325—341.
- Mahood, G. & Hildreth, W., 1983.** Large partition coefficients for trace elements in high-silica rhyolites. *Geochimica et Cosmochimica Acta* 47, 11—30.
- Manning, D. A. C., 1981.** The effect of fluorine on liquidus phase relationships in the system Qz-Ab-Or with excess water at 1 kb. *Contributions to Mineralogy and Petrology* 76, 206—215.
- Martin, H., Chauvel, C., Jahn, B. & Vidal, P., 1983.** Rb-Sr and Sm-Nd ages and isotopic geochemistry of Archaean granodioritic gneisses from eastern Finland. *Precambrian Research* 20, 79—91.

- Masuda, Y. & Aoki, K.-I., 1979.** Trace element variations in the volcanic rocks from the Nasu zone, northeast Japan. *Earth and Planetary Science Letters* 44, 139—149.
- McCallum, I.S. & Charette, M.P., 1977.** Partitioning of Zr between crystals and coexisting high-Ti mare basalt melt. *Lunar Science*, VIII, 637—639.
- McCarthy, T.S. & Hasty, R.A., 1976.** Trace element distribution patterns and their relationship to the crystallization of granitic melts. *Geochimica et Cosmochimica Acta* 40, 1351—1358.
- McDonough, W.F., 1990.** Constraints on the composition of the continental lithospheric mantle. *Earth and Planetary Science Letters* 101, 1—18.
- McDonough, W.F., McCulloch, M.T. & Sun, S.S., 1985.** Isotopic and geochemical systematics in Tertiary-Recent basalts from southeastern Australia and implications for the evolution of the sub-continental lithosphere. *Geochimica et Cosmochimica Acta* 49, 2051—2067.
- McKay, G.A. & Weill, D.F., 1976.** Application of major and trace element crystal/liquid partitioning to the origin of KREEP. *Lunar Science* VII, 527—599.
- Menuge, J.F., 1988.** The petrogenesis of massive anorthosites: a Nd and Sr isotopic investigation of the Proterozoic of Rogaland/Vest-Agder, SW Norway. *Contributions to Mineralogy and Petrology* 98, 363—373.
- Menzies, M., 1983.** Mantle ultramafic xenoliths in alkaline magmas: Evidence for mantle heterogeneity modified by magmatic activity. *In* C.J. Hawkesworth & M.J. Norry (Editors), *Continental basalts and mantle xenoliths*. Shiva, Nantwich, Cheshire, 92—110.
- Menzies, M.A., Leeman W.P. & Hawkesworth, C.J., 1983.** Isotope geochemistry of Cenozoic volcanic rocks reveals mantle heterogeneity below western USA. *Nature* 303, 205—209.
- Meriläinen, K., 1966.** Geological map of Finland, 1:100 000, pre-Quaternary rocks, Sheet 4112+4111, Imatra. Geological Survey of Finland.
- Meriläinen, K., 1976.** The granulite complex and adjacent rocks in Lapland, northern Finland. *Geological Survey of Finland, Bulletin* 281, 129 p.
- Miller, C.F. & Mittlefehldt, D.W., 1982.** Depletion of light rare-earth elements in felsic magmas. *Geology* 10, 129—133.
- Morris, P.A., 1984.** MAGFRAC: a basic program for least-squares approximation of fractional crystallization. *Computers and Geosciences* 10, 437—444.
- Morse, S.A., 1982a.** A partisan review of Proterozoic anorthosites. *American Mineralogist* 67, 1087—1100.
- Morse, S.A., 1982b.** Kiglapait geochemistry V: Strontium. *Geochimica et Cosmochimica Acta* 46, 223—234.
- Mortimer, G.E., Cooper, J.A. & Oliver, R.L., 1988.** Proterozoic mafic dykes near Port Lincoln, South Australia: composition, age and origin. *Australian Journal of Earth Sciences* 35, 93—110.
- Murakami, N., and Imaoka, T., 1985.** Rapakivi granites from Cape of Ashizuri, Kochi Prefecture, southwest Japan. *Journal of the Geological Society of Japan* 91, 179—194 (in Japanese with English Abstract).
- Murthy, V.R. & Griffin, W.L., 1970.** K/Rb fractionation by plagioclase feldspars. *Chemical Geology* 6, 265—271.
- Mysen, B.O. & Kushiro, I., 1976.** Partitioning of iron, nickel, and magnesium between metal, oxide, and silicates in Allende meteorite as a function of fO₂. Annual Report of the Director of the Geophysical Laboratory, Carnegie Institution of Washington, 1975—1976, Geophysical Laboratory, Washington, D.C., 678—684.
- Nagasawa, H. & Schnetzler, C.C., 1971.** Partitioning of rare earth, alkali and alkaline earth elements between phenocrysts and acidic igneous magma. *Geochimica et Cosmochimica Acta* 35, 953—968.
- Nance, W.B. & Taylor, S.R., 1976.** Rare-earth element patterns and crustal evolution — I. Australian post-Archean sedimentary rocks. *Geochimica et Cosmochimica Acta* 40, 1539—1551.
- Nash, W.P. & Crecraft, H.R., 1985.** Partition coefficients for trace elements in silicic magmas. *Geochimica et Cosmochimica Acta* 49, 2309—2322.
- Nelson, B.K. & DePaolo, D.J., 1985.** Rapid production of continental crust 1.7 to 1.9 b.y. ago: Nd isotopic evidence from the basement of the North American mid-continent. *Geological Society of America, Bulletin* 96, 746—754.
- Neymark, L.A., Amelin, Ju.A. & Larin, A.M., in prep.** Isotopic evidence for the lower crustal origin of rapakivi granites and related basic rocks of Salmi batholith, Southern Karelia.
- Nixon, P.H. & Davies, G.R., 1987.** Mantle xenolith perspectives. *In* P.H. Nixon (Editor), *Mantle xenoliths*. John Wiley & Sons, New York, 741—756.
- Noble, D.C. & Hedge, C.E., 1970.** Distribution of rubidium between sodic sanidine and natural silicic liquid. *Contributions to Mineralogy and Petrology* 29, 234—241.
- Nurmi, P.A. & Haapala, I., 1986.** The Proterozoic granitoids of Finland: granite types, metallogeny and relation to crustal evolution. *Bulletin of the Geological Society of Finland* 58, 203—233.
- Nyfors, J., 1954.** Om anortositförekomsten i Kolinummi by, Yläne. Unpublished M.Sc. thesis, Åbo Akademi University, 35 p.
- Öhlander, B., Skiöld, T., Hamilton, P.J. & Claesson, L.-Å., 1987.** The western border of the Archaean province of the Baltic Shield: evidence from northern Sweden. *Contributions to Mineralogy and Petrology* 95, 437—450.
- Palme, H. & Wlotzka, F., 1977.** Trace element fractionation during crystallization of lunar rock 75035. *Lunar Science* VIII, 747—749.
- Papunen, H. & Gorbunov, G.I. (Editors), 1985.** Nickel-copper deposits of the Baltic Shield and Scandinavian Caledonides. Geological Survey of Finland, *Bulletin* 333, 394 p.
- Parker, A.J., Rickwood, P.C. & Tucker, D.H. (Editors), 1990.** Mafic dykes and emplacement mechanisms. A.A. Balkema, Rotterdam, Brookfield, 541 p.
- Paster, T.P., Schauwecker, D.S. & Haskin, L.A., 1974.** The behavior of some trace elements during solidification of the Skaergaard layered series. *Geochimica et Cosmochimica Acta* 38, 1549—1577.
- Patchett, P.J., 1980.** Thermal effects of basalt on continental crust and crustal contamination of magmas. *Nature* 283, 559—561.
- Patchett, P.J. & Arndt, N.T., 1986.** Nd isotopes and tectonics

- of 1.9–1.7 Ga crustal genesis. *Earth and Planetary Science Letters* 78, 329–338.
- Patchett, P.J. & Bridgwater, D., 1984.** Origin of continental crust of 1.9–1.7 Ga age defined by Nd isotopes in the Ketilidian terrain of South Greenland. *Contributions to Mineralogy and Petrology* 87, 311–318.
- Patchett, J. & Kouvo, O., 1986.** Origin of continental crust of 1.9–1.7 Ga age. Nd isotopes and U-Pb zircon ages in the Svecofennian terrain of South Finland. *Contributions to Mineralogy and Petrology* 92, 1–12.
- Patchett, P.J., Kouvo, O., Hedge, C.E. & Tatsumoto, M., 1981.** Evolution of continental crust and mantle heterogeneity: evidence from Hf isotopes. *Contributions to Mineralogy and Petrology* 78, 279–297.
- Patchett, P.J., Todt, W. & Gorbatschev, R., 1987.** Origin of continental crust of 1.9–1.7 Ga age: Nd isotopes in the Svecofennian orogenic terrains of Sweden. *Precambrian Research* 35, 145–160.
- Pearce, J.A. & Norry, M.J., 1979.** Petrogenetic implications of Ti, Zr, Y, and Nb variations in volcanic rocks. *Contributions to Mineralogy and Petrology* 69, 33–47.
- Pearce, J.A., Harris, N.B.W. & Tindle, A.G., 1984.** Trace element discrimination diagrams for the tectonic interpretation of granitic rocks. *Journal of Petrology* 25, 956–983.
- Pearce, T.H., Gorman, B.E. & Birkett, T.C., 1975.** The $\text{TiO}_2\text{-K}_2\text{O-P}_2\text{O}_5$ diagram: a method of discriminating between oceanic and non-oceanic basalts. *Earth and Planetary Science Letters* 24, 419–426.
- Pearce, T.H., Gorman, B.E. & Birkett, T.C., 1977.** The relationship between major element chemistry and tectonic environment of basic and intermediate volcanic rocks. *Earth and Planetary Science Letters* 36, 121–132.
- Pedersen, A.K., 1979.** Basaltic glass with high-temperature equilibrated immiscible sulphide bodies with native iron from Disco, central West Greenland. *Contributions to Mineralogy and Petrology* 69, 397–407.
- Perry, F.V., Baldrige, W.S. & DePaolo, D.J., 1987.** Role of asthenosphere and lithosphere in the genesis of late Cenozoic basaltic rocks from the Rio Grande Rift and adjacent regions of the southwestern United States. *Journal of Geophysical Research* 92, 9193–9213.
- Philpotts, J.A. & Schnetzler, C.C., 1970.** Phenocryst-matrix partition coefficients for K, Rb, Sr and Ba, with applications to anorthosite and basalt genesis. *Geochimica et Cosmochimica Acta* 34, 307–322.
- Pihlaja, P., 1987.** Porin seudun subjotjuniset diabaasit, English abstract: The Subjotnian diabaasites of the Pori region, southwestern Finland. *In* K. Aro & I. Laitakari (Editors), *Suomen diabaasit ja muut mafiset juonikivilajit (Diabaasites and other mafic dyke rocks in Finland)*. Geological Survey of Finland, Report of Investigation 76, 133–150.
- Pipping, F., 1956.** Rapakivimassivet i Suomenniemi. Unpublished M.Sc. thesis, University of Helsinki, Department of Geology, 53 p.
- Pitcher, W.S. & Berger, A.R., 1972.** The geology of Donegal: A study of granite emplacement and unroofing. John Wiley & Sons, New York, London, Sydney, Toronto, 435 p.
- von Platen, H. & Höller H., 1966.** Experimentelle Anatexis des Stainzer Plattengneises von der Koralpe, Steiermark, bei 2, 4, 7 und 10 kb H_2O -Druck. *Neues Jahrbuch für Mineralogie, Abhandlungen* 106, 106–130.
- Pushkar, P., McBirney, A.R. & Kudo, A.M., 1972.** The isotopic composition of strontium in Central American Ignimbrites. *Bulletin volcanologique* 35, 265–294.
- Rämö, O.T., 1989a.** Silicic-basic magmatism associated with rapakivi granites: petrography and petrology of composite diabase-quartz porphyry dykes and K-feldspar diabaasites in the Suomenniemi complex, southeastern Finland. *In* I. Haapala & Y. Kähkönen (Editors), *Symposium Precambrian granitoids abstracts*. Geological Survey of Finland, Special Paper 8, 105–106.
- Rämö, O.T., 1989b.** Petrology and geochemistry of tholeiitic dikes in the eastern Fennoscandian shield: Evolution of a middle Proterozoic continental rift. *International Association of Volcanology and Chemistry of the Earth's Interior 1989 General Assembly Abstracts*. New Mexico Bureau of Mines and Mineral Resources, Bull. 131, 220.
- Rämö, O.T., 1990.** Diabase dyke swarms and silicic magmatism — Evidence from the Proterozoic of Finland. *In* A.J. Parker, P.C. Rickwood & D.H. Tucker (Editors), *Mafic dykes and emplacement mechanisms*. A.A. Balkema, Rotterdam, Brookfield, 185–199.
- Rämö, O.T. & Haapala, I., 1991.** The rapakivi granites of eastern Fennoscandia: a review with insights into their origin in the light of new Sm-Nd isotopic data. *In* C.F. Gower, T. Rivers & B. Ryan (Editors), *Mid-Proterozoic Laurentia-Baltica*. Geological Association of Canada, Special Paper 38, 401–415.
- Rämö, O.T., Vaasjoki, M. & Huhma, H., 1989.** Sm-Nd and Pb-Pb isotopic constraints on the origin of the rapakivi granites and associated tholeiitic dyke rocks in southern Finland. *In* I. Haapala & Y. Kähkönen (Editors), *Symposium Precambrian granitoids abstracts*. Geological Survey of Finland, Special Paper 8, 107–108.
- Rämö, O.T., Huhma, H. & Vaasjoki, M., 1990.** Protolith variation in the Proterozoic rapakivi granites of eastern Fennoscandia: Nd and Pb isotopes. *7th International Conference on Geochronology, Cosmochronology and Isotope Geology Abstract Volume*, Geological Society of Australia, Abstracts 27, 81.
- Rayleigh, J.W.S., 1896.** Theoretical considerations respecting the separation of gases by diffusion and similar processes. *Philosophical Magazine* 42, 493–498.
- Reece, C., Ruiz, J., Duffield, W.A., & Patchett, P.J., 1990.** Origin of Taylor Creek rhyolite magma, Black Range, New Mexico, based on Nd-Sr isotope studies. *In* H.J. Stein & J.L. Hannah (Editors), *Ore-bearing granite systems; Petrogenesis and mineralizing processes*. Geological Society of America, Special Paper 246, 263–273.
- Reid, J.B., Jr., Evans, O.C. & Fates, D.G., 1983.** Magma mixing in granitic rocks of the central Sierra Nevada, California. *Earth and Planetary Science Letters* 66, 243–261.
- Roeder, P.L. & Emslie, R.F., 1970.** Olivine-liquid equilibrium. *Contributions to Mineralogy and Petrology* 29, 275–289.
- Rogers, J.J.W. & Greenberg, J.K., 1990.** Late-orogenic, post-

- orogenic, and anorogenic granites: Distinction by major-element and trace-element chemistry and possible origins. *Journal of Geology* 98, 291—309.
- Rudnick, R.L. & Goldstein, S.L., 1990.** The Pb isotopic compositions of lower crustal xenoliths and the evolution of lower crustal Pb. *Earth and Planetary Science Letters* 98, 192—207.
- Rudnick, R.L. & Presper, T., 1990.** Geochemistry of intermediate/- to high-pressure granulites. *In* D. Vielzeuf & Ph. Vidal (Editors), *Granulites and crustal evolution*. NATO ASI Series C: Mathematical and Physical Sciences 311, 523—550.
- Rudnick, R.L. & Taylor, S.R., 1987.** The composition and petrogenesis of the lower crust: a xenolith study. *Journal of Geophysical Research* 92, B13, 13981—14005.
- Sack, R.O., Carmichael, I.S.E., Rivers, M. & Ghiorso, M.S., 1980.** Ferric-ferrous equilibria in natural silicate liquids at 1 bar. *Contributions to Mineralogy and Petrology* 75, 369—376.
- Sahama, Th. G., 1945.** On the chemistry of the east Fennoscandian rapakivi granites. *Bulletin de la Commission Géologique de Finlande* 136, 15—67.
- Sahama, Th.G., 1947.** Rapakivi amphibole from Uuksunjoki, Salmi Area. *Bulletin de la Commission Géologique de Finlande* 140, 159—162.
- Savolahti, A., 1956.** The Ahvenisto massif in Finland. *Bulletin de la Commission Géologique de Finlande* 174, 96 p.
- Savolahti, A., 1962.** The rapakivi problem and the rules of idiomorphism in minerals. *Bulletin de la Commission Géologique de Finlande* 204, 33—112.
- Schiffries, C.M., 1990.** Crustal contamination and magma evolution: oxygen isotopic data for layered intrusions. *Annual Report of the Director of the Geophysical Laboratory, Carnegie Instn. Washington, 1989—1990*, Geophysical Laboratory, Washington, D.C., 27—29.
- Schnetzer, C.C. & Philpotts, J.A., 1970.** Partition coefficients of rare-earth elements between igneous matrix material and rock-forming-mineral phenocrysts — II. *Geochimica et Cosmochimica Acta* 34, 331—340.
- Sederholm, J. J., 1891.** Ueber die finnländischen Rapakiwigesteine. *Tschermak's Mineralogische und Petrographische Mittheilungen* 12, 1—31.
- Sederholm, J.J., 1934.** On migmatites and associated Precambrian rocks of southwestern Finland, part III, The Åland islands. *Bulletin de la Commission Géologique de Finlande* 107, 68 p.
- Şengör, A.M.C. & Burke, K., 1978.** Relative timing of rifting and volcanism on Earth and its tectonic implications. *Geophysical Research Letters* 5, 419—421.
- Shaw, D.M., 1970.** Trace element fractionation during anatexis. *Geochimica et Cosmochimica Acta* 34, 237—243.
- Sheraton, J.W. & Black, L.P., 1981.** Geochemistry and geochronology of Proterozoic tholeiite dykes of East Antarctica: evidence for mantle metasomatism. *Contributions to Mineralogy and Petrology* 78, 305—317.
- Sibiya, V.B., 1988.** The Gaborone granite complex Botswana, southern Africa: an atypical rapakivi granite-massif anorthosite association. *Free University Press, Amsterdam*, 449 p.
- Siivola, J., 1977.** Baddeleyite — ZrO₂ — from Lovasjärvi diabase, southeastern Finland. *Bulletin of the Geological Society of Finland* 49, 59—64.
- Siivola, J., 1987.** Lovasjärven mafinen intruusio, English summary: The mafic intrusion of Lovasjärvi. *In* K. Aro & I. Laitakari (Editors), *Suomen diabaasit ja muut mafiset juonikivilajit (Diabases and other mafic dyke rocks in Finland)*. Geological Survey of Finland, Report of Investigation 76, 121—128.
- Simonen, A., 1973.** Geological map of Finland, 1:100 000, pre-Quaternary rocks, Sheet 3042 Hamina. Geological Survey of Finland.
- Simonen, A., 1979a.** Geological map of Finland, 1:100 000, pre-Quaternary rocks, Sheet 3044 Vaalimaa. Geological Survey of Finland.
- Simonen, A., 1979b.** Geological map of Finland, 1:100 000, pre-Quaternary rocks, Sheet 3133 Ylämaa. Geological Survey of Finland.
- Simonen, A., 1980.** The Precambrian in Finland. *Geological Survey of Finland, Bulletin* 304, 58 p.
- Simonen, A. & Laitala, M., 1972.** Geological map of Finland, 1:100 000, pre-Quaternary rocks, Sheet 3041 Haapasaari. Geological Survey of Finland.
- Simonen, A. & Tyrväinen, A., 1965.** Geological map of Finland, 1:100 000, pre-Quaternary rocks, Sheet 3132 Savitaipale. Geological Survey of Finland.
- Simonen, A. & Tyrväinen A., 1981.** Savitaipaleen karttalueen kallioperä, English summary: Pre-Quaternary rocks of the Savitaipale map-sheet area, Geological map of Finland 1:100 000, Explanation to the map of pre-Quaternary rocks, Sheet 3132. Geological Survey of Finland, 30 p.
- Simonen, A. & Vormaa, A., 1969.** Amphibole and biotite from rapakivi. *Bulletin de la Commission Géologique de Finlande* 238, 28 p.
- Sparks, R.S.J., 1986.** The role of crustal contamination in magma evolution through geological time. *Earth and Planetary Science Letters* 78, 211—223.
- Stacey, J.S. & Kramers, J.D., 1975.** Approximation of terrestrial lead isotope evolution by a two-stage model. *Earth and Planetary Science Letters* 26, 207—221.
- Stewart, B.W. & DePaolo, D.J., 1990.** Isotopic studies of processes in mafic magma chambers: II. The Skaergaard intrusion, east Greenland. *Contributions to Mineralogy and Petrology* 104, 125—141.
- Streckeisen, A.L., 1973.** Plutonic rocks: classification and nomenclature recommended by the IUGS Subcommittee of the systematics of igneous rocks. *Geotimes* 18, 26—30.
- Sun, S.-S., 1980.** Lead isotopic study of young volcanic rocks from mid-ocean ridges, ocean islands and island arcs. *Philosophical Transactions of the Royal Society of London, A* 294, 409—455.
- Sundsten, H., 1985.** Suomenniemi rapakivimassivets kontakter, inom kartbladet 3141 Ristiina, Finland. Unpublished M.Sc. thesis, Åbo Akademi University, 42 p.
- Suominen, V., 1979.** Geological map of Finland, 1:100 000, pre-Quaternary rocks, Sheet 1014 Föglö. Geological Survey of Finland.
- Suominen, V., 1987.** Lounais-Suomen mafiset juonikivet, English abstract: Mafic dyke rocks in southwestern Fin-

- land. *In* K. Aro & I. Laitakari (Editors), Suomen diabaasit ja muut mafiset juonikivilajit (Diabases and other mafic dyke rocks in Finland). Geological Survey of Finland, Report of Investigation 76, 151—172.
- Suominen, V., 1991.** The chronostratigraphy of SW Finland with special reference to the Postjotnian and Subjotnian diabases. Geological Survey of Finland, Bulletin 356, in print.
- Tatsumoto, M., Knight, R.J. & Allègre, C.J., 1973.** Time differences in the formation of meteorites as determined from the ratio of lead-207 to lead-206. *Science* 180, 1279—1283.
- Taylor, S.R. & McLennan, S.M., 1985.** The continental crust: Its composition and evolution. Blackwell Scientific Publications, Oxford, London, Edinburgh, Boston, Palo Alto, Melbourne, 312 p.
- Teixeira, W., 1990.** The Proterozoic mafic dyke swarms and alkaline intrusions in the Amazonian Craton, South America, and their tectonic evolution based on Rb-Sr, K-Ar and ⁴⁰Ar-³⁹Ar geochronology. *In* A.J. Parker, P.C. Rickwood & D.H. Tucker (Editors), Mafic dykes and emplacement mechanisms. A.A. Balkema, Rotterdam, Brookfield, 285—293.
- Tindle, A.G. & Pearce, J.A., 1981.** Petrogenetic modelling of *in situ* fractional crystallization in the zoned Loch Doon pluton, Scotland. *Contributions to Mineralogy and Petrology* 78, 196—207.
- Thirlwall, M.F. & Jones, N.W., 1983.** Isotope geochemistry and contamination mechanics of Tertiary lavas from Skye, Northwest Scotland. *In* C.J. Hawkesworth & M.J. Norry (Editors), Continental basalts and mantle xenoliths. Shiva, Nantwich, Cheshire, 186—208.
- Thompson, R.N., Dickin, A.P., Gibson, I.L. & Morrison, M.A. 1982.** Elemental fingerprints of isotopic contamination of Hebridean Palaeocene mantle-derived magmas by Archaean sial. *Contributions to Mineralogy and Petrology* 79, 159—168.
- Thompson, R.N., Morrison, M.A., Dickin, A.P., and Hendry, G.L. 1983.** Continental flood basalts ... Arachnids rule OK? *In* C.J. Hawkesworth and M.J. Norry (Editors), Continental basalts and mantle xenoliths. Shiva, Nantwich, Cheshire, 158—185.
- Törnroos, R., 1984.** Petrography, mineral chemistry and petrochemistry of granite porphyry dykes from Sibbo, southern Finland. Geological Survey of Finland, Bulletin 326, 43 p.
- Tuomi, A., 1988.** Maankuoren yläosan rakenteen seismologis-geologinen tulkinta Baltic-luotauslinjalta Kaakkois-Suomesta. Unpublished M.Sc. thesis, University of Helsinki, Department of Geology, 135 p.
- Tyrväinen, A., 1986.** Vuohijärven kartta-alueen kallioperä, English summary: Pre-Quaternary rocks of the Vuohijärvi map-sheet area, Geological map of Finland 1:1000,000, Explanation to the map of Pre-Quaternary rocks, Sheet 3114. Geological Survey of Finland, 35 p.
- Tyrväinen, A., 1990.** Geological map of Finland, 1:100 000, pre-Quaternary rocks, Sheet 3141 Ristiina. Geological Survey of Finland.
- Vaasjoki, M., 1977.** Rapakivi granites and other postorogenic rocks in Finland; Their age and the lead isotopic composition of certain associated galena mineralizations. Geological Survey of Finland, Bulletin 294, 64 p.
- Vaasjoki, M., 1981.** The lead isotopic composition of some Finnish galenas. Geological Survey of Finland, Bulletin 316, 30 p.
- Vaasjoki, M. & Rämö, T., 1989.** The Wiborg rapakivi batholith and associated rocks in southeastern Finland. Precambrian Granitoids, petrogenesis, geochemistry and metallogeny, Excursion A2, Geological Survey of Finland, Guide 30, 32 p.
- Vaasjoki, M. & Sakko, M., 1989.** The radiometric age of the Virmaila diabase dyke: Evidence for 20 Ma of continental rifting in Padasjoki, southern Finland. *In* S. Autio (Editor), Geological Survey of Finland current research 1988. Geological Survey of Finland, Special Paper 10, 43—44.
- Vaasjoki, M., Pihlaja, P. & Sakko, M., 1988.** The radiometric age of the Reposaari granite and its bearing on the extent on the Laitila rapakivi batholith in western Finland. *Bulletin of the Geological Society of Finland* 60, 129—134.
- Vaasjoki, M., Rämö, O.T. & Sakko, M., 1991.** New U-Pb ages from the Wiborg rapakivi area: constraints on the temporal evolution of the rapakivi granite — anorthosite — diabase dyke association of southeastern Finland. *In* I. Haapala & K.C. Condie (Editors), Precambrian granitoids — petrogenesis, geochemistry and metallogeny. *Precambrian Research* 51, 227—243.
- Van Schmus, W.R. & Bickford, M.E., 1981.** Proterozoic chronology and evolution of the midcontinent region, North America. *In* A. Kröner (Editor), Precambrian plate tectonics. Elsevier, Amsterdam, 261—296.
- Velikoslavinskiy, D.A., Birkis, A.P., Bogatkov, O.A., Bukharev, V.P., Velikoslavinskiy, S.D., Gordienko, L.I., Zinchenko, O.V., Kivisilla, J., Kirs, J., Kononov, Yu. V., Levitskiy, Yu. F., Niin, M., Puura, V., Khvorov, M.I. & Shustova, L.E., 1978.** Anortozit-rapakivigranitnaja formatsija Vostotsno-Evropeskij platformy. Nauka, Leningrad, 296 p.
- Villemant, B., Jaffrezic, H., Joron, J.L. & Treuil, M., 1981.** Distribution coefficients of major and trace elements; Fractional crystallization in the alkali basalt series of Chaîne des Puys (Massif Central, France). *Geochimica et Cosmochimica Acta* 45, 1997—2016.
- Varma, A., 1971.** Alkali feldspars of the Wiborg rapakivi massif in southeastern Finland. *Bulletin de la Commission Géologique de Finlande* 246, 72 p.
- Varma, A., 1972.** On the contact aureole of the Wiborg rapakivi granite massif in southeastern Finland. Geological Survey of Finland, Bulletin 255, 28 p.
- Varma, A., 1975.** On two roof pendants in the Wiborg rapakivi massif, southeastern Finland. Geological Survey of Finland, Bulletin 272, 86 p.
- Varma, A., 1976.** On the petrochemistry of rapakivi granites with special reference to the Laitila massif, southwestern Finland. Geological Survey of Finland, Bulletin 285, 98 p.
- Varma, A., 1980.** The Wiborg rapakivi massif. *In* K. Hytönen (Editor), Precambrian bedrock of southern and eastern Finland, Guide to excursions 001 A + C, 26th International Geological Congress Paris 1980. Geological Survey of Finland, 6—8.

- Vorma, A. & Paasivirta, T., 1979.** Contribution to the mineralogy of the rapakivi granites: I. Zircon of the Laitila rapakivi, southwestern Finland. Geological Survey of Finland, Bulletin 303, 40 p.
- Wahl, W., 1925.** Die Gesteine des wiborger Rapakivigebietes. Fennia 45 (20), 127 p.
- Wahl, W., 1947.** A composite lava flow from Lounatkorkia, Hogland. Bulletin de la Commission Géologique de Finlande 140, 287—302.
- Walker, D., Shibata, T. & DeLong, S.E., 1979.** Abyssal tholeiites from the Oceanographer Fracture Zone II. Phase equilibria and mixing. Contributions to Mineralogy and Petrology 70, 111—125.
- Watson, E.B., 1982.** Basalt contamination by continental crust: some experiments and models. Contributions to Mineralogy and Petrology 80, 73—87.
- Watson, E.B. & Harrison, T.M., 1983.** Zircon saturation revisited: temperature and composition effects in a variety of crustal magma types. Earth and Planetary Science Letters 64, 295—304.
- Weaver, B.L. & Tarney, J., 1980.** Continental crust composition and nature of the lower crust: constraints from mantle Nd-Sr isotope correlation. Nature 286, 342—346.
- Weaver, B.L. & Tarney, J., 1981.** The Scourie Dyke Suite: petrogenesis and geochemical nature of the Proterozoic sub-continental mantle. Contributions to Mineralogy and Petrology 78, 175—188.
- Whalen, J.B. & Currie, K.L., 1990.** The Topsails igneous suite, western Newfoundland; Fractionation and magma mixing in an »orogenic« A-type granite suite. In H.J. Stein & J.L. Hannah (Editors), Ore-bearing granite systems; Petrogenesis and mineralizing processes. Geological Society of America, Special Paper 246, 287—299.
- Whalen, J.B., Currie, K.L. & Chappell, B.W., 1987.** A-type granites; Geochemical characteristics, discrimination, and petrogenesis. Contributions to Mineralogy and Petrology 95, 407—419.
- White, A.J.R., 1979.** Sources of granitic magmas. Geological Society of America, Abstracts with Programs 11, 539 p.
- White, A.J.R. & Chappell, B.W., 1977.** Ultrametamorphism and granitoid genesis. Tectonophysics 43, 7—22.
- Wickham, S.M., 1987.** The segregation and emplacement of granitic magmas. Journal of the Geological Society, London, 144, 281—297.
- Wiebe, R.A., 1980.** Anorthositic magmas and the origin of the proterozoic anorthosite massifs. Nature 286, 564—567.
- Wiebe, R.A., 1990.** Evidence for unusually feldspathic liquids in the Nain complex, Labrador. American Mineralogist 75, 1—12.
- Winkler, H.G.F., Boese, M. & Marcopoulos, T., 1975.** Low temperature granitic melts. Neues Jahrbuch für Mineralogie Monatshefte 6, 245—268.
- Wittke, J.H., Smith, D. & Wooden, J.L., 1989.** Origin of Sr, Nd and Pb isotopic systematics in high-Sr basalts from central Arizona. Contributions to Mineralogy and Petrology 101, 57—68.
- Wyborn, L.A.I., Page, R.W. & McCulloch, M.T., 1988.** Petrology, geochronology and isotope geochemistry of the post-1820 Ma granites of the Mount Isa Inlier: Mechanisms for the generation of Proterozoic anorogenic granites. Precambrian Research 40/41, 509—541.
- Wyllie, P.J., 1977.** Crustal anatexis: an experimental review. Tectonophysics 43, 41—71.
- Yu, J., 1989.** Geochemistry of the K-rich acidic-basic complex in the Proterozoic rift trough, Beijing area, China. In I. Haapala & Y. Kähkönen (Editors), Symposium Precambrian granitoids abstracts. Geological Survey of Finland, Special Paper 8, 147.
- Zartman, R.E. & Haines, S.M., 1988.** The plumbotectonic model for Pb isotopic systematics among major terrestrial reservoirs - A case for bi-directional transport. Geochimica et Cosmochimica Acta 52, 1327—1339.

Appendix 1. Chemical composition of the silicic rocks and alkali-feldspar syenites.

Sample	Suomenniemi complex													
	Hornblende-clinopyroxene-fayalite granites				Hornblende granites									
	M415.2	M415.4	A1130	L868.3B	M319.2	A1044	M1.1	M1.2	A1043	M195.2	A1045	O202.1	O211.2	O256.1
SiO ₂ (wt%)	68.50	65.10	67.50	67.30	69.70	70.60	68.10	65.90	66.70	68.00	67.80	67.70	67.20	67.20
TiO ₂	0.67	0.96	0.56	0.58	0.48	0.45	0.66	0.79	0.73	0.68	0.49	0.79	0.74	0.61
Al ₂ O ₃	12.20	11.90	12.80	13.40	12.80	12.70	12.90	13.00	12.90	13.10	13.80	13.00	13.20	13.90
Fe ₂ O ₃	2.25	3.07	1.41	2.02	1.27	1.13	1.26	1.21	2.23	1.41	1.66	2.27	1.56	1.99
FeO	4.10	6.60	4.20	2.80	3.60	3.40	4.80	5.50	4.80	5.00	3.10	4.50	4.50	3.20
MnO	0.10	0.16	0.09	0.07	0.07	0.17	0.09	0.12	0.10	0.10	0.06	0.11	0.10	0.09
MgO	0.26	0.42	0.13	0.39	0.27	0.21	0.35	0.59	0.40	0.39	0.28	0.44	0.48	0.54
CaO	2.31	3.17	1.89	1.82	2.06	1.80	2.38	2.78	2.49	2.34	2.26	2.51	2.27	1.51
Na ₂ O	2.62	2.58	2.72	3.23	2.99	3.08	3.07	2.99	2.83	2.94	2.85	3.01	2.90	2.90
K ₂ O	5.25	4.23	6.01	6.17	5.50	5.76	5.28	5.36	5.21	5.35	6.10	4.94	5.48	6.37
P ₂ O ₅	0.12	0.19	0.08	0.11	0.09	0.06	0.11	0.20	0.13	0.13	0.10	0.15	0.19	0.11
F	0.26	0.2	0.14	0.18	0.16	0.32	0.16	0.23	0.13	0.14	0.29	0.12	0.22	0.11
H ₂ O+	0.60	0.50	0.40	0.70	0.70	0.60	0.40	0.50	0.45	0.50	0.50	0.70	0.60	0.90
H ₂ O-	0.10	0.10	0.10	0.10	0.20	0.10	0.10	0.10	0.10	0.10	0.10	0.10	<0.10	0.10
Total	99.34	99.18	98.03	98.87	99.89	100.38	99.66	99.27	99.17	100.18	99.39	100.34	99.44	99.53
O=F ₂	0.11	0.08	0.06	0.08	0.07	0.13	0.07	0.10	0.05	0.06	0.12	0.05	0.09	0.05
Total	99.23	99.09	97.97	98.79	99.82	100.25	99.59	99.17	99.12	100.12	99.27	100.29	99.35	99.49
NK/A (a)	0.82	0.74	0.86	0.89	0.85	0.89	0.83	0.82	0.80	0.81	0.82	0.79	0.81	0.84
A/CNK (b)	0.86	0.82	0.89	0.88	0.88	0.87	0.85	0.82	0.87	0.88	0.90	0.87	0.89	0.96
Rb/Ba	0.40	0.30	0.17	0.16	0.17	0.29	0.11	0.11	0.10	0.10	0.14	0.08	0.15	0.13
Rb/Sr	2.13	1.53	1.94	1.56	1.27	3.65	1.06	0.99	0.97	0.96	1.63	0.84	1.26	1.36
Ga/Al	3.72	3.49	2.95	3.67	3.40	3.87	3.52	3.20	3.08	3.46	3.29	3.34	3.29	3.40
K/Na	2.00	1.64	2.21	1.91	1.84	1.87	1.72	1.79	1.84	1.82	2.14	1.64	1.89	2.20
C.I.P.W. norms (c):														
Q	27.46	24.96	23.48	20.93	25.71	25.60	22.97	19.73	23.32	22.97	22.39	24.30	22.62	21.16
C	0.00	0.00	0.00	0.00	0.00	0.00	0.00	0.00	0.00	0.00	0.00	0.00	0.00	0.00
Or	31.53	25.40	36.46	37.24	32.88	34.25	31.51	32.17	31.25	31.79	36.59	29.36	32.83	38.24
Ab	22.53	22.19	23.63	27.92	25.60	26.23	26.24	25.70	24.30	25.01	24.48	25.61	24.88	24.93
An	6.12	8.53	5.10	3.92	5.32	3.84	5.88	6.32	7.21	6.78	6.95	7.41	6.91	6.19
Ac	0.00	0.00	0.00	0.00	0.00	0.00	0.00	0.00	0.00	0.00	0.00	0.00	0.00	0.00
Wo	0.00	0.00	0.00	0.00	0.00	0.00	0.00	0.00	0.00	0.00	0.00	0.00	0.00	0.00
Mt	3.32	4.52	2.10	2.99	1.86	1.65	1.84	1.78	3.28	2.06	2.44	3.31	2.29	2.93
Il	1.29	1.85	1.09	1.13	0.92	0.86	1.27	1.52	1.41	1.30	0.94	1.51	1.42	1.18
Hm	0.00	0.00	0.00	0.00	0.00	0.00	0.00	0.00	0.00	0.00	0.00	0.00	0.00	0.00
Ap	0.29	0.46	0.19	0.27	0.22	0.14	0.26	0.48	0.31	0.31	0.24	0.36	0.46	0.26
Hy	3.32	6.66	4.42	1.70	3.62	3.25	5.36	6.76	5.03	6.25	2.69	4.56	5.77	4.51
Di	4.14	5.42	3.53	3.90	3.87	4.17	4.65	5.53	3.89	3.53	3.27	3.58	2.82	0.58
Trace elements in ppm:														
Sc	13.4	12.1	10.0	7.3	6.7	16.7	16.1	19.1	16.6	10.8	19.1	14.2	13.1
Zn	159	181	113	125	126	122	123	129	127	129	124	104	119	105
Sn	9	3	3	4
Ga	24	22	20	26	23	26	24	22	21	24	24	23	23	25
Rb	194	148	198	231	185	241	186	174	169	177	222	160	209	206
Ba	489	498	1200	1480	1080	841	1710	1560	1735	1710	1590	2090	1360	1610
Nb	63	67	33	34	36	52	39	39	43	35	39	23	45	51
Ce	293	298	177	209	210	306	240	245	183	199	215	140	188	221
Sr	91	97	102	148	146	66	175	175	175	184	136	191	166	151
Hf	28	19	20	15	22	17	14	16	17	14	14	13	20
Zr	1160	931	524	728	623	840	603	547	595	637	488	594	542	736
Y	116	94	67	83	80	103	86	91	62	67	75	77	52	84
Yb	8.4	8.5	6.6	6.3	6.1	7.2	5.6	5.9	6.1	5.0	8.0	5.1	5.6	6.7

App. 1, contd.

		Suomenniemi complex														
Sample	Biotite-hornblende granites							Biotite granites								
	O263.1	M214.3	M291.1	M480.1	O63.1	O78.3	A1040	A1042	M114.2	M452.2	M553.1	A1041	O209.2	O242.1	L871.1	
SiO ₂ (wt%)	68.50	70.30	70.10	69.30	70.10	68.10	72.30	72.80	74.60	73.20	71.20	73.70	73.30	74.20	69.20	
TiO ₂	0.43	0.33	0.35	0.58	0.44	0.61	0.36	0.24	0.25	0.26	0.34	0.24	0.24	0.29	0.39	
Al ₂ O ₃	14.40	13.30	13.20	13.30	13.10	13.30	12.30	12.20	11.50	12.80	13.10	12.60	12.50	11.80	14.10	
Fe ₂ O ₃	1.18	0.79	0.94	1.19	0.73	1.42	1.21	0.84	0.98	0.72	1.46	0.76	0.64	1.46	0.92	
FeO	2.30	2.60	2.80	3.90	3.50	3.60	2.00	2.10	1.70	1.60	1.80	1.90	1.20	1.50	2.60	
MnO	0.05	0.05	0.06	0.09	0.07	0.07	0.04	0.04	0.04	0.04	0.05	0.04	0.03	0.04	0.06	
MgO	0.47	0.22	0.26	0.42	0.36	0.50	0.38	0.16	0.17	0.15	0.36	0.20	0.15	0.30	0.43	
CaO	1.58	1.62	1.34	1.97	1.57	1.85	1.39	1.54	1.09	1.15	1.11	1.39	0.77	1.13	1.58	
Na ₂ O	3.05	3.11	2.90	2.99	3.06	2.80	2.85	2.79	2.54	3.08	2.75	2.93	2.62	2.52	3.04	
K ₂ O	6.43	5.76	6.35	5.27	5.75	5.73	5.45	5.43	5.33	5.86	5.86	5.69	6.57	5.36	5.95	
P ₂ O ₅	0.08	0.05	0.05	0.11	0.08	0.13	0.05	0.04	0.02	0.03	0.06	0.03	0.02	0.03	0.08	
F	0.23	0.33	0.28	0.23	0.29	0.19	0.23	0.54	0.48	0.47	0.34	0.53	0.33	0.4	0.36	
H ₂ O+	0.80	0.60	0.70	0.80	0.60	0.80	0.60	0.93	0.50	0.60	0.60	0.40	0.50	0.80	0.90	
H ₂ O-	0.10	0.10	0.20	<0.10	0.10	0.10	0.10	<0.10	<0.10	0.10	0.10	<0.10	0.10	<0.1	
Total	99.60	99.16	99.53	100.15	99.75	99.20	99.26	99.65	99.20	99.96	99.13	100.51	98.87	99.93	99.61	
O=F ₂	0.10	0.14	0.12	0.10	0.12	0.08	0.10	0.23	0.20	0.20	0.14	0.22	0.14	0.17	0.15	
Total	99.51	99.02	99.41	100.05	99.63	99.12	99.16	99.42	99.00	99.76	98.99	100.29	98.73	99.76	99.46	
NK/A (a)	0.83	0.85	0.88	0.80	0.86	0.81	0.86	0.86	0.86	0.89	0.83	0.87	0.91	0.84	0.81	
A/CNK (b)	0.97	0.93	0.94	0.94	0.93	0.94	0.94	0.92	0.96	0.95	1.02	0.93	0.97	0.98	0.99	
Rb/Ba	0.16	0.20	0.22	0.19	0.26	0.17	0.23	0.59	0.81	1.01	0.24	0.62	1.56	0.47	0.21	
Rb/Sr	1.55	1.92	2.45	2.10	2.66	1.62	2.36	4.74	9.05	30.08	2.14	5.90	8.64	5.05	1.83	
Ga/Al	3.28	3.41	3.72	2.98	3.17	3.69	3.23	4.18	4.27	3.69	3.32	3.90	3.63	3.52	3.22	
K/Na	2.11	1.85	2.19	1.76	1.88	2.05	1.91	1.95	2.10	1.90	2.13	1.94	2.51	2.13	1.96	
C.I.P.W. norms (c):																
Q	21.58	25.84	24.90	25.35	25.04	24.26	31.41	32.23	36.88	30.06	29.86	31.19	31.27	36.30	23.77	
C	0.00	0.00	0.00	0.00	0.00	0.00	0.00	0.00	0.00	0.00	0.37	0.00	0.00	0.00	0.00	
Or	38.58	34.68	38.15	31.42	34.40	34.51	32.75	32.68	32.07	35.02	35.30	33.80	39.60	32.11	35.75	
Ab	26.21	26.81	24.95	25.52	26.21	24.15	24.52	24.04	21.88	26.35	23.72	24.92	22.61	21.62	26.15	
An	6.71	5.42	4.32	7.37	5.09	6.93	4.75	4.82	4.31	3.84	5.21	4.45	3.00	5.13	7.38	
Ac	0.00	0.00	0.00	0.00	0.00	0.00	0.00	0.00	0.00	0.00	0.00	0.00	0.00	0.00	0.00	
Wo	0.00	0.00	0.00	0.00	0.00	0.00	0.00	0.00	0.00	0.00	0.00	0.00	0.00	0.00	0.00	
Mt	1.74	1.17	1.39	1.74	1.07	2.10	1.78	1.24	1.45	1.06	2.16	1.11	0.95	2.15	1.36	
Il	0.83	0.64	0.68	1.11	0.85	1.18	0.70	0.46	0.48	0.50	0.66	0.46	0.46	0.56	0.75	
Hm	0.00	0.00	0.00	0.00	0.00	0.00	0.00	0.00	0.00	0.00	0.00	0.00	0.00	0.00	0.00	
Ap	0.19	0.12	0.12	0.26	0.19	0.31	0.12	0.10	0.05	0.07	0.14	0.07	0.05	0.07	0.19	
Hy	3.55	3.19	3.66	5.69	5.17	5.22	2.32	2.07	1.96	1.60	2.58	2.02	1.40	1.77	4.60	
Di	0.61	2.13	1.84	1.53	1.97	1.34	1.64	2.36	0.92	1.51	0.00	1.99	0.66	0.30	0.05	
Trace elements in ppm:																
Sc	6.9	6.9	6.0	12.6	7.4	8.9	3.7	3.6	4.7	4.3	8.2	4.7	6.9	
Zn	66	134	118	124	138	115	122	91	94	69	87	96	50	105	118	
Sn	12	<2	
Ga	25	24	26	21	22	26	21	27	26	25	23	26	24	22	24	
Rb	267	259	238	241	271	223	252	322	380	391	252	366	337	308	292	
Ba	1670	1300	1080	1300	1040	1350	1120	542	470	386	1030	591	216	662	1420	
Nb	38	43	42	48	37	24	27	50	62	48	37	43	25	44	47	
Ce	211	300	320	187	208	185	222	479	424	276	418	369	322	245	
Sr	172	135	97	115	102	138	107	68	42	13	118	62	39	61	160	
Hf	13	15	14	13	14	14	14	17	11	13	4.6	13	14	
Zr	525	500	563	544	571	487	576	368	501	409	366	435	191	491	530	
Y	75	107	107	61	72	62	71	95	153	141	110	12	94	122	61	
Yb	6.0	7.7	6.8	5.7	6.4	5.8	6.2	8.9	9.6	7.5	8.2	6.0	8.9	7.0	

App. 1, contd.

Sample	Suomenniemi complex						Topaz-bearing granites						
	Porphyritic biotite granites												
	M326.1	M589.2	M644.1	O101.1	O195.1	O247.1	M9.1	A1097	M150.1	M577.1	M664.1b	M664.2	M815.1
SiO ₂ (wt%)	71.50	71.90	72.50	72.30	72.40	72.50	74.50	74.10	74.80	72.70	77.00	73.90	73.80
TiO ₂	0.26	0.34	0.30	0.29	0.26	0.25	0.06	0.04	0.13	0.28	0.05	0.08	0.05
Al ₂ O ₃	13.00	13.50	12.80	12.20	13.00	13.10	13.50	14.40	12.10	13.50	13.10	13.50	13.30
Fe ₂ O ₃	0.70	0.92	0.86	0.73	0.91	0.54	1.03	0.81	0.33	0.80	0.27	0.47	0.85
FeO	2.20	1.60	2.20	2.40	2.00	2.00	0.10	0.10	1.50	1.50	0.30	0.80	0.10
MnO	0.04	0.04	0.05	0.05	0.04	0.03	0.03	0.02	0.03	0.03	0.03	0.04	0.01
MgO	0.18	0.31	0.25	0.23	0.16	0.17	0.07	0.01	0.10	0.29	0.10	0.08	<0.01
CaO	1.25	1.01	1.15	0.95	1.33	1.26	0.90	0.99	1.06	0.91	0.41	0.79	0.67
Na ₂ O	3.03	2.97	2.63	2.87	2.98	3.01	3.44	4.32	3.05	2.92	3.74	3.63	3.85
K ₂ O	6.09	5.92	6.29	5.87	6.07	6.11	4.95	4.14	5.20	5.82	4.43	5.10	5.10
P ₂ O ₅	0.04	0.07	0.05	0.04	0.03	0.04	0.02	0.02	0.02	0.11	0.02	0.03	0.02
F	0.49	0.31	0.46	0.34	0.55	0.49	0.72	0.88	0.72	0.41	0.73	0.94	0.58
H ₂ O+	0.70	0.80	0.70	0.60	0.50	0.30	0.70	0.50	0.50	0.50	0.30	0.50	0.70
H ₂ O-	0.10	<0.10	<0.10	0.10	0.10	<0.10	<0.10	0.10	0.10	<0.10	<0.10	0.10	<0.10
Total	99.58	99.69	100.24	98.97	100.33	99.80	100.02	100.43	99.64	99.77	100.48	99.96	99.03
O=F ₂	0.21	0.13	0.19	0.14	0.23	0.21	0.30	0.37	0.30	0.17	0.31	0.40	0.24
Total	99.37	99.56	100.04	98.83	100.10	99.59	99.72	100.06	99.34	99.60	100.17	99.57	98.78
NK/A (a)	0.89	0.84	0.87	0.91	0.88	0.88	0.82	0.80	0.88	0.82	0.84	0.85	0.89
A/CNK (b)	0.94	1.03	0.97	0.95	0.94	0.95	1.07	1.08	0.96	1.06	1.12	1.04	1.02
Rb/Ba	0.54	0.39	0.50	0.88	0.75	0.60	7.14	6.05	1.92	1.22	4.12	4.24	7.96
Rb/Sr	6.00	4.35	4.92	8.63	7.03	7.33	60.08	44.63	15.44	8.39	>62.20	>62.40	18.58
Ga/Al	3.49	2.80	3.25	3.10	4.07	3.89	3.50	3.15	3.90	2.80	3.46	4.06	3.13
K/Na	2.01	1.99	2.39	2.05	2.04	2.03	1.44	0.96	1.70	1.99	1.18	1.40	1.32
C.I.P.W. norms (c):													
Q	27.23	29.19	29.56	30.25	28.38	28.13	34.05	31.38	34.57	30.96	37.39	31.58	31.20
C	0.00	0.55	0.00	0.00	0.00	0.00	0.91	1.07	0.00	1.02	1.46	0.65	0.28
Or	36.61	35.48	37.51	35.42	36.16	36.46	29.67	24.72	31.25	34.79	26.32	30.62	30.83
Ab	26.08	25.49	22.46	24.80	25.42	25.72	29.52	36.94	26.25	24.99	31.82	31.21	33.32
An	3.95	4.62	4.59	3.13	4.20	4.23	4.40	4.83	4.04	3.84	1.91	3.78	3.27
Ac	0.00	0.00	0.00	0.00	0.00	0.00	0.00	0.00	0.00	0.00	0.00	0.00	0.00
Wo	0.00	0.00	0.00	0.00	0.00	0.00	0.00	0.00	0.00	0.00	0.00	0.00	0.00
Mt	1.03	1.35	1.26	1.08	1.33	0.79	0.25	0.27	0.49	1.17	0.39	0.69	0.21
Il	0.50	0.66	0.58	0.56	0.50	0.48	0.12	0.08	0.25	0.54	0.10	0.15	0.10
Hm	0.00	0.00	0.00	0.00	0.00	0.00	0.87	0.63	0.00	0.00	0.00	0.00	0.72
Ap	0.10	0.17	0.12	0.10	0.07	0.10	0.05	0.05	0.05	0.26	0.05	0.07	0.05
Hy	2.66	2.50	3.20	3.43	1.96	2.50	0.18	0.03	2.07	2.44	0.55	1.24	0.03
Di	1.83	0.00	0.73	1.23	1.96	1.59	0.00	0.00	1.04	0.00	0.00	0.00	0.00
Trace elements in ppm:													
Sc	4.8	4.7	4.7	6.8	5.1	4.8	4.6	3.3	4.7	3.9	2.7
Zn	90	67	92	83	92	80	44	28	56	69	45	60	25
Sn	35	12	57	4
Ga	24	20	22	20	28	27	25	24	25	20	24	29	22
Rb	342	335	369	345	408	403	721	714	417	428	622	624	446
Ba	628	854	740	394	541	669	101	118	217	352	151	147	56
Nb	45	33	36	29	45	42	57	68	42	21	56	49	62
Ce	446	138	314	263	422	289	105	73.2	384	203	85	193	82
Sr	57	77	75	40	58	55	12	16	27	51	<10	<10	24
Hf	16	11	13	12	13	11	6.7	2.6	11	7.8	<0.5
Zr	440	362	461	436	451	362	90	39	248	231	68	123	29
Y	109	85	113	76	164	126	102	59	137	71	162	157	126
Yb	8.5	7.5	7.5	5.6	11.0	9.7	15.0	14.8	12.6	4.9	10.0	18.7	17.3

App. 1, contd.

Suomenniemi complex															
Sample	Alkali-feldspar syenites							Quartz-feldspar porphyries							
	M244.1	M265.1	A1164	M292.6	M730	M737	A1111	M227.2	A21b	O53.1	O62.2	A1100	A1046	O101.2	O119.2
SiO ₂ (wt%)	57.30	60.84	63.10	61.40	64.50	62.70	61.50	68.00	70.90	74.00	72.80	71.00	72.00	75.20	71.80
TiO ₂	1.07	0.72	0.35	0.87	0.33	0.61	0.67	0.43	0.28	0.21	0.25	0.42	0.35	0.14	0.32
Al ₂ O ₃	15.20	17.65	16.20	14.70	16.50	15.50	14.70	12.70	13.30	11.80	12.20	13.00	12.60	12.00	12.80
Fe ₂ O ₃	4.69	3.41	3.17	5.06	3.50	5.05	5.37	4.86	0.70	1.93	1.28	1.64	1.75	0.93	0.80
FeO	4.20	2.58	1.10	3.00	0.70	0.80	0.70	1.30	2.30	0.70	1.20	2.80	1.80	1.00	2.20
MnO	0.13	0.08	0.06	0.12	0.07	0.10	0.08	0.08	0.04	0.02	0.04	0.07	0.05	0.03	0.05
MgO	0.73	0.49	0.31	0.71	0.51	0.53	0.47	0.24	0.32	0.22	0.29	0.21	0.34	0.14	0.29
CaO	3.75	1.98	1.62	2.47	1.52	1.73	1.68	2.00	1.42	1.09	1.22	1.65	0.98	1.00	1.09
Na ₂ O	2.79	6.37	5.25	5.87	7.14	5.85	6.13	2.56	2.74	2.88	3.17	2.78	2.88	2.96	3.00
K ₂ O	6.84	4.95	7.00	5.01	4.52	6.09	6.08	5.90	6.02	5.20	4.82	5.71	5.84	5.27	5.91
P ₂ O ₅	0.28	0.16	0.04	0.13	0.03	0.12	0.17	0.07	0.05	0.03	0.05	0.06	0.06	0.02	0.06
F	0.13	0.07	0.10	0.02	0.04	0.03	0.38	0.38	0.5	0.77	0.3	0.26	0.68	0.28
H ₂ O+	0.60	0.47	0.40	0.60	0.40	0.60	0.30	0.70	0.60	0.70	0.40	0.80	0.70	0.40	0.70
H ₂ O-	0.10	0.10	0.10	0.10	0.10	0.10	0.10	0.10	0.10	0.10	0.10	0.10	0.10	0.10
Total	97.81	99.70	98.77	100.13	99.84	99.82	97.98	99.32	99.15	99.38	98.59	100.54	99.71	99.87	99.40
O = F ₂	0.05	0.03	0.04	0.01	0.02	0.01	0.16	0.16	0.21	0.32	0.13	0.11	0.29	0.12
Total	97.76	98.74	100.09	99.83	99.80	97.97	99.16	98.99	99.17	98.26	100.41	99.60	99.58	99.28
NK/A (a)	0.79	0.90	1.00	1.03	1.01	1.05	1.13	0.83	0.83	0.88	0.86	0.83	0.88	0.88	0.89
A/CNK (b)	0.81	0.91	0.85	0.75	0.85	0.80	0.75	0.89	0.98	0.96	0.96	0.95	0.98	0.97	0.96
Rb/Ba	0.14	0.11	0.19	0.42	0.49	0.20	0.15	1.01	0.20	0.74	4.18	0.27	0.32	3.77	0.31
Rb/Sr	1.02	1.34	1.86	5.05	4.57	2.22	1.94	5.27	1.59	8.63	13.85	3.52	3.56	31.06	2.85
Ga/Al	3.36	2.33	3.08	2.06	2.56	2.57	4.02	3.55	1.76	4.18	3.78	3.60	4.09	3.40
K/Na	2.45	0.78	1.33	0.85	0.63	1.04	0.99	2.30	2.20	1.81	1.52	2.05	2.03	1.78	1.97
C.I.P.W. norms (c):															
Q	7.47	0.76	3.72	4.77	3.52	3.77	2.70	27.40	27.71	35.74	33.74	28.38	30.30	35.79	28.49
C	0.00	0.00	0.00	0.00	0.00	0.00	0.00	0.00	0.00	0.00	0.00	0.00	0.00	0.00	0.00
Or	41.67	29.47	42.12	29.80	26.89	36.32	36.83	35.52	36.27	31.33	29.27	33.96	34.98	31.55	35.52
Ab	24.34	54.31	45.16	48.03	60.11	46.24	42.80	22.07	23.64	24.84	27.56	23.68	24.70	25.38	25.82
An	9.02	4.99	0.00	0.00	0.00	0.00	0.00	5.85	6.33	3.99	4.96	6.17	4.26	3.94	4.07
Ac	0.00	0.00	0.06	1.73	0.63	3.27	9.13	0.00	0.00	0.00	0.00	0.00	0.00	0.00	0.00
Wo	0.00	0.00	2.40	2.20	1.61	1.74	1.70	0.88	0.00	0.00	0.00	0.00	0.00	0.00	0.00
Mt	7.01	4.98	2.78	6.52	1.54	1.15	0.59	3.26	1.03	1.75	1.91	2.39	2.57	1.37	1.18
Il	2.10	1.38	0.68	1.66	0.63	1.17	1.30	0.83	0.54	0.41	0.49	0.80	0.67	0.27	0.62
Hm	0.00	0.00	1.29	0.00	2.25	3.17	1.94	2.70	0.00	0.76	0.00	0.00	0.00	0.00	0.00
Ap	0.68	0.38	0.10	0.31	0.07	0.29	0.41	0.17	0.12	0.07	0.12	0.14	0.14	0.05	0.14
Hy	0.81	0.57	0.00	0.00	0.00	0.00	0.00	0.00	3.90	0.08	1.19	3.01	2.14	0.84	3.27
Di	6.90	3.16	1.70	4.99	2.76	2.87	2.59	1.31	0.45	1.03	0.77	1.46	0.23	0.81	0.89
Trace elements in ppm:															
Sc	22.8	9.5	23.1	11.8	11.1	12.0	8.2	5.2	4.4	6.0	7.8	6.2	4.0	5.8
Zn	169	171	99	207	102	94	114	162	88	54	67	131	102	67	74
Sn	5	2	4	5	4	4	5
Ga	27	20	24	18	21	20	27	25	11	27	26	24	26	23
Rb	237	188	270	288	210	242	227	274	260	328	568	264	274	528	274
Ba	1700	1710	1420	683	427	1230	1500	270	1310	441	136	981	844	140	898
Nb	48	45	33	103	34	37	37	42	35	48	48	58	54	26	39
Ce	288	301	288	296	204	195	140	381	323	212	263	264	272	359	267
Sr	232	140	145	57	46	109	117	52	164	38	41	75	77	17	96
Hf	23	30	21	25	16	19	21	12	11	10	16	12	9.8	13
Zr	521	867	443	802	454	433	553	773	427	305	190	654	481	194	438
Y	116	88	105	151	89	77	66	109	78	111	141	100	85	145	90
Yb	8.7	12.3	10.9	10.2	5.8	5.2	7.6	6.1	9.2	13.6	8.6	7.0	12.4	6.7

App. I, contd.

Sample	Wiborg batholith					SW Finland						Soviet Karelia		
	A1163	A18	A29b	A524b	1/IH/89	A606	A690	A710	A295	A762	A373	6896	9202	IYL/79
SiO ₂ (wt%)	72.20	63.00	65.80	75.08	73.10	65.87	71.60	73.10	72.00	69.70	71.10	75.30	74.10	74.50
TiO ₂	0.44	1.07	0.88	0.09	0.03	0.79	0.34	0.25	0.39	0.46	0.21	0.09	0.24	0.16
Al ₂ O ₃	11.50	13.60	12.80	11.52	15.00	13.61	14.42	12.90	12.60	13.30	13.90	12.40	12.40	12.70
Fe ₂ O ₃	1.35	1.91	1.17	0.68	0.27	1.68	0.87	0.42	1.61	1.23	1.06	0.44	0.21	0.44
FeO	3.30	6.20	5.80	1.32	0.86	5.49	1.94	1.80	2.00	2.80	1.30	0.90	1.70	1.30
MnO	0.08	0.11	0.11	0.03	0.04	0.08	0.04	0.04	0.05	0.07	0.03	0.02	0.04	0.04
MgO	0.28	0.81	0.61	0.04	0.13	0.75	0.43	0.31	0.52	0.61	0.27	0.07	0.23	0.13
CaO	1.79	3.60	2.54	1.17	0.77	1.98	1.18	0.93	0.85	1.53	0.90	0.71	0.64	0.77
Na ₂ O	2.33	2.81	2.84	2.81	3.88	2.43	2.85	2.99	3.40	3.43	2.35	4.18	3.45	3.04
K ₂ O	5.05	4.80	5.42	5.66	4.58	4.97	5.73	5.77	5.35	5.27	6.99	4.75	5.08	5.95
P ₂ O ₅	0.07	0.34	0.23	0.02	0.03	0.30	0.09	0.08	0.07	0.11	0.05	0.01	0.03	0.02
F	0.33	0.17	0.18	0.77	1.53	0.25	0.36	0.5	0.15	0.13	0.37	0.41	0.093	0.35
H ₂ O+	0.60	0.50	0.60	0.60	0.30	1.26	0.54	0.50	0.80	0.80	0.50	0.40	0.60	0.50
H ₂ O-	0.10	0.10	0.10	0.14	0.10	0.10	0.03	0.10	0.20	0.20	0.20	0.10	0.10	0.10
Total	99.42	99.02	99.08	99.93	100.62	99.56	100.42	99.69	99.99	99.64	99.23	99.78	98.91	100.00
O=F ₂	0.14	0.07	0.08	0.32	0.64	0.11	0.15	0.21	0.06	0.05	0.16	0.17	0.04	0.15
Total	99.28	98.95	99.01	99.61	99.98	99.45	100.27	99.48	99.92	99.58	99.07	99.61	98.87	99.85
NK/A (a)	0.81	0.72	0.82	0.93	0.76	0.69	0.76	0.87	0.90	0.85	0.82	0.97	0.90	0.90
A _j /CNK (b)	0.92	0.83	0.84	0.89	1.18	1.05	1.11	1.00	0.97	0.94	1.06	0.93	1.01	0.99
Rb/Ba	0.12	0.10	0.19	2.75	>97.4	0.13	0.90	0.78	0.17	0.14	0.38	10.93	0.23	0.26
Rb/Sr	1.02	0.65	1.63	>13.75	46.38	0.86	5.28	3.46	1.71	1.18	3.69	>43.7	2.50	4.86
Ga/Al	3.61	3.89	3.54	10.01	7.05	2.93	3.30	3.41	2.99	5.79	3.81	4.76
K/Na	2.17	1.71	1.91	2.01	1.18	2.05	2.01	1.93	1.57	1.54	2.97	1.14	1.47	1.96
C.I.P.W. norms (c):														
Q	34.35	18.03	20.43	35.09	31.03	25.29	29.26	30.64	28.97	24.82	28.46	31.56	32.38	31.78
C	0.00	0.00	0.00	0.00	2.36	1.38	1.61	0.24	0.00	0.00	0.97	0.00	0.14	0.00
Or	30.33	28.86	32.61	33.98	27.42	29.98	34.03	34.58	31.98	31.61	42.08	28.39	30.59	35.50
Ab	20.04	24.19	24.47	24.16	33.26	20.99	24.24	25.66	29.10	29.46	20.26	35.77	29.75	25.97
An	6.10	10.50	6.28	2.14	3.67	8.03	5.29	4.15	3.36	5.41	4.22	1.06	3.04	3.47
Ac	0.00	0.00	0.00	0.00	0.00	0.00	0.00	0.00	0.00	0.00	0.00	0.00	0.00	0.00
Wo	0.00	0.00	0.00	0.00	0.00	0.00	0.00	0.00	0.00	0.00	0.00	0.00	0.00	0.00
Mt	1.99	2.82	1.73	1.00	0.40	2.49	1.27	0.62	2.36	1.81	1.57	0.65	0.31	0.64
Il	0.85	2.07	1.70	0.17	0.05	1.53	0.65	0.48	0.75	0.89	0.41	0.17	0.46	0.31
Hm	0.00	0.00	0.00	0.00	0.00	0.00	0.00	0.00	0.00	0.00	0.00	0.00	0.00	0.00
Ap	0.17	0.82	0.55	0.05	0.07	0.73	0.21	0.19	0.17	0.26	0.12	0.02	0.07	0.05
Hy	4.03	8.03	7.86	0.21	1.73	9.60	3.44	3.44	2.94	4.41	1.93	0.25	3.26	2.06
Di	2.14	4.68	4.36	3.21	0.00	0.00	0.00	0.00	0.37	1.33	0.00	2.13	0.00	0.22
Trace elements in ppm:														
Sc	8.8	16.9	14.4	5.3	6.3	7.8	0.8	4.8
Zn	124	138	128	69	34	81	79	64	47	105	82
Sn	27	36	<2	28
Ga	22	28	24	61	56	20	22	24	22	38	25	32
Rb	186	146	218	550	974	183	402	370	191	187	328	437	190	214
Ba	1490	1410	1130	200	<10	1434	448	475	1140	1360	870	40	819	829
Nb	54	40	53	100	77	29	29	32	26	86	33	90
Ce	272	191	248	146	266	196	182	239	119	261	296
Sr	182	223	134	<40	21	212	76	107	112	158	89	<10	76	44
Hf	18	18	15	6.8	13	12	12	9.5
Zr	821	703	637	190	37	607	229	226	480	436	214	175	342	227
Y	84	75	87	118	80	78	64	94	138	131	110
Yb	5.4	5.6	7.6	27.6	6.7	6.8	6.2	6.0	13.9	6.5	10.6

App. 1, contd.

Note: The samples were analysed at X-Ray Assay Laboratories Ltd (Canada), except M265.1 that was analysed at the Geological Survey of Finland (GSF). In addition, three previously published analyses are listed: the composition used for sample A524b is from Haapala (1988), that of A606 from Haapala (1977a), and that of A690 from Vormaa (1976). Most of the analysed samples were milled in chrome steel mill. Those agate-milled are A1097, M114.2, M244.1, A1164, A1045, A1042, M553.1, M664.1b, M730, M737, A1111, A1130, M815.1, and O62.2; those milled in an iron pan at GSF are 6896, 9202, IYL/79, A18, A29b, 1/IH/89, A295, A373, A690, A710, A762, M415.4, and M664.2. Major components by XRF, ferrous iron by potassium dichromate titration, fluorine by ion specific electrode, H₂O+ by mixing the sample with PbO and heating the mixture at 110°C for three hours, H₂O- by heating at 110°C for one hour (except sample M265.1 for which the total water content was determined by Leco water analyzer at GSF). Ferrous iron was not measured for samples 1/IH/89 and IYL/79; their Fe³⁺/Fe²⁺ ratios were estimated by the method of Sack et al. (1980) assuming 750 °C and QFM. Analytical methods for the trace elements were:

XRF: Zn; Sn; Rb; Ba; Nb; Sr (except M9.1); Zr (except M214.3); Y

NA: Sc; Ce for M244.1, M265.1, A1045, M730, M737, and M815.1; Hf; Yb (except A18, A1130, A1043, A1041, A1097, A1111, A1064, and A1100)

ICP: Ga (except IYL/79, 1/IH/89, A373, L871.1, A1097, M244.1, A1164, M292.6, A1045, M415.4, A1042, M480.1, M553.1, M664.1b, M664.2, M730, M737, A1111, A1130, M815.1, O202.1, O242.1, O62.2, O78.3, and A1100); Sr for M9.1; Zr for 214.3

ICP/MS: Ga for IYL/79, 1/IH/89, A373, L871.1, A1097, M244.1, A1164, M292.6, A1045, M415.4, A1042, M480.1, M553.1, M664.1b, M664.2, M730, M737, A1111, A1130, M815.1, O202.1, O242.1, O62.2, O78.3, and A1100; Ce (except M244.1, A265.1, A1045, M730, M737, and M815.1); Yb for A18, A1130, A1043, A1041, A1097, A1111, A1164, and A1100

(a) molecular (Na₂O+K₂O)/Al₂O₃ ratio

(b) molecular Al₂O₃/(CaO+Na₂O+K₂O) ratio

(c) weight norms calculated fluorine free

Locations of the samples taken from the Suomenniemi complex (see also the appended map):

Sample	Map	Northing	Easting	Sample	Map	Northing	Easting
M415.2	313205B	6788.49	3513.82	M326.1	313209B	6796.37	3521.64
M415.4	313205B	6788.49	3513.81	M589.2	313203D	6795.20	3507.58
A1130	313209D	6799.26	3528.37	M644.1	313206B	6796.90	3513.68
L868.3B	313209B	6798.88	3522.34	O101.1	313209D	6796.01	3528.81
M319.2	313209	6795.00	3525.59	O195.1	314107C	6802.80	3528.52
A1044	313209A	6791.44	3523.57	O247.1	313209D	6797.14	3525.61
M1.1	313208D	6787.49	3525.18	M9.1	314107A	6801.58	3521.72
M1.2	313208D	6787.50	3525.33	A1097	314107A	6801.54	3521.84
A1043	313208D	6788.76	3528.02	M150.1	314104A	6800.16	3514.65
M195.2	313208B	6786.85	3523.68	M577.1	313203A	6794.44	3503.30
A1045	313205B	6788.64	3513.94	M664.1b	313206D	6799.46	3517.20
O202.1	313209C	6793.32	3529.85	M664.2	313206D	6799.43	3517.25
O211.2	313209C	6793.39	3527.46	M815.1	314107A	6803.58	3523.30
O256.1	313209D	6795.76	3525.45	M244.1	313209C	6791.04	3527.59
O263.1	313209D	6799.30	3526.77	M265.1	313209A	6793.46	3524.77
M214.3	313209A	6794.12	3522.73	A1164	313209D	6795.38	3525.19
M291.1	313209D	6795.35	3525.62	M292.6	313209D	6795.22	3525.83
M480.1	313205D	6787.58	3517.37	M730	313209D	6795.92	3528.58
O63.1	313203A	6793.89	3504.62	M737	313209D	6796.48	3528.55
O78.3	313206B	6799.36	3510.35	A1111	313209D	6796.47	3527.83
A1040	313209B	6797.71	3521.92	M227.2	313209C	6791.98	3527.33
A1042	314104C	6803.94	3519.30	A21b	314104A	6804.19	3512.01
M114.2	314104C	6800.41	3515.02	O53.1	314104A	6802.19	3511.20
M452.2	313205B	6786.04	3514.32	O62.1,2	313203A	6794.56	3503.86
M553.1	313202D	6787.61	3506.26	A1100	313209C	6791.32	3527.96
A1041	314107C	6801.70	3529.38	A1046	313209D	6796.81	3528.97
O209.2	313209C	6793.68	3528.09	O101.2	313209D	6796.00	3528.64
O242.1	314107A	6804.88	3523.18	O119.2	313211D	6789.88	3535.68
L871.1	313209B	6798.66	3522.82	A1163	314101C	6800.04	3507.53

Appendix 2. Chemical composition of the basic rocks.

Sample	Diabase dykes											
	Suomenniemi swarm											
	4.1	9.1	A1063	30.1	35.1	A1064	A1047	A1068	123.3	128.2	133.2	136.2
SiO ₂ (wt%)	49.70	48.00	47.80	47.40	53.20	48.70	52.70	51.70	47.80	47.50	47.85	46.85
TiO ₂	2.39	2.97	2.29	2.89	2.18	2.17	3.17	3.07	2.21	2.42	1.83	2.40
Al ₂ O ₃	14.30	13.90	17.10	13.80	15.00	18.40	13.70	13.20	15.70	15.40	15.72	16.24
Fe ₂ O ₃	2.40	2.63	2.60	2.85	3.60	1.30	7.20	3.40	1.71	2.36	6.13	3.68
FeO	11.70	12.30	10.40	12.10	8.40	9.90	7.10	11.10	11.60	12.00	6.80	10.40
MnO	0.21	0.21	0.17	0.20	0.17	0.15	0.14	0.18	0.19	0.20	0.19	0.21
MgO	4.52	4.70	4.12	4.66	3.57	4.09	2.26	3.15	5.59	5.44	5.58	5.32
CaO	7.71	7.35	8.47	7.67	6.79	8.77	5.97	6.51	8.16	8.32	8.36	7.84
Na ₂ O	2.76	2.48	2.88	2.43	2.71	2.90	2.24	2.55	2.51	2.49	2.36	2.69
K ₂ O	1.73	1.50	1.34	1.59	2.22	1.19	2.49	2.07	1.04	1.33	1.68	1.27
P ₂ O ₅	0.55	0.72	0.49	0.66	0.89	0.43	1.19	1.31	0.48	0.51	0.47	0.68
L.O.I.	0.31	1.54	0.31	0.31	1.23	0.47
Total	98.28	98.30	97.97	96.56	98.73	98.00	98.16	98.24	98.22	98.44	96.97	97.58
An/(An+Ab) (a)	47.96	51.60	54.99	51.75	49.20	57.84	51.32	46.09	57.30	56.09	57.79	55.58
Hy/(Hy+Di) (b)	66.56	75.43	65.65	70.30	80.63	75.08	92.33	82.46	76.85	67.35	66.42	77.76
Mg number (c)	40.62	40.19	40.41	39.99	39.14	43.66	25.87	31.81	47.16	44.68	48.72	44.86
C.I.P.W. norms (d):												
Q	0.81	1.75	0.00	0.71	6.86	0.00	11.47	8.26	0.00	0.00	0.00	0.00
C	0.00	0.00	0.00	0.00	0.00	0.00	0.00	0.00	0.00	0.00	0.00	0.00
Or	10.43	9.16	8.11	9.76	13.30	7.17	15.06	12.45	6.33	8.02	10.28	7.70
Ab	23.83	21.68	24.96	21.36	23.25	25.02	19.39	21.98	21.88	21.50	20.67	23.35
An	21.96	23.11	30.49	22.91	22.52	34.33	20.44	18.79	29.36	27.46	28.30	29.22
Mt	3.42	3.67	3.15	3.69	2.85	2.73	3.35	3.48	3.27	3.49	3.08	3.41
Il	4.63	5.83	4.45	5.70	4.20	4.20	6.16	5.94	4.32	4.69	3.60	4.68
Ap	1.33	1.76	1.19	1.62	2.14	1.04	2.88	3.16	1.17	1.23	1.15	1.65
Hy	22.35	24.93	14.83	24.07	20.06	17.96	19.61	21.39	25.10	19.33	18.79	17.80
OI	0.00	0.00	5.06	0.00	0.00	1.58	0.00	0.00	1.00	4.91	4.62	7.11
Di	11.23	8.12	7.76	10.17	4.82	5.96	1.63	4.55	7.56	9.37	9.50	5.09
Parameters for the 1 atm tholeiite system (e):												
Q	8.18	10.26	4.59	8.72	15.48	5.50	22.51	18.21	7.73	6.09	6.02	5.61
Plag	62.20	62.71	69.94	61.22	69.88	74.01	70.86	66.48	65.41	63.14	63.64	67.45
Cpx	15.25	11.37	9.78	14.06	7.35	7.44	2.90	7.42	9.66	12.08	12.34	6.53
OI	22.56	25.91	20.28	24.73	22.77	18.55	26.24	26.10	24.93	24.78	24.02	26.02
Trace elements in ppm:												
Sc	41.2	42.9	24.0	38.9	35.6	23.6	34.4	33.9	29.1	28.7	37.1	36.5
Ni	21	36	26	37	21	27	17	28	37	35	49	40
Co	43	42	45	45	28	46	24	27	50	55	44	44
Cr	42	52	28	56	33	26	28	14	85	53	55	46
Pb	6.86	20.42	7.57	15.56	11.42
Rb	52	33	36	48	75	38	91	74	42	40	47	47
Ba	541	693	478	561	930	430	1120	770	451	558	350	470
Th	3.7	4.4	2.8	3.8	5.5	2.7	6.3	5.9	2.3	3.7	3.1	2.4
U	0.9	1.2	0.65	0.8	1.61	1.00	1.87	1.51	0.7	0.7	0.6	0.8
Nb	24	23	18	20	24	17	29	31	17	20	17	19
La	56.6	61.4	29.6	50.3	79.0	32.2	67.2	54.9	29.6	29.6	35.3	38.9
Ce	118	112	58	94	135	69	130	119	62	58	71	72
Sr	309	319	375	308	443	367	285	282	311	294	322	297
Nd	43	45	34.56	43	69.09	34.75	70.55	66.29	63	28	53	61
Hf	12.0	13.0	6.4	8.7	10.0	5.7	13.0	14.0	4.7	6.7	6.6	5.6
Zr	238	260	176	275	325	170	415	463	179	186	244	221
Sm	12.0	11.0	7.49	9.2	12.68	7.57	13.77	13.38	6.5	6.1	8.0	8.4
Y	53	58	43	51	54	46	57	57	54	48	44	46
Yb	4.4	4.7	3.1	4.4	4.7	4.2	4.9	5.5	3.2	3.2	4.0	3.7

App. 2, contd.

Sample	Diabase dykes											
	Suomenniemi swarm											
	138.2	140.2	141.1	A1101	145.1	164.1	164.2	A1102	A1118	173.3	175.9	176.1
SiO ₂ (wt%)	52.20	47.50	49.60	48.00	47.50	46.60	45.90	47.00	46.70	53.60	52.10	51.90
TiO ₂	2.06	2.49	2.37	1.97	2.23	2.83	2.78	2.99	2.98	2.26	2.45	3.14
Al ₂ O ₃	17.50	15.70	14.40	18.50	16.80	14.80	15.20	15.40	14.70	14.00	13.80	13.00
Fe ₂ O ₃	2.23	2.62	3.86	2.50	2.61	3.39	4.15	4.60	6.70	2.00	3.40	3.08
FeO	8.70	11.50	10.20	9.10	10.70	11.80	12.10	11.00	10.00	9.90	9.90	11.00
MnO	0.14	0.19	0.20	0.16	0.19	0.22	0.21	0.20	0.19	0.18	0.19	0.20
MgO	2.87	4.98	4.64	4.20	4.72	3.90	5.29	3.45	4.72	3.57	3.89	3.20
CaO	7.10	8.02	7.34	8.56	7.98	7.13	7.00	6.84	6.72	6.81	7.19	6.03
Na ₂ O	2.89	2.53	2.55	2.92	2.69	2.94	2.74	2.89	2.76	2.60	2.52	2.30
K ₂ O	1.97	1.63	1.68	1.35	1.41	1.52	1.44	1.87	1.27	1.53	1.75	2.28
P ₂ O ₅	0.49	0.53	0.54	0.41	0.47	0.60	0.54	0.66	0.61	0.64	0.70	0.95
L.O.I.	0.70	0.54	0.88	1.31	0.85	0.62	0.93	1.00	1.47	1.54	0.62	1.08
Total	98.85	98.23	98.26	98.98	98.15	96.35	98.28	97.90	98.82	98.63	98.51	98.16
An/(An + Ab) (a)	54.22	55.48	51.48	57.46	56.53	47.71	51.81	49.03	50.66	50.01	49.83	48.62
Hy/(Hy + Di) (b)	87.43	68.58	73.58	69.95	74.86	69.67	72.35	77.47	83.90	74.83	70.87	82.07
Mg number (c)	35.98	42.98	41.57	43.70	43.14	35.52	41.20	32.34	38.18	39.03	38.64	32.77
C.I.P.W. norms (d):												
Q	4.99	0.00	2.19	0.00	0.00	0.00	0.00	0.00	0.00	10.43	7.10	9.49
C	0.00	0.00	0.00	0.00	0.00	0.00	0.00	0.00	0.00	0.00	0.00	0.00
Or	11.86	9.86	10.21	8.17	8.56	9.39	8.75	11.42	7.74	9.31	10.57	13.88
Ab	24.92	21.91	22.18	25.31	23.40	26.00	23.84	25.28	24.08	22.65	21.80	20.05
An	29.51	27.30	23.53	34.19	30.43	23.72	25.63	24.32	24.72	22.66	21.65	18.97
Mt	2.63	3.43	3.40	2.81	3.25	3.76	3.94	3.78	3.99	2.91	3.20	3.44
Il	3.99	4.84	4.63	3.83	4.35	5.62	5.43	5.87	5.84	4.42	4.76	6.14
Ap	1.18	1.29	1.32	1.00	1.14	1.49	1.32	1.62	1.49	1.56	1.70	2.32
Hy	18.29	18.01	23.95	12.73	17.66	17.71	14.13	18.33	24.28	19.50	20.70	21.10
Ol	0.00	5.12	0.00	6.50	5.27	4.61	11.56	4.05	3.20	0.00	0.00	0.00
Di	2.63	8.25	8.60	5.47	5.93	7.71	5.40	5.33	4.66	6.56	8.51	4.61
Parameters for the 1 atm tholeiite system (e):												
Q	12.00	5.79	10.39	3.92	5.53	5.64	4.52	5.97	7.67	18.86	15.55	19.97
Plag	76.99	64.82	63.41	73.55	68.90	66.07	64.32	68.23	65.30	68.28	64.50	65.70
Cpx	3.72	10.86	11.93	6.76	7.60	10.25	7.02	7.34	6.24	9.88	12.64	7.76
Ol	19.29	24.32	24.66	19.69	23.51	23.68	28.66	24.43	28.47	21.85	22.86	26.54
Trace elements in ppm:												
Sc	17.4	26.7	27.9	18.8	22.9	36.5	26.6	24.2	24.4	28.6	26.1	27.0
Ni	20	32	24	25	36	34	44	22	36	18	18	17
Co	36	52	51	45	47	45	62	49	66	36	36	40
Cr	33	47	38	24	35	38	50	13	38	43	47	24
Pb	7.73	13.09	6.64
Rb	75	50	62	39	58	59	36	48	41	45	54	60
Ba	601	497	572	462	489	506	572	743	574	898	931	773
Th	5.6	3.5	5.1	1.9	3.3	2.8	4.6	5.5	3.9	9.3	6.1	8.4
U	3.0	0.7	0.9	0.56	0.9	1.1	0.9	1.38	2.71	2.5	1.4	1.4
Nb	19	19	22	16	19	19	20	24	22	22	22	30
La	30.6	31.6	28.1	27.2	53.5	32.3	41.5	36.5	64.1	56.8
Ce	58	65	62	57	104	67	89	71	123	110
Sr	373	345	337	422	349	333	355	346	300	483	507	277
Nd	36	59	77	30	68	36	54	54.19	39.82	64
Hf	5.1	5.2	7.9	4.0	4.0	7.6	6.3	7.9	8.7	6.2	8.4	11.0
Zr	179	193	238	146	166	300	210	280	246	286	284	392
Sm	5.6	7.0	6.5	11.4	6.7	11.6	8.5	8.2	9.9	10.8
Y	37	54	58	36	46	53	61	70	60	61	74	74
Yb	2.4	3.5	3.3	2.7	4.6	3.5	5.1	3.9	4.1	4.6

App. 2, contd.

Sample	Diabase dykes						Häme swarm		Lovasjärvi intrusion	
	Suomenniemi swarm						A808a	A1135	A1069	A1129
	177.2	178.7	A1098	180.2	182.1	239.1				
SiO ₂ (wt%)	49.50	51.50	47.70	48.20	48.10	47.90	46.90	48.40	44.20	37.00
TiO ₂	2.42	3.14	3.10	2.33	2.86	2.09	2.36	2.22	4.67	3.00
Al ₂ O ₃	14.60	13.20	14.30	14.60	14.40	17.70	14.80	18.30	14.70	5.23
Fe ₂ O ₃	3.11	2.84	3.30	4.03	2.86	1.95	2.30	3.30	4.30	3.54
FeO	10.70	11.30	11.70	9.60	11.10	10.30	13.10	8.10	12.90	27.50
MnO	0.19	0.21	0.22	0.20	0.19	0.17	0.20	0.15	0.20	0.35
MgO	4.59	3.42	5.06	4.60	4.12	4.42	7.17	4.14	3.83	17.10
CaO	7.75	6.32	6.40	7.33	7.46	8.37	7.05	8.67	8.48	2.40
Na ₂ O	2.51	2.38	2.36	2.55	2.55	2.79	2.63	3.25	2.69	0.96
K ₂ O	1.58	1.84	1.31	1.60	1.78	1.21	1.32	1.56	1.25	0.50
P ₂ O ₅	0.54	0.94	0.74	0.48	0.71	0.43	0.47	0.52	1.07	0.19
L.O.I.	0.77	1.23	2.23	1.54	1.39	1.08	-0.61	-0.46	0.31	-2.69
Total	98.26	98.32	98.42	97.06	97.52	98.41	97.69	98.15	98.60	95.08
An/(An+Ab) (a)	52.95	49.71	55.15	52.31	51.14	57.69	52.58	52.78	51.68	51.09
Hy/(Hy+Di) (b)	70.85	82.56	93.37	74.04	72.16	76.33	72.25	43.44	57.96	87.77
Mg number (c)	41.63	34.11	41.97	42.17	38.72	43.46	49.78	43.96	32.39	53.89
C.I.P.W. norms (d):										
Q	2.28	9.25	3.06	1.17	1.63	0.00	0.00	0.00	0.00	0.00
C	0.00	0.00	0.00	0.00	0.00	0.00	0.00	0.00	0.00	0.00
Or	9.58	11.20	8.05	9.91	10.94	7.34	7.93	9.36	7.52	3.02
Ab	21.80	20.74	20.77	22.62	22.45	24.25	22.63	27.92	23.18	8.29
An	24.53	20.50	25.54	24.81	23.50	33.07	25.09	31.21	24.79	8.66
Mt	3.35	3.45	3.69	3.36	3.44	2.99	3.73	2.72	4.13	7.58
Il	4.72	6.14	6.12	4.64	5.65	4.08	4.56	4.28	9.03	5.82
Ap	1.31	2.29	1.82	1.19	1.75	1.05	1.13	1.25	2.58	0.46
Hy	22.97	21.82	28.89	23.90	22.11	17.99	15.83	5.76	12.70	13.21
Ol	0.00	0.00	0.00	0.00	0.00	3.66	13.02	10.00	6.85	51.12
Di	9.45	4.61	2.05	8.38	8.53	5.58	6.08	7.50	9.21	1.84
Parameters for the 1 atm tholeiite system (e):										
Q	10.13	19.22	13.13	9.08	9.34	5.51	5.04	1.82	4.20	4.21
Plag	63.62	66.37	66.38	64.50	64.80	71.75	60.81	73.09	65.26	21.29
Cpx	12.98	7.42	2.93	11.39	12.03	6.99	7.75	9.27	12.53	2.31
Ol	23.40	26.21	30.69	24.11	23.17	21.26	31.45	17.63	22.21	76.40
Trace elements in ppm:										
Sc	33.3	6.8	35.5	34.2	38.0	25.3	23.8	39.3	17.7
Ni	26	19	34	35	28	31	82	32	22	395
Co	49	40	51	46	46	45	68	41	51	190
Cr	42	28	55	38	48	32	69	37	4	1190
Pb	10.56	6.24	5.93	7.98	2.2
Rb	43	64	43	55	58	33	37	37	36	29
Ba	584	811	809	481	628	441	452	558	55	231
Th	3.8	8.3	5.7	3.0	4.9	2.5	4	1
U	0.9	1.9	1.01	0.7	1.4	0.5	0.62	0.59	0.85	0.36
Nb	21	33	22	20	22	16	23	29	41	39
La	38.2	46.3	41.9	50.7	40.1	10.9
Ce	96	96	82	74	71.3	74.6	88.1	22.9
Sr	310	297	308	309	358	393	339	511	19	98
Nd	43	49.93	62	33	31.39	34.31	46.75	11.15
Hf	5.4	1.7	6.8	7.9	6.8	4.4	4.9	6.0	3.0
Zr	233	393	276	256	253	157	197	202	20	86
Sm	10.44	8.1	6.53	6.88	9.96	2.28
Y	56	81	67	40	58	41	26	25	48	12
Yb	4.5	4.8	3.9	5.1	2.9	2.5	3.5	0.9

App. 2, contd.

Gabbroic and anorthositic rocks

Sample	Väärälampi body		Ahvenisto complex			Ylijärvi	SW Finland	
	A1048	A1048b	A1110	A118	MH87a	A119	A691b	7890
SiO ₂ (wt%)	50.70	50.60	48.70	53.40	53.60	53.00	52.50	50.70
TiO ₂	1.05	1.51	0.79	1.01	0.30	0.91	2.42	1.23
Al ₂ O ₃	21.70	17.80	22.50	22.10	25.50	24.10	17.30	20.80
Fe ₂ O ₃	2.32	1.29	1.77	1.54	0.59	1.34	0.91	2.51
FeO	4.50	8.20	6.70	4.20	2.60	3.40	9.80	5.60
MnO	0.13	0.13	0.11	0.09	0.05	0.07	0.14	0.12
MgO	2.95	3.70	4.75	1.92	1.71	1.42	2.20	3.01
CaO	7.25	7.73	9.81	9.47	9.88	9.83	7.22	10.10
Na ₂ O	3.26	2.87	3.25	3.68	4.08	4.31	3.08	3.20
K ₂ O	1.89	1.74	0.68	1.48	1.01	1.25	1.68	0.58
P ₂ O ₅	0.22	0.32	0.15	0.46	0.06	0.20	0.62	0.22
L.O.I.	2.08	0.77	0.08	0.23	0.47	0.08	0.85	1.16
Total	98.05	96.66	99.29	99.58	99.85	99.91	98.72	99.23
An/(An+Ab) (a)	55.59	55.71	61.96	55.86	58.31	53.95	52.16	60.03
Hy/(Hy+Di) (b)	100.00	79.03	59.66	70.98	96.71	47.49	84.43	67.04
Mg number (c)	48.43	45.33	54.56	41.88	53.39	39.26	30.29	44.56
C.I.P.W. norms (d):								
Q	1.68	2.37	0.00	2.54	0.69	0.00	6.84	1.86
C	1.71	0.00	0.00	0.00	0.00	0.00	0.00	0.00
Or	11.65	10.72	4.05	8.81	6.01	7.40	10.13	3.50
Ab	28.77	25.31	27.73	31.35	34.74	36.54	26.60	27.64
An	36.02	31.84	45.17	39.68	48.59	42.81	29.00	41.52
Mt	1.66	2.36	2.02	1.36	0.76	1.12	2.62	1.94
Il	2.08	2.99	1.51	1.93	0.57	1.73	4.69	2.38
Ap	0.54	0.79	0.36	1.10	0.14	0.47	1.50	0.53
Hy	15.89	18.66	3.55	9.39	8.22	3.60	15.72	13.83
Ol	0.00	0.00	13.21	0.00	0.00	2.34	0.00	0.00
Di	0.00	4.95	2.40	3.84	0.28	3.98	2.90	6.80
Trace elements in ppm:								
Sc	16.3	24.6	8.5	14.1	11.0	25.5	21.0
Ni	32	56	46	17	7	12	7	40
Co	24	33	40	17	13	24	28
Cr	36	39	41	7	37	23	19	49
Pb	14.13	13.01	2.41	7.15	2.79	5.72	10.46	3.58
Rb	116	87	11	37	25	26	45	19
Ba	413	478	252	546	400	355	518	331
Th	3.0	3.2	3.0	2.0
U	0.66	0.93	0.13	0.71	0.081	0.40	0.66	0.29
Nb	11	15	17	19	8	6	36	11
La	16.0	24.0	9.2	32.0	15.5	37.4	14.4
Ce	33.8	50.9	18.4	66.5	10.5	32.4	77.0	30.1
Sr	494	414	699	714	976	642	360	489
Nd	18.35	27.8	9.53	32.89	4.92	16.57	42.23	17.05
Hf	2.2	5.2	3.0	5.6	3.0	7.7	2.5
Zr	117	179	39	218	62	36	281	87
Sm	3.83	5.79	1.91	6.37	0.83	3.22	8.77	3.96
Y	23	32	5	19	5	15	34	23
Yb	1.8	2.6	0.8	2.0	1.4	3.8	1.8

App. 2, contd.

Note: The samples were analysed at X-Ray Assay Laboratories Ltd (Canada), except samples 35.1, A1064, A1047, A1068, 133.2, and 0136.2 which were analysed for major components and Ba at Rautaruukki Oy (Finland). Most of the analysed samples were agate-milled; those milled in an iron pan at GSF are A808a, A1135, A1129, A1069, A118, A119, A691b, A1110, MH87a, and 7890. Major components by XRF (L.O.I. = loss of ignition, one hour at 950 °C), ferrous iron by potassium dichromate titration. Analytical methods for the trace elements were:

XRF: Ni (except MH87a); Cr; Rb; Ba; Th for MH87a; Nb (except A119); Sr; Zr; Y (except A1110)

NA: Sc; Co; Th (except A118, 7890, and MH87a); La & Yb (except A1068, A1069, A1129, A1048, A1048b, A118, A119, A691b, A1110, and 7890); Ce (except A1068, A1069, A1129, A1048, A1048b, A118, A119, A691b, A1110, 7890, and MH87a); Nd & Sm (except the ID samples); Hf

ICP: Y for A1110

ICP/MS: Th for A118 and 7890; La for A1068, A1069, A1129, A1048, A1048b, A118, A119, A691b, A1110, and 7890; Ce for A1068, A1069, A1129, A1048, A1048b, A118, A119, A691b, A1110, 7890, and MH87a

ID: U, Pb, Nd, and Sm for A1063, 35.1, A1064, A1047, A1068, A1101, A1102, A1118, A1098, A808a, A1135, A1069, A1129, A1048, A1048b, A118, A119, A691b, A1110, MH87a, and 7890

DCP: Ni for MH87a

DNC: U (except the ID samples)

Analyses A1063, 35.1, A1064, A1047, A1068, A1101, A1102, A1118, A1098, A808a, A1135, A1069, and A1129 have been previously published by Rämö (1990).

(a) $100 \cdot \text{normative An} / (\text{An} + \text{Ab})$

(b) $100 \cdot \text{normative Hy} / (\text{Hy} + \text{Di})$

(c) molecular $100 \cdot \text{Mg} / (\text{Mg} + 0.85 \cdot \text{Fe}_{\text{tot}})$

(d) weight norms calculated with $\text{Fe}^{2+} = 0.85 \cdot \text{Fe}_{\text{tot}}$

(e) see Cox et al. (1979)

Locations of the samples taken from the Suomenniemi complex (see also the appended map):

Sample	Map	Northing	Easting	Sample	Map	Northing	Easting
4.1	314107B	6807.28	3522.48	164.1	314101D	6805.69	3508.19
9.1	314107B	6807.71	3521.66	164.2	314101D	6805.69	3508.19
A1063	314107B	6808.84	3520.20	A1102	314101C	6802.71	3506.94
30.1	314107B	6809.10	3520.65	A1118	314104A	6803.64	3510.17
35.1	314104D	6805.46	3518.44	173.3	314105A	6813.43	3512.45
A1064	313211D	6789.32	3537.48	175.9	314105A	6812.24	3513.37
A1047	313209D	6796.81	3528.97	176.1	314105A	6813.28	3512.34
A1068	313211D	6789.99	3535.58	177.2	314105A	6815.00	3513.74
123.3	313212C	6790.34	3535.01	178.7	314105B	6817.08	3514.23
128.2	313212C	6791.77	3535.45	A1098	314105B	6817.05	3514.23
133.2	313212C	6792.02	3536.17	180.2	314105C	6813.87	3515.67
136.2	313212B	6798.04	3531.43	182.1	314105C	6813.22	3517.90
138.2	313212C	6793.42	3535.68	239.1	314107B	6807.07	3522.32
140.2	313212B	6795.20	3534.22	A1069	313202C	6783.80	3507.64
141.1	313212B	6796.10	3534.16	A1129	313202C	6784.92	3505.93
A1101	313212B	6795.76	3533.77	A1048	313206B	6799.37	3510.38
145.1	313209D	6796.46	3529.86	A1048b	313206B	6799.46	3510.44

Appendix 3. Crystal/liquid partition coefficients used in modeling partial melting and fractional crystallization.**Partial melting of rapakivi granite protolith and fractional crystallization of rapakivi granite magma**

	Hornblende	Biotite	Plagioclase	Alkali-feldspar	Orthopyr.	Clinopyr.	Fayalite	Quartz	Magnetite	Ilmenite	Zircon	Apatite	Allanite	Garnet
Rb	0.014	2.24 (5.5)	0.041	0.34	0.0027	0.032	0	0.014	0.5	0	0	0	0	0.01
Sr	0.022	0.12	4.4 (9)	3.87	0.0085	0.516	0	0	0.7	0	0	5	0	0.15
Ba	0.044	6.4	0.308	6.12	0.0029	0.131	0	0.023	0.4	0	0	0	0	0.015
Zr	1.4	2	0.1	0.1	0.2	0.5	0	0	0.8	1	4500	0.1	2	0.5
La	0.33	0.11	0.3	0.05	0.1	0.3	1.5	0.015	0.89	7.1	2	20	2,600	0.35
Ce	1.52	0.32	0.27	0.044	0.15	0.5	1.4	0.014	1.1	7.8	2.64	34.7	2,250	0.35
Nd	4.26	0.29	0.21	0.025	0.22	1.11	1.1	0.016	1.65	7.6	2.2	57.1	1,620	0.5
Sm	7.77	0.26	0.13	0.018	0.27	1.67	0.75	0.014	2	6.9	3.14	62.8	850	2.6
Eu	5.14	0.24	2.15	1.13	0.17	1.56	0.25	0.056	0.47	2.5	3.14	30.4	110	1
Tb	12	0.35	0.06	0.006	0.65	1.8	0.43	0.017	2.45	6.5	100	20	270	35
Yb	8.38	0.44	0.049	0.012	0.86	1.58	0.95	0.017	1.1	4.1	270	23.1	30	40
Lu	5.5	0.33	0.046	0.006	0.9	1.54	1.27	0.014	1.05	3.6	323	20.2	30	30

Partial melting of mantle lherzolites**Fractional crystallization of diabase magma**

	Olivine	Orthopyr.	Clinopyr.	Spinel	Garnet		Olivine	Clinopyr.	Plagioclase	Magnetite	Ilmenite
						Rb	0.01	0.02	0.04	0	0
						Sr	0.0004	0.08	2	0	0
						Ba	0.01	0.05	0.25	0.001	0
						Th	0.02	0.02	0.012	0.01	0.01
						U	0.04	0.02	0.01	0.01	0.01
La	0.008	0.002	0.058	0.03	0.03	La	0.008	0.058	0.14	0.015	0.098
Ce	0.007	0.024	0.1	0.03	0.03	Ce	0.007	0.1	0.14	0.016	0.11
Nd	0.007	0.033	0.22	0.04	0.087	Nd	0.007	0.22	0.08	0.026	0.14
Sm	0.007	0.054	0.45	0.05	0.22	Sm	0.007	0.45	0.08	0.024	0.15
Eu	0.007	0.054	0.48	0.05	1	Eu	0.007	0.48	0.32	0.025	0.1
Tb	0.009	0.04	0.59	0.08	3	Tb	0.009	0.59	0.07	0.019	0.14
Yb	0.014	0.034	0.58	0.11	5	Yb	0.014	0.58	0.07	0.018	0.17
Lu	0.016	0.042	0.53	0.09	5.5	Lu	0.016	0.53	0.08	0.018	0.17
						Nb	0.01	0.1	0.01	1	0.8
						Zr	0.01	0.1	0.01	0.1	0.28
						Hf	0.02	0.1	0.008	0.4	0.2
Cr	1	0.87	5	85.2	2	Cr	1	10	0.04	20	12
						Ni	16	2	0.04	10	6

Note: numbers in parentheses denote values used in partial melting modeling if different from those used for crystallization modeling.

Partition coefficient sources:

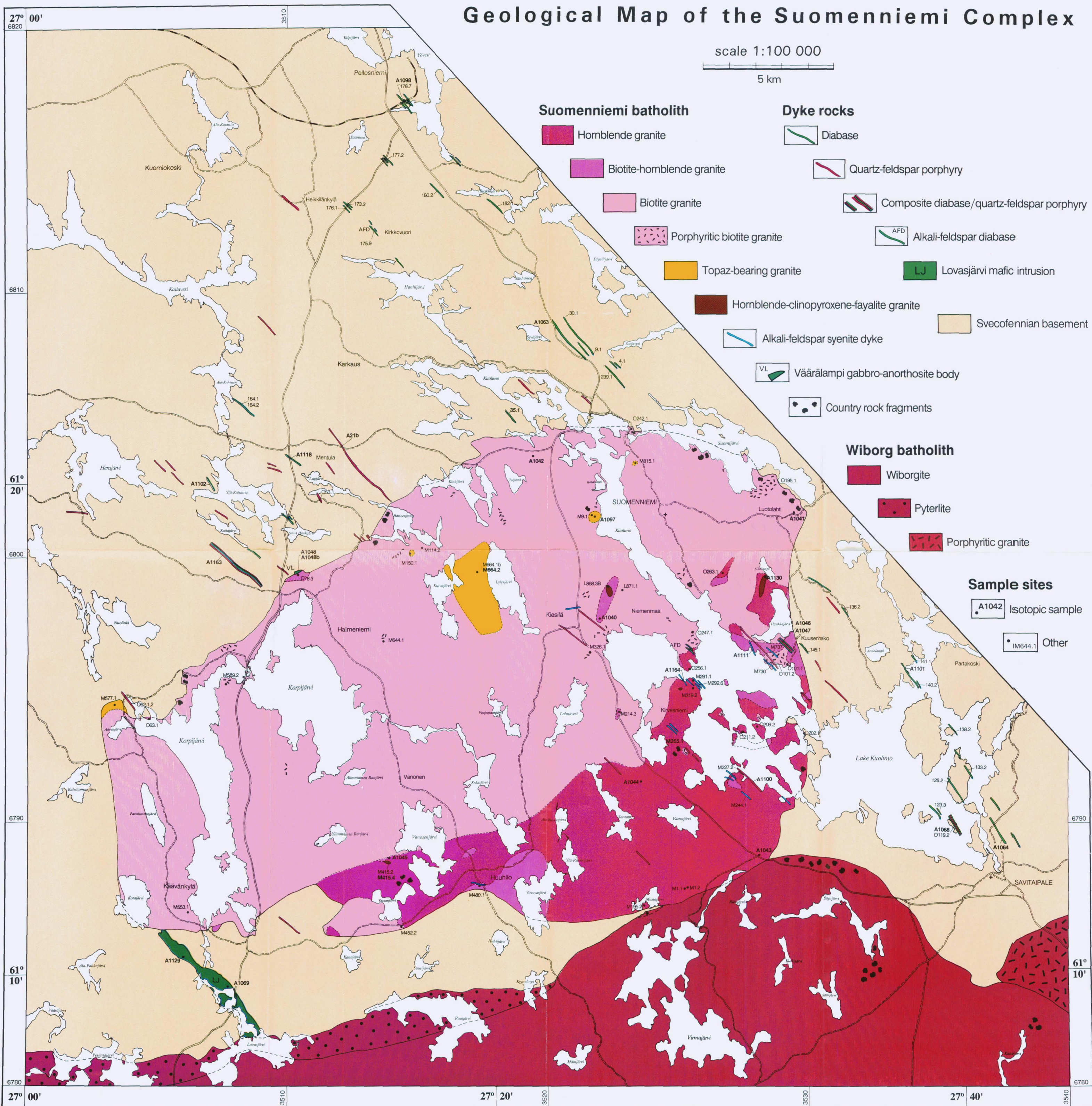
Silicic rocks: Cullers et al. (1981), Higuchi and Nagasawa (1969), Knoper (1989), Mahood and Hildreth (1983), Nagasawa and Schnetzler (1971), Nash and Crecraft (1985), Noble and Hedge (1970), Philpotts and Schnetzler (1970), Schnetzler and Philpotts (1970), Villemant et al. (1981), Watson and Harrison (1983), and Whalen and Currie (1990).

Basic and ultrabasic rocks: Allègre et al. (1977), Arth (1976), Bickle et al. (1977), Dostal et al. (1976), Dostal et al. (1983), Häkli and Wright (1967), Haskin and Korotev (1977), Henderson (1984), Irving (1978), Irving (1980), Irving and Frey (1978), Irving and Frey (1984), Irving et al. (1978), Knoper (1989), Kogarko et al. (1980), Kushiro et al. (1972), Larsen (1979), Lopez-Escobar et al. (1981), Masuda and Aoki (1979), McCallum and Charette (1977), McKay and Weill (1976), Morse (1982b), Murthy and Griffin (1970), Mysen and Kushiro (1976), Palme and Wlotzka (1977), Paster et al. (1974), Pearce and Norry (1979), and Pedersen (1979).

Geological Map of the Suomenniemi Complex

scale 1:100 000

5 km





Tätä julkaisua myy

**GEOLOGIAN
TUTKIMUSKESKUS (GTK)**
Julkaisumyynti
02150 Espoo

☎ 90-46931

Teleksi: 123 185 geolo sf

Telekopio: 90-462 205

**GTK, Väli-Suomen
aluetoimisto**
Kirjasto
PL 1237
70101 Kuopio

☎ 971-205 111

Telekopio: 971-205 215

**GTK, Pohjois-Suomen
aluetoimisto**
Kirjasto
PL 77
96101 Rovaniemi

☎ 960-297 219

Teleksi: 37 295 geolo SF

Telekopio: 960-297 289

Denna publikation säljes av

**GEOLOGISKA
FORSKNINGSCENTRALEN (GFC)**
Publikationsförsäljning
02150 Esbo

☎ 90-46931

Telex: 123 185 geolo sf

Telefax: 90-462 205

**GFC, Mellersta Finlands
distriktsbyrå**
Biblioteket
PB 1237
70101 Kuopio

☎ 971-205 111

Telefax: 971-205 215

**GFC, Norra Finlands
distriktsbyrå**
Biblioteket
PB 77
96101 Rovaniemi

☎ 960-297 219

Telex: 37 295 geolo SF

Telefax: 960-297 289

This publication can be obtained
from

**GEOLOGICAL SURVEY
OF FINLAND (GSF)**
Publication sales
SF-02150 Espoo, Finland

☎ 90-46931

Telex: 123 185 geolo sf

Telefax: 90-462 205

**GSF, Regional office of
Mid-Finland**
Library
P.O. Box 1237
SF-70101 Kuopio, Finland

☎ 971-205 111

Telefax: 971-205 215

**GSF, Regional office of
Northern Finland**
Library
P.O. Box 77
SF-96101 Rovaniemi, Finland

☎ 960-297 219

Telex: 37 295 geolo SF

Telefax: 960-297 289

ISBN 951-690-439-4

ISSN 0367-522-X